Exploration de nouvelles approches pour les études de RCPG au niveau moléculaire : application aux récepteurs de chimiokines

Lina Siauciunaite Siauciunaite-Gaubard

UNIVERSITÉ DE GRENOBLE

THÈSE

Pour obtenir le grade de

DOCTEUR DE L'UNIVERSITÉ DE GRENOBLE

Spécialité : **Biologie structurale et nanobiologie**

Arrêté ministériel : 7 août 2006

Présentée par

Lina Šiaučiūnaitė - Gaubard

Thèse dirigée par **Franck Fieschi** et
codirigée par **Corinne Vivès**

Préparée à **l'Institut de Biologie Structurale Jean-Pierre Ebel**
dans **l'École Doctorale Chimie et Sciences du Vivant**

Exploration de nouvelles approches pour les études de RCPG au niveau moléculaire: application aux récepteurs de chimiokines

Thèse soutenue publiquement le **15 Mai 2012**,
devant le jury composé de :

Prof. Eva PEBAY-PEYROULA	Président
Dr. Renaud WAGNER	Rapporteur
Dr. Jean-Louis BANÈRES	Rapporteur
Dr. Jean-Luc POPOT	Examinateur
Prof. Franck FIESCHI	Directeur de thèse
Dr. Corinne VIVÈS	Co-directeur de thèse

Acknowledgments

I give my sincere thanks to my supervisors Dr. Corinne Vivès and Prof. Franck Fieschi who accepted me to work on this project and who gave me the possibility to acquire the PhD degree.

I would like to express my gratitude to my supervisor, Dr. Corinne Vivès, who was very supportive through all the joys and miseries and whose expertise, understanding, and patience, contributed considerably to my experience. I appreciate her assistance in writing reports and this thesis, which significantly improved my writing skills. I am also grateful for her generous help to translate the thesis summaries to French language. Without her help probably no french would have understood what I wrote.

I would like to thank my thesis director Prof. Franck Fieschi who accepted me as a PhD student to work as a part of his team and for the assistance he provided at all levels of the research.

I am grateful to the jury members Prof. Eva Pebay-Peyroula, Dr. Renaud Wagner, Dr. Jean-Louis Banères and Dr. Jean-Luc Popot who kindly agreed to evaluate my work and who gave me very helpful comments on this work.

I would like to thank to my tutor from the SBMP network, Dr. Jean-Luc Popot, for his valuable and helpful comments and discussions. I am also grateful for the possibility to visit his laboratory where I learned to work with amphipols and the cell free expression. I would like to thank Emmanuelle Billon-Denis and Francesca Zito for the supervising during my stay at IBPC in Paris.

A very special thanks goes to Dr. Antoine Picciocchi who joined the group as a post-doc and was involved in the project and whose motivation and encouragement was leading me every day.

I would like to thank to Ieva Sutkevičiūtė for her valuable help with the analysis of the Biacore results. Taip pat ačiū už palaikymą, visada buvo be galo malonu bendrauti.

Dr. Richard Kahn was the scientist who truly made a difference in my life. He provided me with direction, support and became more of a mentor and friend. I owe him my eternal gratitude.

A big thanks goes to all the former and current members of the MIT: Corinne, Franck, Isabelle, Céline, Antoine, Ieva, Michel, Eric, Julien, Jérôme, Christine. I would like to thank to people from the channels group for the electrophysiology experiments: Dr. Christophe Moreau, Dr. Michel Vivaudou, Dr. Argel Estrada-Mondragón, Dr. Lydia Caro, Jean Revilloud.

I would like to thank Rabia Sadir for the chemotaxis experiments. For the mass spectrometry analysis my thanks to Izabel Bérar and Luca Mollica. I am grateful to Isabelle Bally and Nicole Thielens for the SPR (Biacore technology) platform. For the N-terminal sequencing I would like to thank Jean-Pierre Andrieu.

I am grateful to our collaborators Dr. Bernard Mouillac, Dr. Jean-Louis Banères for the work with the GPCRs and Dr. Jean-Luc Popot who kindly provided amphipols to us. Thank you all! Without your collaborations this work would be hard to imagine.

Thanks to Dr. Federico Martin-Ruiz for the kind gift of the protease clone.

I would also like to thank to my previous colleagues from CNIO. Ya hace un tiempo, pero fue un placer a trabajar con vosotros. No toda nuestra experiencia fue divertida pero yo aprendí muchísimo. Gracias a tod@s! Fede, Miguel, Jose, Carmen, Nayra, Mer, Sandrea, Jero... Muchísimas gracias por vuestro apoyo! Gracias que no olvidáis y que vengáis a visitarme en Grenoble.

Taip pat ačiū svarbiausiems - šeimai ir draugams kurie yra visada šalia. Ačiū tėvams už paramą, kurią jie suteikė man per visą mano gyvenimą. Ir visų svarbiausia, norėčiau padėkoti savo vyrui bei geriausiam draugui, Yohann, be kurio meilės, padrąsinimo ir redagavimo pagalbos, aš nebūčiau baigus šios tezės.

Last but not least, I recognize that this research would not have been possible without the financial assistance. The research leading to these results have received funding from the [European Community's] Seventh Framework Programme [FP7/2007-2013] under grant agreement n° [211800].

Contents

List of Figures

List of Tables

Abbreviations

A_{2A}AR A_{2A} Adenosine Receptor

A8-35 A particular type of anionic amphipol

AA Amino Acid

AC Adenylyl Cyclase

ADP Adenosine Diphosphate

APol Amphipols

ATP Adenosine-5'-Triphosphate

AUC Analytical Ultracentrifugation

β2AR β2-Adrenergic Receptor

BAPol Biotinylated Amphipol

BRET Bioluminescence Resonance Energy Transfer

C8E4 Octyltetraoxyethylene

cAMP cyclic Adenosine Mono-Phosphate

CCR5 CC Chemokine Receptor 5

CMC Critical Micelle Concentration

CRD Cysteine-Rich Domain

CSC Critical Solubilization Concentration

CTC Cubic Ternary Complex model

CXCR4 CXC Chemokine Receptor 4

D3R Dopamine D3 receptor

DAG Diacylglycerol

DARC Duffy Antigen Receptor for Chemokine

DDM n-Dodecyl-β-D-maltoside

DG n-decyl-beta-D-glucopyranoside

DM n-decyl-β-D-maltopyranoside

DOR δ-opioid Receptor

DPC Dodecyl Phosphocholine

DTT Dithiothreitol

EDC N'-(3-dimethylaminopropyl) carbodiimide hydrochloride

EDTA Ethylenediaminetetraacetic acid

ECL Extracellular Loop

ER Endoplasmic Reticulum

ETC Extended Ternary Complex model

F-TAC C6F13C2H4- S-poly-Tris-(hydroxymethyl) aminomethane

FAPol Fluorescently labeled Amphipols

FBS Fetal Bovine Serum

FRET Fluorescence (or Förster) Resonance Energy Transfer

FZD Frizzled receptors

GABA γ-aminobutyric acid

GABAbR γ-aminobutyric acid b receptor

GAG Glycosaminoglycan

GDP Guanosine Diphosphate

GuHCl Guanidine hydrochloride,

GEF Guanine nucleotide Exchange Factor

GIRK G protein regulated Inward Rectifier potassium channel

GPCR G Protein-Coupled Receptor

GPS GPCR Proteolytic Site

GRAFS Glutamate, Rhodopsin, Adhesion, Frizzled/Taste2 and Secretin

GRK G Protein–coupled Receptor Kinases

GST Glutathione S-Transferase

GuHCl Guanidine hydrochloride

H1R Histamine H1 Receptor

HEPES 2-[4-(2-hydroxyethyl) piperazin-1-yl] ethanesulfonic acid

HFS Hemifluorinated Surfactant

HIV Human Immunodeficiency Virus

HS Heparin Sulphate

HSC Hematopoietic Stem Cells

IB Inclusion Bodies

ICL Intracellular Loop

IL-2 Interleukin-2

INS Inelastic Neutron Scattering

IP3 Inositol trisphosphate

JAK Janus Kinase

kDa kilo Dalton

LDAO N,N-dimethyldodecylamine-N-oxide

LPA Lysophosphatidic acid

LT Lanthanoid Binding Tag

MALS Multi Angle Light Scattering

MAP Mitogen-Activated Protein

MAPK Mitogen-Activated Protein Kinase

MBP Maltose Binding Protein

MD Molecular Dynamics

MIP Macrophage Inflammatory Protein

MSP Membrane Scaffold Protein

MW Molecular Weight

nAChR nicotinic Acetylcholine Receptor

NAPol Non-ionic Amphipol

NBD 7-nitrobenz-2-oxa-1, 3- diazol-4-yl

NBD Nucleotide Binding Domain

NDPK Nucleoside Diphosphate Kinase

NG n-nonyl-beta-D-glucopyranoside

NHS N-hydroxysuccinimide

NK Natural-Killer

NMR Nuclear Magnetic Resonance

OG n-octyl-β-D-glucopyranoside

OG Octylglucoside

OM n-octy-beta-D-maltopyranoside

PBS Phosphate-Buffered Saline

PC Phosphorylcholine

PC-APol Phosphorylcholine-based Amphipol

PCR Polymerase Chain Reaction

PDE Phosphodiesterase

PI3K Phosphatidyl inositol 3-kinase

PIP2 Phosphatidylinositol 4, 5-biphosphate

PKC Protein Kinase C

PKD Protein Kinase D

PLA Phospholipase A

PLC Phospholipase C

PLC-β Phospholipase C-β

PrePro PreScission protease

PurF Glutamine Phosphoribosyl Pyrophosphatase Amidotransferase

R Receptor

R* Activated Receptor

RANTES Regulated on Activation, Normal T cell Expressed and Secreted

RGS Regulators of G protein Signaling

RU Response (or Resonance) Units

SA Streptavidin

SANS Small Angle Neutron Scattering

SAPol Sulfonated Amphipol

SAXS Small Angle X-ray Scattering

SDS Sodium Dodecyl Sulfate

SDS-PAGE Sodium Dodecyl Sulfate Polyacrylamide Gel Electrophoresis

Smo Smoothened Receptor

SPR Surface Plasmon Resonance

T4L T4 lysozyme

TC Ternary Complex Model

TEVC Two-Electrode Voltage Clamp method

TM Transmembrane

Tris 2-Amino-2-hydroxymethyl-propane-1, 3-diol

VDCC Voltage-Dependent Ca^{2+} Channels

Standard one- and three-letter codes used for the amino acids.

Amino acid	Three-letter code	One-letter code
Alanine	Ala	A
Arginine	Arg	R
Asparagine	Asn	N
Aspartic acid (Aspartate)	Asp	D
Cysteine	Cys	C
Glutamine	Gln	Q
Glutamic acid (Glutamate)	Glu	E
Glycine	Gly	G
Histidine	His	H
Isoleucine	Ile	I
Leucine	Leu	L
Lysine	Lys	K
Methionine	Met	M
Phenylalanine	Phe	F
Proline	Pro	P
Serine	Ser	S
Threonine	Thr	T
Tryptophan	Trp	W
Tyrosine	Tyr	Y
Valine	Val	V
Unspecific aa	Xaa	X

Table 0.1.: Amino acids and their abbreviations.

Standard one-letter codes used for the nucleotides.

Nucleotide	One-letter code
Adenosine	A
Cytidine	C
Guanosine	G
Thymidine	T

Table 0.2.: Nucleotides and their abbreviations.

Part I.

Introduction

1. G Protein-Coupled Receptors

1.1. GPCR background

G Protein-Coupled Receptors (GPCRs) form one of the largest and most studied gene families of mammalian genomes. GPCRs are found only in eukaryotes, including yeast, plants, choanoflagellates, and animals. From the sequenced human genome over 800 GPCR genes were identified [1].

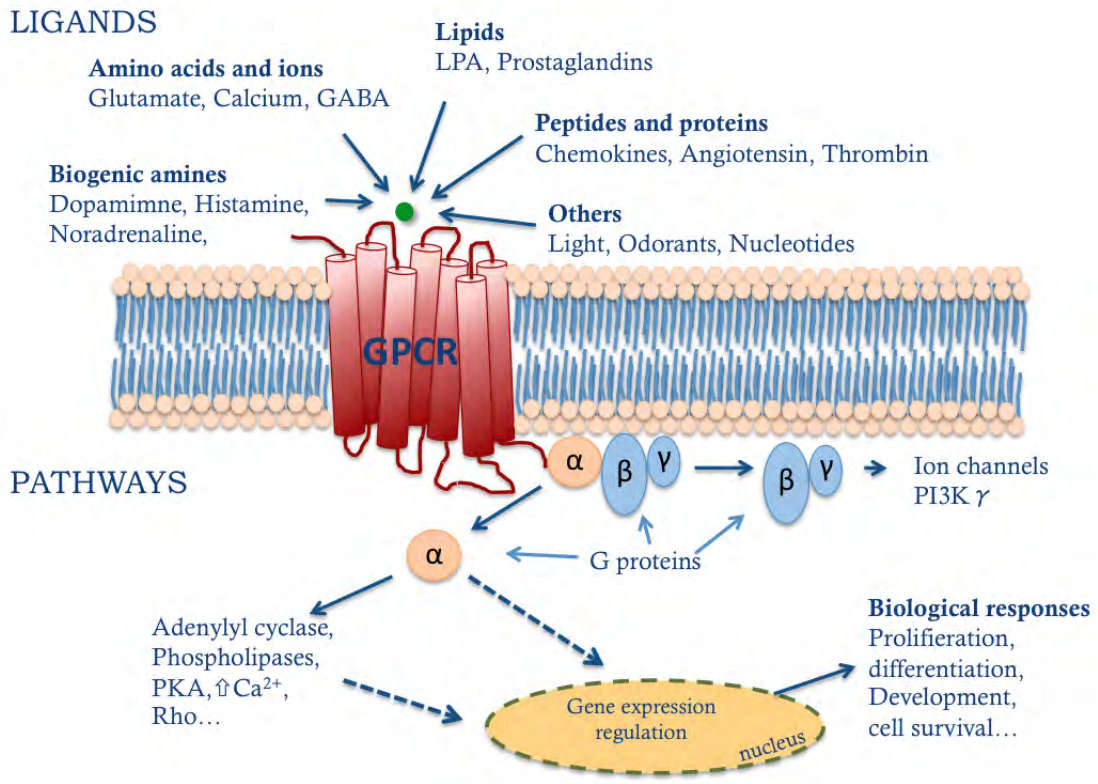

Figure 1.1.: GPCR signaling.

GPCRs bind to a very broad range of ligands such as hormones, neurotransmitters, cytokines, lipids, various small molecules such as odors and are reactive to light (Figure 1.1) [2, 3]. GPCRs modulate variety of cell functions through coupling to heterotrimeric G proteins and regulating downstream effectors such as adenylyl cyclases, phospholipases, protein kinases, ion channels and other intracellular messengers [4].

1.1.1. Topology

Members of the GPCR superfamily share a common membrane topology: an extracellular N-terminal domain, an intracellular C-terminal domain and seven hydrophobic transmembrane (TM) helices, which are connected by three intracellular loops (ICL) and three extracellular loops (ECL) (Figure 1.2). Each transmembrane helical domain is composed of about 24 amino acids, while the C- and N- terminal regions as well as the loops can widely vary in length with up to hundreds of amino acids. Each of these variable regions provides specific properties to GPCRs.

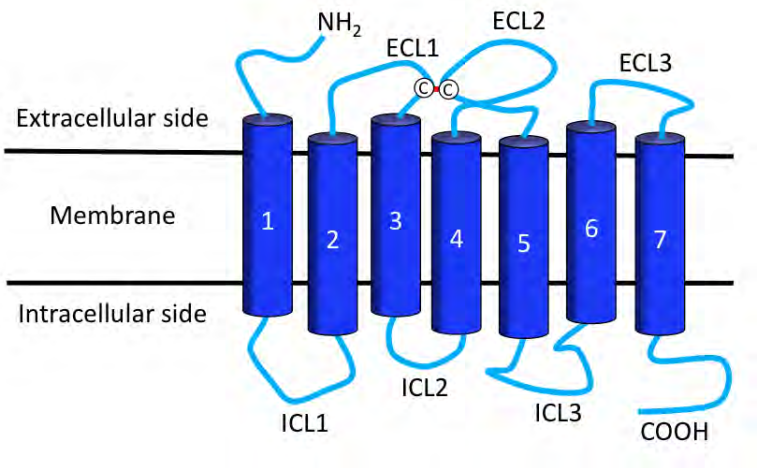

Figure 1.2.: GPCR common topology.

Most of the GPCRs have two well-conserved cysteine residues, one in extracellular loop 1 (ECL1) and one in extracellular loop 2 (ECL2). They form a disulphide bridge important for packing and stabilization of the helical bundle. The extracellular parts of the receptor can be glycosylated.

1.1.2. Ligands of GPCRs

Ligands that bind and activate the GPCRs can be classified by type as follows [5]:

- BIOGENIC AMINES such as noradrenaline, dopamine, histamine;
- AMINO ACIDS AND IONS such as glutamate, GABA, calcium;
- LIPIDS such as LPA, prostaglandins;
- PEPTIDES AND PROTEINS such as chemokines, angiotensin, thrombin;
- OTHERS such as light, odorants, and nucleotides.

GPCRs naturally exist in multiple conformations ranging from the fully inactive ground state (R) to the fully active state (R*), which couples to G proteins and leads to signal transduction. For any given receptor, equilibrium exists between these two states that determine the basal level of its activity in cells.

Depending on the GPCR activation state the ligands can be divided into five classes: full agonist, partial agonist, antagonist, inverse partial agonist and inverse full agonist. Figure 1.3 represents the receptor activation effects produced by different types of ligands.

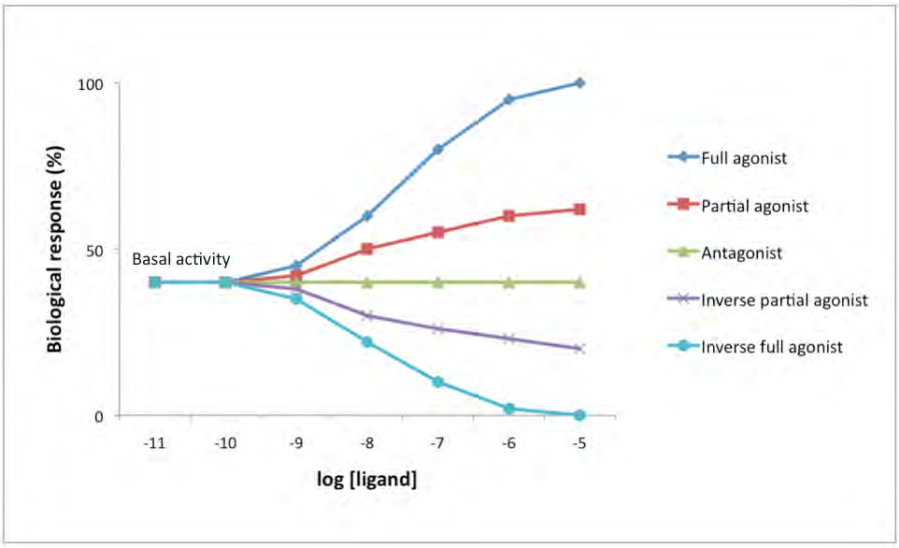

Figure 1.3.: Schematic representation of dose response curves by different types of GPCR ligands.

Full agonist binds and activates the receptor displaying its full efficacy. Efficacy in this case refers to the maximum response achievable from a ligand. Partial agonist binds and activates the receptor but has only partial efficacy compared to full agonist. Both agonists increase the percentage of receptors in the active state above basal activity level. Inverse agonist inhibits the basal activity of the receptor. Antagonist does not provoke a biological response itself upon binding to the receptor but inhibits the action of other ligands and the receptor basal activity state is restored.

GPCR ligands can also be classified according to the receptor-binding site. The majority of known GPCR ligands bind to the same site as the endogenous agonists, the orthosteric site. However, recent studies have described the identification of allosteric ligands for GPCRs, which interact at a distinct site from the orthosteric one [6, 7]. The allosteric sites are of particular pharmacological interest for selective drug design as these sites have not been under specific selective pressure during evolution. Besides, the allosteric sites are quite distinct between highly homologous receptors. Accordingly, they provide excellent targets for highly selective drugs.

1.1.3. Classification of G Protein-Coupled Receptors

Several classification systems have been used to organize the GPCR superfamily. Some are based on the ligand binding modalities others on physiological and structural features.

One of the most frequently used systems uses A, B, C, D, E, and F, classes, which is based on sequence homology and functional similarity [4, 8, 9]. This A–F classification system covers all GPCRs, from vertebrates and invertebrates. Therefore, some families in the A–F classification system do not exist in humans.

More recently, GPCRs have been classified into five distinct groups based on phylogenetic analyses of sequences, from the human genome. This classification system has been named GRAFS, which is an acronym for the five different groups: **G**lutamate, **R**hodopsin, **A**dhesion, **F**rizzled/Taste2 and **S**ecretin [1]. The different groups of GRAFS classification system are described below.

1.1.3.1. Glutamate group

Glutamate family contains 22 members; more than half of these family members remain orphan receptors[1].

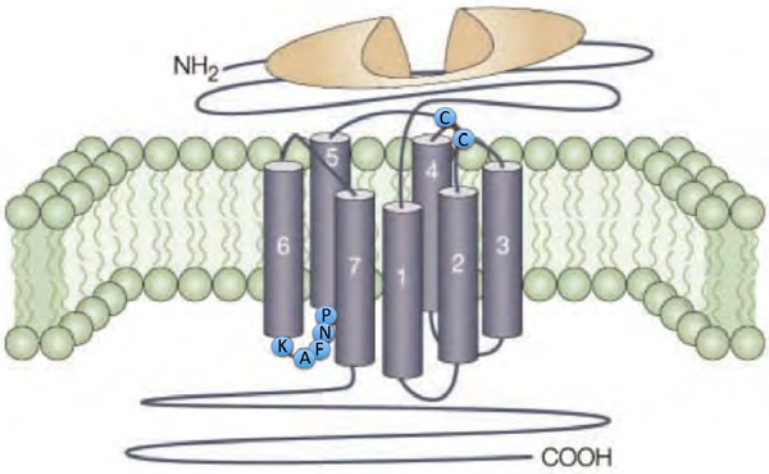

Figure 1.4.: Schematic representation of Glutamate family receptor.
The ICL3 is short and contains highly conserved amino acids [10].

The Glutamate family (also referred to as Class C or Family 3) (Figure 1.4) comprises in metabotropic glutamate receptors, GABA receptors, calcium sensing receptor, taste receptors

[1]Orphan receptors are those for which endogenous ligand has not yet been identified.

(for sweet and *umami*[2]) and several orphan receptors. Ligands of Glutamate receptors family are cations, amino acids, carbohydrates, and other small organic compounds.

These receptors are characterized by a long N- and C- termini and a short and highly conserved third intracellular loop. The N-terminus forms two distinct lobes separated by a cavity in which ligand binds, forming a so-called Venus fly trap domain. The extracellular region also has a cysteine-rich domain (CRD), which contains nine conserved cysteine residues forming three disulphide bridges, which connect the ligand-binding domain and the intracellular signaling domain located within TM regions [11].

GPCRs that belong to the Glutamate family, form constitutive dimers and are used as model proteins to study functional relevance of GPCR dimerization [12].

1.1.3.2. Rhodopsin group

The Rhodopsin family contains 672 members in the human genome including 388 odorant receptors. Despite the fact that this is the largest family there are only 63 orphan receptors[13].

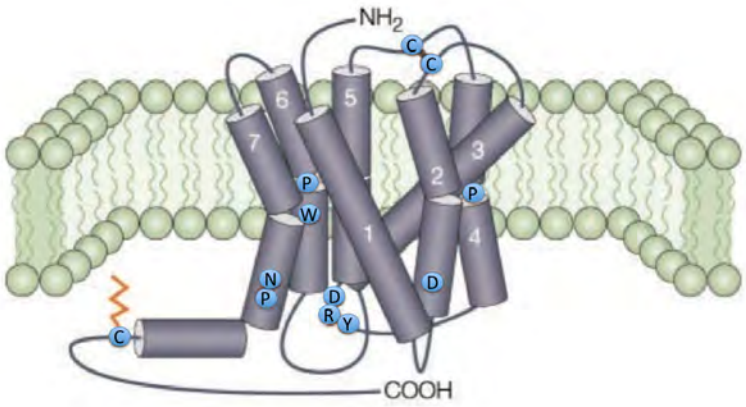

Figure 1.5.: Schematic representation of Rhodopsin family receptor.
Conserved amino acids among the members of the family are represented as well as the palmitoylated cysteine residue in the C-terminal part [10].

Rhodopsin family (Figure 1.5) (also referred to as Class A or Family 1) is by far the largest subgroup and contains receptors for odorants, important neurotransmitters, such as dopamine and serotonin, as well as neuropeptides and glycoprotein hormones. These family members are characterized by several highly conserved amino acids such as NSxxNPxxY motif in the transmembrane helix 7 (TMVII) and the DRY motif or D(E)-R-Y(E) at the border between TMIII and ICL2 [1]. These conserved sequences have been proposed to be important for the receptor

[2] *Umami* is one of the five basic tastes together with sweet, sour, bitter, and salty. *Umami* is a loanword from the Japanese *umami* meaning "pleasant savory taste". This particular writing was chosen by Professor Kikunae Ikeda from *umai* "delicious" and *mi* "taste".

activation or for maintaining the receptor in the inactive state [14]. A conserved disulphide bridge connects the first and second extracellular loops. Most of these receptors also have a palmitoylated cysteine residue in the intracellular C-terminal tail, which serves as an anchor to the membrane.

For small molecules, the ligand binding site is located within the transmembrane part, whereas in the case of peptides and glycoproteins, it is located at the N-terminal part and extracellular loops.

The determination of the crystal structure of rhodopsin [15] has indicated that the transmembrane domains of rhodopsin family receptors are 'tilted' and 'kinked', due to the presence of amino acids such as proline that distort the helical transmembrane domain.

Chemokine receptors belong to this GPCR family.

1.1.3.3. Adhesion group

In the A-F classification system the adhesion receptors belong to class B but in the new GRAFS classification system they are considered as a separate group. Among 33 members of the group there are only 3 receptors, which are no longer orphans. The ligands of these receptors are extracellular matrix molecules such as peptides and glycosaminoglycans.

The family name "adhesion" relates to the long N-terminal part, which contains motifs that participate to cell adhesion. The N-terminal domain is variable in length, from about 200 to 2800 amino acid long and is often rich in glycosylation sites and proline residues that might be important for cell-cell contact [1].

Adhesion GPCRs display the GPCR proteolytic site (GPS). The GPS domain acts as an intracellular autocatalytic processing site that produces two non-covalently attached subunits. The proteolytic cleavage of the receptor protein occurs in the endoplasmic reticulum or in the early compartment of the Golgi apparatus and is necessary to transport the receptor to the membrane [16].

1.1.3.4. Frizzled/Taste2 group

This group includes two distinct clusters without any obvious similarities, the Frizzled receptors and the Taste2 receptors (also referred to as Class F or family 6). However, Taste2 and Frizzled receptors, share several consensus sequences: IFL in the second TM, SFLL in the fifth TM, and SxKTL in the seventh TM. Frizzled/Taste2 family includes 36 members. There are no orphans among the 11 Frizzled family members, but most of the Taste2 GPCRs remain orphans.

Frizzled/Smoothened This family includes ten Frizzled receptors (FZD1-10) and the Smoothened receptor (Smo). The Frizzled receptors mediate signals from secreted glycoproteins and in this way they control cell fate, proliferation, and are involved in embryonic development, particularly, in cell polarity and segmentation. The Frizzled family receptors have a 200-amino acid long N-terminus which contains several conserved cysteines. Their ligands are proteins.

Taste2 receptors The human genome contains 25 functional Taste2 receptors. They are expressed in the tongue and palate epithelium and function as bitter taste receptors. Their ligands are small organic compounds. Several of the Taste2 receptors are still orphans. Taste2 receptors consist of 290 - 340 amino acids and display short N- and C- termini domains. Taste2 receptors lack the well-conserved cysteine bridge between extracellular loops 1 and 2. Despite few conserved residues that are common for the ligand binding site, these receptors are highly variable between the species.

1.1.3.5. Secretin group

Secretin family comprises 50 members with none of them being orphan receptors (also referred to as Class B or Family 2). Secretin family GPCRs (Figure 1.6) are characterized by a relatively long N-terminus, which contains several cysteines that form a network of disulphide bridges. This extended N-terminal domain together with extracellular loops is implicated in ligand binding. Ligands of secretin family GPCRs include high molecular weight hormones such as glucagon, secretine, calcitonin and Black widow spider toxin.

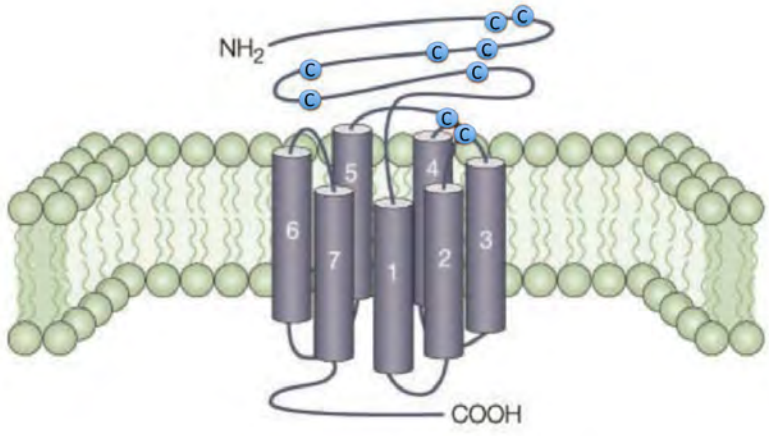

Figure 1.6.: Schematic representation of Secretin family receptor.
Relatively long N-terminus contains several conserved cysteins [10].

The topology of secretin family receptors is similar to some of the rhodopsin family receptors, however the palmitoylation site is missing and the conserved residues and motifs are different from those in the rhodopsin family receptors.

Little is known about the orientation of the TM domains, but given the divergence in amino-acid sequence, they are likely to be different from rhodopsin family receptors. As in rhodopsin family, the secretin family receptors contain several conserved proline residues within the TM segments, which are essential for the conformational dynamics of the receptors.

1.2. GPCR activation

Receptor activation studies started early before the term of receptor was applied. The studies started by observing how different tissues reacted to the drugs. J. N. Langley in 1878 postulated that a drug has to bind to a specific part of the tissue in order to produce an action on that tissue. After a while, he described "side chain molecules" present on different muscles that reacted differently to the drug (nicotine). He named them "receptive substances" that are diverse in different muscles [17]. Lately this term was widely adapted as "receptor".

For a long time receptor activation was represented by a simple model with a bimodal switch between inactive and active forms. However, increasing experimental evidence provided information that GPCRs are dynamic and exist in different conformational states [18].

1.2.1. Simple linear Two-State Model

The first models used to describe the activation mechanism of GPCRs were based on the law of mass action. The interaction between the receptor (R) and the agonist (A) depends on the equilibrium association constant (K_a) resulting in receptor activation (Figure 1.7).

Figure 1.7.: Simple linear two-state model.
A - Agonist, R - Receptor, R* - Activated Receptor.

An agonist (A) binds to the receptor (R) to form an agonist-receptor complex (AR). The level of the AR complex present at thermodynamic equilibrium can be defined by the value of the K_a. A physiological response can be expected only when the AR complex is formed, and a maximal response will occur when the agonist occupies all receptor sites.

In 1980, this idea was modified taking into account receptor properties such as intrinsic activity, efficiency, conformational changes and G protein binding.

1.2.2. Ternary Complex Model

Studying the β2 Adrenergic Receptor (β2AR), A. De Lean and co-workers established the Ternary Complex (TC) Model [19] (Figure 1.8). This model originated form the simple linear two-state model.

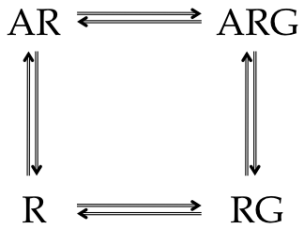

Figure 1.8.: Ternary complex model.
A - Agonist, R - Receptor, G - G Protein.

The initial ternary complex model describes the interactions between ligand, receptor, and G protein. This model implies that the receptor recognizes the agonist and the G protein in a random order.

1.2.3. Extended Ternary Complex Model

Continuous research and discoveries led to the further model development. In 1993, the studies of the β2AR activation indicated that a GPCR could activate G proteins without being stimulated by a ligand [20, 21]. At this stage the Extended Ternary Complex (ETC) model was introduced to include the spontaneous activation of a receptor that can interact with a G protein even in the absence of agonist binding (Figure 1.9).

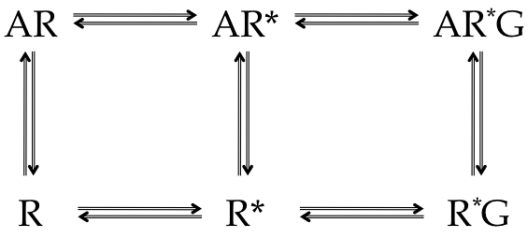

Figure 1.9.: Extended ternary complex model.
A - Agonist, R - Receptor, R* - Activated Receptor, G - G Protein.

This model allows both the spontaneous and ligand induced active-state receptor (R*). R* can then interact with the ligand or activated G protein. In this model, the agonists have

stronger affinity to R* than for R, shifting the equilibrium toward the active form of the receptor. Antagonists have similar affinity for both forms and do not affect the balance. Inverse agonists have a tendency to bind to R and therefore move the equilibrium towards the inactive-state R form.

1.2.4. Cubic Ternary Complex Model

In 1996, to introduce receptor activation and G protein coupling the Cubic Ternary Complex (CTC) was established [22]. The CTC model adds a possibility of an active receptor and G protein association that does not cause signaling. This non-signaling complex is required thermodynamically.

The CTC model takes into account that receptor can be in active (R*) or inactive (R) conformation and bound to the G protein (R*G and RG) or not (Figure 1.10). In this model, the receptor can interact with a G protein and/or a ligand at the same time. In addition, different receptors both active and inactive receptors may compete for the same ligand or G protein.

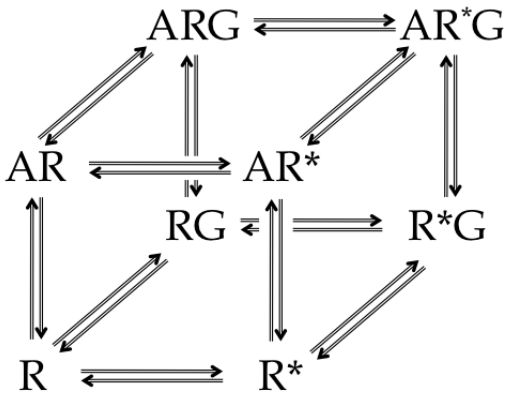

Figure 1.10.: Cubic ternary complex model.
A - Agonist, R - Receptor, R* - Activated Receptor, G - G Protein.

However, the model does not include receptor homo- or hetero-oligomerization [23, 10, 24, 25, 26, 27], or the possibility that GPCRs can form stable complexes with downstream proteins [28].

1.2.5. Constitutive activity

The constitutive activity of GPCRs can be defined as the ability of a receptor to present an intrinsic activity in the absence of agonist. The evidence of constitutive activity of GPCRs has been described in the studies of the δ-opioid receptor [29], and purified β2AR [30]. Inverse agonist binding can block the constitutive activity of receptors.

Most if not all GPCRs can exist in at least two states: an active state favored by agonist and an inactive state favored by inverse agonist [31, 32, 33].

Mutants with increased constitutive activity of GPCRs were later discovered. GPCR mutations in the region near the interface at the end of the third intracellular loop and at the beginning of transmembrane helix VI result in the elevated levels of constitutive activity [34, 35].

1.3. G protein signaling pathway

Heterotrimeric G proteins composed of Gα, Gβ and Gγ subunits constitute one of the most important components of the cell signaling cascade [36]. They transmit signals from transmembrane receptors, ion channels and further to intracellular effector enzymes.

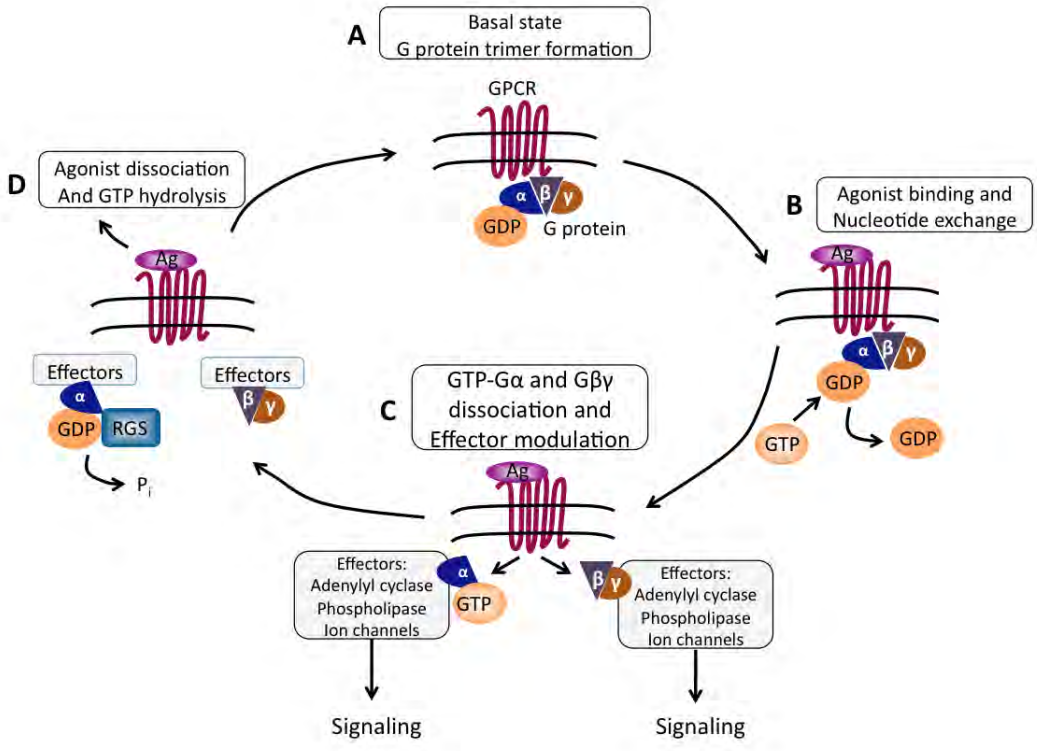

Figure 1.11.: GPCR activation cycle.
In the receptor inactive state (A), the Gα subunit in a GDP bound form is associated to the Gβγ complex. Upon agonist binding (B), the receptor undergoes a conformational change that activates its Guanine nucleotide Exchange Factor (GEF) , which catalyzes the exchange of GDP to GTP in the Gα subunit. GTP-bound Gα and the Gβγ complex dissociates and that activates downstream signaling (C). Hydrolysis of GTP to GDP, which may be stimulated by Regulators of G protein Signaling (RGS) proteins, leads to re-association of Gα and Gβγ subunits and termination of G protein signaling (D).

In the absence of a stimulus, the GDP-bound Gα subunit (Gα·GDP) and the Gβγ complex are associated (Figure 1.11). Ligand binding to the GPCR causes a conformational change in the

GPCR, which allows it to act as a Guanine nucleotide Exchange Factor (GEF). The GPCR can then activate an associated heterotrimeric G protein by exchanging its bound GDP to GTP [37].

The binding of GTP to the Gα subunit results in conformational changes within the three flexible switch regions of Gα (see Section 1.3.1.1), and leads to the dissociation of Gβγ from the heterotrimeric complex. Activated Gα and Gβγ proteins bind to various effectors that transmit signals to different second messengers such as adenylyl cyclases, phospholipases, and ion channels.

Gα signaling is terminated upon GTP hydrolysis. Although Gα has a slow capability to hydrolyze GTP, the rate of this reaction is often accelerated by allosteric modulating proteins called Regulators of G protein Signaling (RGS) (Figure 1.11 D). Re-association of Gβγ with Gα·GDP terminates all interactions with effectors and form the initial inactive heterotrimeric complex [38, 39].

1.3.1. G-protein subunits

At present, there have been 16 Gα, 5 Gβ and 12 Gγ subunit genes identified [40]. Various combinations of heterotrimeric G proteins are possible. Each of the subunits possesses specific properties, which enable the transmission of specific signals.

1.3.1.1. The Gα subunit

There are at least 16 Gα genes in the human genome. When alternative splicing and post-translation modifications are taken into account - there are at least 23 known Gα proteins [41]. The molecular mass of Gα subunit varies from 39 to 45 kDa. Crystallographic studies revealed that the Gα subunit is composed of two major domains: a GTPase binding domain and an α-helical domain (Figure 1.12).

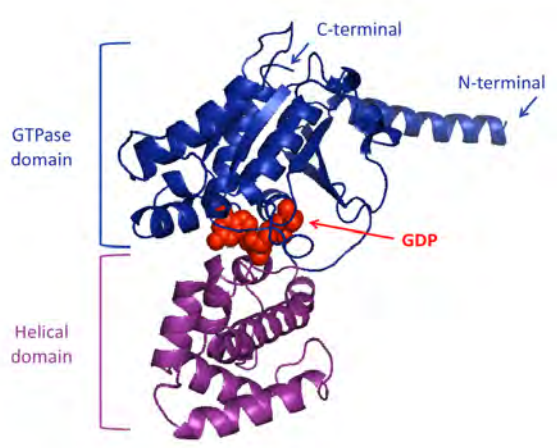

Figure 1.12.: Structure of *Bos taurus* Gα subunit.
PBD code: 1GOT [42].

GTPase domain is conserved among all members of the G protein superfamily. This domain hydrolyses GTP and provides the binding surfaces for the Gβγ dimer, GPCRs and effector proteins. GTPase domain contains three flexible loops, named switches I, II and III, where significant structural differences between GDP-bound and GTP-bound conformations of Gα were identified [43, 44, 45, 46]. The N- and C- terminal parts of the Gα subunit are important for the interaction with GPCRs [47].

The helical domain is unique for each Gα protein and is composed of a bundle of six α-helices that form a cover over the nucleotide-binding pocket, hiding them in the core of the protein (Figure 1.12).

On the basis of the sequence homology Gα proteins are divided into four major classes. Each class can be subdivided into several families (Table 1.1) [48, 41].

Class	**Family**	**Effector**
$G\alpha_S$	α_{SL1}, α_{SL2}, α_{SS1}, α_{SS2}, α_{Olf}	Adenylyl cyclase (+)
$G\alpha_{i/o}$	α_{i1}, α_{i2}, α_{i3}	Adenylyl cyclase (-), Cl^- and K^- channels (+), Phospholipase C and A2 (+)
	α_{t1}, α_{t2}, α_{Gus}	cGMP phosphodiesterase (+)
	α_{o1}, α_{o2}	Voltage dependent Ca^{2+} channels (-), K^+ channels (+)
	α_z	Adenylyl cyclase (-)
$G\alpha_{q,11}$	α_q, α_{11}, α_{14}, α_{15}, α_{16}	Phospholipase C (+)
$G\alpha_{12,13}$	α_{12}, α_{13}	Phospholipase A2 (+), c-Jun NH(2)-terminal kinase (+)

Table 1.1.: Gα subunit classes and their effectors.
(+) Activation, (-) Inhibition.

All Gα subunits, except $G\alpha_t$, are post-translationally modified with the fatty acid palmitate at the N-terminus. Members of the $G\alpha_i$ family are also myristoylated at the N terminus. All these modifications regulate membrane localization and protein – protein interactions [49].

Each Gα class is involved in specific signaling mechanisms (Figure 1.13). Although there are many exceptions and the signaling pathways are not that distinct between different classes of Gα proteins, however, three basic signaling patterns could be identified.

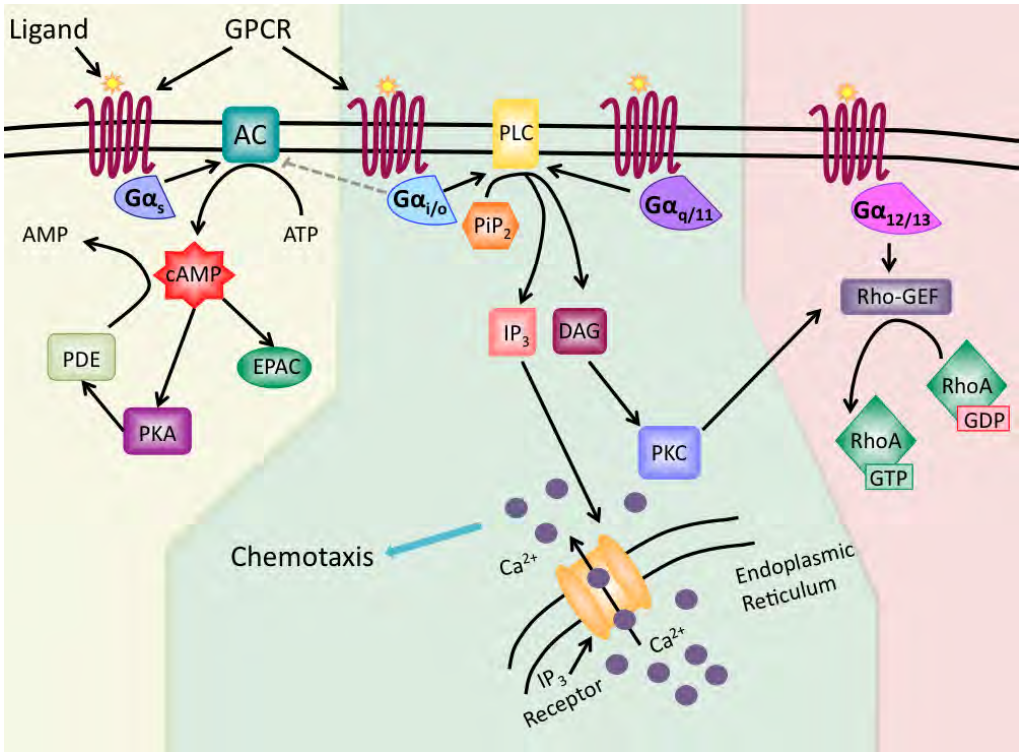

Figure 1.13.: Typical patterns of Receptor-Gα protein signaling in the cells.
AC- Adenylyl Cyclase, PKA - Protein Kinase A, EPAC - Exchange Proteins directly activated by cAMP, PDE - Phosphodiesterase, PLC - Phospholipase C, PIP2 - phosphatidylinositol 4,5-biphosphate, DAG - diacylglycerol, IP3 inositol triphosphate.

The Gα_S class

The Gα_S class contains several families of Gα_S and a Gα_{Olf} family, which couples to the olfactory receptors. They activate the Adenylyl Cyclase (AC), which stimulates the production of cAMP from ATP.

The downstream signaling of cAMP is mediated by its interactions with effector molecules, Protein Kinase A (PKA) or EPAC (Exchange Proteins directly activated by cAMP), which have been shown to modulate phagocyte functions.

The production of cAMP could be regulated by microbial pathogens [50]. Pertussis toxin and cholera toxin cause elevated cAMP levels through ADP-ribosylation of either the Gα_i subunit to prevent its inhibition of Adenylyl Cyclase or of the Gα_S subunit to constitutively activate Adenylyl Cyclase, respectively. Phosphodiesterase (PDE), which degrades cAMP to AMP, is another regulator of intracellular cAMP levels. PDE inhibitors prevent such degradation, resulting in accumulation of intracellular cAMP [51].

The G$\alpha_{i/o}$ class

The G$\alpha_{i/o}$ class contains several families of Gα_i , Gα_t, Gα_o, one Gα_z, and one Gα_{Gus} protein family. Gα_i can inhibit Adenylyl Cyclase, which results in inhibition of the production of cAMP from ATP [52]. The Gα_t and Gα_{Gus} activate the Phosphodiesterase, which degrades cAMP to AMP, when coupled to Rhodopsin and Taste receptors respectively. Gα_i can inhibit the voltage-dependent Ca^{2+}channels and activate Cl^- and K^+ channels.

Upon the dissociation of G$\alpha_{i/o}$ from G$\beta\gamma$ subunits, Phospholipase C (PLC) could be activated. Phospholipase C hydrolyzes phosphatidylinositol 4,5-biphosphate (PIP2) to diacylglycerol (DAG) and inositol triphosphate (IP3). Diacylglycerol acts as a second messenger and activates the Protein Kinase C (PKC). IP3 binds to its receptors on the endoplasmic reticulum causing the increase of intracellular [Ca^{2+}] levels that triggers currently unknown signaling pathways, which could cause cell chemotaxis [53].

The Gα_q class

There are five families of Gα_q proteins and all of them activate the Phospholipase C. The signaling of GPCRs that couple to Gα_q results in the increase of intracellular [Ca^{2+}] that has an effect on DAG-PKC interaction, which is crucial for activating downstream effectors [54].

G$\alpha_{12,13}$ class

The G$\alpha_{12,13}$ class proteins activate the GTPases of the Rho family. They are related to cytoskeleton functions, smooth muscle contractions and neuronal morphogenesis [55]. The activation of Rho-GEF requires not only G$\alpha_{12,13}$ but also PKC-mediated phosphorylation of Rho-GEF [56].

1.3.1.2. The G$\beta\gamma$ dimer

Five different genes encode the Gβ subunits, whereas Gγ subunits are encoded by 11 different genes [57]. Due to alternative splicing there are 6 Gβ members, while Gγ type has 12 members. Their molecular mass range from 35 to 37 kDa for Gβ, and 6 to 8 kDa for Gγ. The Gβ and Gγ subunits form a functional heterodimer, which is a stable structural unit. Most of the Gβ subunits can interact with different Gγ subunits, though not all of the possible dimer combinations occur. The existing G$\beta\gamma$ dimer combinations are specific for the tissue or cell type.

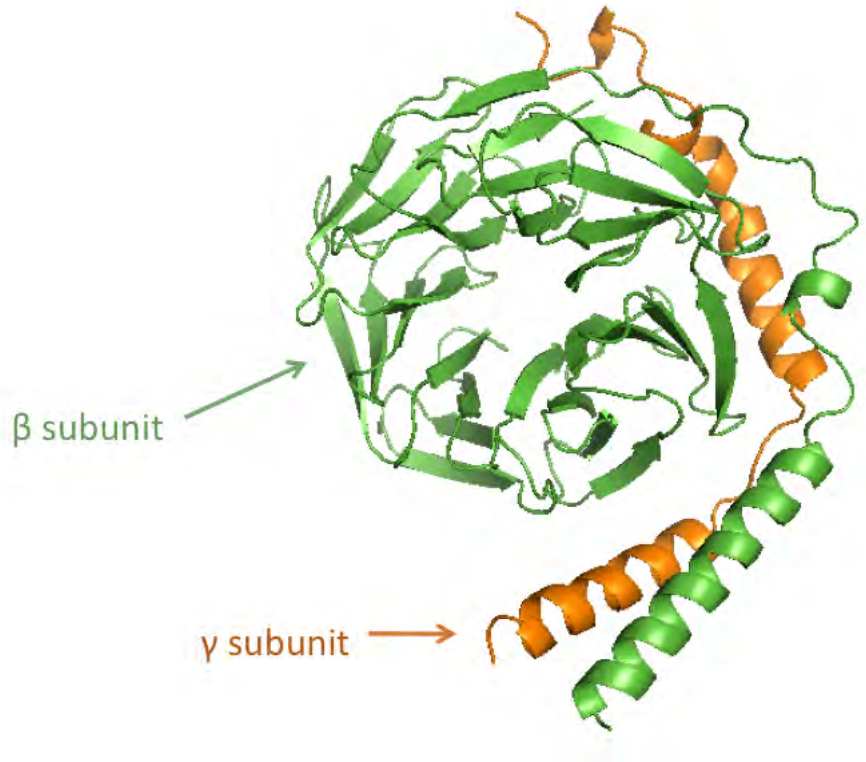

Figure 1.14.: Structure of *Bos taurus* Gβγ dimer.
PBD code: 1GOT [42].

All Gβ subunits contain seven WD-40 repeats, a Tryptophan-Aspartic acid (WD) sequence that repeats about every 40 amino acids and forms small antiparallel β strands that mediates protein-protein interaction (Figure 1.14) [47]. Crystal structures of the Gβγ dimer and Gαβγ trimer demonstrated that these seven WD-40 repeats of the Gβ subunit folds into a seven-bladed β-propeller structure. The N-terminal part of the Gβ subunit forms an α-helix structure [58].

The Gγ subunit folds into two α-helices; the N-terminal helix forms a coiled-coil with the N-terminal α-helix of Gβ subunit, while the C-terminal helix makes extensive contacts with the base of the Gβ subunit seven-bladed β-propeller structure.

Several posttranslational modifications of Gβ have been characterized. The N-terminus of Gβ subunit undergoes the removal of the methionine at position 1, followed by N-acetylation of serine at position 2 [59]. Phosphorylation of $G\beta_1$ histidine 266 by nucleoside diphosphate kinase (NDPK) was predicted as a mechanism of G protein activation [60].

G protein localization at the cytoplasmic face of the plasma membrane of the cells is critical for the signaling [61]. This sub-cellular localization is facilitated due to Gγ subunit lipidation [62, 63]. The Gγ subunit post-translational modifications at the N- and C-terminus, such as C-terminal processing, the absence of prenylation, the N-terminal processing and phosphorylation, are critical for the G protein function[64]. All these post-translational modifications bring more diversity into the G protein heterotrimers and specificity for the signal transduction.

Unlike the conformationally flexible Gα subunit, the Gβγ heterodimer does not undergo conformational change when it dissociates from the G-protein heterotrimer. The Gβγ heterodimer is able to interact with many effectors and also contribute to signal transduction. However, Gβγ association with Gα prevents Gβγ from activating its effectors. Table 1.2 identifies the main effectors of these proteins.

Class	**Family**	**Effector**
Gβ	β1 to β6	Phospholipase C and A2 (+)
Gγ	γ1 to γ12	Adenylyl cyclase I (-), II and IV (+), GIRK (+), Ca^{2+} channels (-), MAPK (+), Na^{+} channels (+), c-Jun NH(2)-terminal kinase (+), PI3 kinase (+), PKC and PKD (+)

Table 1.2.: Gβγ subunit classes and their effectors.
(+) Activation, (-) Inhibition.

Activated Gα and Gβγ proteins bind to various effectors that transmit the signal to different second messengers. Many effectors are regulated by both Gα and Gβγ subunits. Initially the Gβγ complex was considered as a passive partner of the Gα subunit. However, now it is clear that Gβγ subunit can regulate various effectors. The Gβγ complex mediated signaling includes regulation of ion channels such as G protein regulated inward rectifier potassium channel (GIRK) and Voltage-Dependent Ca^{2+} Channels (VDCC).

In addition to the ion channels, the Gβγ complex was shown to be a positive regulator of a large number of effectors including Adenylyl Cyclase, phospholipase C-β (PLC-β), phospholipase A (PLA), phosphoinositide-3-kinase (PI3K), Protein Kinase C (PKC), Protein Kinase D (PKD) and β-Adrenergic Receptor kinase [38].

1.3.2. G protein independent signaling

For many years it was considered that G protein activation is a necessary step in all signal transduction pathways induced by GPCRs. Growing number of receptor binding protein discoveries suggested that there are alternative signaling mechanisms (Figure 1.15). Some of these GPCR binding proteins have properties of signaling molecules with enzymatic activity; others appear to act as adaptor proteins that can promote kinase binding to the receptor. Such mechanisms allow direct cross-talk with other transduction pathways without GPCR interaction with G proteins.

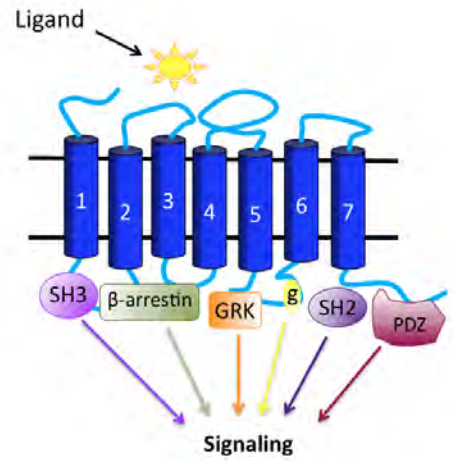

Figure 1.15.: G protein independent signaling.
Following agonist binding, GPCRs can associate with members of diverse families of intracellular proteins, including polyproline-binding proteins such as those containing SH3 domains (SH3), β-arrestins, G Protein–coupled Receptor Kinases (GRK), small GTP-binding proteins (g), SH2 domain–containing proteins (SH2) and PDZ domain–containing proteins (PDZ). All these interactions allow GPCRs to initiate multiple intracellular signaling pathways.

GRKs and Arrestins

Ligand activated GPCR, in addition to heterotrimeric G protein activation, is phosphorylated by a family of specific G protein coupled receptor kinases (GRKs) (Figure 1.16) [65]. This phosphorylation allows the cytosolic proteins known as β-arrestin to interact with the GPCR. Usually arrestins bind to the third intracellular loop and the C-terminal part of the GPCRs, the same region as G proteins. The association of arrestins with GPCRs does not simply uncouple receptors from G protein pathways (signaling to effector proteins), but rather induces a switch in receptor signaling from classical G protein mediated pathways to a process termed desensitization described thereafter.

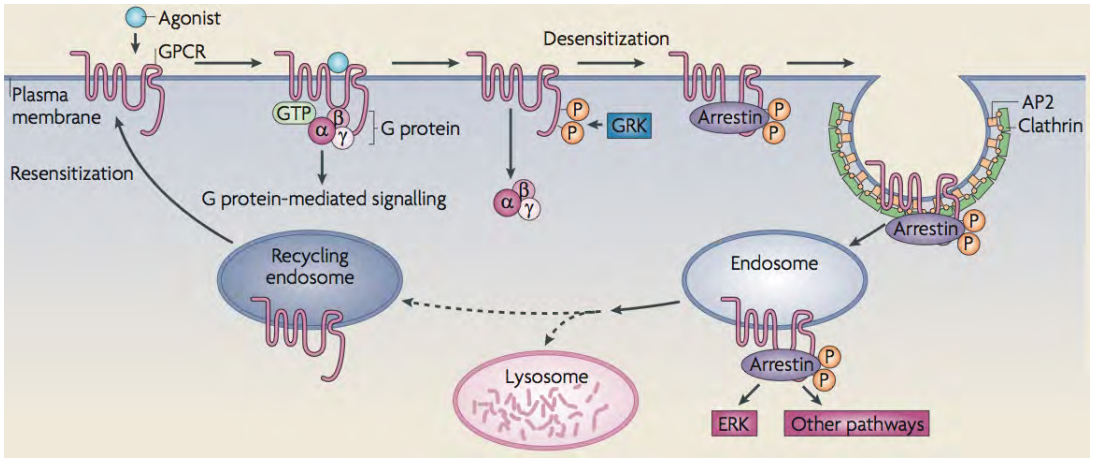

Figure 1.16.: The signaling mediated by GRKs and Arrestins.
Adapted from[66].

GRK and β-arrestins play additional roles in GPCR regulation and signaling. The agonist-induced interaction of β-arrestin with the phosphorylated GPCR allows the β-arrestin mediated recruitment of clatrin, thus triggering receptor internalization, dephosphorylation and recycling (Figure 1.16) [67]. In addition β-arrestin can interact with the cytosolic tyrosine kinase c-Src and promote its recruitment to the receptor signaling complex, suggesting a key role for GRK and β-arrestin function in modulation of mitogen-activated protein kinase (MAPK) cascades by GPCRs.

The β-arrestin activates the GPCR-stimulated Mitogen-Activated Protein (MAP) kinase. This pathway was analyzed in a study of the β2AR [68].

SH2 domain-containing signaling proteins

GPCRs and SH2 domain based signaling complexes act similarly as receptor tyrosin kinases and GRKs [69]. Following stimulation with Angiotensin II the heptahelical Angiotensin AT1 receptor activates JAK2 tyrosine kinase. This mechanism involves Src mediated tyrosine phosphorylation of the AT1 receptor[70].

Small GTP binding proteins

GPCR mediates regulation of small GTP binding proteins such as Ras, Rab, Rho and ARF, which can activate the phospholipase D. It was demonstrated that GPCR activated phospholipase D is not blocked by the inhibitors of the heterotrimeric G protein pathways, which confirms that this activation is independent of G proteins [71].

PDZ domain containing proteins

GPCRs can also interact with the PDZ domain containing proteins. These PDZ domains generally bind to the C-terminal motif (S/T-x-L) of target proteins [72, 73].

Polyproline binding proteins

Some GPCRs exhibit polyproline regions on their third intracellular loop or C-terminal tails. These polyproline regions are known to mediate binding of conserved protein domains such as SH3 domains, WW domains (two highly conserved tryptophans) and EVH (Enabled/VASP homology) domains [74, 75, 76, 77].

1.3.3. Desensitization

Desensitization reduces receptor activity and plays a role in signal duration, intensity and quality. Desensitization is initiated by phosphorylation of Serine and/or Threonine residues in the third intracellular loop and C-terminus of the receptor. Two types of desensitization are known: heterologous and homologous [78]. Both types are the result of receptor phosphorylation.

1.3.3.1. Homologous desensitization

Homologous desensitization is specific for agonist-occupied GPCR. The conformational change in GPCR caused by the agonist binding further allows GRK to interact with the receptor. Serine and Threonine in the intracellular loop and the C-terminal part of the GPCR are phosphorylated by GRK. This mechanism was demonstrated for the Rhodopsin and β2AR [79, 80]. Agonist activated and GRK phosphorylated GPCR binds to β-arrestin, which serves to inhibit G protein coupling. This way the active state of GPCR is terminated, and may also direct the receptor to clathrin-coated pits for internalization.

1.3.3.2. Heterologous desensitization

Heterologous desensitization is much less selective than the homologous desensitization. This mechanism uses kinases (PKA, PKC) that are activated by second messengers that phosphorylate all receptors present in the membrane without discriminating the active and inactive states. Consequently, a receptor can be activated by its ligand and cause a desensitization of another GPCR present in the same cell [81].

Just as GRK, the PKA and the PKC catalyse the phosphorylation of Ser/Thr residues that are located at the intracellular loops and the C-terminus of GPCR. The following process is similar to

that of GRK: the presence of phosphate groups recruits β-arrestin that prevents communication between GPCR and heterotrimeric G proteins.

1.3.4. Internalization

Receptor desensitization, initiated by phosphorylation of the receptor by PKA, PKC or GRKs, can be subsequently followed by receptor internalization.

Upon internalization, receptors can be dephosphorylated and returned to the plasma membrane, fuzed with larger endosomes and slowly recycled, or degraded in lysosomes. Internalization may regulate receptor desensitization and contribute to a positive regulation of receptor signaling [82, 83, 84].

1.4. Dimerization of GPCRs

Even though classical models predict that GPCRs function as monomers, several recent studies suggest that GPCRs exist as dimers or even oligomers. Homodimers or heterodimers can be formed between members of the GPCR family [85].

GPCR dimerization has functional consequences on each step of the life cycle of the receptor including ligand binding, signal transduction and internalization.

There are two GPCR dimerization processes that occur either in the endoplasmic reticulum or at the cell surface. In the endoplasmic reticulum the receptors are gathered together as dimers or multimers and then transported to the cell surface. Otherwise, receptors are synthesized as momomers and then transported to the cell surface where they assemble into dimers/oligomers [23].

Dimeric receptors possess several properties that monomers do not have [86, 87, 88].

Targeting membrane expression and internalization

Heteromerization is involved in receptor maturation, folding and expression at the cell surface by modulating its targeting from the endoplasmic reticulum or internalization.

In some cases dimerization has a role in receptor maturation and allows the correct transport of GPCRs from endoplasmic reticulum (ER) to the cell surface. Oligomer formation at the ER masks specific retention signals or hydrophobic patches of the momomers. For the metabotropic γ-aminobutyric acid b (GABAb) receptor dimerization is essential for its function [23, 89, 90].

This receptor consists of an obligate heterodimer of the GABAbR1 and GABAbR2 subunits. Each of the subunits belongs to the Glutamate family. When expressed alone the GABAbR1 is retained in the ER whereas GABAbR2 subunit is expressed at the cell surface and couples to the G proteins but does not bind agonist [91]. When both subunits are co-expressed, the heterodimer is formed allowing proper targeting of a functional GABA heterodimer to the plasma membrane [92, 93, 94].

In other cases early heterodimerization between wild type and mutant receptors leads to their retention in ER. In case of naturally occurring mutations this could have pathophysiological consequences. GPCR dimerization in an early secretory pathway was shown for CCR5 chemokine receptor. CCR5Δ32 is a natural genetic mutation where there is an internal 32-nucleotide deletion within the CCR5 open reading frame [95]. When expressed alone the CCR5Δ32 is retained in the ER while CCR5 reaches the cell surface. When CCR5 and CCR5Δ32 were co-expressed in the same cell a significant reduced cell surface expression of wild type CCR5 was observed, suggesting that in the case of dimerization, CCR5Δ32 act as a dominant negative inhibitor of CCR5 expression. CCR5/CCR5Δ32 heterodimerization contributes to the delayed onset of AIDS in HIV-infected patients with a CCR5/CCR5Δ32 genotype [95].

Ligand binding

Ligand binding to an allosteric site is able to induce receptor conformational change. It can promote or inhibit the dimerization. In case of heterodimerization, one monomer can induce changes in the active conformation of another monomer, leading to novel pharmacological properties of the receptors.

In some cases heterodimerization could lead to the creation of new binding sites. Two functional opioid receptors κ and δ form a heterodimer κ-δ, which results in the generation of a novel ligand binding site and functional properties [96]. This also occurs with μ- and δ-opioid receptors [97]. This phenomenon has a pharmacological importance: it provides new opportunities for the development of more selective compounds that would target specific heterodimers without affecting the individual monomers [10].

In some cases ligand binding regulates dimerization at the plasma membrane. Ligand binding to the chemokine receptors CCR2b, CCR5 and CXCR4 promotes receptors homodimer formation [98, 99, 100].

Signal transduction

G protein coupling could be promoted or attenuated by receptor heterodimerization (Figure 1.17) [101].

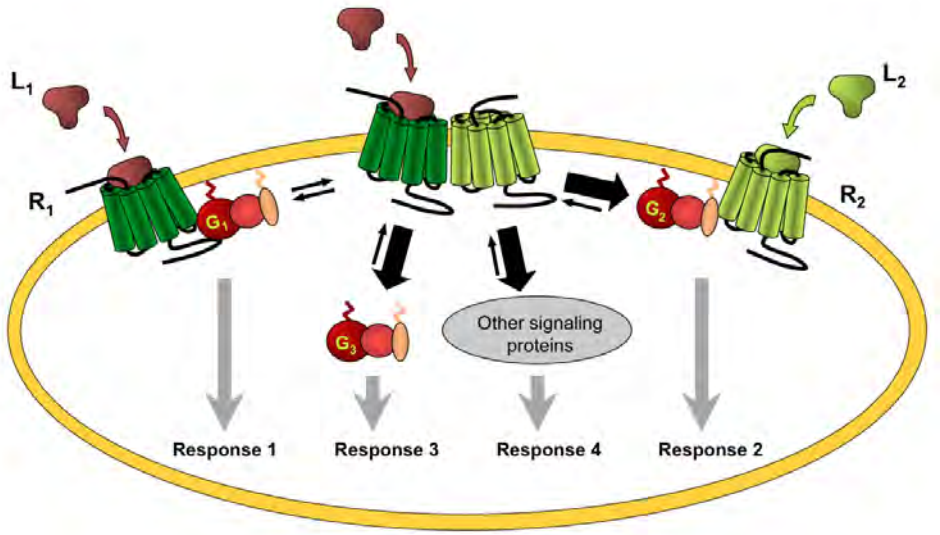

Figure 1.17.: GPCR heteromerization role signaling.
R1: receptor 1, R2: receptor 2, L1: ligand 1, L2: ligand 2, G1: G protein 1, G2: G protein 2, G3: G protein 3.

In some cases, this regulation by receptor heterodimerization can open new signaling pathways to a new G protein coupling or a switch to the recruitment of other signaling protein such as β-arrestin.

Heterodimerization has also been proposed to promote changes in the selectivity of some GPCRs towards the different G-protein subfamilies. In cells that co-express CCR5 and CCR2 chemokine receptors, heterodimers are formed, which activates different signaling pathways such as $G\alpha_{q/11}$ association and delayed activation of phosphatidyl inositol 3-kinase (PI3K), while monomeric receptors couple to $G\alpha_i$ [102].

Recently, it was shown that serotonin type 4 receptor (5-HT4R) homodimer activates G protein twice as much comparing to receptor monomer activation [103]. In case of leukotriene B4 receptor (BLT2), it was shown that dimer formation reduced the signaling ability [104].

1.5. GPCRs as pharmaceutical targets

GPCRs remain the target of many drug design programs due to their central role in most of physiological systems. Approximately 30% of all approved drugs target GPCRs, highlighting the clinical importance of this protein family (Figure 1.18).

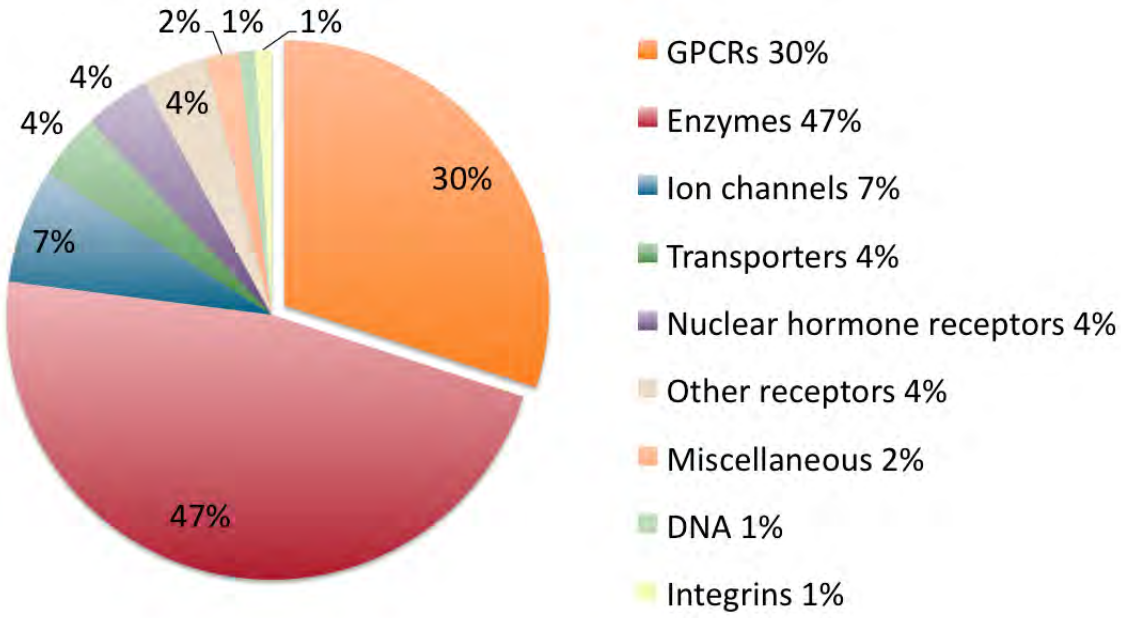

Figure 1.18.: Schematic representation of actual drug targets in the pharmaceutical market. Adapted from [105].

Mutations in GPCRs can have dramatic impacts on cell signaling and it might cause various diseases. Perturbation of their activity can result in a multitude of diseases, including obesity, diabetes, congestive heart failure, hormone-dependent cancers, infertility, etc. Table 1.3 lists human diseases, for which the responsible GPCR has been determined and drugs created.

Disease	**GPCR**
Cardiovascular	βAR, αAR
Obesity	MC4, $5HT_6$, CB1
Diabetes	CB1, AT1
Cancer	CCR5, CXCR4
Asthma	βAR, Adenosine A_{2A}
Schizophrenia	$5HT_{2A}$, Dopamine D_2
Parkinson's	Dopamine D_2, Adenosine A_{2A}
HIV	CCR5, CXCR4

Table 1.3.: Disease associated GPCRs.

Among the top 10 best selling drugs (2008 and 2009 ratings) there are four that target GPCRs, i.e. Plavix (Atherosclerosis), Advair (Asthma), Diovan (Hypertension) and Abilify (Schizophrenia) (Table 1.4).

Nr	Name	Company	Indications	2008 US $bln	2009 US $bln
1	Lipitor	Pfizer, Astellas	High cholesterol	13.35	12.5
2	**Plavix**	BMS & Sanofi-Aventis	Atherosclerosis	9.4	9.39
3	Enbrel	Amgen, Pfizer, Takeda	Arthritis, Psorias	7.7	8.0
4	**Advair**	GSK	Asthma	7.65	7.76
5	Remicade	J & J, Merck	Arthritis	6.2	6.9
6	**Diovan**	Novatis	Hypertension	5.7	6.0
7	Avastin	Roche	Cancer	4.8	5.9
8	Rituxan	Roche	Arthritis	5.4	5.8
9	**Abilify**	Otsuka, BMS	Schizophrenia	4.8	5.6
10	Humira	Abbott	Arthritis	4.5	5.5

Table 1.4.: The list of top 10 blockbuster drugs.
Plavix works by irreversibly inhibiting a receptor called P2Y12, an adenosine diphosphate (ADP) chemoreceptor on platelet cell membranes. **Advair** - is a Beta2-adrenergic agonist which also acts on cholinergic M2 receptors and alpha-1 adrenoreceptors. **Diovan** is a specific and selective type-1 angiotensin II receptor (AT1) antagonist which blocks the blood pressure increasing effects of angiotensin II via the renin-angiotensin-aldosterone system (RAAS). **Abilify** possesses affinity for and acts on the following receptors: Dopamine receptor D2, 5-HT7 receptor and histamine receptor.

In the past years, traditional GPCR drug design was focused on targeting the orthosteric-binding site of the receptor. This approach addressed a classical orthosteric ligand development that directly activated or blocked the targeted receptor. However, the disadvantages of this approach were soon faced, mostly because of the high homology between receptor subtypes, the selective targeting of orthosteric sites were hindered [106]. New approaches emerged based on small molecules that target topographically distinct allosteric sites on GPCRs [107, 108, 109]. The binding events evoke conformational changes in the receptors while still allowing the simultaneous binding of orthosteric ligands. Allosteric drugs present better selectivity of action. However, the most challenging steps of the new GCPR targeting drug candidate development and validation remain for the future [110].

Heteromeric GPCR complexes having unique biochemical and functional properties provide important new targets for drug discovery [10, 111, 112, 113].

1.6. Solved GPCR structures

One of the first bottlenecks for structural studies of GPCRs is to obtain sufficient amounts of proteins. The natural low abundance of GPCRs limits their purification in biochemically relevant amounts. To overcome this problem, various heterologous expression systems were developed. Eukaryotic expression systems present the advantage of direct folding of the GPCRs in the

cell membranes. Yeast [114, 115, 116, 117], insect [118, 119] and mammalian [120, 117] cell expression systems were developed. Proteins produced in eukaryotic expression systems undergo post-translational modifications. Nevertheless, expressed proteins not always were stable and needed engineering to improve stability and crystallizability [121, 122, 123].

Bovine rhodopsine was the first GPCR whose X-ray structure was solved in 2000 [15], which was crystallized in mixed micelles. This was the only GPCR structure with no sequence modifications, as the receptor was obtained from a natural source.

Another seven years of extensive research and technology developments were needed to obtain the high-resolution structure of the human β2AR [124, 123]. Several problems that prevented β2AR structure solving were indicated. First of all, the large and flexible ICL3 and C-terminus caused problems for crystallization. T4-lysozyme (T4L), a well structured protein, replaced the third intracellular loop to stabilize helices V and VI and to increase the polar surface to facilitate crystallization process (Figure 1.19) [123]. The engineered protein was crystallized in two lipidic environments: bicelles and lipidic cubic phase. Only the crystals grown in lipidic cubic phase led to a diffraction data set, from which the structure was solved by molecular replacement using T4 lysozyme as a model.

However ICL3 is functionally important for G protein activation, therefore the β2AR-T4L protein did not couple to $G\alpha_S$ [123].

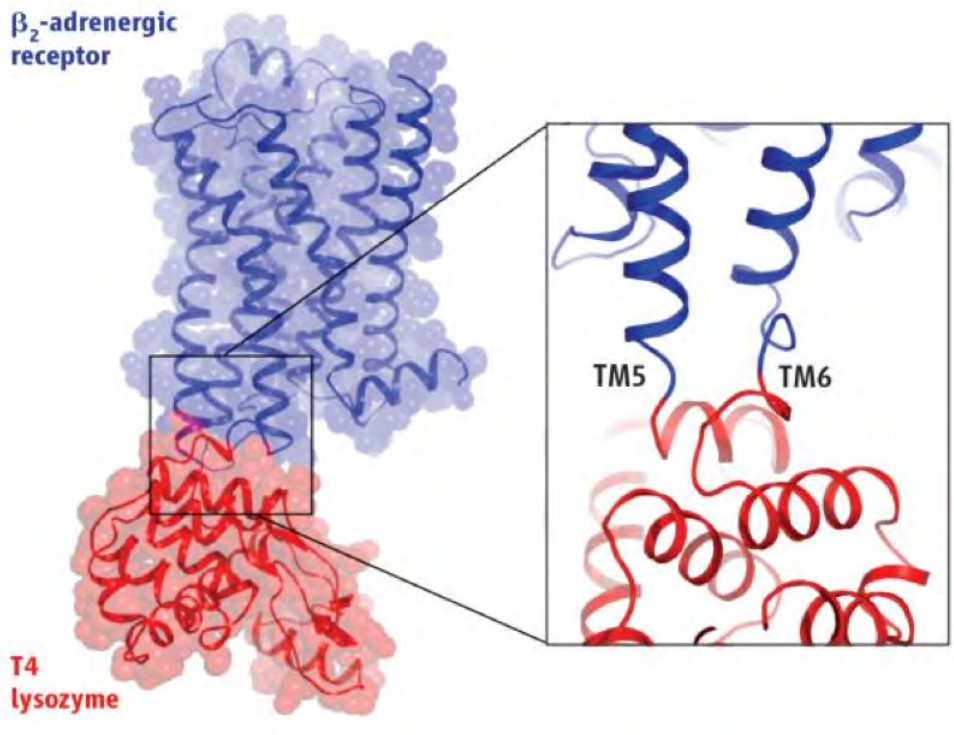

Figure 1.19.: Structure of human β2AR.
The large flexible third intracellular loop between TM5 and TM6 was replaced by lysozyme to constrain helices V and VI [123].

Until the end of 2011, several GPCR of the Rhodopsin-like class were crystallized using a similar approach (in lipidic cubic phase environments) and structures were solved for the following (Table 1.5): β1AR [125], A_{2A} Adenosine Receptor ($A_{2A}AR$) [126], chemokine CXCR4 [127], Dopamine D3 receptor (D3R) [128], and Histamine H1 Receptor (H1R) [129].

Nr.	GPCR	T4L	Mutations	Ligands	Additives	Expression
1	**Rhodopsin** human	-	Thermo stabilized mutant Fully deglycozylated	Inverse agonist Agonist		Natural source Mammalian cells
2	**β1 Adrenergic Rec** turkey	Yes/-	Thermo stabilized Partial IL3 deletion	Antagonist Agonist Partial agonist Inverse agonist		Insect cells (Sf9)
3	**β2 Adrenergic Rec** human	Yes	Stabilising mutations	Antagonist Agonist Partial agonist Inverse agonist Nanobody **(Activated form)**	Cholesterol, Lipid DMPC, Detergent CHAPSO, Dodecylmalthoside, High density lipoprotein (HDL)	Insect cells (Sf9)
		No	N-term fusion	Agonist G protein **(Activated form)**		
4	**A_{2A} adenosine Rec** human	Yes	+/- Stabilising mutations	Antagonist Agonist **(Activated form)**	Lipids, Co-factors (SO_4)	Insect cells (Sf9)
5	**CXCR4 Chemokine Rec** human	Yes	Stabilizing mutations	Antagonist	Cholesterol	Insect cells (Sf9)
6	**Dopamine D3 Rec** human	Yes	Thermo stabilizing mutation	Antagonist	Cholesterol (LCP)	Insect cells (Sf9)
7	**Histamine R1 Rec** human	Yes		Inverse agoniste	Cholesterol (LCP)	*Pichia pastoris*

Table 1.5.: Solved GPCRs structures by the end of 2011.

Apart from the structure of the Rhodopsin, all other GPCR structures have truncated/modified N- or C- termini. The sequences were further engineered to thermostabilize the proteins.

A large diversity in the ligand-binding pockets was observed when comparing the different GPCR structures: they greatly vary in shape, size and electrostatic properties. GPCR subtypes that bind to the same endogenous ligand have a greater degree of binding pocket conservation. The β1AR and the β2AR crystal structures represent 100% conserved contact residues for different antagonists [130].

In most crystal structures analyzed, the GPCR molecules pack in non-functional antiparallel orientations. Only CXCR4 crystals were packed in parallel arrangement [127]. All five different crystal-packing forms of CXCR4 complexes with peptide or small-molecule antagonist suggested that CXCR4 dimer is functionally relevant.

GPCRs agonist bound form corresponds to the active state but it spontaneously relaxes into an inactive form in the absence of stabilization via G protein binding. To diminish protein dynamics, GPCRs were therefore crystallized in inactive conformation, and finally bound to agonist, antagonist, or inverse agonist. So far, there are only three GPCR structures solved in an activated form [131, 132, 133].

Recently the crystal structure of the active ternary complex composed of agonist-occupied monomeric β2AR and nucleotide-free G protein heterotrimer was solved [132]. Although this construct contains sequence of the T4 lyzozyme between helices 5 and 6 it is still able to intercat with the $G\alpha_S$ protein. This provides the first high-resolution structural information for GPCR signaling across the membrane (Figure 1.20).

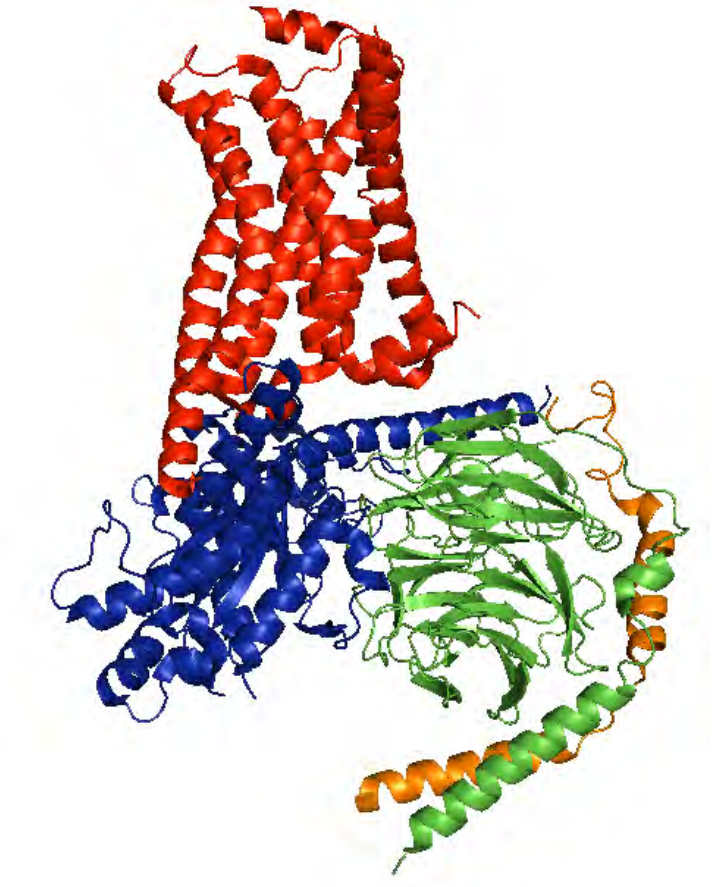

Figure 1.20.: Structure of GPCR in complex with G proteins.
The receptor is colored red, Gα blue, Gβ green and Gγ orange (PDB entry 3SN6).

Comparing the active and inactive β2AR structures, the differences found are in the TM5 and TM6, as in the inactive conformation structure the T4L was inserted between the cytoplasmic ends of TM5 and TM6. Another difference was observed in the second intracellular loop (IL2), which forms an α-helix in the β2AR-Gs complex.

Since crystallography can only provide one structure at a time, active or inactive conformation, the mechanism by which GPCRs transition between inactive and active states remains unclear. It was suggested that GPCRs could adopt multiple conformational states in response to the binding of different ligands. Using molecular dynamics (MD) simulations a detailed activation mechanism for β2AR was proposed and is presented in the Figure 1.21.

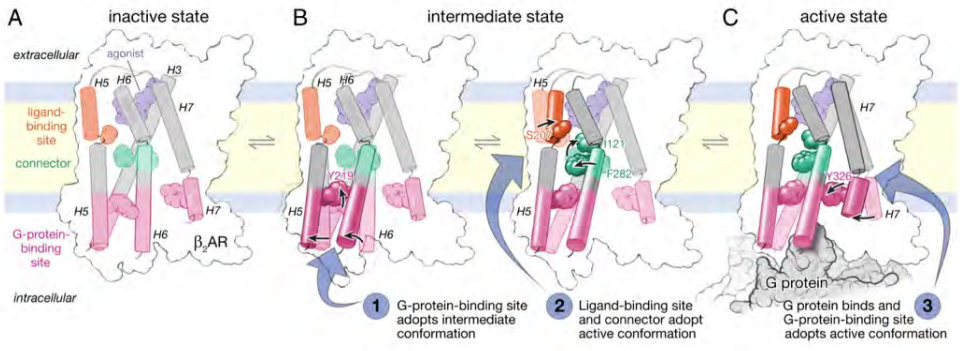

Figure 1.21.: The β2AR activation mechanism.
(A) An agonist bound to an inactive receptor. (B) The activation process begins on the receptor intracellular side with an outward motion of helix 6 bringing the receptor to an intermediate state. Here, the connector and the ligand-binding site are in equilibrium between inactive and active conformations; the bound agonist stabilizes the active conformation. (C) A G protein may bind to the intermediate state, favoring the final step on the activation pathway: conformational change in the NPxxY motif (helix 7) [134].

2. The model proteins

2.1. Chemokine receptors

There have been 23 chemokine receptors identified in humans. They form a structurally distinct subfamily among the class A GPCR and signal through coupling with G_i class of G proteins.

Their major shared biological function is leukocyte trafficking. After the interaction with specific chemokine ligands, chemokine receptors trigger an intracellular calcium ion flux. This causes directional cell migration called chemotaxis.

2.1.1. Chemotaxis

Chemotaxis is a directional movement of the cells in response to a chemokine gradient towards chemoattractant agents (Figure 2.1). Establishment of chemokine concentration gradients on endothelial layers and in the surrounding tissue provides directional cues to guide cell movement.

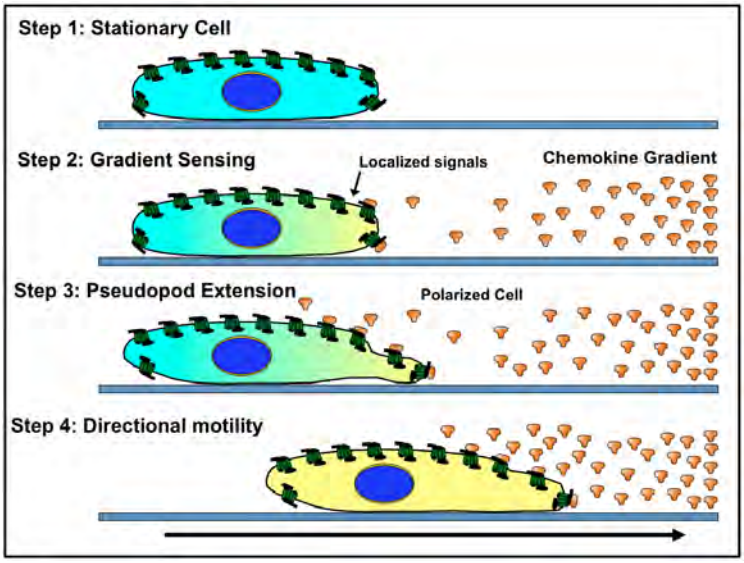

Figure 2.1.: Gradient sensing and chemotaxis.

Chemotaxis is the result of three separate steps: chemosensing, polarization and locomotion [135]. Depending on the cell type and the microenvironment, migration can involve single unattached

cells or multicellular groups [136]. Besides immune cells such as granulocyte, monocyte and lymphocyte there are other type of cells that are mobile such as fibroblasts and endothelial cells. Chemotaxis has a high significance in early embryogenesis, as it is involved in organogenesis. Under pathological conditions chemotaxis can cause tumor growth, cancer metastasis and inflammatory diseases, such as asthma, arthritis and atherosclerosis [137].

2.1.2. Leukocyte extravasation

Leukocyte extravasation from the blood into the tissues is a regulated multistep process involving series of coordinated interactions between leukocytes and endothelial cells. Several families of molecular regulators, such as selectins, integrins, and chemokines control different aspects of this process (Figure 2.2).

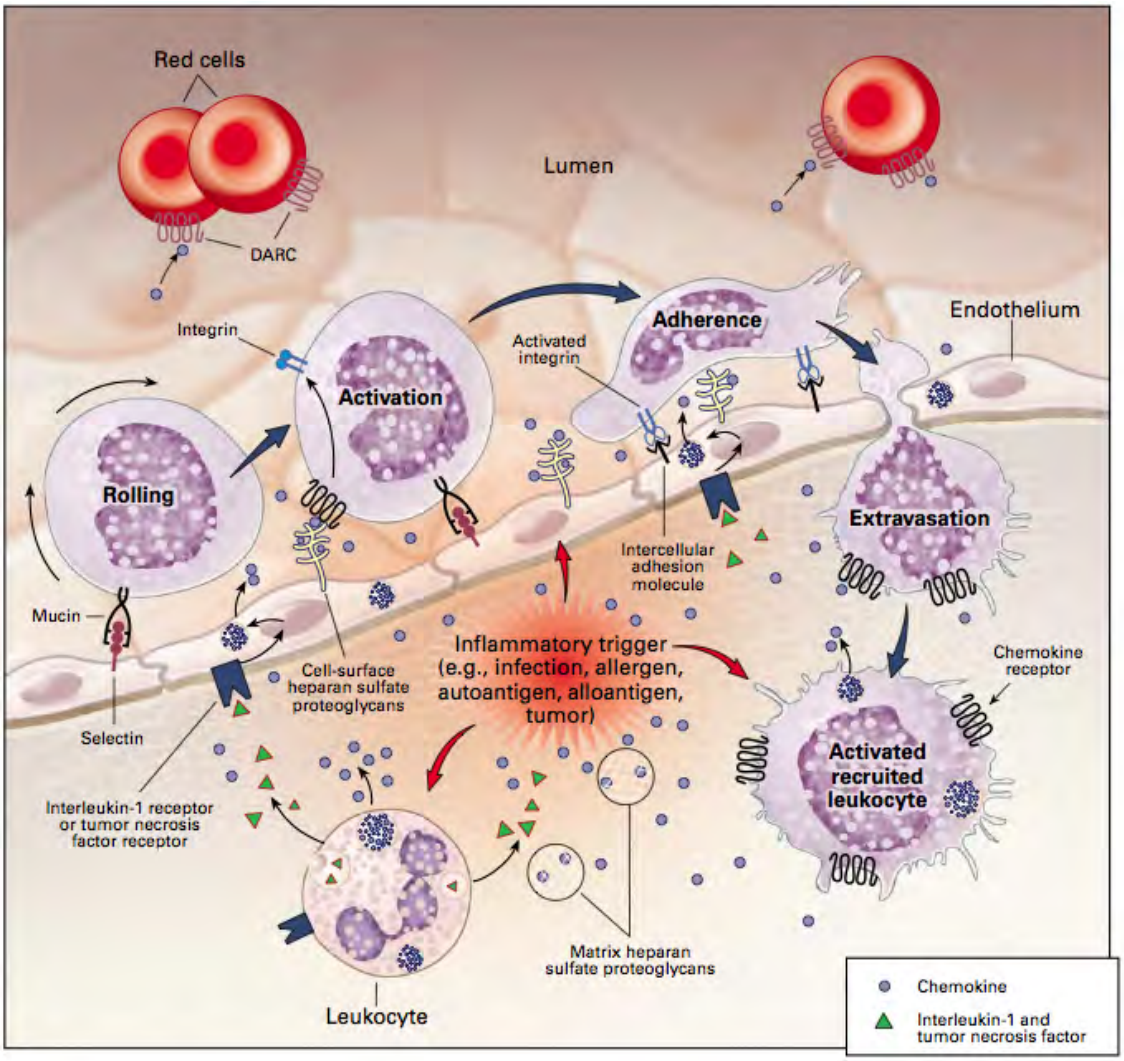

Figure 2.2.: Leukocyte entry into site of inflammation.
Adapted from [138].

At sites of inflammation and infection, leukocytes and cytokine-activated endothelial cells secrets the chemokines. Chemokines establish a local concentration gradient surrounding the inflammatory stimulus by being retained on cell-surface heparan sulfate proteoglycans. Selectins facilitate the movement of leukocytes, called rolling, along the surface of endothelial cells. In this manner the leukocyte surface GPCRs are brought into contact with chemokines retained on cell-surface heparan sulfate proteoglycans. Chemokine/GPCR interaction leads to subsequent clustering of integrins inside lipid rafts and leukocyte activation. Activated integrin interaction with intracellular adhesion molecules displayed at the surface of the endothelium cells forms strong interactions that immobilize the rolling leukocyte at the site of inflammation. Additional signaling events cause the reorganization of the cytoskeleton resulting in the spreading of one edge of the leukocyte. This edge inserts itself between endothelium cells and the leukocyte migrates through the blood vessel wall into the inflamed tissue. Rolling, activation, adhesion and transendothelium migration are the four steps of the process called leukocyte extravasation [138].

Because of high local chemokine concentration the recruited leukocytes activated by proinflammatory cytokines may become desensitized to further chemokine signaling. The Duffy Antigen Receptor for Chemokines (DARC), a non-signaling erythrocyte chemokine receptor, controls the inflammation process [139]. DARC functions as a sink, removing chemokines from the circulation and consequently helping to maintain a chemokine gradient.

Once leukocytes have entered the target tissue they can perform various immune activities, such as pathogen elimination and tissue repair [140]. Remarkably, this extravasation process occurs with little or no damage to the endothelium cells [141].

2.1.3. Classification of chemokine receptors

According to the chemokines they bind, chemokine receptors are classified into four groups: CCR, CXCR, CR and CX3R (Table 2.1) (Chapter 2.2.1). The family also includes several decoy receptors, the Duffy antigen receptor for chemokine (DARC), D6 and CCX-CKR, which are involved in chemokine clearance at inflammation sites.

Chemokine decoy receptors topology is identical to classical chemokine receptors. They are also called “silent” chemokine receptors. Chemokine decoy receptors are unable to couple to G proteins and therefore there is no ligand-induced signaling pathway through these receptors [142]. Chemokine decoy receptors are neither capable to mediate chemotaxis. Instead they efficiently internalize their cognate chemokine ligands. These receptors are involved in controlling the local levels of chemokines.

2.1.4. Characterization of chemokine receptors

Chemokine receptors share from 25 to 80% amino acid identity; their sequence length vary from 340 to 370 amino acids [143]. The short extracellular N-terminal domain is acidic and might

Receptor	Ligand (high affinity)
CCR1	MIP-1α, δ, RANTES, MCP-1, MCP-3, MPIF-1, HCC-1, 2, 4
CCR2	MCP-1, 3, 4, 5
CCR3	Eotaxin 1, 2, 3, MCP-2, 3, 4, RANTES, MIP-1δ
CCR4	MIP-1, RANTES, TARC, MDC
CCR5	MIP1α, MIP1β, RANTES
CCR6	MIP-3α
CCR7	MIP-3β, 6Ckine
CCR8	I-309, TARC, MIP1β
CCR9	MIP1α, MIP1β, MCP-1, 3, 5
CCR10	CTACK
CCR11	MCP-1-4, Eotaxin
CXCR1	IL8, GROα, β, χ, ENA-78, GCP-2
CXCR2	IL8, GROα, β, χ, NAP-2, ENA-78, GCP-2
CXCR3	IP-10, MIG, I-TAC
CXCR4	SDF1α, β
CXCR5	BCA-1
CXCR6	SR-PSOX
CXCR7	
CX3CR1	Fractalkine
XCR1	Lymphoatractin SCM-1β
DARC	IL-8, GRO-α, RANTES, MCP-1, MCP-3, MCP-4, Eotaxin
D6	
CCX-CKR	

Table 2.1.: Human chemokine receptors

be sulfated on tyrosine residues and contain N-linked glycosylation sites. The third intracellular loop is short and basic. The intracellular C-terminus contains serine and threonine residues that act as phosphorylation sites for receptor regulation. Extracellular loops 1 and 2 are linked by highly conserved disulphide bond. The second intracellular loop contains the conserved motif DRYLAIVHA or a variation of it.

2.1.5. Receptor dimerization

It is known that several chemokine receptors can homo- or heterodimerize: CCR2, CCR5, CXCR1, CXCR2, CXCR4 and Duffy antigen receptor for chemokine (DARC) [144]. Fluorescence Resonance Energy Transfer (FRET), Co-immunoprecipitation, and Bioluminescence Resonance Energy Transfer (BRET) techniques demonstrated that such multimers exist in cells naturally co-expressing these chemokine receptors.

It is hard to establish general rules for the chemokine receptor multimerization. However receptor

dimerization can be triggered by different events.

Ligand binding induced dimerization

In vivo studies showed that at lower chemokine concentration CCR2 and CCR5 undergo ligand-mediated heterodimerization that results in activation of different signaling pathways such as $G_{q/11}$ association, and delays activation of phosphatidyl inositol 3-kinase. The consequences of such change are a pertussis toxin resistant Ca^{2+} flux and triggering of cell adhesion rather than chemotaxis [102].

Dimerization upon co-expression

Dimers can be formed during biosynthesis prior to arriving at the cell surface as shown for CXCR1/CXCR2 heterodimers [145].

At physiological concentrations the CCR5 exist as constitutive oligomers that are formed early after biosynthesis, in the endoplasmic reticulum as described earlier in Chapter 1.4 [146, 95].

Signaling modulation upon dimerization

CXCR4 and the δ-opioid receptor (DOR) are both expressed on the surface of monocytes and other immune cells. In the presence of both receptors ligands they form heterodimers. The formation of the CXCR4/DOR heterodimer prevents each of them from signaling [147, 148].

Although the functional importance of dimerization remains incompletely characterized many experiments suggest that receptor dimerization has important *in vivo* pharmacological effects.

2.1.6. Chemokine receptors of interest

2.1.6.1. CCR5

CCR5 (CC chemokine receptor 5) is predominantly expressed on macrophages, dendritic cells, brain microglial cells and memory T-cells [149]. CCR5 plays a role in inflammatory responses to infection, though its exact role in normal immune function is unclear [150].

In 1996, several groups described a 32-base-pair deletion within the coding region of the CCR5, which results in a frame shift and generates a non-functional receptor [151, 152, 153]. It has been hypothesized that CCR5-Δ32 allele was favored by natural selection either during the bubonic

plague or smallpox in the Middle Ages [154] or, occurred even before, as the frequency of CCR5-Δ32 in the Bronze Age is similar to that seen today [155]. The CCR5-Δ32 mutation occurs at high frequency in European Caucasians but is rare among African, Native American, and East Asian populations [154].

The CCR5-Δ32 mutation prevents the entry of CCR5 tropic strain of Human Immunodeficiency virus (HIV). Two copies of this allele provide strong protection against HIV infection. Homozygous individuals have nearly complete resistance to HIV-1 infection despite repeated exposure [156, 157]. Individuals with the Δ32 allele of CCR5 are healthy, suggesting that CCR5 is largely dispensable. However, CCR5 plays a role in mediating resistance to West Nile virus infection in humans, as CCR5-Δ32 individuals are enriched in cohorts of West Nile virus symptomatic patients, indicating that all CCR5 functions may not be compensated by other receptors [158].

CCR5 consists of 352 amino acid residues. It has multiple natural chemokine ligands, including Macrophage Inflammatory Protein 1 α (MIP1α), MIP1β, RANTES and monocyte chemotactic protein 2 (MCP-2). Among these ligands, RANTES and MIP-1α can bind to other CC chemokine receptors, while MIP-1β is known to be specific to CCR5 [159].

Maraviroc (UK-427,857) was identified as a small-molecule ligand [160]. Maraviroc is a selective CCR5 antagonist with potent anti-HIV-1 activity; it is a HIV entry inhibitor. Maraviroc has been approved for the treatment of patients infected with only CCR5-tropic viruses [160, 161].

Combining site-directed mutagenesis and homology modeling using solved GPCR structures a CCR5 topology model (Figure 2.3) with ligand binding sites was proposed [162].

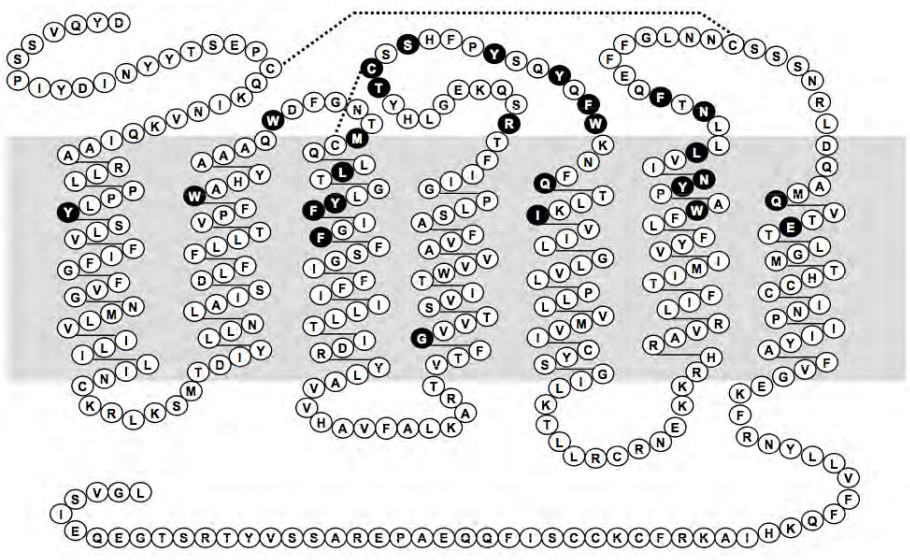

Figure 2.3.: Snake-like plot of human CCR5 sequence.
Residues surrounding the proposed hydrophobic binding pocket for small molecule CCR5 inhibitors are highlighted with a black circles [162].

Signal transduction through CCR5 is known to play important roles in both physiological and pathological processes, including inflammation and hematopoiesis [163].

2.1.6.2. CXCR4

CXCR4, a CXC chemokine receptor 4, is expressed on brain, lung, colon, heart, kidney, and liver cells [164]. CXCR4 is widely expressed on T-lymphocytes, B-lymphocytes, monocytes, macrophages, neutrophils, eosinophils [149, 164]. CXCR4 is also expressed on astrocytes, neuronal cells, and smooth muscle progenitors [164]. CXCR4 plays a significant role in development of metastatic diseases, particularly in directing tumor cells towards the specific sites of metastases [165, 164].

CXCR4 consists of 352 amino acid residues. Unlike the other chemokine receptors that have a number of distinct ligands, CXCR4 has only one endogenous natural ligand known as SDF1 [166]. However, CXCR4 can also be recognized by an antagonistic ligand, vMIP-II, encoded by the Kaposi's sarcoma-associated herpes virus [167].

CXCR4 or SDF1 gene knockout mice result in impaired hematopoiesis exhibited as a defect in either trafficking of hematopoietic stem cells (HSC) from the fetal liver to the embryonic bone marrow, or in heart and brain development, and vascularization. Thus, CXCR4 and SDF-1 knockouts are embryonic lethal [168, 169, 170, 171, 172].

CXCR4 structure

The three dimensional structure of the chemokine receptor CXCR4 recently has been solved [127]. The authors used approaches already used to solve other GPCR structures. The flexible C-terminal part was truncated from residue 320 or 326.

Previous studies performed on the β2-Adrenergic Receptor demonstrated that the removal of the poorly structured third intracellular loop (IL3) would favor crystallization [123]. This truncation would diminish the movement of the transmembrane helices but would also reduce the polar surface area important to form protein-protein contacts in the crystal. Therefore this loop was replaced by the well-structured T4 lysozyme (T4L) to increase the polar surface and to constrain the transmembrane helices.

Previous studies with β2-Adrenergic Receptor showed that engineering of the TM4-TM3-TM5 interface might provide a general strategy for the stabilization of other receptors [173]. Therefore, the thermostabilizing mutation L125W was introduced in CXCR4 to increase the yield of functionally folded receptor.

All these modifications resulted in several CXCR4 constructs with small variations. The prepared constructs differed in: the precise T4L junction; the position of the C-terminal truncation; additional T240P mutation (in one construct). Stabilized constructs were expressed in baculovirus-infected *Spodoptera frugiperda* (Sf9) insect cells and were selected for structural studies on the basis of thermal stability, monodispersity and lipid matrix diffusion.

Prepared constructs required further stabilization with ligands to facilitate crystallization in lipidic cubic phase. Five independent crystal structures of CXCR4 were solved in inactive antagonist small molecule IT1t and cyclic peptide CVX15 bound conformation [127].

Architecture of CXCR4

The solved structure includes 293 residues (27 to 319) of the 352 total residues of CXCR4 and residues 2 to 161 of T4L (Figure 2.4).

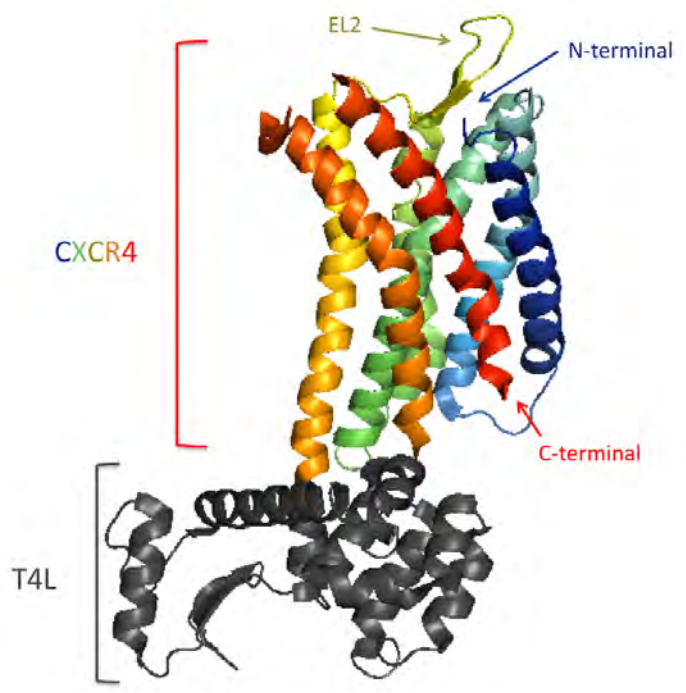

Figure 2.4.: Solved CXCR4 structure.
The CXCR4 helices are shown in colors where T4L appears in gray. PBD code: 3OE9 [127].

The overall fold of CXCR4 is similar to the other previously solved GPCR structures. The extracellular interface of CXCR4 consists in 34 N-terminal residues. The Extracellular loop 1 (EL1) is from residues 100 to 104 (4 residues in total) and links helices II and III. The EL2, the largest extracellular loop, contains 18 residues (from 174 to 192 residues) and links helices IV and V. The EL3 is 6 residues long (from 267 to 273 residues) and links helices VI and VII.

The structure shows that both conserved disulphide bonds at the extracellular side of CXCR4 constrain EL2 and the N-terminal segment and shape the entrance to the ligand-binding pocket.

The intracellular side of CXCR4 contains intracellular loop 1 (IL1) from residue 65 to 71, which links helices I and II. The IL2 contains four residues (140 to 144) linking helices III and IV. The IL3 contains five residues (225 to 230) and links helices V and VI.

Structural alignment of CXCR4 with other GPCR high-resolution structures indicates that the intracellular part of CXCR4 is more conserved than the extracellular part.

Comparison with other GPCR

Comparing the CXCR4 structure with other solved GPCR structures showed that the intracellular part of the CXCR4 helix VII is one turn shorter, ending just after the GPCR conserved NPxxY motif. All five CXCR4 solved structures lacked the short helix VIII that is considered as a regular structural element for all class A GPCRs (Figure 2.5).

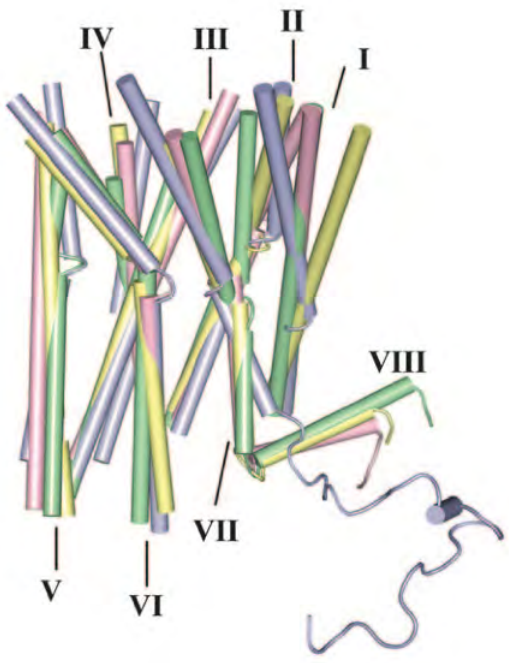

Figure 2.5.: CXCR4 transmembrane helices comparison with other GPCR structures. CXCR4 (blue); b2AR (PDB ID: 2RH1; yellow); A2AAR (PDB ID: 3EML; green); and rhodopsin (PDB ID: 1U19; pink) [127].

CXCR4 lacks a putative palmitoylation site at the end of helix VIII, which anchors the C-terminal part of many GPCRs to the lipid membrane [127].

Structures of CXCR4 bound to an antagonist small molecule IT1t and a cyclic peptide CVX15 ligand-binding sites considerably overlap. Comparing the ligand binding sites of CXCR4 to other GPCRs highlights the structural plasticity of GPCR binding sites [130].

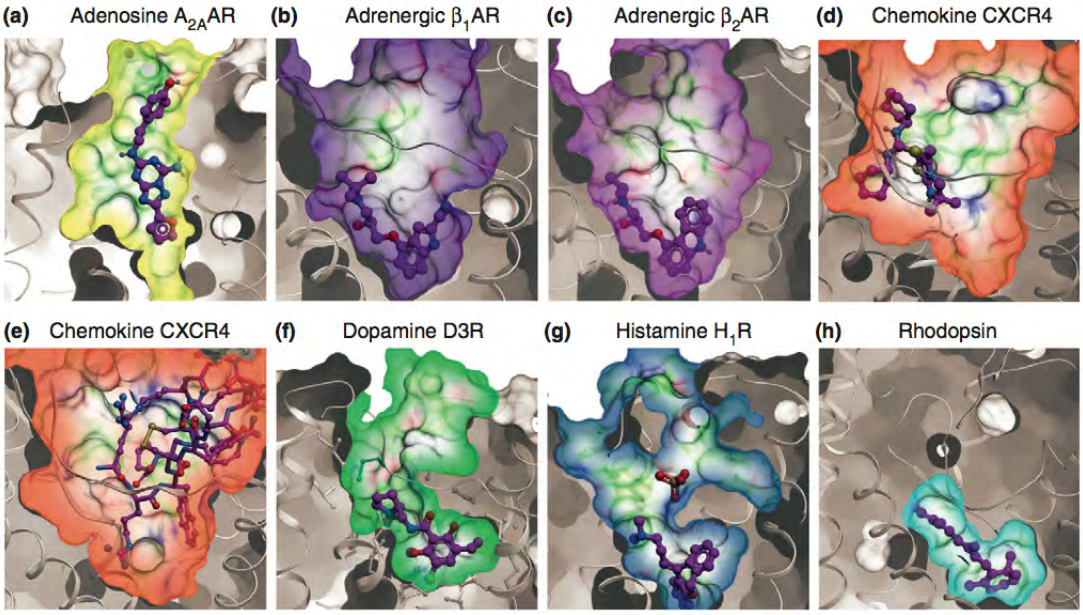

Figure 2.6.: Diversity of ligand binding pocket shapes in GPCR crystal structures. (a) The Adenosine A2AAR is bound to the antagonist ZM241385 (PDB ID 3EML). (b) The Adrenergic β1AR antagonists cyanopindolol (PDB ID 2VT4). (c) The Adrenergic β2AR is bound to an antagonists carazolol (PDB ID 2RH1). (d) The chemokine CXCR4 receptor is bound to a small molecule IT1t (PDB ID 3ODU). (e) The chemokine CXCR4 receptor is bound to a cyclic peptide CVX15 (PDB ID 3OE0). (f) The Dopamine D3R is bound to an antagonist eticlopride (PDB ID 3PBL). (g) The Histamine H1R is bound to the antagonist Doxepin where a PO43– ion modulates the ligand access to the pocket (PDB ID 3RZE). (h) The Rhodopsin is bound to its agonist retinal (PDB ID 1GZM). All pockets are shown in the same orientation. Adapted from [130].

Compared with previous GPCR structures the ligand-binding cavity of the CXCR4 is larger, more open and located closer to the extracellular surface (Figure 2.6) [130].

CXCR4/SDF-1α binding model

Chemokine activity is initiated by the agonist-chemokine binding to the GPCR. A two-step model has been suggested for the receptor activation. The first step corresponds to the chemokine specific recognition and its binding to the receptor. The first binding site is located in the exposed area of the loop between the second and third cysteine residues of the chemokine. This site considered as a low affinity region of interaction and binds to the extracellular N-terminus of the receptor. This is followed by chemokine conformational change due to the flexible N-terminus. The second binding site is the N-terminal part of the chemokine which specifically interacts with the receptor and that leads to receptor activation [174].

NMR studies provided structural evidence for the two-step CXCR4/SDF1α binding model (Figure 2.7) [175].

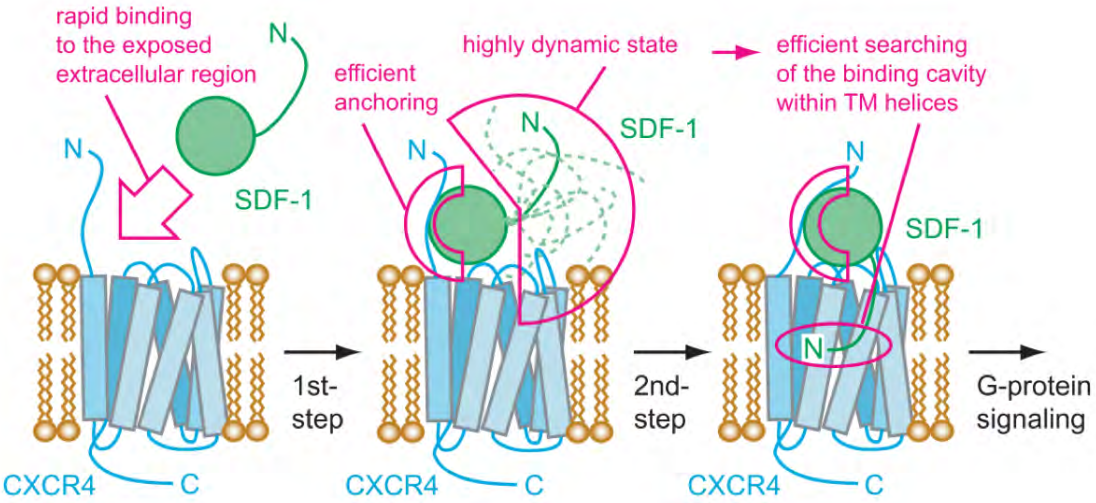

Figure 2.7.: Schematic diagram of the two-step mechanism for the CXCR4/SDF1α interaction. Adapted from [175].

The 1st step interaction occurs between the SDF1α N-loop, β-sheet and 50-s loop and the CXCR4 extracellular region. This interaction facilitates the rapid binding and efficient anchoring of SDF1α on the extracellular side of CXCR4. Consequently, the 2nd step interaction between the N- terminus of the SDF1α and the CXCR4 transmembrane region is formed. The SDF1α N-terminus triggers the conformational changes in the CXCR4 transmembrane region to induce G-protein signaling [175].

The solved structures of CXCR4 provide new clues about the interactions between CXCR4 and SDF1α. The crystal structures of CXCR4 suggest the possibility of a three-step interaction between CXCR4 and its ligand. The first step would be the electrostatic interaction of the body of the chemokine with the complementary surface of CXCR4. The second step would be the insertion of the N-terminal of chemokine into the cavity defined by the TM helices and some extracellular domains. The third step would be the folding of the N-terminus of CXCR4 across the top of the docked chemokine [163].

Although CXCR4 structure has been solved the CXCR4/SDF1α complex stoichiometry is still speculative. Due to the oligomeric nature of CXCR4 and the complementary electrostatic surfaces of the ligand and receptor, SDF1α could bind to the receptor as a 1:1, 1:2, or 2:2 (ligand:receptor) complex (Figure 2.8). No information on the orientation of SDF1α with respect to CXCR4 is implied from the models presented in the Figure 2.8.

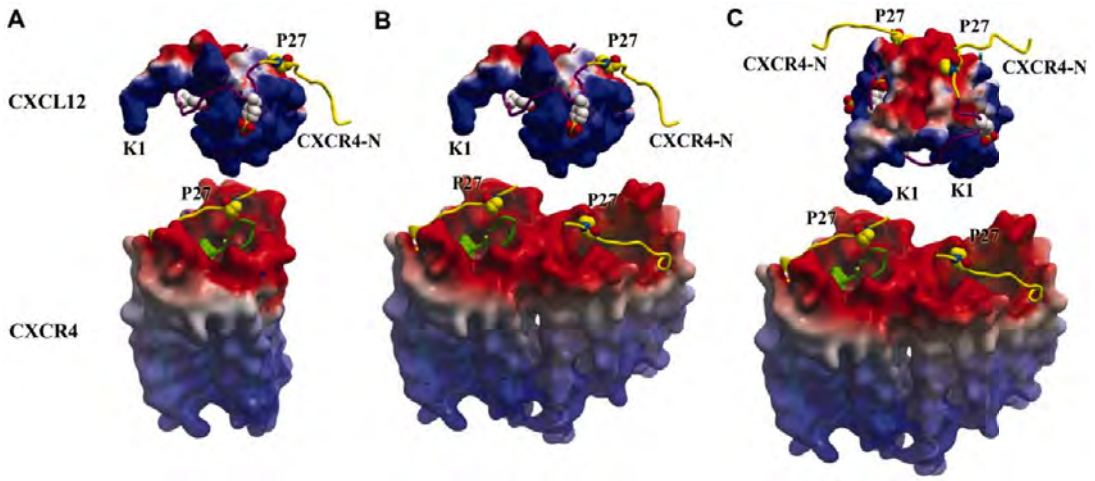

Figure 2.8.: Stoichiometry of possible CXCR4-SDF-1α complexes.
Adapted from [127].

Additional experiments will still be necessary to fully define the relevance and functional implications of different chemokine: receptor stoichiometries.

2.1.6.3. Chemokine receptors and human health

CCR5 and CXCR4 are specifically implicated in HIV-1 infection [176, 177, 178] and cancer metastasis [179, 180, 181, 182].

Human immunodeficiency virus

For some years it has been known that chemokines such as RANTES, MIP1α, MIP1β have the ability to block HIV replication in laboratory experiments. This is explained by the fact that chemokines compete with HIV to attach to chemokine receptors and also trigger receptor internalization and its clearance from the cell surface. Chemokine receptors represent thus an attractive therapeutic target to block HIV infection.

CXCR4 and CCR5 are the major HIV-1 co-receptors that mediate virus entry into CD4+ cells. There are two main HIV-1 strains: T-cell-tropic (X4) and macrophage M-tropic (R5) which uses CXCR4 and CCR5 as their co-receptors, respectively [183, 184, 185]. In the early HIV infection the CCR5 tropic strains represent the major virus phenotype [183, 186]. CCR5-using viruses (R5 viruses) are transmitted from person to person and are dominant in the early and chronic phases of HIV-1 infection [177]. The emergence of CXCR4 using viruses is correlated with a faster CD4+ T-lymphocyte depletion and rapid disease progression toward AIDS [187].

Therefore, HIV-1 tropism refers to the ability of the virus to establish infection in alternative CD4+ cell types, and is influenced by co-receptor usage. M-tropic viruses can infect primary

CD4+ T cells and macrophages and principally use CCR5; T-cell tropic viruses can infect CD4+ T cells and T-cell lines via CXCR4; and dual-tropic viruses can infect the three different cell types and can use CCR5 and/or CXCR4 [177, 188, 189].

Chemokine receptors constitute an important target for the development of anti-HIV therapies. This idea was strongly supported by the fact that Caucasian individuals with a homozygous 32 bp deletion in the CCR5 gene are relatively resistant against HIV-1 infection [153]. The SDF1α and RANTES cooperate to strongly (93%) inhibit the viral replication of the dual-tropic (R5/X4) HIV-1 strain [176]. The HIV co-receptor antagonists AMD3100 (CXCR4 antagonist) and maraviroc (CCR5 antagonist) showed antiviral efficacy against a wide variety of X4 and R5 strains, respectively [190, 160].

Figure 2.9 shows the chemokine receptors as co-receptors for HIV entry into cells and chemokine inhibition of HIV entry.

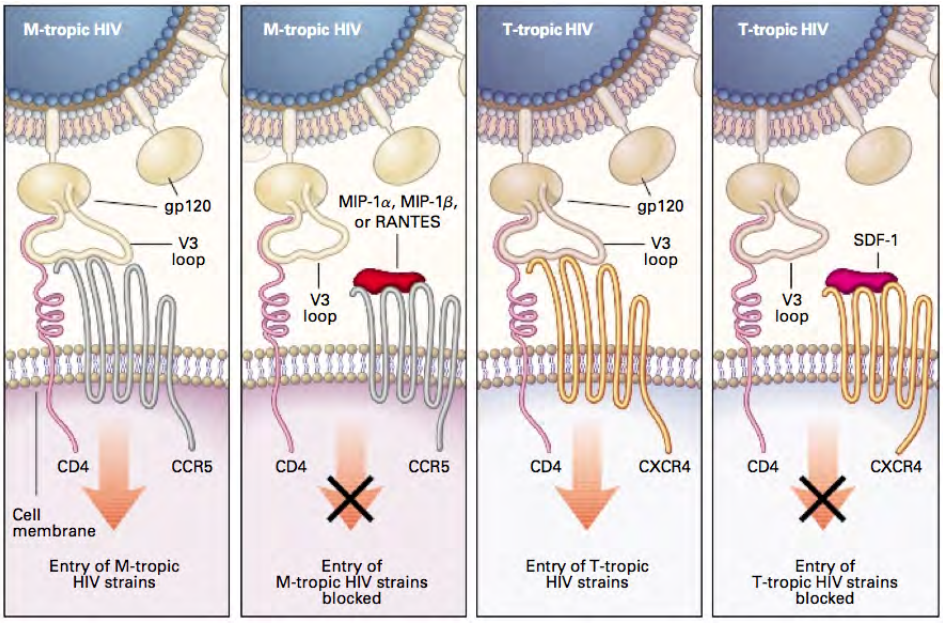

Figure 2.9.: Chemokine inhibition of HIV entry.
Adapted from [138].

The molecular interaction between HIV-1 glycoprotein 120 (gp120), in its trimeric conformation, and the CD4 (primary receptor) on the host cell surface represents the first step of the HIV infection cycle. Upon this interaction, the co-receptor-binding site on gp120 is exposed, enabling the binding to chemokine coreceptors expressed on the surface of CD4+ lymphocytes [191]. To gain entry into cells M-tropic HIV-1 uses principally CCR5 and T-tropic HIV-1 uses the CXCR4 for the most cases. Macrophage inflammatory proteins MIP1α, MIP1β and RANTES are the chemokine ligands for CCR5, which block M-tropic HIV-1 from entering target cells. SDF1α is a ligand for CXCR4 and blocks T-tropic HIV-1 from entering target cells.

The initial binding of HIV gp120 to CD4 triggers a conformational change in gp120 that exposes the V3 loop and permits subsequent interaction with the co-receptor (the chemokine receptor). The interaction of CD4-bound gp120 with co-receptor induces further conformational changes and exposes the N-terminus of the transmembrane glycoprotein gp41, which contains a fusion peptide that embeds into the host cell membrane. The HIV gp41 ectodomain forms an extended coiled coil conformation and a six-helix bundle structure, which promotes the juxtaposition of the viral and target cell membranes. This results in an energetically stable structure, facilitating fusion between the viral and cellular membranes and release of the viral core into the cell [192, 193].

The binding of the gp120-CD4 complex to chemokine coreceptors not only mediates HIV entry but also activates intracellular signaling cascades; mimicking chemokine signaling induced by binding to cognate receptors [194, 195].

The co-receptors post-translational modifications on N-terminal and EC loops may mediate the efficient binding to the HIV gp120. In general, extracellular domains may undergo N-linked or O-linked glycosylation and tyrosine sulfation, while modifications of intracellular loops include palmitoylation, phosphorylation, and ubiquitination [196, 197, 198, 199].

Cancer and metastases

Apart from their role in organogenesis and cell migration, chemokines and their receptors are involved in various pathological mechanisms, such as development of tumors and metastases [200]. Indeed, tumor cells usually modify the expression of their chemokine receptors. While some chemokine receptor expression is reduced or inhibited, others are over-expressed.

The migration of metastatic cells is not random but is determined by the receptors they express and therefore the type of cancer they come from [201]. CXCR4 is the most common chemokine receptor expressed in human tumors such as breast cancer, colorectal cancer, and ovarian cancer, and SDF1α is highly expressed at sites of metastasis including lung, bone marrow, lymph nodes, and liver [202, 203]. SDF1α is indeed a powerful potent chemoattractant and is expressed in many tissues. An interaction between CXCR4 and its ligand SDF1α plays an important role in the directional regulation of hematopoiesis, migration of hematopoietic cells, angiogenesis, and migration of metastatic tumor cells [204]. Moreover, SDF1α promotes the survival and growth of tumor cells and induces the secretion of cytokines [205].

RANTES and CCR5 are over-expressed in case of melanoma metastases which metastasizes to regional lymph nodes, subcutis, and brains [182]. RANTES/CCR5 enhanced the metastatic behavior of breast cancer cells [206] and are required for lung cancer metastasis [207]. The change of RANTES/CCR5 expression pattern may be highly relevant for cancer metastases in general [182].

Currently, the involvement of chemokines and their receptors in the development of lymphoproliferative diseases is an important subject of research. Its understanding will lead to new therapeutic interest for the fight against human leukemia and cancer in general.

2.2. Chemokines

Chemokines (CHEMOtactic cytoKINES) are small-secreted proteins that belong to the family of cytokines and have important functions in intracellular communication. Chemokines regulate biological processes such as proliferation, apoptosis, angiogenesis, lymphoid organ development, hematopoiesis, T-cell differentiation and phagocyte activation. However the main role of chemokines is to activate and control the migration of leukocytes in hematopoiesis and in innate and adaptive immunity. Chemokines play a key role in many disease processes including inflammation, autoimmune diseases, infectious diseases (such as HIV infection) and cancer.

The superfamily of human chemokines contains about 46 members that bind to 20 GPCRs and three decoy receptors. Many chemokines bind multiple receptors and most receptors bind multiple chemokines, suggesting the possibility of functional redundancy.

Chemokines are small and positively charged proteins that vary in size from 6 to 14 kDa. The sequence identity between chemokines varies from less than 20% to over 90%. Nevertheless, chemokines from different subfamilies adopt essentially the same monomer fold. Each monomer has a flexible N-terminal domain, a three-stranded antiparallel β-sheet region, and a C-terminal α-helix (Figure 2.10) [208, 209].

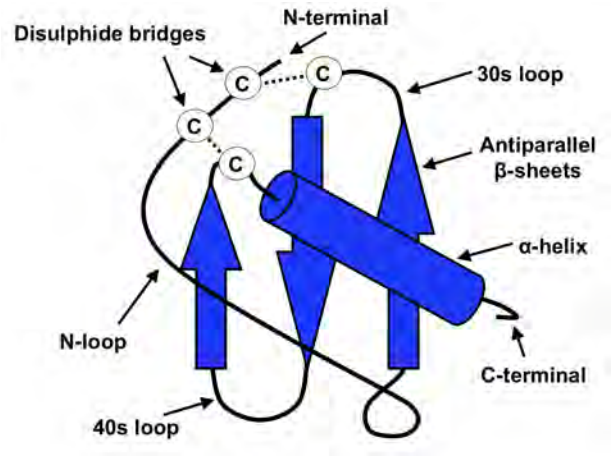

Figure 2.10.: Schematic representation of chemokine three dimensional structure.

Most chemokines have four cysteine residues in highly conserved positions that form two disulfide bridges, one between the first and third cysteine residues, and the other between the second and fourth cysteine residues [210].

2.2.1. Chemokine classification

The discovery of chemokine has been rapid and somehow chaotic. Therefore, several groups reported the same molecule under different names, contributing to a significant confusion in the field. A new classification system has been adopted in 2000 [143].

Depending on the number of amino acids present between the first two cysteines of the N-terminal domain, chemokines are classified into four classes: CC, CXC, CX_3C, and C (where X stands for any amino acid) (Figure 2.11). Modeling studies suggest that the three-dimensional structure of chemokines can only accommodate 0, 1, or 3 amino acids between the first two cysteins, explaining the absence of a CX_2C chemokine class [210].

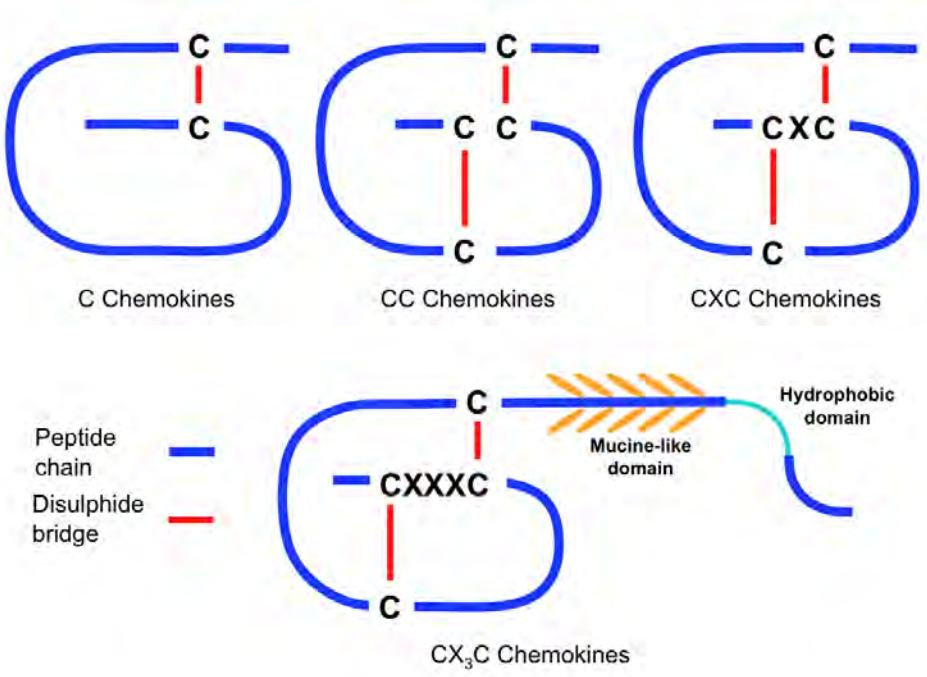

Figure 2.11.: Schematic representation of chemokine classes.

2.2.1.1. CC chemokines

The CC chemokines have two neighboring cysteines, near the amino terminus. There are about 27 members of this family reported in mammals (Table 2.2). CC chemokines induce the migration of monocytes and other cell types such as lymphocytes, NK cells and dendritic cells but not neutrophils.

Examples of CC chemokines include the monocyte chemoattractant protein-1 (MCP-1 or CCL2), which stimulates monocytes to leave the bloodstream and enter the surrounding tissue to become tissue macrophages. RANTES or CCL5 attracts cells such as T cells, eosinophils and basophils that express the receptor CCR5.

Name	Other name(s)	Receptor
CCL1	I-309, TCA-3	CCR8
CCL2	MCP-1	CCR2
CCL3	MIP-1α, LD78α	CCR1
CCL4	MIP-1β	CCR1, CCR5
CCL5	RANTES	CCR5
CCL6	C10, MRP-2	CCR1
CCL7	MARC, MCP-3	CCR2
CCL8	MCP-2	CCR1, CCR2B, CCR5
CCL9/ CCL10	MRP-2, CCF18, MIP-1	CCR1
CCL11	Eotaxin	CCR2, CCR3, CCR5
CCL12	MCP-5	CCR2
CCL13	MCP-4, NCC-1, Ckβ10	CCR2, CCR3, CCR5
CCL14	HCC-1, MCIF, Ckß1, NCC-2, CCL	CCR1
CCL15	Leukotactin-1, MIP-5, HCC-2, NCC-3	CCR1, CCR3
CCL16	LEC, HCC-4, LMC, Ckβ12	CCR1, CCR2, CCR5, CCR8
CCL17	TARC, dendrokine, ABCD-2	CCR4
CCL18	PARC, DC-CK1, AMAC-1, Ck7, MIP-4	Unknown
CCL19	ELC, Exodus-3, Ck11, MIP3β	CCR7
CCL20	LARC, Exodus-1, Ckβ4, MIP3α	CCR6
CCL21	SLC, 6Ckine, Exodus-2, Ckß9, TCA-4	CCR7
CCL22	MDC, DC/β-CK	CCR4
CCL23	MPIF-1, Ckß8, MIP-3, MPIF-1	CCR1
CCL24	Eotaxin-2, MPIF-2, Ckß6	CCR3
CCL25	TECK, Ckß15	CCR9
CCL26	Eotaxin-3, MIP-4a, IMAC, TSC-1	CCR3
CCL27	CTACK, ILC, Eskine, PESKY, skinkine	CCR10
CCL28	MEC	CCR3, CCR10

Table 2.2.: CC chemokines and their main receptors.

2.2.1.2. CXC chemokines

In the CXC subfamily the two N-terminal cysteines are separated by one amino acid (Table 2.3). CXC chemokines are potent chemoattractants and activators of neutrophils but not monocytes.

Name	Other name(s)	Receptor
CXCL1	Gro-α, GRO1, NAP-3, KC	CXCR2
CXCL2	Gro-ß, GRO2, MIP-2a	CXCR2
CXCL3	Gro-γ, GRO3, MIP-2ß	CXCR2
CXCL4	PF-4	CXCR3B
CXCL5	ENA-78	CXCR2
CXCL6	GCP-2	CXCR1, CXCR2
CXCL7	NAP-2, CTAPIII, ß-Ta, PEP	CXCR2
CXCL8	IL-8, NAP-1, MDNCF, GCP-1	CXCR1, CXCR2
CXCL9	MIG, CRG-10	CXCR3
CXCL10	IP-10, CRG-2	CXCR3
CXCL11	I-TAC, ß-R1, IP-9	CXCR3, CXCR7
CXCL12	SDF-1α/β, PBSF	CXCR4, CXCR7
CXCL13	BCA-1, BLC	CXCR5
CXCL14	BRAK, Bolekine	Unknown
CXCL15	Lungkine, WECHE	Unknown
CXCL16	SRPSOX	CXCR6
CXCL17	DMC, VCC-1	Unknown

Table 2.3.: CXC chemokines and their receptors

CXCL12 (or SDF1α) together with its receptor CXCR4 plays a central role in the interactions of hematopoietic stem cells, lymphocytes, and developing neutrophils in the marrow [211].

The CXC subfamily is further subdivided into two categories depending on the presence or absence of an ELR motif (glutamate-leucine-arginine) upstream of the first cysteine residue. ELR-CXC chemokines (CXCL1, CXCL2, CXCL3, CXCL5 and CXCL8) specifically recruit neutrophils into inflamed tissues in a multi-step process by rolling, adhesion and transmigration [212, 213]. One characteristic of ELR-CXC chemokines (CXCL4, CXCL9 and CXCL10) is their ability to promote angiogenesis [214, 215]. In contrast, non-ELR CXC chemokines inhibit the angiogenesis induced by ELR-CXC chemokines [216].

2.2.1.3. CX_3C chemokines

The CX_3C chemokines have three amino acids between the first two cysteine residues (Table 2.4). The only member of this family is CX_3CL1 - previously called fractalkine. This chemokine totally differs from the others, as it is the only membrane bound chemokine [217].

Name	Other name(s)	Receptor
CX_3CL1	Fractalkine, Neurotactin, ABCD-3	CX_3CR1

Table 2.4.: CX_3C chemokine and its receptor.

2.2.1.4. C chemokines

The C class chemokines lack the first and third conserved cysteines (Table 2.5). This family has two members called XCL1 (lymphoatractin-α) and XCL2 (lymphoatractin-β) [218].

Name	Other name(s)	Receptor
XCL1	Lymphotactin α, SCM-1α, ATAC	XCR1
XCL2	Lymphotactin β, SCM-1β	XCR1

Table 2.5.: C chemokines and their receptors.

According to the nomenclature: CCL1 stands for the ligand 1 of the CC-family of chemokines, and CCR1 for its respective receptor.

This structural classification is now used as a reference nomenclature but some common names are still widely used, such as RANTES (CCL5), SDF1α (CXCL12), MCP-1 (CCL2), etc...

2.2.2. Functional chemokine classification

Based on their expression patterns and functions chemokines have been divided into two groups: inflammatory chemokines and homeostatic chemokines [219, 220, 215].

Inflammatory chemokines, are produced by the immune system cells such as leukocytes or related cells such as epithelial and endothelial cells, fibroblasts and others. Inflammatory chemokines can be activated after contact with a pathogen. They participate in the development of the immune and inflammatory reactions [220].

Chemokines that are constitutively expressed in specific tissues or cells in discrete locations in the absence of apparent activating stimuli have been classified as homeostatic chemokines. Homeostatic chemokines are constitutively expressed in the lymphoid organs and in non-lymphoid organs such as skin and mucous membranes. The functions of the homeostatic chemokines are more diverse than those of the inflammatory chemokines. They are involved in cell migration. Homeostatic chemokines regulate lymphocyte trafficking and localization of lymphocytes [221, 222].

However, the division between inflammatory and homeostatic chemokines is not absolute, certain chemokines belong to both families.

2.2.3. Chemokine 3D structure

The 3D structure of many chemokines has been solved by Nuclear magnetic resonance (NMR) spectroscopy and/or crystallography.

Despite their functional diversity the structural fold of CXC and CC chemokine monomers is very conserved (Figure 2.12) [208].

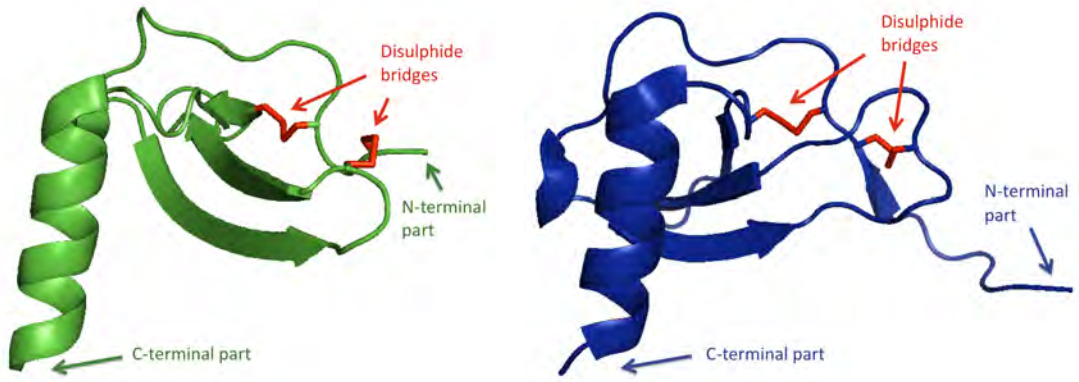

(a) SDF1α (b) RANTES

Figure 2.12.: 3D structures of SDF1α and RANTES monomers.
PDB codes: 1VMC for SDF1α [223] and 1EQT for RANTES [224].

Both monomers have unstructured N-terminal part which forms a long loop. The main secondary structure elements comprise three antiparallel β sheets and a C-terminal α helix. The two characteristic disulphide bridges define and stabilize the overall architecture of chemokines.

2.2.4. Oligomerization

It has been demonstrated that chemokines bind and signal through their receptors as monomers [225, 226] nevertheless the ability of chemokines to oligomerize is important for *in vivo* function [227]. NMR studies showed that chemokines can dimerize [228, 225]. All chemokines oligomerize into dimers [209], and some form tetramers [229] or higher molecular mass oligomers [208, 230]. Although each chemokine has its own set of unique properties there are some general mechanisms of oligomerization.

Despite having similar monomer folds, CXC and CC dimers associate differently [209].

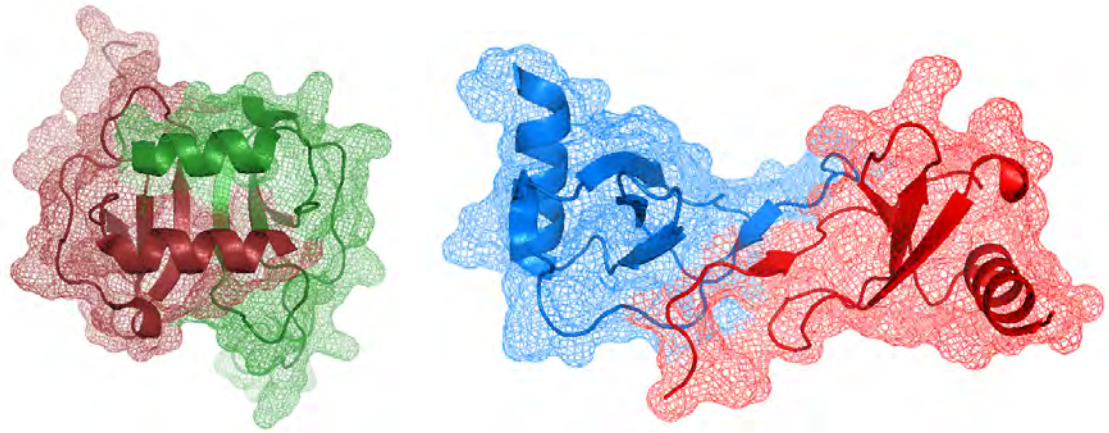

(a) CXC dimer. (b) CC dimer.

Figure 2.13.: 3D structures of chemokine dimers.
The 3D structures are: (a) SDF1α, PDB code 2J7Z; (b) RANTES, PDB code 1EQT [231, 224].

The more globular CXC-type dimer is formed by extension of the three-stranded β-sheet from each monomer into a six-stranded β-sheet, on top of which run the two C-terminal antiparallel α-helices (Figure 2.13a). The CC chemokines form elongated end-to-end type dimers. Their contacts are formed between their N-terminus, which are unstructured in the monomer, but form a β-sheet in the dimer (Figure 2.13b). The two C-terminal helices run almost perpendicular to each other on opposite sides of the molecule.

CXC chemokine dimerization is independent of pH and salt concentration. CC chemokine dimer is stable at very low pH and is also independent of salt concentration [232].

Chemokines bind to glycosaminoglycans (GAGs) on the cell surface which increases their local concentration. Chemokines binding to GAGs facilitate their accumulation in localized areas, allowing them to function as directional cues for migrating cells [233]. GAGs also induce chemokine oligomerization [234]. Reciprocally, oligomerization plays an important role in chemokine-GAG interaction, which is necessary for some *in vivo* chemokine activity. It has been shown that oligomerization-deficient and GAG-binding-deficient chemokine variants result in impaired migration *in vivo* [233].

Chemokine oligomerization and the ability to bind GAG represent essential structural features for their ability to recruit leukocytes *in vivo* [233]. Several analyses show that some, but not all chemokines either bind as dimers or dimerize after binding to GAG on endothelial cells [235], which is necessary for their function [236].

In addition to cell migration, oligomeric forms of chemokines may also be involved in other processes such as cellular activation associated with inflammatory responses.

Heterodimerization

Heterodimerization has been observed for both CXC and CC chemokines. Homodimers of chemokines can be substituted by heterodimers if the arrangement of individual residues at the monomer-monomer interface is energetically and sterically more favorable than in homodimer [228].

The change of chemokine concentration could result in chemokine homodimerization / heterodimerization at a particular site [228]. It is known that different quaternary states of chemokines play different biological roles. Heterodimerization dramatically modulates the biological activities of chemokines. For example, the presence of angiogenic CXCL8 in solution with anti-angiogenic CXCL4 induces the formation of the CXCL8-CXCL4 heterodimer which increases the anti-proliferative activity of CXCL4 against endothelial cells [230]. In the case of RANTES–CXCL4-heterodimerization, the RANTES-induced monocyte arrest on atherosclerotic or inflamed endothelium is enhanced by CXCL4 [237, 238].

2.2.5. Biological activity of chemokines

Chemokines play a key role in numerous biological processes, from organogenesis and leukocyte trafficking to host immune response to infection [239]. Chemokine-dependent signaling is necessary for inflammation, hematopoiesis, angiogenesis and tumors. In addition, chemokines can control HIV-1 infection [239].

Chemokine interaction with receptor

Biological activity of chemokines is mediated by their receptors. Chemokine activity is initiated by the chemokine binding to its specific receptor the GPCR. The activation of the GPCR was previously described in Chapter 1.3. Like other GPCRs, some chemokine receptors initiate their ligand-induced signaling cascade by receptor dimerization (Figure 2.14).

Ligand binding to chemokine receptor activates signaling cascade events represented in Figure 2.14, and results in diverse physiological processes including gene expression, cell polarization and chemotaxis [240, 239, 241].

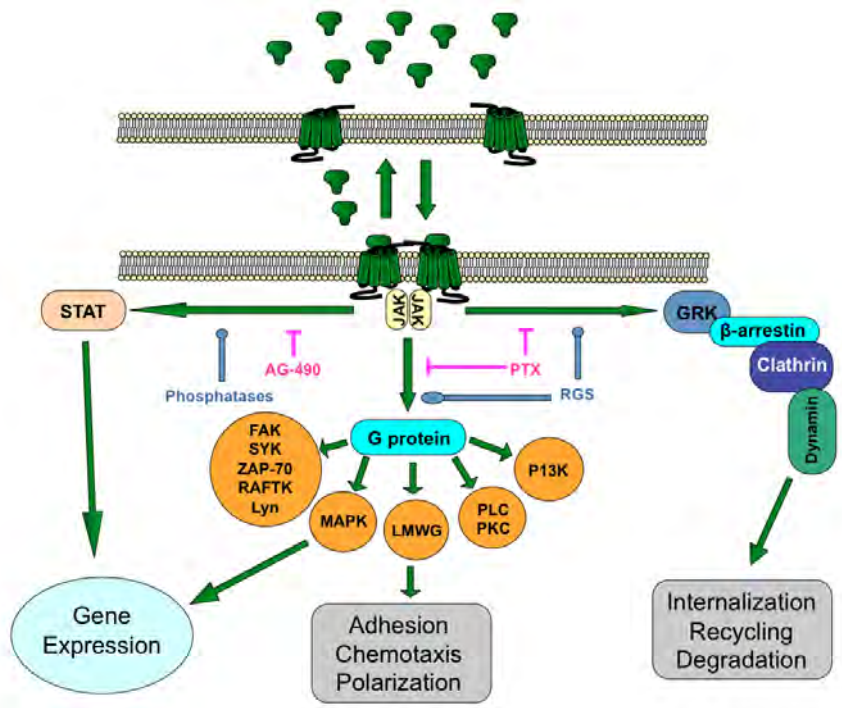

Figure 2.14.: Schematic model representing chemokine receptor activated signaling pathways. Adapted from [241].

It was suggested that chemokine receptor dimerization and JAK/STAT pathway activation is common for CC and CXC class chemokine receptors [241]. This is the case for CCR5 and CXCR4, both of which induce activation of different JAK/STAT family members. In the absence of JAK activation, chemokine signaling through chemokine receptors does not occur. This was confirmed by the observation that G protein–mediated signaling events are blocked by JAK kinase inhibitors [242].

Chemokine interaction with glycosaminoglycans

In addition to GPCR, chemokines also interact with glycosaminoglycans (GAGs) of the heparin/heparan sulfate family. GAGs serve to present chemokine to their receptors expressed on leukocytes. This chemokine-GAG interaction avoids chemokine dilution within lymph or blood vessels.

Chemokine interaction with cellular or extracellular matrix GAGs is important for their biological activity. GAGs are highly sulfated oligosaccharides characterized by high degree of structural heterogeneity. Chemokines interact with GAGs via typical BBXB heparin-binding motif (where B stands for a basic residue and X for a hydropathic residue) [243].

Chemokines control the selective migration of leukocytes in immune surveillance, inflammation and atherogenesis [244, 245]. This involves not only the directed migration of leukocytes along

chemokine gradients within the extracellular matrix but also the arrest of circulating leukocytes on activated endothelium under flow (Chapter 2.1.2).

The immobilization of chemokines to endothelium via binding to glycosaminoglycans (GAGs) has been implicated in triggering leukocyte arrest, as well as transmigration in flow [246, 247]. Chemokine binding to GAGs is essential for presentation of chemokines on endothelial layers and *in vivo* leukocyte migration [236, 248]. This interaction is not required for *in vitro* chemotactic activity.

2.2.6. Chemokines of interest

2.2.6.1. RANTES

The chemokine RANTES (Regulated on Activation, Normal T cell Expressed and Secreted) is 8-kDa protein that belongs to the CC chemokine class and is also called CCL5.

RANTES is a proinflammatory chemokine secreted by both endothelial cells and activated leukocytes to attract leukocytes to sites of inflammation. RANTES is chemotactic for T cells, eosinophils and basophils. Together with other cytokines such as Interleukin-2 (IL-2) and Interferon-gamma (IFN-γ) that are produced by T cells, RANTES induces the proliferation and activation of natural-killer (NK) cells [249, 250].

RANTES expression has been associated with more then 100 human diseases such as transplant rejection, atherosclerosis, arthritis, airway inflammatory disorders, and cancer [251, 252, 253].

RANTES is one of the most potent natural chemokine inhibitor of M-tropic HIV-1 infection [254]. High concentration can also act as a stimulator, enhancing viral infection. Indeed, in the early stage of the HIV infection the virus uses CCR5 for entry, high RANTES concentrations shift the virus to use the CXCR4 for entry and towards AIDS development [255, 256].

RANTES is the most effective antiviral CCR5 binding chemokine and is being investigated as a potential anti HIV agent. However, an *in vivo* use of RANTES is impaired by the proinflammatory properties of this chemokine triggered upon receptor binding and subsequent signal transduction. These potential difficulties encourage the search for modified RANTES analogues or small peptide derivatives that are not implicated in the signal transduction.

RANTES has been shown to interact with CCR3 [257, 258], CCR5 [258, 259, 260], and CCR1 [258, 260]. Apart from the chemokine receptors it was shown that RANTES activates another GPCR class receptor - GPR75 [261].

N-terminal modifications

It was reported that the extension of recombinant human RANTES by a single residue at the N-terminus (Met-RANTES) is sufficient to produce a potent and selective antagonist [262]. Series of Met-RANTES analogs were created (Table 2.6).

Chemokine	**N-terminal sequence**	**Properties**	**Signaling**	**Ref.**
RANTES wild-type	SPYSSDTTPCC-	Antiviral properties, Ca^{2+}mobilization, Chemotactic activity	Yes	[263, 264, 265, 266, 267, 174, 262]
Met-RANTES	MSPYSSDTTPCC-	Antiviral activity	No	[262]
L-RANTES	L-SPYSSDTTPCC-	Antiviral activity reduced, Ca^{2+}-mobilization, Chemotactic activity	Decreased	[268]
C1.C5 RANTES	CPYSCDTTPCC-	Antiviral activity reduced, Ca^{2+}-mobilization, Chemotactic activity	Decreased	[268]
RANTES 3-68	--YSSDTTPCC-	Antiviral activity, No chemotactic and Ca^{2+}-mobilization activity	Controversial	[265, 266]
RANTES 9-68	--------PCC-	Antiviral activity, No chemotactic and Ca^{2+}-mobilization activity	No	[269]
AOP-RANTES	AOP-SPYSSDTTPCC-	Antiviral activity reduced, Chemotactic activity reduced, Ca^{2+}-mobilization, Inhibit the recycling of internalized CCR5	Yes	[270]
NNY-RANTES	NNY-SPYSSDTTPCC-	Antiviral activity, Inhibit the recycling of internalized CCR5		[271]
PSC-RANTES	PSC-SPYSSDTTPCC-	Antiviral activity, Induce internalization, Inhibit the re-expression of the receptor	Yes	[272]
5P12-RANTES	GPPLMATQS-RANTES	Antiviral activity, Inhibit the re-expression of the receptor	No	[273]
5P14-RANTES	GPPLMSLQV-RANTES	Antiviral activity	No	[273]
6P4-RANTES	GPPGDIVLA-RANTES	Antiviral activity, Inhibit the re-expression of the receptor	No	[273]

Table 2.6.: N-terminal RANTES modifications.

Engineered versions in particular PSC-, AOP- RANTES lead to significantly stronger inhibition of HIV-1 replication [270, 268].

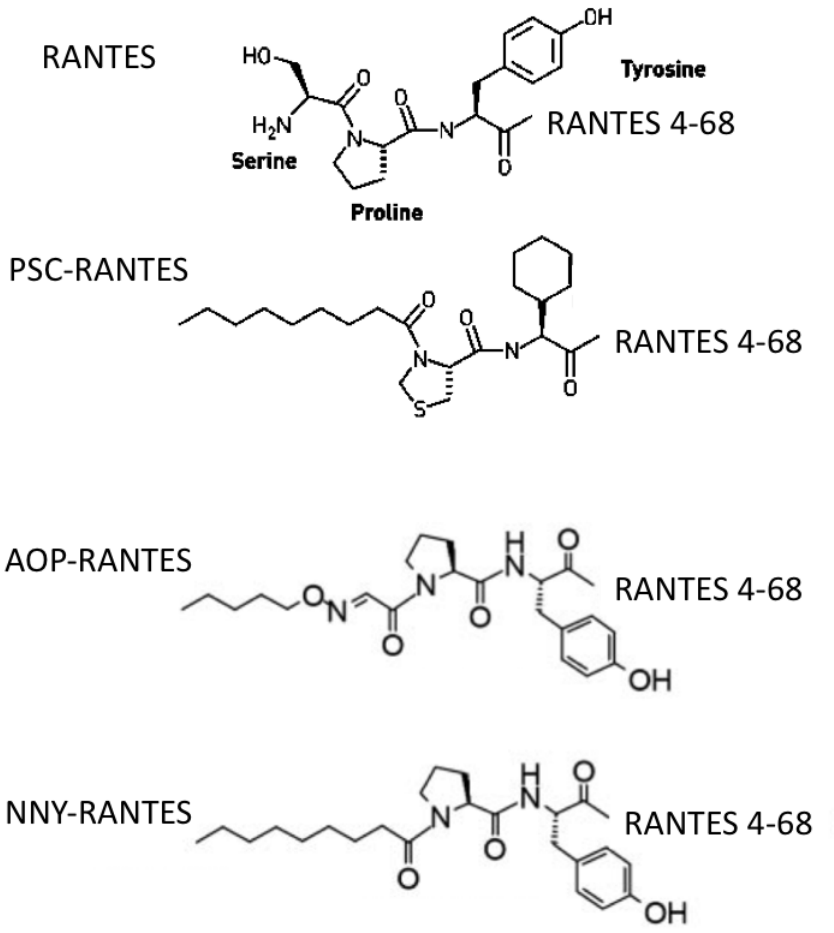

Figure 2.15.: Substitution of the first three residues of RANTES dramatically changes the protein's ability to prevent entry of HIV into cells.

L-RANTES bears an additional hydrophobic amino acid (Leu) at the N-terminus. AOP-RANTES (aminooxypentane-RANTES) is a rationally designed analogue of Met-RANTES. NNY-RANTES (Nα-nonanoyl-RANTES) is a further-optimized molecule based on AOP-RANTES [271]. PSC-RANTES (L-Thia-Pro2,L-α-cyclohexyl-Gly3-NNY-RANTES) is a further optimized analogue [272].

PSC-RANTES is a highly potent inhibitor of CCR5-dependant HIV entry *in vitro* [274, 275]. PSC-RANTES required a chemical synthesis step during production. PSC-RANTES analogs that contain only natural amino acids were also produced. Three mutants 5P12-RANTES, 5P14-RANTES, and 6P4-RANTES, were identified with anti-HIV properties [273].

RANTES aggregation

Recombinant human RANTES tends to oligomerize and even to form large aggregates. To characterize the pH effect on RANTES oligomerization a titration from pH 5.0 to pH 2.5 was performed. The results demonstrated that RANTES is extensively aggregated in solution above pH 4.0 and at pH 3.7 the protein is mostly dimeric [276].

Latter the tetrameric E26A and the dimeric E66A RANTES mutants have been described [277]. The biology of RANTES aggregation has been investigated using RANTES and disaggregated variants, enabling comparison of aggregated, tetrameric, and dimeric RANTES forms [277].

RANTES aggregation may be responsible for a proportion of its proinflammatory activity. The relative inability of RANTES E66S to stimulate the protein tyrosine kinase pathway and to activate leukocyte suggests that dimeric RANTES is noninflammatory. Disaggregated RANTES will be a valuable tool to explore the biology of RANTES action in human immunodeficiency virus infection and in inflammatory disease.

Combining complementary data from multiple techniques such as available crystal structures of dimers, solution NMR data, SAXS data, and hydroxyl radical foot-printing MS an oligomerization model of RANTES has been generated (Figure 2.16) [278].

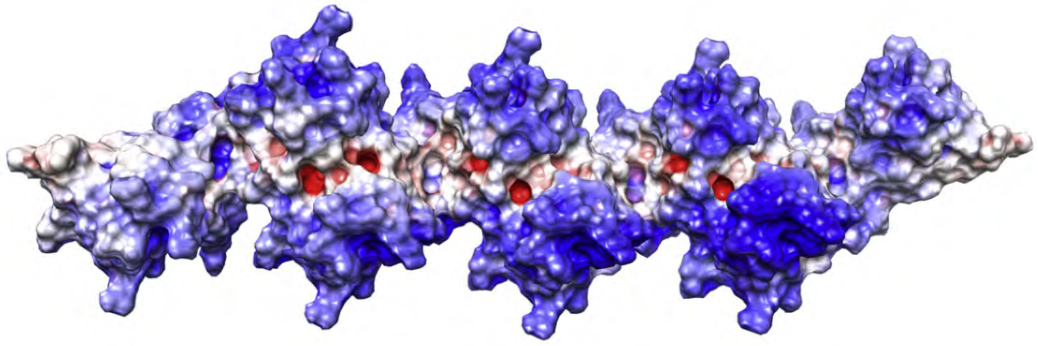

Figure 2.16.: Octameric structure of RANTES.
Basic regions are shown in blue. Positive charges form an elongated RANTES surface. Adapted from [278].

It has been shown that RANTES is able to oligomerize without significantly changing its dimeric structure (Figure 2.17b). While other CC class chemokines such as MCP-1 and IP-10 have globular tetrameric structure (Figure 2.17a) [279, 280], RANTES forms an elongated tetramer, where its interacting dimer units form a long linear polymeric chain containing an even number of monomer units.

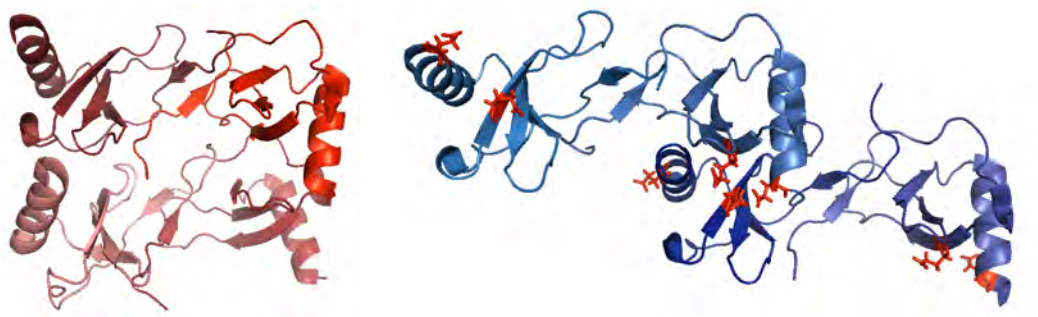

(a) MIP1α tetramer. (b) RANTES tetramer. Residues E26 and E66 shown in red.

Figure 2.17.: Comparison of MIP1α tetramer with RANTES tetramer .
A single dimer unit from each tetramer is arranged in identical orientation. PDB code: MIP1α - 2X69, RANTES - 2L9H. Adapted from [278].

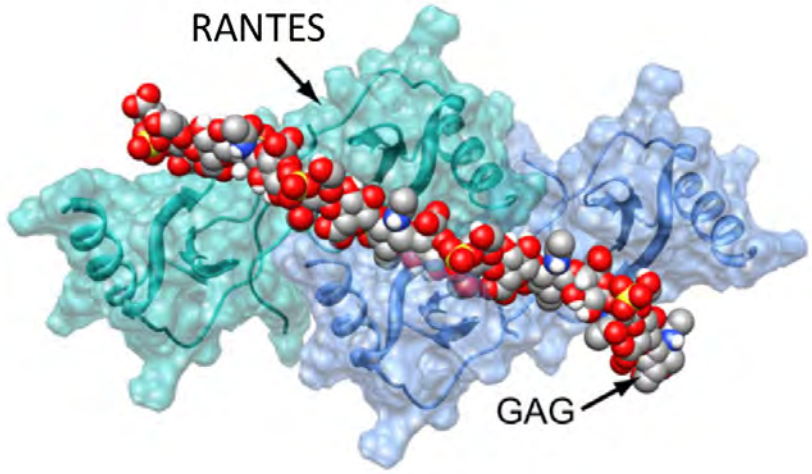

Figure 2.18.: The model of tetrameric RANTES binding GAG.
Graphical Abstract [278].

RANTES forms linear oligomeric complexes, allowing extended interactions with glycosaminoglycan (GAG) chains (Figure 2.18). The basic residues on the surface of RANTES oligomer are arranged linearly and form GAGs binding sites.

Signaling

Numerous elements of the RANTES signaling cascade have been characterized, but the whole process remains poorly understood [281]. It has been shown that depending on the affinity and protein concentration RANTES act via two different signal transduction pathways in T cells [282].

At relatively low concentrations of RANTES it activates the high affinity GPCR signaling through Gi protein mediating chemotaxis, transient calcium mobilization, and suppression of HIV infection.

The other signaling pathway at high concentrations of RANTES involves protein tyrosine kinase (PTK) activation pathway resulting in a prolonged mobilization of calcium [283, 284]. This RANTES induced stimulation leads to T cell activation, including proliferation of T cells, induction of interleukin-2 (IL-2) expression and increases in expression of cell surface molecules such as the IL-2 receptor (CD25) [282, 283]. This G protein independent CCR5 activation can induce apoptosis [277, 285].

The existence of two different signaling pathways suggests that oligomeric RANTES activates different signaling pathways than those induced by monomeric RANTES [277, 285]. Aggregated RANTES activates human T cells, monocytes, and neutrophils. Disaggregated, dimeric RANTES has lost its cellular activating activity, rendering it noninflammatory and does not enhance HIV infection [256]. *In vivo* study showed that engineered, non-oligomerizing chemokine are less effective in recruiting cells along a chemokine gradient [233].

Depending on the N-terminal RANTES modification CCR5 undergoes different recycling pathways (Figure 2.19).

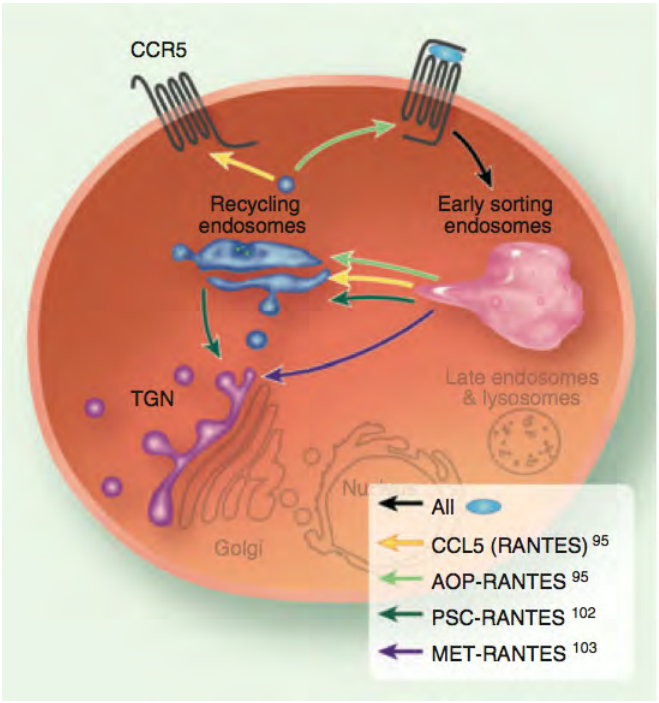

Figure 2.19.: Trafficking routes of CCR5 upon different RANTES treatment. Adapted from [286].

After interaction with the natural chemokine RANTES the receptor follows internalization and is located in Recycling Endosomes (RE) before re-accumulating in the plasma membrane. Af-

ter binding to CCR5 the chemically modified aminooxypentane AOP-RANTES the receptor is cycling back from the cell surface to the RE. The receptor exposed to Nα-(n-nonanoyl)-des-Ser1-[l-thioproline2, l-α-cyclo-hexyl-glycine3] PSC-RANTES becomes trapped in the Trans-Golgi Network (TGN). The receptor interaction with Met-RANTES bypasses the RE and then receptor accumulates in the TGN [286].

2.2.6.2. SDF1α

SDF1 is an acronym for Stromal cell-Derived Factor 1, also called CXCL12. It belongs to the large family of chemokines that initiate the migration of effector cells.

There are six human SDF1 isoforms, SDF1α, SDF1β, SDF1γ, SDF1δ, SDF1ε, and SDF1Φ [287]. SDF1α and SDF1β were generated through alternative splicing; SDF1β has an additional 4 amino acids at the C-terminus. The other SDF1 isoforms (γ to Φ) are also splice variants. They all share the same first three exons, but the fourth exon is different. SDF1α/β share similar expression patterns and tissue distribution; their highest expression levels are in liver, pancreas and spleen. The human SDF1γ is only expressed in the heart. All human SDF1 isoforms can stimulate cell migration once bound to CXCR4.

For a long time it was thought that SDF1 was the only ligand for CXCR4 and that CXCR4 was the only receptor for SDF1. Even though SDF1α preferentially binds to CXCR4 it was shown that SDF1α also binds to and signals through the orphan receptor RDC1 in T-lymphocytes [288].

In vitro studies showed that SDF1α exist in equilibrium between monomeric and dimeric forms. It was shown that the N-terminal 38 residue of CXCR4 promotes SDF1α dimerization [289] by contacting specific sulfotyrosine recognition sites on both sides of the dimer interface [290]. A stable SDF1α dimer was created by double mutation (L36C/A65C) where introduced Cys residues formed a pair of symmetric intermolecular disulphide bounds [290]. This disulphide bridge stabilized dimer enabled the resolution of the SDF-1α and N-terminus of CXCR4 complex by NMR.

In vitro studies of SDF1α interaction with GAGs demonstrated that SDF1α binds selectively to heparan sulphate (HS) and heparin [291]. Electrostatic calculations showed that the SDF1α dimer association allows the formation of a crest constituted by the positively charged Lys-27, Arg-41, Lys-24, and Lys-43, creating a possible binding site for the negatively charged heparin (Figure 2.20) [292].

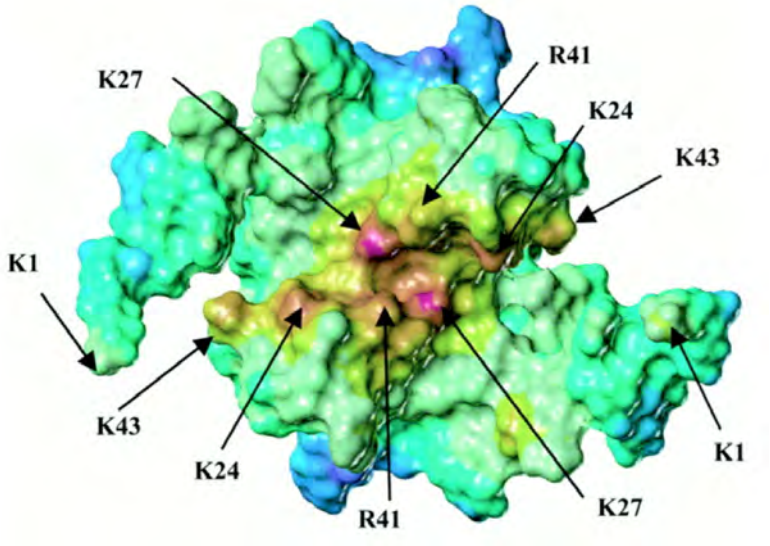

Figure 2.20.: SDF1α dimer.
The surface of the SDF1α dimer color-coded according to the electrostatic potential, blue - negative regions and red - positive regions [292].

Several SDF1α mutants were created to identify the amino acids involved in heparin binding. It was shown that a double mutant K24S/K27S was unable to bind heparin. Single mutants K24S and K27S strongly diminished the binding, indicating that both K24 and K27 are involved in the complex formation. However, the binding of these mutants to the heparin increased at higher concentrations [292].

A 3D model of the interaction between SDF1α and heparin was proposed (Figure 2.21) [293].

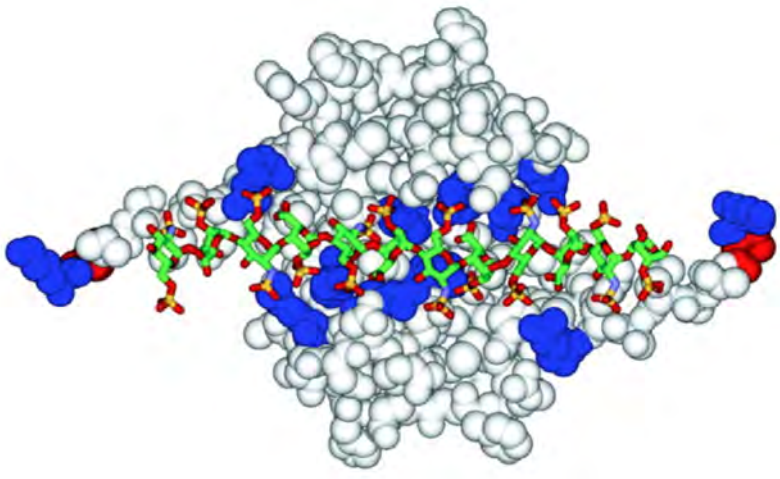

Figure 2.21.: Model of SDF1α and heparin complex.
SDF1α dimer in complex with a heparin-derived dodecasaccharide. The basic amino acids involved in the complex are shown in blue, the proline residue at position 2 is shown in red, and the heparin oligosaccharide is represented as sticks [293].

It was suggested that the N-terminal lysine residue of the SDF-1α interaction with the extended dodecasaccharide terminal sugar residues protects the chemokine from cleavage by the CD26/dipeptidyl peptidase IV (DPP IV) a serine protease, which mediates the selective removal of the N-terminal dipeptide of SDF1α [293]. Heparin and HS specifically prevent the processing of SDF1α. Chemokine mutants that do not bind the HS are cleaved by DPP IV. Processed chemokines lose their biological activity [294]. Therefore, chemokine/GAGs interaction mediates a control mechanism of selective protease cleavage events that directly affect the chemokine activity [293].

3. Biochemistry of membrane proteins

GPCRs are integral membrane proteins and their handling obeys "classical" membrane biochemistry rules.

3.1. Solubilizing membrane proteins

Biological membranes are generally rich in proteins. In order to study *in vitro* structure and function of membrane proteins it is necessary to extract the proteins from their native environment, the membrane.

The hydrophobic domains of membrane proteins make them difficult to manipulate once they have been extracted. Usually membrane proteins tent to precipitate and/or form insoluble aggregates. They have to be handled in an environment that resembles the native membrane. Hydrophobic interactions play a major role in defining the native tertiary structure of the proteins. In water-soluble proteins, hydrophobic domains are folded-in together and protected from aqueous environment. In membrane proteins, some hydrophobic domains are exposed to the aqueous environment and therefore are surrounded by a mixture of lipids and other components.

Membrane proteins are usually extracted from cell membranes and maintained soluble in aqueous solution thanks to surfactants. The most common used surfactants are detergents. The selection of detergents suitable for the solubilization and purification of a specific membrane protein is a critical step in the purification of membrane proteins.

However, detergents can destabilize the protein. The structure and function of membrane protein can depend on associated lipids and cofactors, which are often lost upon detergent extraction. That leads to protein destabilization and frequently to aggregation. Many membrane proteins require specific types of phospholipids to maintain active function. This is a hard task to achieve while working with the detergents. Liposome preparation was used for these cases to incorporate membrane proteins. However, they are heterogeneous in size and difficult to prepare with precisely controlled size and stoichiometry. Membrane proteins when extracted with detergents are in monomeric state, while in the native membrane they are often in oligomeric state. That is another frequent protein destabilization problem, which leads to the loss of protein function.

Membrane proteins solubilized in detergents tend to form mixed detergent-protein-lipid micelles. Free micelles often co-concentrate with the protein and that can interfere with many techniques such as absorbance and light scattering.

3.2. Detergents

3.2.1. General introduction

Detergents are small, amphipatic molecules classified as surfactants. Detergents have similar dual properties as lipid molecules; they have hydrophobic tail and hydrophilic head. Detergents vary in both nature of the hydrophilic head groups (sugar-based, phospholipid like) and length and composition of hydrophobic alkyl tails. Many different detergents with various combinations of hydrophobic and hydrophilic groups are available. It is crucial to choose the right detergent while working with membrane proteins.

Detergents at low concentration in solution exist as monomers. However, at a specific concentration called the Critical Micelle Concentration (CMC) the detergent molecules form micelles due to hydrophobic interaction of the alkyl chains. The CMC is a function of the specific detergent and is varying according to the composition of the solvent. The CMC is related to the length of the alkyl chain of the molecule: the longer alkyl chain the smaller CMC value. At concentrations below the CMC the detergent is a monomer in solution. At the concentration equal to the CMC, the detergent spontaneously aggregates into a micelle. At the concentration above the CMC, there is equilibrium between monomers and an increasing concentration of micelles [295]. In order to effectively solubilize membrane proteins detergents must be used at concentrations above their CMC [296].

At the CMC, detergent start to disrupt the interactions between membrane protein and the lipid bilayer. Detergents solubilize membrane proteins by mimicking the lipid bilayer environment. The hydrophobic protein regions are covered by detergents and hydrophilic regions are exposed to the water environment. Depending on the concentration of detergent used it is possible to obtain a mix of protein-lipids-detergent or just protein-detergent.

The CMC varies with the salt concentration and temperature. These features are important to bear in mind while working with MPs.

3.2.2. Detergent classification

According to the nature of the hydrophilic head group, detergents can be classified as ionic, nonionic and zwitterionic.

Ionic detergents contain a head with a net charge (either negative or positive). Ionic detergents contain either a hydrocarbon (alkyl) straight chain or a more complicated rigid steroid structure. Ionic detergents are rather denaturing; they strongly bind to membrane proteins. Due to the charged nature of their head groups, the CMC, the micellar structure and behavior will be strongly dependent on solution parameters such as ionic strength and pH.

Non-ionic detergents contain uncharged, hydrophilic head groups that consist on either polyoxyethylene moieties or glycosidic groups. In general, non-ionic detergents are better suited for breaking lipid-lipid and lipid-protein interactions than protein-protein interactions. Nonionic detergents are less aggressive and allow the isolation of MP in a native state.

Zwitterionic detergents are unique in that they offer combined properties of ionic and non-ionic detergents; they do not show any net charges. Like non-ionic detergents they do not possess a net charge, they lack conductivity and electrophoretic mobility, and do not bind to ion exchange resins and are relatively mild for membrane proteins. They are suitable for the extraction of membrane proteins and can be used in the subsequent purification and crystallization steps.

3.2.3. Physical properties of detergents

The difference between detergents and biological lipids is that detergents tend to assemble into relatively small, well-defined micelles when biological lipids form extended structures typical of lipid bilayers. The reason is geometric. In the membrane, the polar and apolar moieties of lipids occupy comparable areas, as lipid molecules look more or less cylindrical: the combination of many molecules forms a flat monolayer, two of which form the membrane. In detergents, the apolar part is less bulky than the polar one, which bends the interface, generating spheres, ellipsoids, or cylinders, called micelles.

For the detergent interaction with proteins the head group has a strong influence, while the length of the alkyl chain affects the CMC and aggregation number. For detergents with the same alkyl chain length, those with bigger polar head groups tend to be milder. For example, OM (n-octy-beta-D-maltopyranoside) is milder than OG (octyl-beta-D-glucopyranoside). Detergents with longer hydrophobic tails will be milder than the ones with shorter tails provided that they have the same polar head. For instance, NG (nonyl-beta-D-glucopyranoside) is milder than OG but harcher than DG (n-decyl-beta-D-glucopyranoside). The solubility of detergents decreases as the alkyl tails gets longer [296].

3.2.4. Extraction/solubilization from membranes

For the extraction and solubilization of membrane proteins a key concept is the Critical Solubilization Concentration (CSC). The CSC is the minimal detergent concentration required to

disrupt a membrane system into a predominantly micellar dispersion. The CSC depends on the starting conditions such as the lipid concentration, the membrane system and the detergent.

Selective solubilization of proteins at detergent concentrations below the CSC can be a very effective purification strategy.

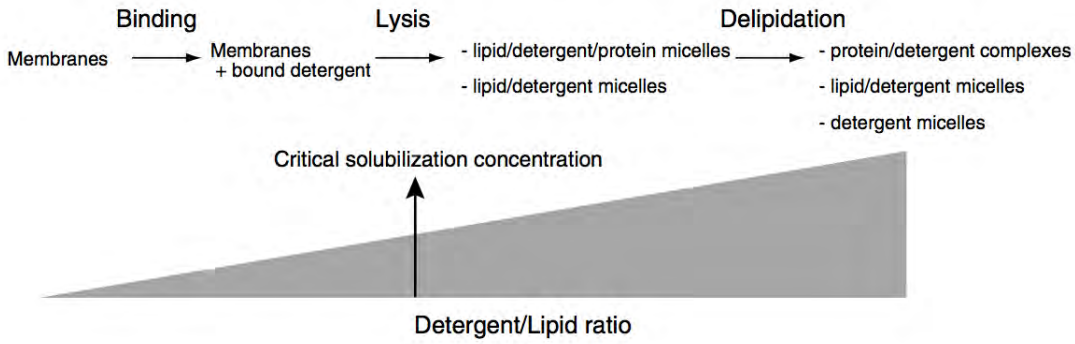

Figure 3.1.: Solubilization of membranes by detergents.
Adapted from [296].

In many cases the membrane preparation is completely solubilized when the target protein is fully extracted from the membrane (Figure 3.1 and Figure 3.2).

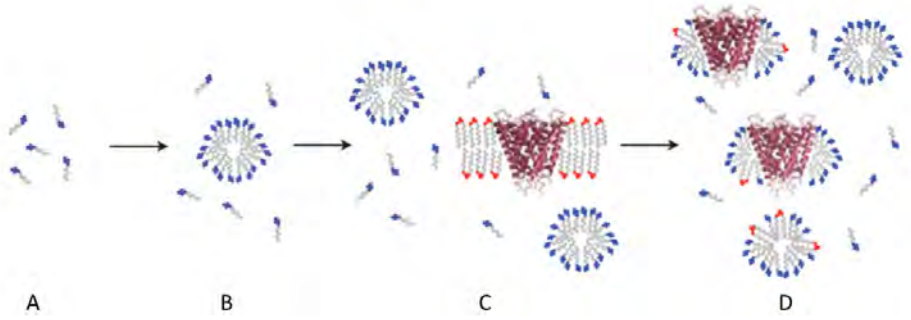

Figure 3.2.: Schematic representation of the solubilization process.
Free detergent monomers (A) associate to form detergent micelles (B) at concentrations above the CMC. When added to a membrane preparation (C), the micelles extract membrane proteins from the lipid bilayer yielding a solution containing detergent/protein complexes, free lipid-detergent micelles and detergent monomers (D) [297].

The temperature factor is very important and should be controlled depending on the requirements of the protein solubilization. The lipid concentration in the starting membrane suspension is the most critical parameter to control and to ensure batch-to-batch reproducibility during detergent solubilization [298, 299, 300].

3.2.5. Protein denaturation and aggregation

Sometimes the detergent may not be able to fully mask the transmembrane regions of a protein. This typically results in the aggregation and precipitation of the protein. In some cases the precipitate may be resolubilized by the addition of more detergent, or of a more effective detergent. In most cases, protein aggregation is irreversible leading to non-specific interactions between surfaces that are normally buried in the folded protein.

Despite the large number of detergents that are commercially available, no single ‘‘universal detergent’’ is ideally suited to all biochemical applications. As a result, the choice of detergent is one of the most fundamental decisions that must be made in developing a new protocol for a given membrane protein.

3.2.6. Commonly used detergents

In general, membrane proteins are more stable in detergents with long alkyl chains such as dodecyl-β-D maltoside (DDM) than those with shorter chains such as octylglucoside (OG). Alkylglucosides, such as n-dodecyl-β-D maltoside (DDM), are increasingly used in membrane protein solubilization as many proteins can be readily solubilized in a functional state in DDM but with retention of functional properties [301].

Detergent	Structure	CMC
LDAO	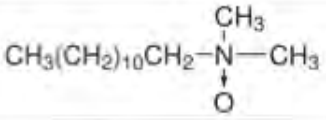	1mM
OG	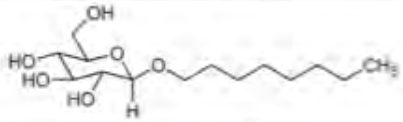	24 mM
C8E4		7.2 mM
DM	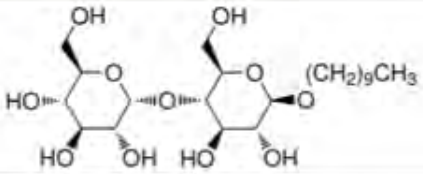	1.6 mM
DDM	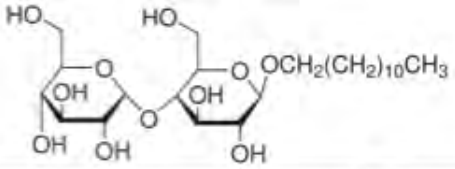	0.2 mM
SDS		8.2 mM
DPC	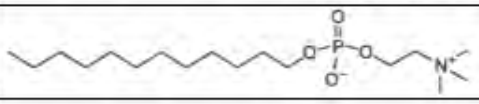	1.1 mM

Table 3.1.: Structures and properties of detergents commonly used to solubilize membrane proteins.

The most commonly used detergents to study membrane proteins are: N,N-dimethyldodecylamine-N-oxide (LDAO), n-octyl-β-D-glucopyranoside (OG), octyltetraoxyethylene (C8E4), n-decyl-β-D-maltopyranoside (DM) and n-dodecyl-β-D-maltopyranoside (DDM), sodium dodecyl sulfate (SDS), dodecyl phosphocholine (DPC) and CHAPS (Table 3.1) [296].

3.3. Nanodiscs

The Nanodisc is a non-covalent assembly of phospholipids and a genetically engineered Membrane Scaffold Protein (MSP) [302]. MSP is derived from human serum apolipoprotein AI [303]. The phospholipids associate as a bilayer while two molecules of MSP wrap around the edges of the disc-like structure in a belt-like configuration. The MSP sequence is a highly engineered synthetic gene, optimized for *Escherichia coli* expression and can contain various affinity tags (6xHis, FLAG, Cys, etc.) [304]. There are different MSP sequence lengths that allow controlling the overall nanodisc size [305]. When prepared properly, nanodiscs are uniform in size allowing a native local environment for a chosen membrane protein *in vitro* study.

The membrane in nanodiscs can be composed of different mixtures of phospholipid types as well as other components such as cholesterol. Nanodiscs are the ideal model for membrane protein system with defined size and phospholipid composition [303]. Membrane proteins which function depends on association with cellular lipids, co-factors and additives could be addressed in nanodiscs [306].

The work carried out by Leitz and co-workers illustrates the use of nanodisc for GPCRs [307].

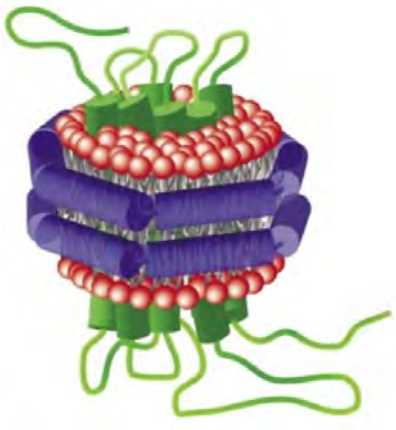

Figure 3.3.: Schematic representation of β2AR assembled in Nanodisc.
Adapted from [307].

Purified and solubilized in detergent the β2AR monomers assembled into Nanodiscs (Figure 3.3). Receptor functionality was confirmed by a ligand binding assay and a functional receptor/G protein complex formation [307].

3.4. Fluorinated Surfactants

New types of surfactants have been designed to keep membrane proteins soluble.

Fluorinated Surfactants were designed based on the observation that alkanes and perfluorinated alkanes while being hydrophobic are poorly miscible [308, 309]. Chemically the fluorinated surfactants looks similar to classical detergents with a hydrophobic tail containing fluorine atoms; they are both hydrophobic and lipophobic [310]. The first Fluorinated Surfactant successfully tested was C6F13C2H4- S-poly-Tris-(hydroxymethyl) aminomethane (F-TAC) (Figure 3.4) [311, 312].

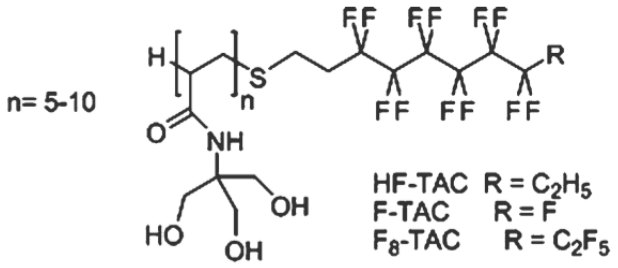

Figure 3.4.: Chemical structure of Fluorinated Surfactant.
For F-TAC the R=F, in case of HF-TAC the R=C_2H_5 [308].

Fluorinated Surfactants alone cannot extract membrane proteins from their membranes. The micellar phase of Fluorinated Surfactants is a poor solvent for lipids and other stabilizing hydrophobic co-factors [308, 313]. Classical detergents used for membrane protein solubilization can be substituted by Fluorinated Surfactants [311]. Fluorinated Surfactants are less aggressive and less efficient than detergents at disrupting protein/protein interactions.

However, perfluorinated chains have little affinity for the hydrogenated transmembrane surface of membrane proteins and are inefficient at keeping them from aggregating. To improve interactions with the protein, a hydrogenated tip was grafted at the end of the fluorinated tail, yielding hemifluorinated surfactants (HFSs) [308, 310].

It was shown that three membrane proteins: bacteriorhodopsin, the transmembrane domain of OmpA and the cytochrome b6f complex remained soluble when transferred in (H)F-TAC. The bacteriorhodopsin and the b6f, were stable when stored in (H)F-TAC, as compared to storage in equivalent concentrations of detergent [311, 312].

Fluorinated Surfactants were used for membrane proteins cell-free synthesis [314, 315] and for their thermodynamic studies [316].

3.5. Amphipols

Amphipols (APol) are small amphipatic polymers. They are highly flexible and remain soluble despite the presence of multiple hydrophobic chains. They can stabilize and keep soluble membrane proteins in aqueous solutions without detergent (Figure 3.5) [317].

Figure 3.5.: Membrane protein trapped in APols.
Cartoon by P.L. Porté.

APols are poorly dissociating surfactants; therefore they are not efficient at solubilizing biological membranes [318, 319]. Usually, membrane proteins are first extracted and purified in buffer containing detergent and then transferred to buffer with APols [317].

Membrane proteins trapped in APols have been implemented in functional and/or ligand binding studies. APols have successfully been used for both β-barrels and α-helical membrane proteins studies. Examples of β-barrel membrane proteins functionally solubilized in APols includes OmpF [320], while the α-helical proteins includes the bacteriorhodopsin (BR) [321, 322], the calcium ATPase [318, 323], the nicotinic acetylcholine receptor (nAChR) [324, 325], followed by several GPCRs trapped in APols which maintained their functionality: rhodopsin [320], the leukotriene receptors 1 and 2 (BLT1 and BLT2) [326], the $5HT_{4(a)}$ serotonin receptor, the CB1 cannabinoid receptor 1, the GHSR-1a ghrelin receptor [326, 327, 328] and the chemokine receptor CCR5 described in this thesis manuscript.

3.5.1. Amphipol A8-35

The first designed and most extensively studied APol is the A8-35 (Figure 3.6) [317, 329, 330]. The A8-35 contains a polyacrylate chain of about 70 residues, in which around 17 carboxylates are grafted at random position with octylamine and around 28 carboxylates with isopropylamine.

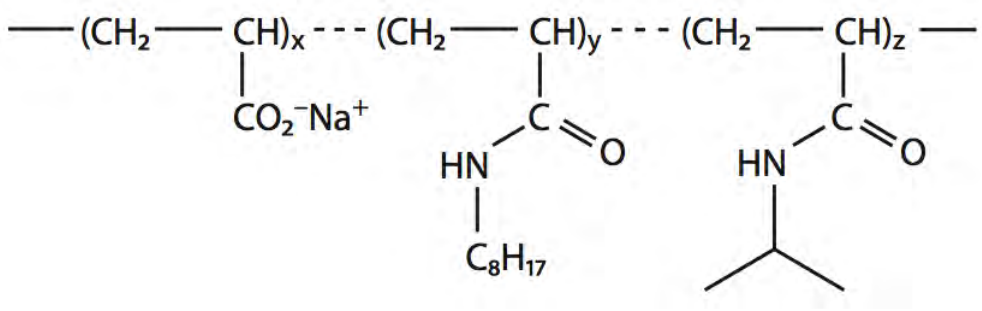

Figure 3.6.: A8-35
Amphipol A8-35 where x, y, and z corresponds to 35, 25, and 40%, respectively [329, 313].

The average MW of A8-35 molecule is 9-10 kDa. A8-35 is highly water-soluble and in aqueous solutions forms well defined, small, globular particles [330]. A8-35 self-assembles into well-defined clusters consisting of four 9-10 kDa macromolecules [321, 330].

Extensive study of the A8-35 led to the discovery of some APol limitations which are important while working with membrane proteins. The solubility of A8-35 depends on the presence of ionized carboxylates, it is highly sensitive to their protonation, as well as to the presence of multivalent cations, in particular of Ca^{2+} ions [318, 331, 330, 329, 323].

To overcome some limitations of A8-35 such as precipitation at pH below 7.0 and in the presence of divalent cations series of new APols have been synthesized including SAPols, PC-APols and NAPols [332, 331, 323].

3.5.2. Non-ionic Amphipol (NAPol)

NAPols are nonionic β-D-glucose-based amphipols. Previously the glucose-based NAPols were synthesized by free-radical co-telomerization of hydrophilic and amphiphilic monomers [333]. Even though it was expected that the hydroxyl groups will provide a good solubility, however, these NAPols had rather poor solubility, which limited their use in biochemistry approaches [333]. Therefore, the strategy of the synthesis was firstly improved by employing the homo-telomerization of a glucosylated acrylamide monomer carrying two hydroxyl groups, onto which undecyl alkyl chains are subsequently grafted through a urethane bond [334, 335]. These glucosylated NAPols were tested using two model membrane proteins: bacteriorhodopsin (BR) and OmpA [334]. It was demonstrated that there was no difference in stability whether the BR was trapped into A8-35 or in NAPol.

The further improvement was achieved by creating new NAPols through free-radical homo-telomerization of an acrylamide-based monomer comprising of C_{11} alkyl chain and two glucose moieties, using a thiol as a transfer reagent (Figure 3.7) [336]. The advantage of this new strategy is that there are less batch-to-batch variations. In this way only one type of monomer undergoes

free-radical polymerization. Thus the reproducibility was improved allowing the larger-scale synthesis [337].

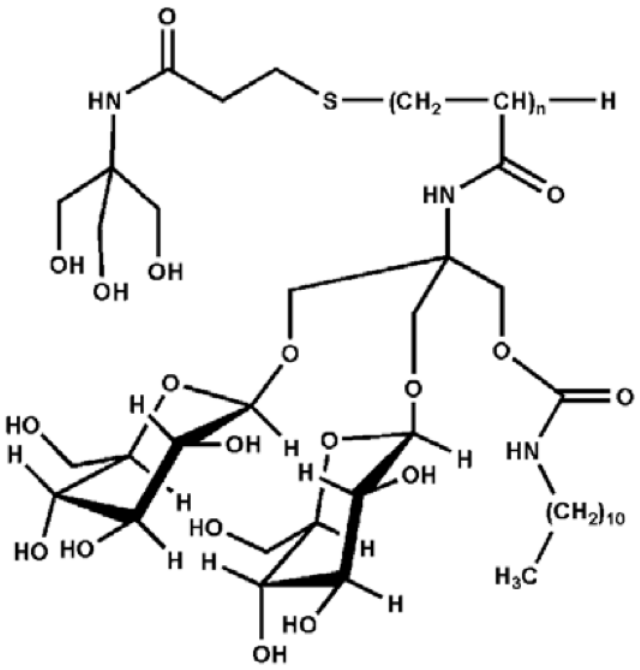

Figure 3.7.: NAPol.
Where n ranges from 9 to 90[336].

New glucosylated NAPols are highly water-soluble molecules. In aqueous buffers they form small, compact, globular particles. The average molecular weight of the NAPols varies from 8 to 63 kDa [336]. NAPol, which is an electrically neutral surfactant, is less aggressive while working with membrane proteins. Membrane proteins trapped in NAPols are suitable for applications, such as NMR, where the overall size of the particles is important [334].

Recently, the studies of the outer membrane protein X from *E. coli* (OmpX), BR and the ghrelin G protein-coupled receptor GHS-R1a stabilized in NAPols were extended to further applications to membrane protein folding, cell-free synthesis and Solution Nuclear Magnetic Resonance [337].

3.5.3. Sulfonated Amphipol

Addressing the A8-35 incompatibility with calcium ions and pH sensitivity the Sulfonated Amphipols (SAPols) were designed (Figure 3.8). SAPols are anionic at any pH, with an average molecular mass of about 11 kDa [323, 332].

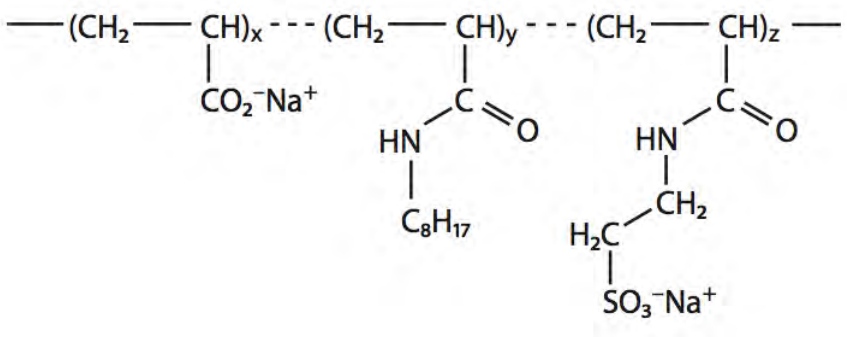

Figure 3.8.: SAPol.
SAPol where x, y, and z corresponds to 35, 25, and 40%, respectively[323, 313]

The ability of SAPols to keep membrane proteins soluble in aqueous solution was tested using two membrane proteins an α-helical membrane protein from *Halobacterium salinarum* the bacteriorhodopsin (BR) and the transmembrane β-barrel domain (tOmpA) of *Escherichia coli* outer membrane protein A [338, 321, 332]. Tested tOmpA/SAPol complex remained soluble and monodisperse at tested pH 6.5 as regards the dispersity of protein/SAPol complexes [332].

SAPols are insensitive to the presence of multivalent cations. The sarcoplasmic reticulum $Ca^{2+}-ATPase$ trapped in A8-35 was stabilized but inactive, trapped in SAPol it remained stable and fully functional [323].

3.5.4. Phosphorylcholine-based Amphipol

New neutral amphipols were developed bearing phosphorylcholine-based (PC) units (Figure 3.9).

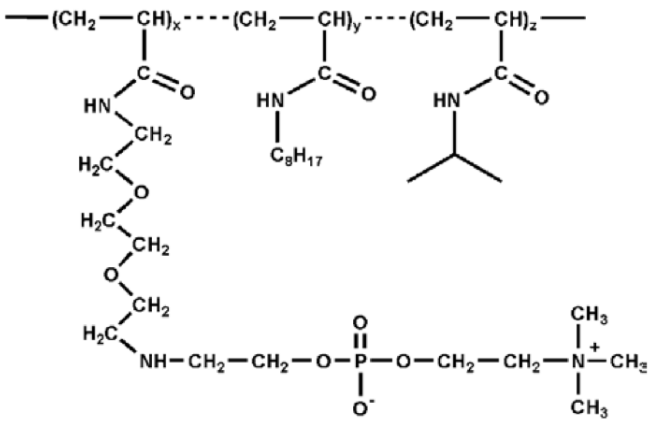

	x	y	z
C45-68:	0.00	0.68	0.32
C60-44:	0.26	0.44	0.30
C60-30:	0.33	0.30	0.37
C22-43:	0.30	0.43	0.27

Figure 3.9.: PC-APol.
[331]

The phosphorylcholine groups ensure PC-amphipol solubility. This type of polar group is highly soluble over a wide range of conditions, including low pH and the presence of divalent ions. In

addition, the phosphorylcholine group is a good mimic of the polar moiety of phosphatidylcholine, which represents a large proportion of membrane lipids in eukaryotic organisms [331].

3.5.5. Labeled Amphipols

APols can be labeled during their chemical synthesis. So far, labeling was applied only to A8-35 and A8-75 (which differs from A8-35 by the absence of isopropyl grafts) [317]. Isotopically labeled APols include ^{14}C-labeled A8-75 and ^{3}H-labeled A8-35, which have been used to follow the distribution of the polymers during fractionation experiments and to quantify their binding to membrane proteins [321, 320, 339].

A A8-35 version where the short-chain parent polymer chain was hydrogenated and isopropylamine and octyl groups were perdeuteriated [329] has been heavily used for SANS, AUC and NMR experiments [326, 340, 321, 330, 329, 341].

3.5.6. Biotinylated Amphipols

A biotinylated version of A8-35 termed BAPol (Figure 3.10) has been used for the immobilization of APol trapped membrane proteins onto solid supports coated with streptavidin (SA) [325]. This allows the study of immobilized membrane proteins for ligand-binding experiments such as Surface Plasmon Resonance (SPR).

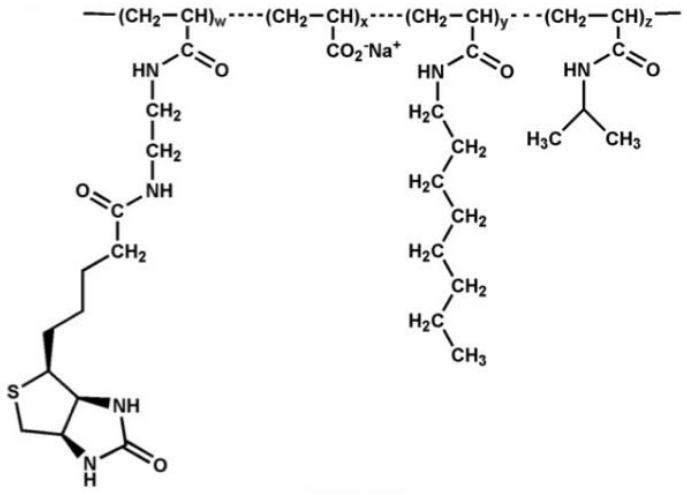

Figure 3.10.: BAPol.
Where w = 0.7% - 1.4%, x = 30% - 35%, y = 21% - 25%, z = 36% - 41% [325].

Membrane proteins trapped in BAPol are stabilized and functionalized for specific immobilization onto surfaces

3.5.7. Fluorescent Amphipols

A fluorescently labeled version of A8-35 has been synthesized (FAPol) in order to study the size and dispersity of membrane proteins and APols complexes and understand the dynamics of their interactions (Figure 3.11) [338].

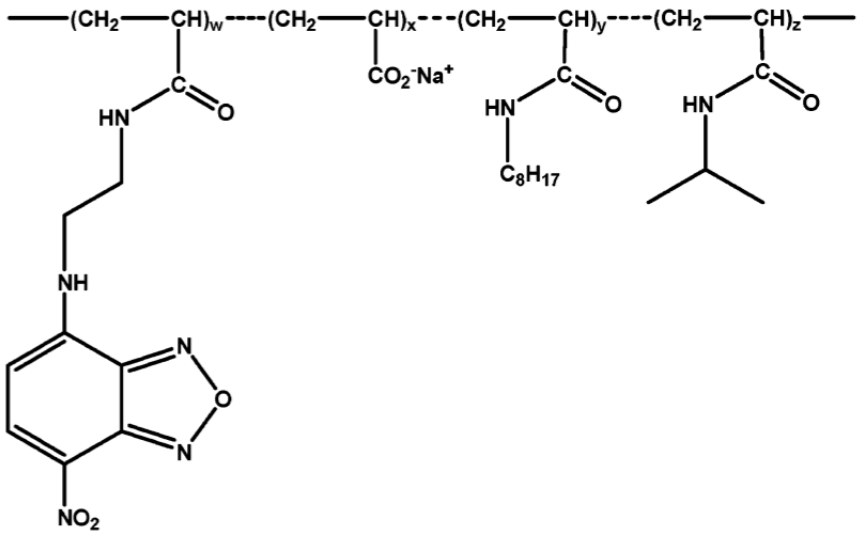

Figure 3.11.: FAPol.
Where x=35%, y=23.5% and z=34% [338].

First of all the A8-35 carrying a reactive arm (UAPol, non-fluorescent precursor of fluorescent amphipol) was synthesized to which any desirable label could be bound. The subsequent binding of NBD (7-nitrobenz-2-oxa-1, 3- diazol-4-yl) yielded a fluorescent amphipol (FAPol) (Figure 3.11).

NBD was chosen as the fluorophore for its low absorbance at 280 nm. Using FRET it could be excited through tryptophans which are acting as donors. As NBD is weakly hydrophobic it is a good reporter for the APol backbone.

Upon being trapped with such APols, any membrane protein become noncovalently but permanently functionalized, without having to be genetically or chemically modified [338]. FAPols have been used in FRET experiments [338].

3.6. Applications for amphipols

Initially developed for membrane protein solubilization and stabilization in the recent years some applications for amphipols have been developed. Membrane proteins trapped in amphipols have been studied by size exclusion chromatography, equilibrium and sedimentation velocity analytical

ultracentrifugation (AUC), dynamic and static light scattering, small angle X-ray scattering (SAXS), Small Angle Neutron Scattering (SANS), Förster Resonance Energy Transfer (FRET) and solution NMR Inelastic Neutron Scattering (INS) [313, 328].

Folding membrane proteins to their native state

Targeting the over-expression of membrane proteins towards *E. coli* inclusion bodies allows large amounts of protein production. However, folding those inactive membrane proteins into their native state is difficult. Several GPCRs were successfully folded *in vitro* using detergents, detergent/lipid mixtures or lipid vesicles.

Some GPCRs have been produced in *E. coli* as inclusion bodies, purified and solubilized in detergents such as SDS [342, 327, 104]. Receptors folding in amphipols were achieved by supplementing the SDS solution with either A8-35 or A8-35–lipid mixture. The SDS was removed by precipitation with KCl followed by dialysis (Figure 3.12) [322].

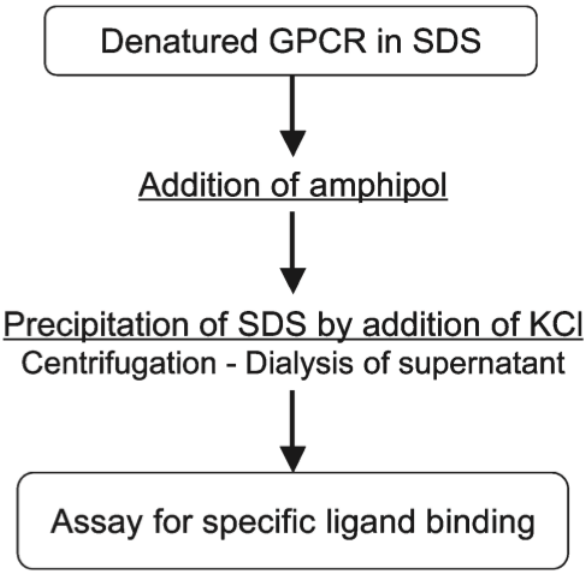

Figure 3.12.: Schematic representation of GPCR folding and functional assay.
Adapted from [327].

The amount of ligand-binding competent receptor obtained after folding the SDS-unfolded receptors in fos-choline-16/asolectin (D + L), A8-35 (AP), and A8-35 plus asolectin (AP + L) was compared for four GPCRs: leukotriene BLT1, serotonin 5-HT4(a), leukotriene BLT2, and cannabinoid CB1 receptors (Figure 3.13).

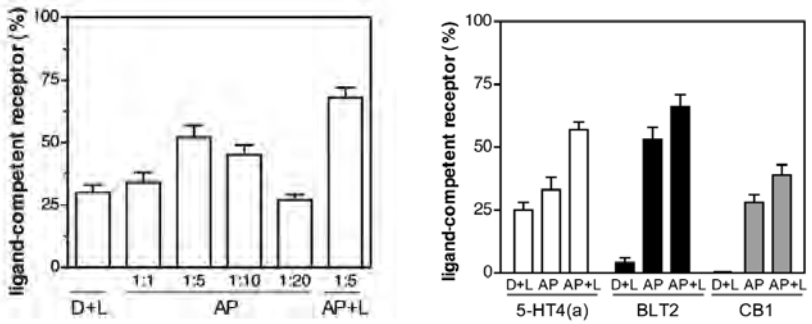

(a) (b)

Figure 3.13.: Amphipol assessed GPCRs folding.
(A) Comparing the folding of leukotriene BLT1 receptor in fos-choline-16/asolectin (D+L) and in A8-35 at increasing amphipol/protein ratios (AP), and in A8-35 in the presence of asolectin (1:5:1 protein/amphipol/asolectin weight ratio; AP+L). (B) Folding of serotonin 5-HT4(a), leukotriene BLT2, and cannabinoid CB1 receptors in detergents or A8-35 and lipids. Adapted from [327].

In case of leukotriene BLT1 receptor the use of A8-35 increased the amount of functional receptor comparing to folding in detergent. The receptor/amphipol ratio is important as using not enough or too much amphipol can dramatically decrease the amount of functional receptor. The addition of lipids to the amphipol mix increased the receptor-folding yield to 65-70 %. The most advantageous use of A8-35 versus detergents is shown in Figure 3.13b. After folding in detergent only 5% of leukotriene BLT2 receptor was able to bind its ligand, while using A8-35 with or without lipids 60-75% of functional receptor was obtained. Results obtained with cannabinoid CB1 receptor were even more interesting since functional refolding could only be obtained with amphipols.

Besides folding in amphipols enhanced receptor thermostability (Figure 3.14).

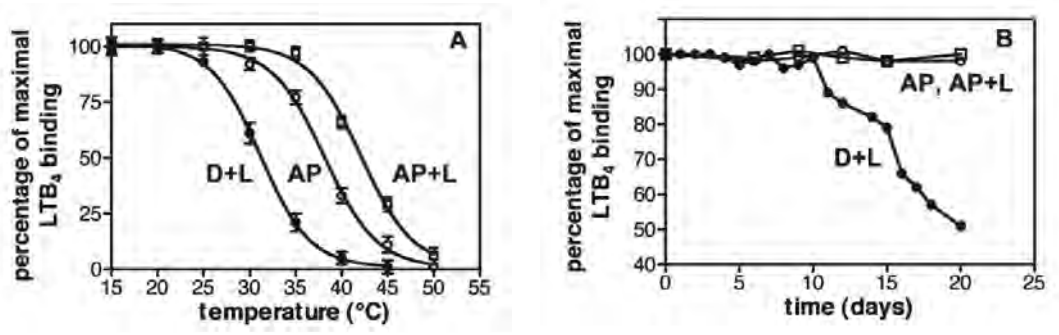

(a) (b)

Figure 3.14.: Stability of BLT1 trapped in A8-35.
The temperature (A) and time-dependent (B) stability of leukotriene BLT1 receptor folded in amphipols (1:5 protein/amphipol weight ratio; AP), and amphipols plus lipids (1:0.2 amphipol/lipid weight ration; AP + L), compared to that of BLT1 folded in fos-choline-16/asolectin mixed micelles (2:1, w/w; D + L) . Adapted from [327].

BLT1 thermostability and time stability were tested using ligand-binding assay. In the Figure 3.14 shows that BLT1 folded in amphipols and in the amphipol/lipid mixture is able to bind the ligand at higher temperature and retain its functionality over 20 days.

Cell-free Synthesis of Membrane Proteins

Not all APols are suitable for cell free synthesis. It has been reported that both A8-35 and SAPols inhibit the synthesis of membrane proteins [315]. Great results were obtained when NAPol was used for barteriorhodopsin synthesis. Using NAPol the yield of protein synthesis was higher and more reproducible than that observed while using DDM [337]. Also the majority of the protein remained soluble over several months in NAPols while in DDM it tended to precipitate[337]. The use of NAPol for the cell-free synthesis could be applied to GPCRs.

Immobilizing Membrane Proteins onto Solid Supports for Ligand-Binding Studies

The immobilization of BAPol-trapped membrane proteins could be achieved on streptavidin-coated chips or beads. Trapping membrane proteins with APols does not interfere with ligand biding (Figure 3.15) [325].

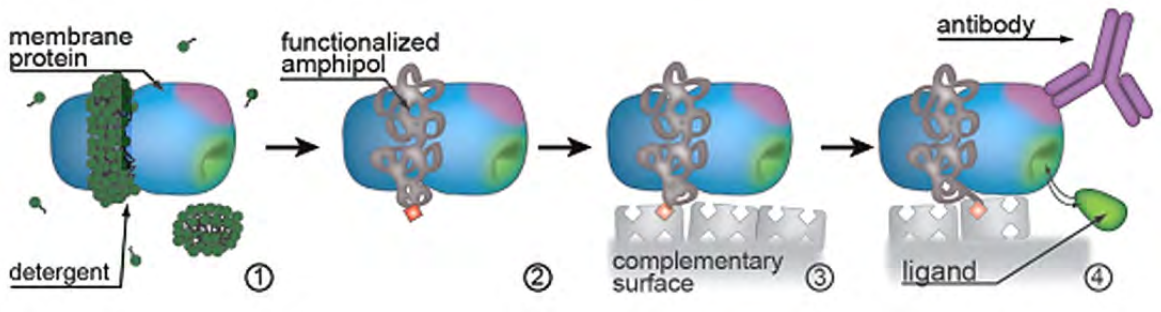

Figure 3.15.: Immobilization of BAPol trapped membrane protein.
Membrane protein solubilized in detergent (1) is transferred to BAPol. The complex (2) is applied to a support, which exposes a functional streptavidin group to which BAPol can associate (3). Protein ligands are applied (4) and their interaction can be detected by any convenient method. Adapted from [325].

This strategy of immobilization presents several advantages. Once the protein is successfully folded in BAPols their association is irreversible as long as amphipols are not displaced by another surfactant. Protein/amphipol complex resists to the extensive washes with surfactant-free buffer therefore there is no need to supply the buffers with amphipols.

BAPol mediated immobilization should be more favorable to the ligand binding assays than classical amine coupling. The latter one is non-specific and it cross link the proteins via their NH_2 groups leading to a random orientation of the proteins and could impair the access to the

ligand-binding sites. Immobilization via BAPol should offer a more accessible ligand-binding site and facilitate the interaction with the tested analyte.

Trapping a membrane protein with a functionalized APol therefore results in a permanently functionalized complex. This way functionalized membrane proteins are suitable for the ligand binding studies as the ligand binding site is exposed and accessible [325, 328, 308].

Other APol applications

Membrane proteins trapped in APols are suitable for many other applications.

Fragile membrane proteins and their super-complexes trapped in amphipols could be used for electron microscopy studies [343, 344, 345].

APols could be used for the membrane protein delivery to pre-existing membranes. APols do no lyse target membranes (lipid vesicles or black films, cell plasma membrane) and can therefore be used to deliver to them hydrophobically charged proteins such as membrane proteins [328, 322, 346, 316].

Usually for membrane proteins the solution NMR conditions are highly aggressive. The A8-35 and sulfonated A8-35 - SAPol stabilize membrane proteins at higher temperatures. Another advantage is that A8-35 and SAPol are easier to deuterate than most detergents. A8-35 aggregates at pH < 7, preventing the study of solution-exposed amide protons, while the pH insensitive SAPol overcome that limitation [340, 326, 347, 348, 332, 349, 350, 341].

The mass spectrometry analysis of APol trapped membrane proteins along with weakly bound partners could be useful to identify membrane protein bound lipids and co-factors, that tend to dissociate in detergent solutions [322].

4. Objectives

Since its discovery in the XIXth century, for a long period of time, rhodopsin was the GPCR the most studied by scientists. In the late XXth century other GPCRs were extensively studied at the cellular level and their interaction with G proteins was discovered. Molecular studies have been until recently hindered by the difficulty to express and purify GPCRs. Recently the first GPCR structure from recombinant source has been obtained and now more than 30 structures of almost ten different GPCRs are known. Most of these GPCRs were produced using insect cell expression system, which is an expensive system and is not affordable for many laboratories. To allow expression the proteins were highly modified with many mutations and insertions. The expressed GPCRs were so highly modified that they were far from the natural proteins. Despite this breakthrough at the structural level, functionality was assessed only for a few of those modified GPCRs. High amounts of purified, stable and functional receptor would open the way to studies at the molecular level such as: receptor dimerization, stoichiometry of receptor/ligand complex, interactions with intracellular proteins such as G proteins, β-arrestins and others. Therefore, there is still need for alternative production protocol where GPCRs would be expressed in high yield, functional and with minimal amount of modifications.

Corinne Vivès, in the team of Franck Fieschi has been already working on alternative expression strategies for CCR5 and CXCR4. CXCR4 and CCR5 genes were optimized for *E. coli* expression to avoid the limitation due to rare codons. To circumvent the toxicity linked to membrane protein expression, the collaboration with the group of J.-L. Banères and B. Mouillac (Montpellier) led to the design of fusion proteins targeting the expression to *E. coli* inclusion bodies [104]. With this fusion and inclusion body strategy we could access to high yields of purified receptors. The receptor production was already started to be developed and its folding was assessed with detergents and amphipols. It was shown that only a small amount of receptor was maintained soluble in detergent solution where only 4% of it was functional. Folding in amphipols gave promising results, higher amount of receptor was solubilized, but its functionality was not yet assessed. Therefore, the receptor folding using alternative methods to detergents, the amphipols, developed by J.-L. Popot (Paris), will be attempted [317].

To assess the functionality of folded receptor we needed to produce their functional ligands. Therefore, the first step of my work was to produce functional CXCR4 and CCR5 ligands: SDF1α (specific for CXCR4) and RANTES (specific for CCR5). Once chemokines will be produced it is essential to confirm that they are functional. Collaboration with C. Moreau and

M. Vivaudou (IBS, Grenoble) was established which allows us to test chemokine functionality independent of receptor folding. Therefore, receptor binding and signaling will be assessed using an electrophysiology recording strategy.

Once the production of functional ligand will be established, I will concentrate on the initial goal of the project – on the functional GPCR production. I will produce CCR5 and CXCR4 using *E. coli* inclusion body production strategy and their folding in amphipols will be assessed. Several different amphipols will be tested as well as the presence of lipids will be investigated on the receptor folding impact. Folded receptor functionality will be tested at the molecular level by setting up an interaction with their ligands using Surface Plasmon Resonance (SPR) technique.

The access of high yields functional GPCRs and their ligands will open the ways for further investigations at the molecular level and in solution studies of those GPCRs in complex with their ligands to reply to remaining unanswered questions such as the complex stoichiometry.

5. Résumé de l'introduction et des objectifs en français

Depuis sa découverte au 19ème siècle, et pendant une longue période, la rhodopsine était le récepteur couplé aux protéines G (RCPG) le plus étudié par les scientifiques. Récemment, d'autres RCPGs ont été étudiés au niveau cellulaire et leurs interactions avec les protéines G ont été mises en évidence. Les études moléculaires ont été jusqu'à récemment entravées par les difficultés à produire et purifier les RCPGs. Récemment, la première structure de RCPG recombinant a été obtenue, et actuellement, plus de 30 structures de 10 RCPG différents sont connues. La plupart de ces RCPGs ont été produits avec des systèmes d'expression utilisant des cellules d'insectes, or ces systèmes sont onéreux et ne peuvent être utilisés par tous les laboratoires. Pour permettre l'expression, les protéines sont modifiées de manière importante avec un grand nombre de mutations et d'insertions. Les RCPGs produits sont ainsi parfois très éloignés des protéines naturelles. Malgré cette avancée au niveau structural, la fonctionnalité a été évaluée seulement pour quelques uns des RCPGs modifiés. Une grande quantité de récepteurs purifiés, stables et fonctionnels pourrait permettre des études au niveau moléculaire comme la dimérisation des récepteurs, la stœchiométrie du complexe récepteur/ligand, les interactions avec les protéines intracellulaires comme les protéines G, les β-arrestins ou autres. Ainsi, il est nécessaire de trouver des moyens de production alternatifs permettant d'obtenir des RCPG fonctionnels en grande quantité, avec un minimum de modifications.

Les récepteurs de chimiokines sont des régulateurs essentiels de la migration des cellules dans le cadre de la surveillance immunitaire, l'inflammation et le développement. Les RCPGs, CCR5 et CXCR4, sont spécifiquement impliqués dans de nombreux cancers et l'infection par le VIH-1. L'entrée du VIH dans les cellules cibles nécessite l'interaction sequentielle de la protéine virale gp120 avec CD4 (récepteur primaire) et un co-récepteur, CCR5 ou CXCR4 pour respectivement les virus M- et T-tropique.

Depuis plusieurs années, il a été montré que les chimiokines RANTES et MIP1-α (ligands naturels de CCR5) ont la possibilité de bloquer la réplication du VIH dans les expériences de laboratoire [351]. Ceci s'explique par le fait que les chimiokines entre en compétition avec le VIH dans la liaison au récepteur et aussi déclencher l'internalisation du récepteur et sa disparition de la surface cellulaire. Les récepteurs de chimiokines représentent donc une cible thérapeutique pour bloquer l'infection par le VIH.

Corinne Vivès, dans l'équipe de Franck Fieschi travaille depuis plusieurs années sur une stratégie alternative d'expression de CCR5 et CXCR4. Les codons rares des gènes CXCR4 et CCR5 ont été optimisés afin de faciliter l'expression des protéines chez *E. coli*. Pour éviter la toxicité liée à l'expression des protéines membranaires, une collaboration avec le groupe de J.-L. Banères et B. Mouillac (Montpellier) a permis de concevoir des protéines de fusion permettant l'adressage vers les corps d'inclusion d' *E. coli* [104]. Grace à cette stratégie, nous avons pu obtenir un rendement élevé de récepteurs purifiés. Le repliement de ces récepteurs obtenus en conditions dénaturantes avait été avait testés avec des détergents et des amphipoles développés par J.-L. Popot (Paris). Il avait été démontré que seulement une petite quantité des récepteurs était maintenu soluble par les détergents et que seulement 4% de ces récepteurs étaient fonctionnels. Le repliement en présence d'amphipoles donnait des résultats prometteurs, une plus grande quantité de récepteurs était soluble, mais la fonctionnalité n'avait pas été évaluée. C'est sur ces approches alternatives (repliement en amphipoles) que nous souhaitions nous concentrer [317].

Pour évaluer la fonctionnalité du récepteur replié, nous avions besoin de produire des ligands fonctionnels. Ainsi, la première étape de mon travail a été de produire les ligands de CXCR4 et CCR5: SDF1α (ligand spécifique à CXCR4) et RANTES (Ligand spécifique à CCR5). Une fois les chemokines produites, il était essentiel de confirmer leur fonctionnalité. Une collaboration avec C. Moreau and M. Vivaudou (IBS, Grenoble) fut établie et nous a permis de tester la fonctionnalité des chemokines indépendamment du repliement du récepteur. Ainsi, les interactions et la signalisation du récepteur ont été évaluées en utilisant une stratégie d'enregistrement électro-physiologique et chimiotactisme.

Un fois la production du ligand fonctionnel établie, je me suis concentrée sur le but premier du projet, la production du RGPGs. J'ai produit les protéines CCR5 et CXCR4 (you did not produce CXCR4) en utilisant la production en corps d'inclusion chez *E. coli* et le repliement en amphipoles. Différents amphipols ont été testés et l'impact de la présence de lipides sur le repliement a été évaluée. La fonctionnalité du récepteur replié a été testée en étudiant l'interaction avec les ligands en utilisant la résonance des plasmons de surface.

L'accès à des rendements élevés de RCPG fonctionnels et de leurs ligands ouvrira la voie à de futures études en solution de RCPG en complexe avec leur ligand, ce qui permettra de répondre à des questions encore ouvertes telles que la stœchiométrie du complexe.

Part II.

Materials and methods

6. Materials

6.1. Product lists

***E. coli* strain**	**Company**	**Reference**
BL21(DE3)	Novagene	70235-3
Rosetta2 (DE3)	Novagene	71400-3
Top 10	Invitrogen	C4040-03
XL 10 Gold	Agilent	200315

Table 6.1.: Bacterial strains.

Product	**Company**	**Reference**
Quick change site-directed mutagenesis kit	Stratagene	200519.5
Mass ruler DNA Ladder Mix	Frementas	SM0403
HiSpeed Plasmid Midi kit	Qiagen	12643
QiaQuick gel extraction kit	Qiagen	28704
QiaPrep Spin Mini-prep kit	Qiagen	27106
Pfu turbo	Stratagene	600250-52
Ultra Pure Agarose	Invitrogen	15510-019
Rapid DNA Ligation kit	Fermentas	K1422
PCR Purification kit	Qiagen	28106
PCR Master Mix	Fermentas	K0171
QuikChange XL Site-Directed Mutagenesis Kit, 30 rxn	Agilent	200516

Table 6.2.: Products for Molecular Biology.

Product	**Company**	**Reference**
Ni-NTA superflow resin	Qiagen	30430
Glutathione Sepharose High Performance	Amersham	17527901
HiTrap Capto S 5ml	GE Healthcare	17-5441-22
HiTrap Capto Q 5ml	GE Healthcare	11-0013-02
Superdex 200 prep grade 150 ml	GE Healthcare	17-1043-01
PD 10 (desalting) Columns	GE Healthcare	17-0851-01
Amylose resin	NEB Ozyme	E80215
Ecno_Pac chromatography columns (empty)	Biorad	732-1010
Strep Trap HP 5 ml	GE Healthcare	28-9075-47

Table 6.3.: Columns and resins.

Product	Company	Reference
Anti-His Antibody	Amersham	27471001
Strep-Tactin horseradish peroxidase (HRP) conjugate	IBA	2-1502-001
Monoclonal anti-polyhistidine peroxydase conjugate	Sigma	A7058-1VL
Anti-Rhodopsin, C-terminus, last 9 amino acids, clone Rho 1D4	Millipore	MAB5356

Table 6.4.: Antibodies.

Product	Company	Reference
Amicon Ultra 4, 10 kDa	Millipore	UFC801024
Amicon Ultra 3K 15 ml	Dutscher	UFC900324
Dialysis Membrane 12-14,000	Spectrum Laboratories, Inc.	059026
Filter 0.2 µm	Dutscher	146560
Membrane MCE 0.22 µm	Dutscher	044121

Table 6.5.: Concentrators and membranes.

Product	Company	Reference
SDS 20%	Euromedex	151-21-3
Acrylamide	Euromedex	EU0088-B
Unstained Protein Ladder	Fermentas	SM0661
Pre-stained Protein Ladder	Fermentas	SM0671
Immunoblot PVDF membrane	Bio-Rad	162-0177
Trans-Blot Nitrocellulose membrane	Bio-Rad	162-0097
SIGMAFAST™ 3,3´-Diaminobenzidine tablets	Sigma	D4168
Paper Blotting Whatman 3mm CHR 460 x 570	Dutscher	036347
Ammonium persulfate (APS)	Sigma	A3678
TEMED	Euromedex	50406
Brilliant blue R	Sigma	B7920

Table 6.6.: Materials for gels.

Product	Company	Reference
Sensor Chip CM4	GE Healthcare	BR-1005-39
Amine coupling kit	GE Healthcare	BR-1000-50
Sensor Chip SA	GE Healthcare	BR-1000-32
Sensor Chip NTA	GE Healthcare	BR-1004-07
HBS-N	GE Healthcare	BR-1003-69

Table 6.7.: SPR products.

Product	Company	Reference
Ampicillin	Euromedex	EU0400-D
Choramphenicol	Sigma	C0378
LB Broth (Lennox)	AthenaES	0102
LB agar	Sigma	L2897
Glucose	Athenaes	0108
IPTG	Euromedex	EU0008c
Complete EDTA-free	Roche	11873580001
Na_2HPO_4	Sigma	S0876
NaH_2PO_4	Sigma	S0751
Acetic acid	Sigma	33209
Sodium acetate	Euromedex	EU0310
HABA	Sigma	HS126
DTT	Fluka	43817
L-Glutathione reduced	Sigma	G4251
L-Glutathione oxidized	Sigma	G4376
DNase	Euromedex	1307
Factor Xa protease	Qiagen	33223
Thrombin	Sigma	T6884
Asolectin	Sigma	11145
Tricine	Sigma	T0377
Triton X-100	Anatrace	T1001
EDTA	Euromedex	EU0007
Tris-HCl	Euromedex	26-128-3094-B
KCL	Euromedex	P017
Guanidine hydrochloride	Euromedex	EU0045
D-Desthiobiotin	Sigma	D-1411
Maltose	Sigma	M5885
HEPES	Sigma	H4034
NaCl	Euromedex	1112-A
Imidazole	Sigma	56749
NaOH	Euromedex	2020
KH_2PO_4	Sigma	P0662
K_2HPO_4	Sigma	P5504
β-Mercaptoethanol	Carl Roth GmbH + Co. KG	4227
$CaCl_2$	Sigma	C5080
Urea	Sigma	51456
Ethanol	Carlo Erba	528151
HCl 37%	OM Group	CAS-7647-01-0
Terbium	Sigma	204560
RTS 100 *E. coli* HY Kit	5 PRIME	2401100

Table 6.8.: Biochemistry Products.

7. Methods

7.1. Chemokine production

7.1.1. Molecular biology

7.1.1.1. MBP chemokine construct preparation

Optimized synthetic human chemokine genes encoding SDF1α, RANTES and RANTES-LT designed for efficient production in *E. coli* cloned in standard pUC57 plasmids were ordered from GeneCust (Evry, France) (sequences are listed in the Appendix 18). One construct contained an additional double Lanthanoid Binding Tag (LT) in the C-terminal part of the protein [352].

The pUC57 plasmid containing SDF1α was digested using XbaI and BamHI enzymes. The pUC57 plasmid containing RANTES was digested using BamHI enzyme. The pUC57 plasmid containing RANTES-LT was digested with BamHI and SalI. The pMAL-c4x vector was digested with BamHI, BamHI/XbaI and BamHI/SalI enzyme pairs. Digested chemokine sequences were purified from the 1% agarose gel using Qiagen gel extraction kit. Each chemokine was ligated into expression vector using Rapid DNA Ligation kit resulting in MBP-Xa-SDF1α-Strep, MBP-Xa-RANTES-Strep and MBP-Xa-RANTES-LT-Strep. The Top 10 calcium-competent cells were transformed with ligation reaction products. Mini-preps were prepared for each construct and sequences were verified by sequencing (Beckman Coulter Genomics).

Factor Xa cleavage site was replaced by Prescission protease cleavage site by site directed mutagenesis. New created constructs were named MBP-PrePro-RANTES-Strep, MBP-PrePro-RANTES-LT-Strep and MBP-PrePro-SDF1α-Strep.

The double Lanthanoid Binding Tag was added to the SDF1α construct by multiple PCRs (sequences of primers are listed in the Appendix 17). First, the LT sequence was amplified using MBP-PrePro-RANTES-LT-Strep as a DNA template with a SDF-LT-fw and M13RV primers. With the second PCR, the SDF sequence was amplified using MALE-Fw and SDF-LT-rv primers and the MBP-PrePro-SDF-Strep clone as a DNA template. For the third PCR both results from the previous two PCRs were mixed and used as a DNA template with the MALE-Fw and M13RV primers. The product of the latter PCR (SDF1α-LT-Strep sequence) was digested with HindIII and EcoRI enzymes and cloned into pMAL-c4x expression vector previously digested

with the same enzyme pair. The new created construct was named MBP-PrePro-SDF1α-LT-Strep (sequences are listed in the Appendix 18).

7.1.1.2. Constructs for the chemokine expression in *E. coli* inclusion bodies

The cDNA encoding chemokine sequences was amplified by PCR using MBP-chemokine constructs as templates with primers (see in Appendix 17) and sub-cloned into the pET-20b expression plasmid. Chemokine constructs were prepared with or without the LT. The SDF1α clones contained C-terminal non-cleavable polyhistidine tag or Strep-Tag, which can be cleaved by PreScission protease (SDF1α-His, SDF1α-LT-His, SDF1α-PrePro-Strep, SDF1α-LT-PrePro-Strep).

SDF1α-His was prepared by PCR using pc4X-SDF as a template with primers SDF-NdeI and SDF-XhoI. SDF1α-LT-His was prepared by PCR using pc4x-SDF-LT as a template with primers SDF-NdeI and SDF-LT-XhoI.

Three RANTES constructs were prepared, where one had a C-terminal Strep-Tag (RANTES-Strep), the second one was the same construct with LT (RANTES-LT-Strep) and the last construct did not contained any tags (RANTES). All cloned DNA sequences were verified by sequencing (Beckman Coulter Genomics) (sequences are listed in the Appendix).

7.1.2. MBP-chemokine expression

The *E. coli* BL21 (DE3) calcium-competent cells were transformed with plasmids bearing chemokine constructs and selected on ampicilin containing Luria Bertani (LB)-agar Petri dishes. A single colony was isolated and a 10 ml pre-culture of Luria Bertani (LB) medium containing 100 μg/ml ampicilin was prepared. One liter of LB medium containing 100 μg/ml ampicilin was inoculated with 5 ml of overnight culture and grown at 37°C to an absorbance at 600 nm of 0.6 to 0.8. The recombinant protein expression was induced by addition of IPTG to a final concentration of 1 mM for the MBP constructs, SDF1α-His, SDF1α-LT-His, SDF1α-Strep, SDF1α-LT-Strep and RANTES-LT-Strep and 0.5 mM for RANTES and RANTES-Strep. Cells were further incubated for 3 h at 37°C (SDF1α-His, SDF1α-Strep, RANTES-Strep, RANTES) or 16 h at 20°C (MBP constructs, SDF1α-LT-His, SDF1α-LT-Strep, RANTES-LT-Strep). Cultures were harvested by centrifugation for 30 min at 5 000 g using Sorvall Evolution RC Superspeed Centrifuge with the rotor SLC6000 (Kendro laboratories). The purification of the recombinant proteins was proceeded immediately or bacterial pellet were stored at -20°C.

7.1.3. MBP-chemokine purification

The bacterial pellet was resuspended in 50 ml of lysis buffer containing 100 mM Tris-HCl pH 8.0, 150 mM NaCl, 1 mM EDTA and supplemented with 1 tablet of Complete Protease Inhibitors.

Bacterial pellet was disrupted twice using a Microfluidizer M-110P (Microfluidics international, Newton, MA) at 10 000 psi. After ultracentrifugation for 45 min at 20 000 g, the supernatant was filtered and loaded to the Strep-Trap column (5 ml) at 4°C previously equilibrated in 20 mM HEPES pH 8.0, 150 mM NaCl buffer. Recombinant protein was eluted with the same buffer containing 2.5 mM desthiobiotin. Purified MBP-fusions were cleaved with the PreScission protease (1.75 U protease/mg of fusion proteins) overnight at 4°C. Sample was centrifuged for 45 min at 20 000 g. To eliminate the GST tagged PreScission protease the supernatant was loaded on the GST-Sepharose column equilibrated in the same 20 mM HEPES pH 8.0, 150 mM NaCl buffer. The flow-through containing the protein of interest was collected and loaded to an Amylose column to eliminate MBP proteins. Amylose column was previously equilibrated in 20 mM HEPES pH 8.0, 150 mM NaCl buffer. The flow-through containing the protein of interest was collected and concentrated up to a volume of less than 2 ml. Further chemokines were purified on gel filtration Superdex 200 column in 20 mM HEPES pH 8.0, 150 mM NaCl buffer. Proteins were concentrated using 3 kDa cut-off concentrator and stored at –80°C.

7.1.4. Chemokines purification from *E. coli* inclusion bodies

7.1.4.1. Preparation of inclusion bodies

Bacterial pellet were resuspended in 50 ml of 50 mM Tris-HCl pH 8.0 (buffer A) supplemented with 1 tablet of Complete EDTA-free Protease Inhibitors and bacterial pellet was disrupted twice using a Microfluidizer M-110P (Microfluidics international, Newton, MA) at 10 000 psi. After centrifugation for 30 min at 20 000 g, inclusion bodies were pelleted and washed with buffer A supplemented with 2 M Urea and 5 % Triton X-100, then with buffer A containing 2 M Urea and finally with only buffer A.

7.1.4.2. SDF1α-His, SDF1α-Strep purification and refolding

Inclusion bodies were solubilised in 50 ml of 50 mM Tris-HCl pH 8.0 (buffer A) with 7.5 M guanidine hydrochloride (GuHCl) and 20 mM DTT by incubating for 20 min at 50°C. Refolding was performed by rapid dilution in buffer A up to 1 M GuHCl . The mixture was gently stirred overnight at 4°C after addition of Complete protease inhibitors, diluted 4 times with buffer A and loaded onto a 5 mL Capto S column equilibrated in 50 mM Tris-HCl pH 7.5. Chemokines were then eluted with a linear NaCl gradient (0-1 M, length 25 ml), concentrated and further purified on a gel filtration Superdex 200 column (Amersham Biosciences) previously equilibrated in 20 mM Na_2HPO_4 pH 6.0. Purified proteins were analyzed by ion-spray mass spectrometry and stored at –80°C.

7.1.4.3. Rantes-Strep and RANTES purification and refolding

Inclusion bodies were solubilized in 50 mM Tris-HCl pH 8.0, 6 M GuHCl and 1 mM DTT incubating 30 min at 60°C. Sample was centrifuged for 20 min at 29 434 g and dialyzed against 4 liters of 1% acetic acid for 3 hours at room temperature. Protein sample was centrifuged at 29 434 g for 30 min. The supernatant was filtered using 0.2 µm filter and concentrated. Protein sample was then diluted up to 1 mg/ml final concentration in the 50 mM Tris-HCl pH 8.0, 6 M GuHCl, 1 mM DTT buffer. Refolding was performed by 10 fold dilution of protein sample into 20 mM Tris-HCl pH 8.0, 0.01 mM oxidized glutathione, 0.1 mM reduced glutathione overnight at 4°C with gentle stirring. Refolded protein was centrifuged for 20 min at 29 434 g and the pH of the supernatant was adjusted to 4.5 with acetic acid. Sample was filtered using 0.2 µm filter and loaded onto CaptoS column (GE Healthcare) previously equilibrated in 50 mM Na-Acetate pH 4.5 buffer. Chemokines were then eluted with a linear NaCl gradient (0-2 M, length 25 ml). Fractions containing chemokines were pooled, concentrated and further purified on a gel filtration Superdex 200 column (Amersham Biosciences) previously equilibrated in 20 mM Na-Acetate pH 6.0, 150 mM NaCl. Purified proteins were concentrated using 3 kDa cut-off Amicon concentrator and stored at –80°C until use.

7.1.4.4. SDF1α-LT-His, SDF1α-LT-Strep and RANTES-LT-Strep purification and refolding

Inclusion bodies were solubilized by rotation on a wheel for 1 h at room temperature in 100 mM Tris-HCl pH 8.0, 6 M Urea, 100 mM NaCl, 0.5 mM EDTA, 5 mM DTT buffer. Sample was centrifuged at 29 434 g for 20 min. Refolding was achieved by drop-wise 100 fold dilution of the supernatant in 100 mM Tris-HCl pH 8.0, 0.5 mM EDTA, 0.1 mM oxidized glutathione and 1 mM reduced glutathione buffer. The refolding solution was stirred overnight at 4°C. Sample was centrifuged at 29 434 rpm for 20 min. Supernatant was loaded onto a 10 mL Q-Sepharose column (Amersham Biosciences) previously equilibrated in 50 mM Tris-HCl pH 8.0. Chemokines were eluted with a 0-100% linear 50 ml length gradient of 50 mM Tris-HCl pH 8.0, 1 M NaCl buffer. Fractions containing the refolded chemokines were pooled, concentrated and further purified on a gel filtration Superdex 200 column equilibrated in 50 mM Tris-HCl pH 8.0, 150 mM NaCl buffer. Purified proteins were concentrated using 3 kDa cut-off Amicon Ultrafree and stored at –80°C until further use.

7.2. Receptor production

7.2.1. Expression

The *E. coli* Rosetta2 (DE3) strain were transformed with the pET-21a-α5I-CCR5 expression vector (sequence is listed in the Appendix 18) following the manufacturer's (Novagen) instructions

and grown overnight at 37°C on LB-agar plates containing 100 μg/ml ampicillin. An isolated colony was picked from the plate and the bacteria were grown in 5 ml of LB broth containing 100 μg/ml ampicillin at 37°C overnight. This pre-culture was used to inoculate 100 ml of LB medium containing 100 μg/ml ampicillin and 37 μg/ml chloramphenicol and grown overnight at 37°C. 15 ml of the pre-culture were used to inoculate 1 liter of LB medium supplemented with 100 μg/ml ampicillin and 34 μg/ml chloramphenicol, and bacteria were grown at 37°C until the OD_{600} nm reached 1. Then, 0.2 % glucose and 1 mM IPTG were added to the culture to induce expression of the recombinant proteins. Bacteria were harvested 4 hours later, pelleted by centrifugation for 15 min at 4 000 g using Sorvall Evolution RC Superspeed Centrifuge with the rotor SLC6000 (Kendro laboratories) and stored at – 80°C.

7.2.2. Extraction and purification

The cell pellet was thawed and resuspended in 30 ml of ice-cold lysis buffer containing 50 mM NaH_2PO_4, 1 M Urea, 300 mM NaCl at pH 8.0 supplemented with 1 tablet of Complete Protease Inhibitors and DNAse. Bacterial pellet was disrupted twice using a Microfluidizer M-110P (Microfluidics international, Newton, MA) at 10 000 psi. The lysates were centrifuged at 20 000 g for 45 min. The lysis, sonication, and centrifugation steps were repeated. The resulting pellet was suspended in 30 ml wash buffer containing 50 mM NaH_2PO_4 pH 8.0, 2 M Urea, 300 mM NaCl. The lysates were centrifuged at 20 000 g for 45 min. The pellet wash step was repeated twice.

Solubilization of inclusion bodies (IB) was carried out in 20 ml of solubilization buffer (10 mM Tris-HCl, 6 M Urea, 100 mM NaH_2PO_4, 10% glycerol, 0.4 % SDS, 4 mM β-mercaptoethanol [pH 8.00]) overnight at room temperature on a rotating wheel. The solubilized sample was centrifuged at 20 000 g for 45 min and the supernatant was collected.

The supernatant was incubated overnight at room temperature with 3 ml of Ni-NTA (Nickel-nitrilotriacetic acid) superflow slurry equilibrated with solubilization buffer. The sample-resin suspension was allowed to settle down into a 1 cm diameter empty column. The resin was first washed with 30 ml of solubilization buffer and then with 30 ml of solubilization buffer supplemented with 20 mM imidazole. The recombinant CCR5 fusions were eluted with 20 ml of elution buffer (10 mM Tris-HCl, 6 M Urea, 100 mM NaH_2PO_4, 10% glycerol, 0.4 % SDS, 4 mM β-mercaptoethanol and 500 mM imidazole [pH 8.00]). The eluted fractions were analyzed using 12% SDS-polyacrylamide gel and visualized by Coomassie blue staining.

Fractions containing CCR5 fusions were pooled and dialyzed overnight at room temperature using a 12-14 kDa molecular weight cut-off membrane against 500 ml of 25 mM Tris-HCl, 150 mM NaCl [pH 8.0]. Dialysis buffer was changed 4 times. After dialysis, the SDS concentration was decreased enough to be compatible with thrombin cleavage. The protein sample was centrifuged.

The optimal thrombin cleavage is achieved when the protein concentration is 0.3-0.5 mg/ml. 1 U of thrombin to 100 µg of protein was added to the protein sample and supplemented with 2.5 mM $CaCl_2$. An optimized incubation time was determined. The reaction was stopped by adding 6 M Urea and 0.4% SDS and incubated for several hours.

The mixture was applied on the 3 ml of Ni-NTA (Nickel-nitrilotriacetic acid) superflow slurry equilibrated with solubilization buffer and incubated overnight at room temperature. The sample-resin suspension was allowed to settle down into a 1 cm diameter column. The resin was washed with 30 ml of solubilization buffer. The recombinant CCR5 were eluted with 20 ml of elution buffer (10 mM Tris-HCl, 6 M urea, 100 mM NaH_2PO_4, 10% glycerol, 0.4 % SDS, 4 mM β-mercaptoethanol and 500 mM imidazole [pH 8.00]). The eluted fractions were analyzed using 12% SDS-polyacrylamide gel and visualized by Coomassie blue staining.

Fractions containing CCR5 were pooled and dialyzed overnight at room temperature using a 12-14 kDa molecular weight cut-off dialysis membrane (MWCO) against 50 mM Tris-HCl, 0.8 % SDS [pH 8.0]. Dialysis buffer changed twice. At this stage the receptor sample is stable at room temperature during several month.

7.2.3. Receptor folding in amphipols

It was observed that the receptor folding was working better when protein concentration was 0.3 - 0.5 mg/ml, therefore the receptor sample was diluted or concentrated accordingly. The amphipols were prepared by dissolving their powder in H_2O at final 100 mg/ml concentration. The mix of lipids - asolectin was prepared at 10 mg/ml concentration in 50 mM Tris HCl, 0.8 %SDS [pH 8.0] buffer. The amphipols and lipids were added to the protein solution to reach a protein:amphipol:lipid mass ration 1:5:1 for A8-35 and BAPol and 1:10:1 mass ration for NAPol and were incubated at room temperature for one hour. Then SDS were precipitated by addition of KCl to reach a final concentration equal to concentration of detergent with additional 150 mM and was incubation for 30 min under vigorous stirring at room temperature. The formed KDS crystals were removed by two centrifugations at 15 000 g for a 10 min, at room temperature. Protein sample was dialyzed to remove residual dodecylsulphate against 100 times larger volume of 30 mM Potassium phosphate (30 mM KH_2PO_4 + 30 mM K_2HPO_4), 150 KCl [pH 8.0] buffer.

7.3. Protein characterization methods

7.3.1. Transwell (Boyden Chamber) Cell Migration Assay

To study the characteristic movements of the cells along a chemical concentration gradient towards the chemical stimulus, the Boyden chamber was used (Figure 7.1). It implies that cells undergo directed motion in a chemokine gradient.

The Boyden chamber is composed of two compartments separated by a filter membrane that cells can easily pass through. The chemokines were located in the lower compartment and the cells in the upper compartment. After an incubation, the amount of cells in the lower compartment was determined.

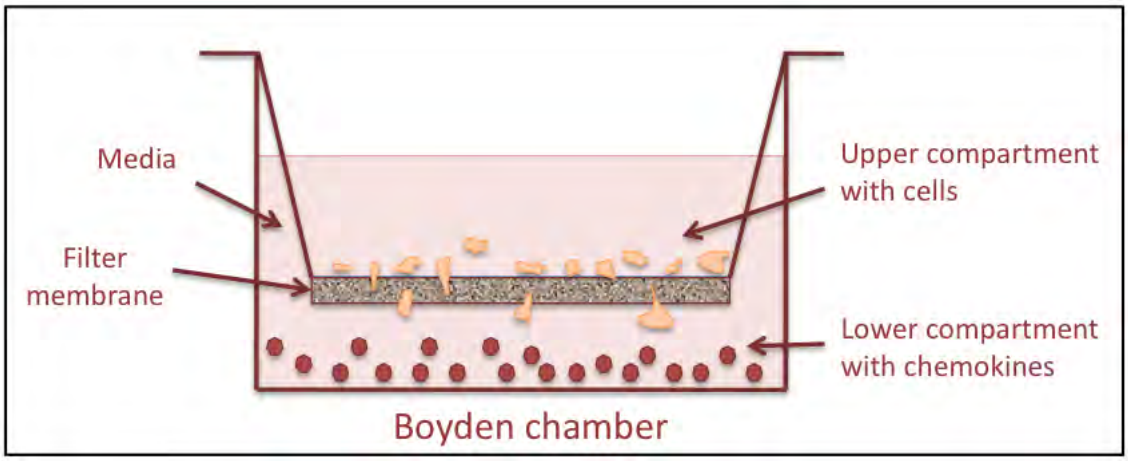

Figure 7.1.: Schematic representation of Boyden/transwell chamber.

The human Jurkat T cell line was purchased from the American Type Culture Collection and grown in RPMI 1640 medium (Invitrogen) supplemented with 10% fetal bovine serum (FBS) at 37°C in 5% CO_2. For the chemotaxis studies, Jurkat cells were stained with 5 mM calcein-AM (Molecular Probes) in PBS - 1% BSA for 30 min at 37°C in 5% CO_2. Stained cells were washed twice with PBS buffer and resuspended at the density of 2 x 106 cells/ml in RPMI 1640 containing 20 mM HEPES and 1% human AB serum (Institut J. Boy, Reims). T cell migration was evaluated using 5 µm pore polycarbonate filters in 96-well transwell chambers (Corning, Sigma). 2 x 105 cells in 100 µl RPMI medium supplemented with 20 mM HEPES and 1% human AB serum were added to the upper chamber of a transwell culture insert. The same media (250 µl) with or without chemokine (range from 3 to 300 nM) were placed in the lower chamber. Each condition was set up in triplicate. Chemotaxis proceeded for 3 hours at 37°C in humidified air containing 5% CO_2. Migration of calcein-stained cells through the filter to the lower chamber wells was evaluated by fluorescence (485-525 nm) using a Victor fluorescent plate reader (Perkin-Elmer).

7.3.2. Surface Plasmon Resonance (SPR) analysis

7.3.2.1. Materials

A Biacore 3000 machine, NTA Sensor Chip, SA Sensor Chip, CM4 Sensor chip, amine coupling kit and HBS-N (10 mM Hepes, 150 mM NaCl [pH 7.4]) from GE-Healthcare were used. The 1D4 antibody (Anti-Rhodopsin, C-terminus, last 9 amino acids, clone Rho 1D4, Cat. Nr. MAB5356) was purchased from Millipore.

7.3.2.2. Immobilization of CCR5-His on NTA Sensor Chip

Experiments were performed using 30 mM KPhosphate, 150 mM KCl, 50 μM EDTA [pH 8.0] as a running buffer and the flow rate was 5 μl/min.

For CCR5-His immobilization on NTA Sensor Chip receptor folded in A8-35/L, NAPol/L, and BAPol/L was used. The two first flow cells (Fc1 and Fc2) of the NTA Sensor Chip, using extra clean option, was washed with 5 μl injection of 175 mM EDTA and then with 5 μl injection of 10 mM NaOH, 200 mM NaCl solution. On the Fc2 Ni^{2+} was loaded by 5 μl injection of 30 mM KPhosphate, 150 mM KCl, 500 μM $NiCl_2$ buffer. The receptor was immobilized by several (two or three) 20 μl injections or, for later experiments, by one 70 μl injection of CCR5/NAPol/L or CCR5/BAPol/L, or CCR5/A8-35/L at 60 μg/ml concentration.

To reuse Ni-NTA surface, the coupled receptors were removed injecting 20 μl of running buffer with 500 mM imidazole, followed by 10 μl injection of 25 mM EDTA, 50 mM Glycine NaOH, 0.15 % Triton X-100 [pH 12.0] buffer.

7.3.2.3. Chemokine interaction with the receptor on CCR5-His functionalized NTA Sensor Chip

Firstly, chemokine interaction with receptor was tested at the flow rate of 20 μl/min by injecting 20 μl at 500 nM SDF1α-Strep or 500 nM RANTES-Strep.

For RANTES-Strep titration, a range of concentrations from 4 nM to 1000 nM was prepared by 3 fold serial dilutions of 1 mM RANTES-Strep stock solution. RANTES-Strep titration was performed at 20 μl/min flow rate injecting 20 μl of each RANTES-Strep concentration. The injections were performed from the lowest to the highest concentration to minimize accumulation of analyte on the receptor surface. No regeneration was done between analyte injections.

7.3.2.4. Immobilization of CCR5-His-C9 on CM4 Sensor Chip

Experiments were performed using HBS-N (10 mM HEPES, 150 mM NaCl [pH 7.4]) as a running buffer and the flow rate was 5 μl/min.

7.3.2.4.1. 1D4 antibody pre-concentration test The 1D4 antibody (5 μg/ml) was prepared in 10 mM Na Acetate buffer at pH 4.0, 4.5. 5.0 and 5.5. Then 5 μl of 1D4 antibody at each buffer pH was injected onto the surface.

7.3.2.4.2. 1D4 antibody immobilization on CM4 Sensor Chip The 1D4 antibody was immobilized on a CM4 sensor chip using standard amine-coupling chemistry. The CM4 sensor chip was activated by 50 µl injection of 0.2 M 1-ethyl-3-(3-diethylaminopropyl)-carbodiimide (EDC)/0.05 M N-hydroxysuccinimide (NHS). The antibody was coupled on the surface with 35 µl injection of 1D4 antibody at 100 µg/ml concentration diluted in 10 mM Na Acetate [pH 4.5] buffer. Remaining activated groups were blocked with 50 µl injection of 1 M Ethanolamine [pH 8.5].

7.3.2.4.3. CCR5-His-C9 capture The C9-tagged CCR5/NAPol/L was captured by 1D4 immobilized on the surface of CM4 chip by 30 µl injection at 100 µg/ml concentration.

7.3.2.4.4. CCR5-His-C9 surface regeneration To remove the receptor from 1D4 surface the buffer of 10 nM NaOH, 1% n-octyl-β-D-glucopyranoside was used.

7.3.2.5. Chemokine interaction with the receptor on CCR5-His-C9/1D4 functionalized CM4 Sensor Chip

Experiments were performed using 50 mM HEPES, 150 mM NaCl [pH 7.0] as a running buffer and the flow rate was 100 µl/min.

Chemokine RANTES-Strep and SDF1α-His were injected (90 µl) over the captured receptor at 200 nM concentration. The analyte injection was followed by a blank injection of buffer to reference the surface. No regeneration was performed between analyte injections.

7.3.2.6. Immobilization of CCR5-His on SA Sensor Chip

For CCR5-His immobilization on SA Sensor Chip, receptor folded in BAPols/L was used. First, the sensor chip was washed with 5 µl injection of 50 mM NaOH, 1M NaCl at the 5 µl/min flow rate. On the Fc1, the reference surface, 55 µl of BAPol was injected at 60 µg/ml concentration. On the Fc2 the 55 µl of CCR5/BAPol/L was injected at 60 µg/ml concentration.

7.3.2.7. Immobilization of RANTES-Strep on CM4 Sensor Chip

Experiments were performed using HBS-N (10 mM HEPES, 150 mM NaCl [pH 7.4]) as a running buffer.

7.3.2.7.1. RANTES-Strep pre-concentration test The RANTES-Strep (7 µg/ml) was prepared in 10 mM Na Acetate buffer at pH 4.0, 4.5. 5.0, 5.5 and 6.0. Then 5 µl of RANTES-Strep in each buffer pH was injected at the flow rate of 5 µl/min.

7.3.2.7.2. RANTES-Strep immobilization on CM4 Sensor Chip The RANTES-Strep was immobilized on a CM4 sensor chip using standard amine-coupling chemistry. The CM4 sensor chip was activated by 50 µl injection of 0.2 M EDC/0.05 M NHS mixture. The RANTES-Strep was coupled to the surface with 35 µl injection of RANTES-Strep at 1.76 µg/ml concentration diluted in 10 mM Na Acetate [pH 5.0] buffer. Remaining activated groups were blocked with 50 µl injection of 1 M Ethanolamine [pH 8.5]. The flow rate was 5 µl/min.

7.3.2.7.3. Chemokine interaction with amphipols Experiments were performed at 20 µl/min and 100 µl/min flow rates. 10 µl of each amphipol (NAPol or A8-35) at 1.17 mg/ml and 0.234 mg/ml concentrations were injected over the captured RANTES-Strep. The surface was regenerated by 10 µl injection of 10 mM NaOH.

7.3.3. Electrospray mass spectrometry

Masses and purities of purified chemokines were confirmed using electrospray mass spectrometry.

Sample preparation Purified chemokines were prepared in 50 mM Tris, 150 mM NaCl [pH 8.0] buffer. Two samples of each chemokine were prepared in volume of 10 µl at 200 µM concentration and one sample additionally contained 100 mM of DTT. Then 10 µl of each protein sample were diluted in 90 µl FA 0.1%; 100 µl of this dilution was desalted on line.

Methods All solvents were HPLC grade. HPLC (Agilent 1100 series) was coupled with electrospray TOF mass spectrometer (Agilent, LC/MSD TOF). MacroTrap (Michrom) was used for desalting with 0.03 % FA in water and for elution with 70 % solvent B (95% acetonitrile, 5% water, 0.03 % FA).

7.4. Introduction to Lanthanoids[1]

Lanthanoid metals are elements from 57 to 71 in the periodic table of elements (Figure 7.2). They are also called “Rare Earth” metals, not because of their rare natural abundance but because of the difficulties encountered in their purification [353]. The informal chemical symbol Ln is used in general discussions of lanthanoid chemistry.

[1]The current IUPAC recommendation is that the name lanthanoid be used rather than lanthanide, as the suffix "-ide" is preferred for negative ions whereas the suffix "-oid" indicates similarity to one of the members of the containing family of elements. However, lanthanide is still favored in most (90%) scientific articles.

57 138.91	58 140.12	59 140.91	60 144.24	61 (145)	62 150.36	63 151.96	64 157.25	65 158.93	66 162.50	67 164.93	68 167.26	69 168.93	70 173.04	71 174.97
La	**Ce**	**Pr**	**Nd**	**Pm**	**Sm**	**Eu**	**Gd**	**Tb**	**Dy**	**Ho**	**Er**	**Tm**	**Yb**	**Lu**
LANTHANUM	CERIUM	PRASEODYMIUM	NEODYMIUM	PROMETHIUM	SAMARIUM	EUROPIUM	GADOLINIUM	TERBIUM	DYSPROSIUM	HOLMIUM	ERBIUM	THULIUM	YTTERBIUM	LUTETIUM

Figure 7.2.: Lanthanoid metals.

In our approach we used terbium to bind to Lanthanoid Binding Tag (see paragraph 9.2.1.1).

Many lanthanoid ions (including Tb^{3+}) exhibit distinct luminescence emission spectra, due to $f - f$ electronic transitions (Figure 7.3).

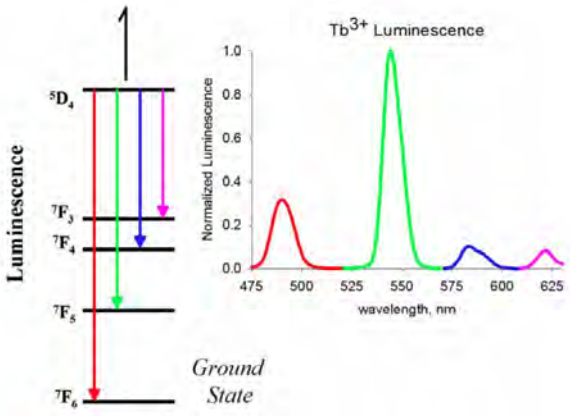

Figure 7.3.: Emission spectrum of Tb^{3+} .
The origin of the peaks are highlighted in color.

Because $f - f$ electronic dipole transitions are forbidden by parity rules (Laporte-forbiden), it is much easier to excite Ln^{3+} ions via an organic fluorophore (Figure 7.4). First, an organic fluorophore (in our case, the side-chain indole of tryptophan) is excited (A) by irradiation from a source such as UV light, making an excited singlet. This singlet may release a photon and fluoresce (B), or it may undergo intersystem-crossing and become an excited triplet. If the triplet releases a photon, the process is known as phosphorescence (C), but it may instead undergo another (non-radiative) exchange of energy with a nearby Tb^{3+} ion. The energy of this now-excited Tb^{3+} may be lost by a non-radiative process, or the Tb^{3+} may luminesce (D), giving rise to the spectrum in Figure 7.3. It should be noted that this process is formally known as "luminescence", and is referred as such throughout this work, because the ground state of Tb^{3+} is not a singlet (having six unpaired f electrons) and therefore is neither fluorescence nor phosphorescence.

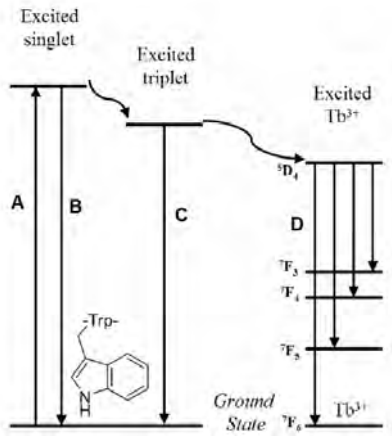

Figure 7.4.: Excitation of Tb^{3+} luminescence.
A. An organic fluorophore (the indole ring of tryptophan) is excited by UV light. B. The excited state singlet may fluoresce. C. If the excited singlet undergoes intersystem crossing, the excited triplet state may phosphoresce. D. Or, the energy may be transferred to the nearby Tb^{3+} , which can luminesce.

The direct absorption of Ln^{3+} cations is very weak, and for this reason they have very low molar absorption coefficients, which limits their practical use. In order to circumvent these low extinction coefficients, the luminescent metal ion can be chelated to a chromophore-containing group, which functions as an 'antenna,' absorbing incident light, then transferring this excitation to the metal ion, which can then deactivate by undergoing its typical luminescent emission (Figure 7.5).

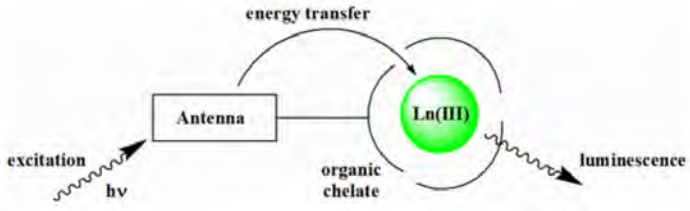

Figure 7.5.: Antenna effect.
An illustration of the 'antenna' effect, wherein incident excitation is first absorbed by a chelating organic chromophore and then transferred to the metal.

While many lanthanoid ions are capable to luminesce, terbium is the only one that can be sensitized by the side chain of the tryptophan. Although sensitizing Tb^{3+} via tryptophan at 280 nm is acceptable for most *in vitro* applications, such high-energy radiation would be damaging to living cells.

Ubiquitin was the first protein with LT, for which the structure was determined (Figure 7.6) [354].

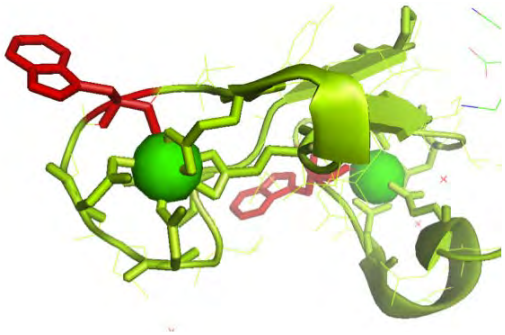

Figure 7.6.: LT tag bound terbium ions.
The side chains that chelate Tb^{3+} ion (dark green) are shown in clear green. Tryptophan (shown in red) serve as antenna. The indole ring is excited at 280 nm, thereby sensitizing Tb^{3+} which emits at 544 nm. The structure was determined by NMR, the PDB code is 2OJR [354].

LT tagged proteins can be directly visualized in SDS polyacrylamide gels by UV illuminator [352, 355]. The gel has to be soaked in buffer containing terbium prior to illumination with UV.

Lanthanoids and lanthanoid luminescence has an interesting application in the security measures of banknotes. Luminescent europium chelates are responsible for the red color that shows up on the Euro paper currency under UV light (Figure 7.7).

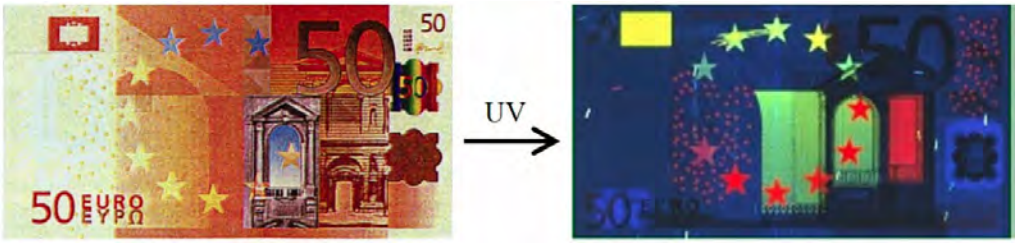

Figure 7.7.: The security measures on euro banknotes.
50 euro banknotes containing europium chelates that emit red luminescence under UV light.

7.4.1. Lanthanoid binding tag

Lanthanoid binding tags are short peptide sequences that tightly and selectively bind lanthanoid ions and can sensitize terbium luminescence [352]. Increasing the number of bound lanthanoids would improve the capabilities of these tags [352].

The similarity of trivalent lanthanoids to Ca^{2+} in ionic radius and oxophilicity has enabled their direct incorporation into calcium-binding proteins. Using information about calcium-binding loops, short polypeptides comprising 20 or fewer encoded amino acids that bind tightly and selectively lanthanoids were designed, engineered and developed. Therefore, on the base of using a structurally well-characterized single lanthanoid binding tag sequence, a double lanthanoid binding tag was designed. (Figure 7.8). It was shown that double lanthanoid binding tag improved

up to 3-fold luminescence intensity [352]. A lanthanoid binding sequence can be integrated as a protein co-expression tag via molecular biology strategies.

Figure 7.8.: Double lanthanoid binding tag.
[352]

These tags have been used for many applications, such as luminescence-based visualization on gels [355], as magnetic-field paramagnetic alignment agents in protein NMR experiments [356, 357], in fluorescence microscopy [358], as partners in luminescence resonance energy transfer (LRET) studies [359], and in the dissociation-enhanced lanthanoid fluorescent immunoassay (DELFIA) technology for ligand screening assays [360].

7.4.1.1. Terbium titration

Titrations were recorded on Photon Technology International Quanta Master I fluorimeter using 1 cm path length quartz cuvette and slit widths of 2 and 4 nm. Tryptophan-sensitized Tb^{3+} luminescence was collected at room temperature by exciting the sample at 280 nm. The purified SDF1α-LT-His protein (2 ml at 75 µM in Hepes 20 mM, NaCl 100 mM [pH 8.0]) was titrated by adding ten 2 µl aliquots of 15 mM Tb^{3+}. After each addition, the solution was mixed and the fluorescence emission spectra was recorded between 450 and 550 nm.

8. Résumé de matériel et méthodes en français

8.1 Matériel

8.1.1 Liste des produits

8.2 Méthodes

8.2.1 Production des chimiokines

8.2.1.1 Biologie moléculaire

8.2.1.1.1 Préparation des constructions MBP-chimiokine

8.2.1.1.2 Constructions pour l'expression des chimiokines en corps d'inclusion chez *E. coli*

8.2.1.2 Expression des MBP-chimiokines

8.2.1.3 Purification des MBP-chimiokines

8.2.1.4 Purification dess chimiokines en corps inclusion d'*E. coli*

8.2.1.4.1 Préparation des corps d'inclusion

8.2.1.4.2 Purification et repliement de SDF1α-His et SDF1α-Strep

8.2.1.4.3 Purification et repliement de RANTES-Strep et RANTES

8.2.1.4.4 Purification et repliement de SDF1α-LT-His, SDF1α-LT-Strep et RANTES-LT-Strep

8.2.2 Production des récepteurs

8.2.2.1 Expression

8.2.2.2 Extraction et purification

8.2.2.3 Repliement des récepteurs en amphipoles

8.2.3 Méthodes de caractérisation des protéines

8.2.3.1 Transwell (chambre de Boyden) essais de migration des cellules

8.2.3.2 Analyse par résonance des plasmons de surface (SPR)

8.2.3.2.1 Matériels

8.2.3.2.2 Immobilisation de CCR5-His sur puce NTA

8.2.3.2.3 L'interaction des chimiokines avec le récepteur sur la surface des puces NTA fonctionnalisé avec CCR5-HIS

8.2.3.2.4 Immobilisation de CCR5-His-C9 sur puce CM4

8.2.3.2.4.1 Essai de pré-concentration de l'anticorps 1D4

8.2.3.2.4.2 Immobilisation de l'anticorps 1D4 sur puce CM4

8.2.3.2.4.3 Capture de CCR5-His-C9

8.2.3.2.4.4 Régénération de la surface CCR5-His-C9

8.2.3.2.5 Interaction des chimiokines avec le récepteur sur puce CM4 fonctionnalisée avec CCR5-His-C9/1D4

8.2.3.2.6 Immobilisation de CCR5-HIS sur puce SA

8.2.3.2.7 Immobilisation de RANTES-Strep sur puce CM4

8.2.3.2.7.1 Essai de pré-concentration de RANTES-Strep

8.2.3.2.7.2 Immobilisation de RANTES-Strep sur puce CM4

8.2.3.2.7.3 Interaction des chimiokines avec des amphipoles

8.2.3.3 Spectrométrie de masse en electrospray

8.2.3.3.1 Préparation des échantillons

8.2.3.3.2 Méthodes

8.2.4 Introduction au Lanthanides

8.2.4.1 L'étiquette Lanthanide

8.2.4.1.1 Titration au terbium

Part III.

Results

9. Chemokine production

This first part of the results will describe the engineering of various versions of two HIV co-receptor ligands, RANTES (for CCR5) and SDF1α (for CXCR4). Those recombinant chemokines constitute critical tools to assess the functionality of the folded receptor and later on will be used to investigate receptor/ligand complex. The commercially available chemokines are very expensive, therefore the production of recombinant chemokine receptors ligands was carried out in *E. coli*. Choosing this way of chemokine production the advantage was taken to produce them in a functionalized form bearing different tags for several purposes. Several modifications were introduced including different tags such as Strep-Tag, His-Tag and Lanthanoid Binding Tag. The Strep-Tag was introduced to form chemokine/receptor complex and to constitute affinity chromatography. The Lanthanoid binding tag was introduced for luminescence experiments. In order to set up a chemokine production strategy protocols already published in the literature were examined. Two different approaches were considered.

The first method consisted in fusing the Maltose Binding Protein (MBP) to the N-terminal part of the chemokines [361]. It has been shown that MBP fusion improves protein solubility, proper folding, overall purification via affinity chromatography and protects against proteolysis [362, 363, 361]. In this article, DNA fragments encoding MBP, RANTES and SDF1α were amplified by PCR and cloned into pET20b vector with a N-terminal hexahistidine tag for purification of the recombinant proteins via immobilized metal affinity chromatography. The authors produced MBP-RANTES and MBP-SDF1α chemokines in *E. coli* under variety of culture conditions. The use of MBP-fusion for RANTES and SDF1α protein expression improved yields of soluble protein under optimized culture conditions, using a relatively simple purification scheme. According to the authors this MBP-fused chemokine strategy resulted in high-yield expression of functional chemokines. It was stated that using a double fusion system comprising a His-tag and MBP-fusion partner increased the purity of chemokines. Recombinant chemokine MBP-RANTES and MBP-SDF1α binding activity to their receptor was confirmed by flow cytometry using EL-4 cells expressing CCR5 and CXCR4 receptors on their surface [361].

The second approach consisted in chemokine production in *E. coli* inclusion bodies [364]. This method requires cell lysis and inclusion body isolation followed by protein solubilization and renaturation.

At the beginning of my PhD the first approach was looking more promising than the second one as functional chemokines were directly produced, avoiding the delicate step of refolding. Besides,

MBP fusion strategy was already reported to improve the expression of soluble recombinant proteins in *E. coli* [365, 366, 367]. Moreover it was demonstrated that the purified MBP-fused proteins were functional. Therefore, chemokines were first produced using this strategy.

9.1. Chemokines

9.2. MBP constructs

9.2.1. Molecular biology

The chemokine genes of RANTES, RANTES-LT and SDF1α were ordered as synthetic genes, where all nucleotides were optimized for *E. coli* expression.

The frequency of usage of redundant codons differs in human and in bacteria. The disponibility of the corresponding tRNA directly reflects this frequency. Therefore human genes that contain some codons that are poorly used in *E. coli* may be inefficiently expressed. Rare codons can cause premature termination of the synthesized protein or misincorporation of amino acids. Clusters of rare codons stand a higher chance to create translation errors and reduce the expression level. Working with synthetic genes solve this problem and codons that are more frequently used in *E. coli* were introduced. Sequences of the constructs can be find in Annex 18 .

9.2.1.1. Features

Besides their optimized sequence each synthetic construct contained several features.

MBP Constructs contained a N-terminal fusion with the Maltose Binding Protein (MBP) which is a fusion partner for better protein expression.

The Factor Xa cleavage site The Factor Xa cleavage (Xa) allowed the cleavage of the MBP from the chemokine.

Strep tag The chemokine also had a C-terminal Strep tag (Strep), which facilitated the purification step and could allow the subsequent creation of an affinity column.

Thrombin cleavage site (T) Thrombin cleavage site allowed the cleavage of the Strep tag from the purified chemokine.

Lanthanoid binding tag (LT) Lanthanoid binding tags (LTs) are short polypeptide sequences that were derived from calcium binding motifs [355]. These tags selectively bind lanthanoid ions and can sensitize terbium (Tb^{3+}) luminescence [352]. The size of the LT is minimal; therefore the impact on the structure and function of the proteins to which they are fused should be limited. A double lanthanoid binding tag was designed, which concatenates two lanthanoid binding motifs. Comparing with other luminescent tags the lanthanoid binding to LT tag can achieve up to 3-fold greater luminescence intensity [352]. The goal of this double lanthanoid binding tag was to incorporate two Tb^{3+}- binding sites within a contiguous sequence, potentially conferring advantages in luminescence output, X-ray scattering power, and anisotropic magnetic susceptibility, together with reduced mobility relative to the tagged protein due to the larger mass [352].

The double lanthanoid binding tag (LT) was first introduced for RANTES construct and later on added to SDF1α chemokine. The purpose of this tag in our case was to facilitate the tracking of the chemokine by luminescence [355] and also, in the future, it could be used for a chemokine/co-receptor complex structure solving [368] as well as for a time-resolved FRET strategy in cell lines [369].

9.2.1.2. Cloning

The pMAL-c4X vector was chosen for the MBP fusion cloning for cytoplasmic protein expression. The *malE* gene on pMAL-c4X vector has a deletion of the signal sequence, leading to cytoplasmic expression of the fusion protein.

Figure 9.1.: Schematic representation of MBP-chemokine constructs.

The synthetic chemokine genes cloned into pMAL-c4X vector are schematized in Figure 9.1. The final constructs contained a N-terminal MBP fusion followed by the Factor Xa site, which enables the subsequent cleavage of the fusion protein. Constructs contained a C-terminal Strep tag, which is cleavable by thrombin. One RANTES construct comprised an additional double Lanthanoid binding Tag (LT).

9.2.2. Expression

First of all, to determine the best expression conditions, small-scale expression tests were carried out. The expression of the constructs MBP-Xa-SDF1α-Strep, MBP-Xa-RANTES-Strep and MBP-Xa-RANTES-LT-Strep were performed. Expression, induced by IPTG addition (1 mM) was tested at two different temperatures at 37°C for 4 hours and 20°C for overnight growth. Three different growth medias were tested: LB, TB and auto-induction. Comparison of the results (Figure 9.2) indicated that expression was similar in LB and TB media while very poor in auto-induction media. In regards to the temperatures, MBP-Xa-SDF1α-Strep was similarly poorly expressed in either conditions while MBP-Xa-RANTES-Strep expression was improved at 20°C.

It was surprising to see that MBP-Xa-RANTES-LT-Strep was better expressed than the one without the LT tag with the same tendency – better expression at 20°C.

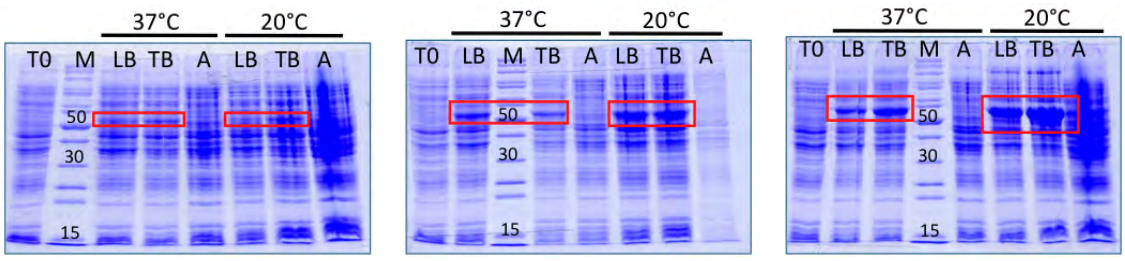

(a) MBP-Xa-SDF1α-Strep (b) MBP-Xa-RANTES-Strep (c) MBP-Xa-RANTES-LT-Strep

Figure 9.2.: SDS-polyacrylamide gels showing expression of MBP-chemokine constructs. (a) MBP-Xa-SDF1α-Strep (b) MBP-Xa-RANTES-Strep and (c) MBP-Xa-RANTES-LT-Strep expression in different conditions. M - marker, T0 - sample before induction; LB - LB medium, TB - TB medium, A - auto-induction medium indicates the culture medium ; 37°C and 20°C indicates at which temperature cultures were grown after induction.

The next step consisted in examining the amount of soluble protein. Two constructs MBP-Xa-RANTES-Strep and MBP-Xa-RANTES-LT-Strep grown in LB, medium at 20°C overnight were compared. The bacterial cultures were harvested (sample corresponding to "total extract") and centrifuged. Bacterial pellets were resuspended in lysis buffer and sonicated. After ultracentrifugation the supernatant containing the soluble proteins (supernatant) was separated from the pellet, where cell membrane and inclusion bodies remained (pellet) (Figure 9.3).

The presence of the LT tag clearly enhanced the solubility of the protein since the MBP-Xa-RANTES-Strep mostly remained in the pellet fraction while the MBP-Xa-RANTES-LT-Strep was mostly soluble (Figure 9.3 b).

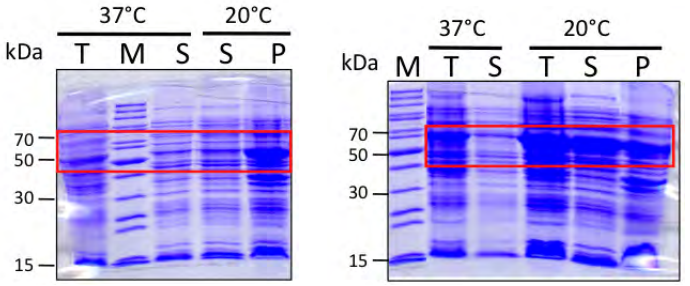

(a) MBP-Xa-RANTES-Strep (b) MBP-Xa-RANTES-LT-Strep

Figure 9.3.: SDS-polyacrylamide gels representing solubility test of RANTES with and without LT tag.
M - marker, T – total extract, S – supernatant, P –pellet.

Therefore, cultures for MBP chemokine fusion expression were carried out in conditions that allowed soluble protein expression: in LB medium supplied with the relevant antibiotic, induced with 1 mM of IPTG and incubated at 20°C overnight.

9.2.3. Purification

The purification was first attempted with MBP-Xa-RANTES-LT-Strep construct, which in the small-scale expression test was better expressed, and where larger proportion of protein was obtained in the soluble fraction. All the purifications described were performed form one liter of bacterial culture.

9.2.3.1. MBP-Xa-RANTES-LT-Strep

A first step of the MBP-Xa-RANTES-LT-Strep chemokine purification was carried out on a Strep-Trap column (Figure 9.4). The soluble fraction of the protein was applied to the column equilibrated in the protein buffer.

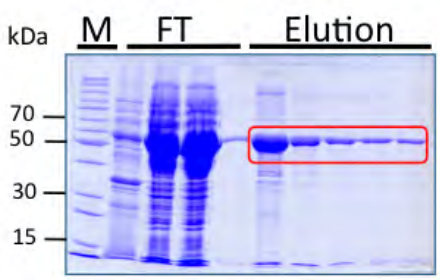

Figure 9.4.: SDS-polyacrylamide gel showing MBP-Xa-RANTES-LT-Strep purification on Strep-Trap column.
M - marker, FT - flow-through fractions, Elution - elution fractions from the Strep-Trap column.

The flow-through (FT) fraction still contained a lot of protein demonstrating that the column was saturated. Protein was eluted from the column with a buffer containing desthiobiotin. Elution fractions containing the MBP-Xa-RANTES-LT-Strep protein were pooled together, dialyzed and Factor Xa digestion was performed to cleave off the MBP protein from the chemokine (Figure 9.5).

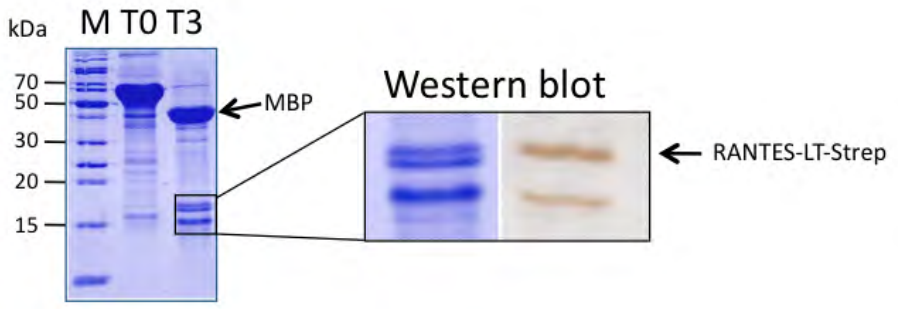

Figure 9.5.: SDS-polyacrylamide gel and Western blot showing MBP-Xa-RANTES-LT-Strep Factor Xa digestion.
M – marker; T0 – non-digested protein; T3 – protein after 3 hours of digestion.

Digestion of MBP-Xa-RANTES-LT-Strep by Factor Xa analyzed on SDS-polyacrylamide gel revealed three distinct bands that could correspond to RANTES-LT (Figure 9.5). The N-terminal sequencing analysis of the 3 bands confirmed that the two upper bands started with the expected amino acid sequence: ISEFS, while the lower band N-terminal sequence was AHIK which corresponds to the sequence from RANTES 22nd amino acid. Western blotting using a Strep-Tactin HRP indicated that the upper and the lower bands contained the Strep tag. Even though the middle band was confirmed by the N-terminal sequencing having an expected amino sequence, the C-terminus lacked the Strep tag and was not revealed by the Western blot. Therefore, we can conclude that only the upper band corresponded to the full length RANTES-LT and that there were two other Factor Xa cleavage sites resulting in two additional bands. Thus Factor Xa was not optimal for the MBP cleavage and another cleavage site was required.

PreScission protease was directly tested on MBP-Xa-RANTES-LT-Strep construct in order to determine if it could led to a non-specific cleavage (Figure 9.6).

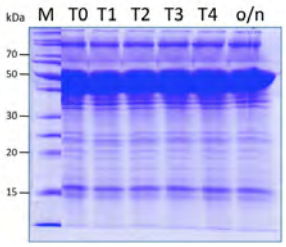

Figure 9.6.: SDS-polyacrylamide gel showing MBP-Xa-RANTES-LT-Strep digestion test with PreScission protease.
M - marker, T0 - non-digested sample, T1-4 - sample after 1, 2, 3, 4 hours digestion, o/n - sample after overnight digestion.

No non-specific cleavage was observed, therefore, Factor Xa cleavage site was replaced by PreScission protease site (PrePro) by site direct mutagenesis in all constructs resulting in MBP-PrePro-RANTES-LT-Strep, MBP-PrePro-RANTES-Strep and MBP-PrePro-SDF1α-Strep.

9.2.3.2. MBP-PrePro-RANTES-LT-Strep Purification

The MBP-PrePro-RANTES-LT-Strep chemokine was expressed following the previously mentioned protocol. The amount of the expressed protein was examined on SDS-polyacrylamide gel (Figure 9.7).

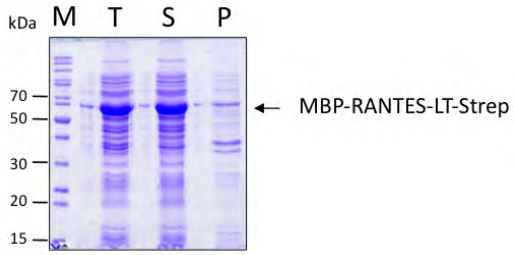

Figure 9.7.: SDS-polyacrylamide gel representing MBP-PrePro-RANTES-LT-Strep solubility test.
M - marker, T – total extract, S – supernatant, P –pellet, the arrow indicates the expected position of the protein.

Changing Factor Xa cleavage site to PreScission protease cleavage site improved the overall protein solubility. Almost all expressed protein was soluble while the previous construct led to a 50/50 soluble/insoluble protein ratio (Figure 9.3).

As before a first step of MBP-PrePro-RANTES-LT-Strep purification was carried out on a Strep-Trap column (Figure 9.8a). Expression of the protein was so strong that the flow-through and wash fractions contained quite a lot of protein. The used column was clearly saturated.

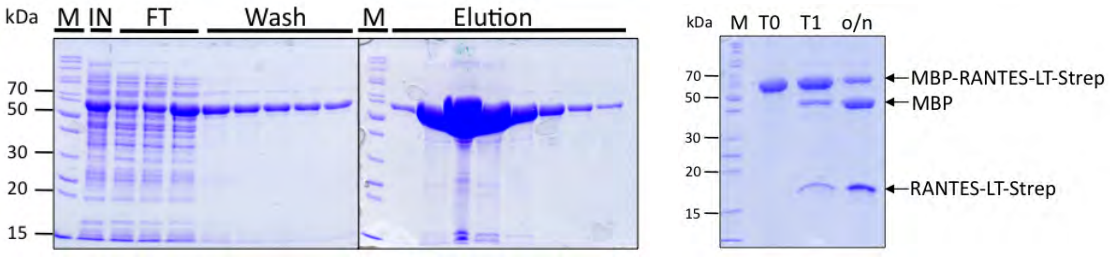

(a) (b)

Figure 9.8.: SDS-polyacrylamide gel representing MBP-PrePro-RANTES-LT-Strep purification. (a) MBP-PrePro-RANTES-LT-Strep purification on Strep-Trap column. M - Marker, IN - input sample, FT - flow-through sample, Wash - wash fractions, Elution - elution fractions from the Strep-Trap column. (b) Purified MBP-PrePro-RANTES-LT-Strep digestion with PreScission protease. T0 - non-digested sample, T1 - sample after 1 hour of digestion, o/n - sample after overnight digestion with PreScission protease.

The specificity of the PreScission protease digestion was verified on a small fraction of purified MBP-PrePro-RANTES-LT-Strep (Figure 9.8b). After analyzing results on a SDS-polyacrylamide gel the PreScission protease digestion was performed on the whole preparation. The PreScission protease contained a GST tag therefore it was removed by applying the whole digested sample was applied to a GST resin: the cleaved MBP, chemokine and the non-cleaved protein were collected in the flow-through fraction while the PreScission protease was retained by the GST resin. With the next step, the non-digested protein and the MBP were removed by using an amylose column. The MBP binds to the amylose resin: including the non-digested sample (MBP-RANTES-LT-Strep) and the cleaved MBP, while the cleaved chemokine was collected in the flow through fractions (Figure 9.9).

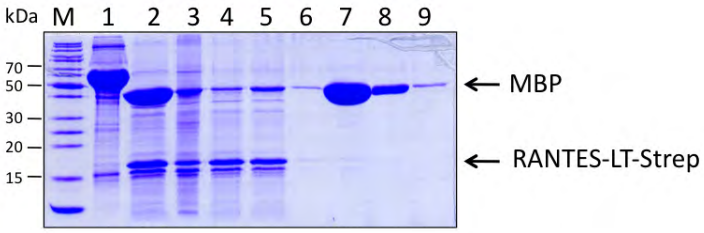

Figure 9.9.: SDS-polyacrylamide gel representing the RANTES-LT-Strep purification after digestion with PreScission protease.
M - marker, 1 - non-digested sample, 2 - MBP-PrePro-RANTES-LT-Strep after overnight digestion with PreScission protease, 3, 4, 5 - flow through fractions from GST column, 6, 7, 8, 9 - elution fractions from amylose column.

As the flow through fractions still contained a big amount of the MBP they were reloaded one more time on the amylose column, to remove MBP contamination. RANTES-LT-Strep was further purified by gel filtration column to characterize the oligomeric status of the protein (Figure 9.10).

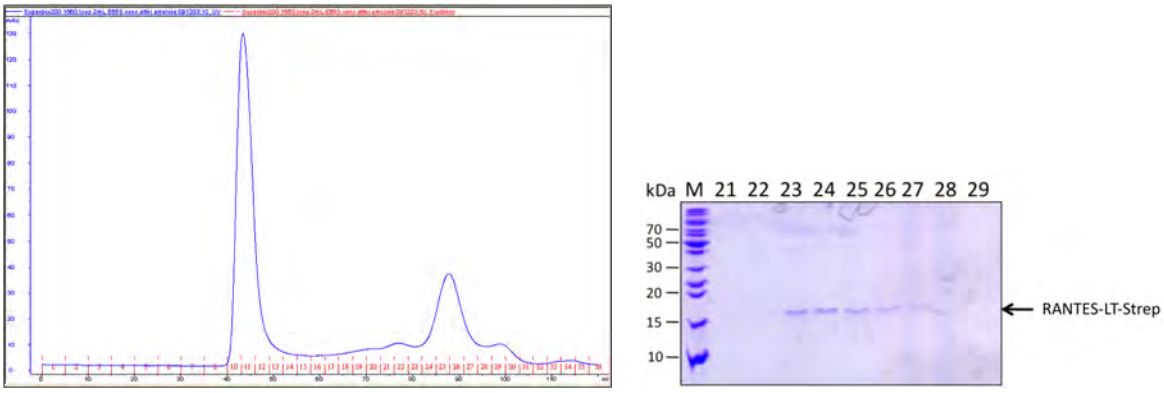

(a) (b)

Figure 9.10.: RANTES-LT-Strep elution profile on Superdex 200 column.
(a) RANTES-LT-Strep elution from Superdex 200 column, (b) SDS-polyacrylamide gel representing 22-29 fractions from Superdex 200 column. M - marker.

The gel filtration Superdex 200 column elution profile indicated that RANTES-LT-Strep elutes with different oligomeric states: probably corresponding to monomers, dimers and mostly higher oligomers (Figure 9.10).

At the end of the purification we obtained about 2.5 mg of dimer-monomer protein per one liter of bacterial culture. The presence of two disulphide bridges, required for proper protein folding was confirmed by Mass Spectroscopy analysis. The protein was analyzed in oxidized and reduced conditions (in the presence of DTT). A 4 Da mass increase (from 13820 Da to 13824 Da) confirmed the presence of the two awaited disulphide bridges for these chemokines (Figure 9.11).

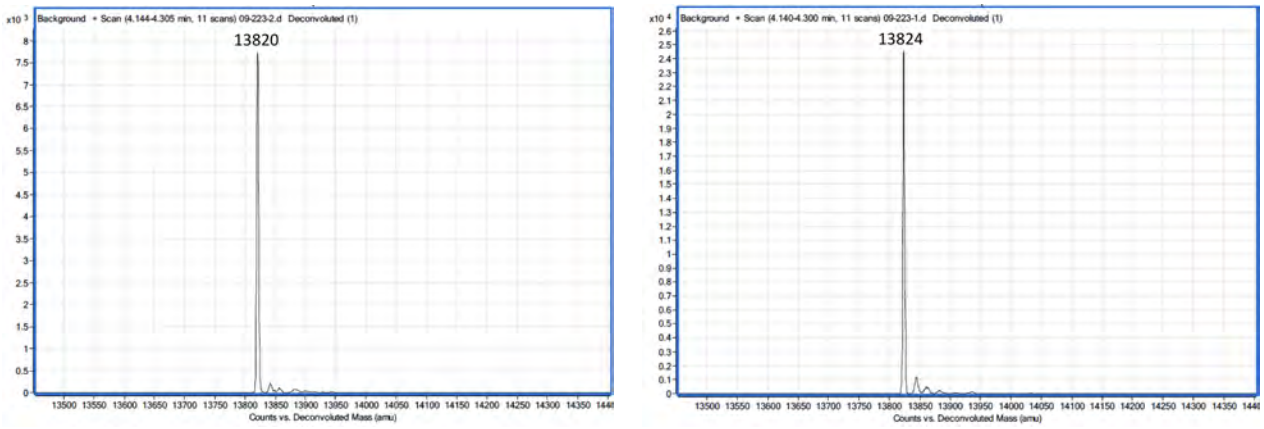

(a) (b)

Figure 9.11.: MALDI Spectrum of RANTES-LT-Strep.
(a) RANTES-LT-Strep sample corresponds to the 13820 Da mass, (b) RANTES-LT-Strep sample with DTT was reduced and a 4 Da increase (13824 Da) confirmed the presence of two disulfide bridges.

We wanted to characterize RANTES oligomerization and to examine if the produced RANTES behaves similarly as it was previously described [370]. It was stated that at high protein concentration (1-10 μM) and low salt - 0.15 M sodium chloride concentration RANTES behaves as a high molecular mass aggregate (100-200 kDa). The aggregation is reversible and protein dilution as well as the presence of high sodium chloride concentration (0.5 M) reduce aggregation of RANTES. Thus, in the presence of 0.5 M sodium chloride and at the same 1-10 μM protein concentration, RANTES is a dimer.

Different protein concentrations (0,7 mg/ml and 1,4 mg/ml) and two salt concentrations (0.150 M and 0.5 M of NaCl) were used to determine the influence of those two parameters on the oligomeric state of RANTES-LT-Strep. The gel filtration elution profiles of those different conditions are represented in Figure 9.12. In either case of low protein and low salt concentration or high protein and high salt concentration RANTES-LT-Strep had a tendency to oligomerize or aggregate. Just a small fraction of protein is in the dimer-monomer equilibrium fraction (Figure 9.12 A and B).

In the presence of high salt concentration and low protein concentration the amount of oligomers decreased and the dimer-monomer fraction increased (Figure 9.12 C).

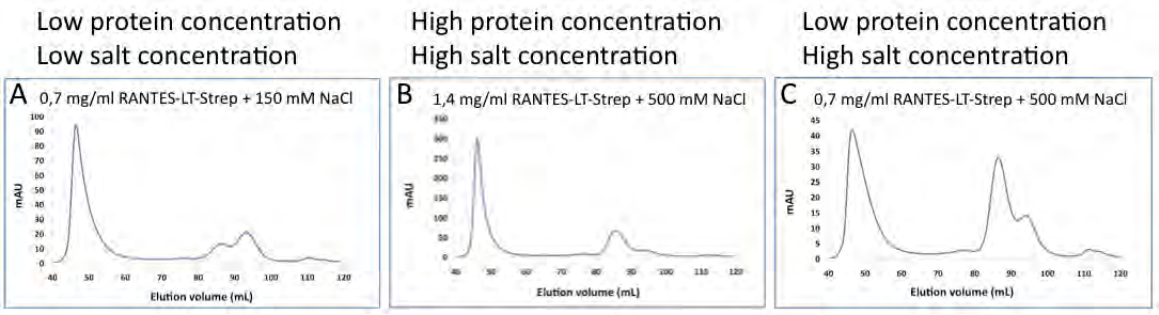

Figure 9.12.: RANTES-LT-Strep oligomerization states monitored in gel filtration column. A Superdex 200 column was used for all elution (a) RANTES-LT-Strep at 0.7 mg/ml concentration elution profile in buffer containing 0.15 M NaCl. (b) RANTES-LT-Strep at 1.4 mg/ml concentration elution profile in buffer containing 0.5 M NaCl. (c) RANTES-LT-Strep at 0.7 mg/ml concentration elution profile in buffer containing 0.5 M NaCl.

To shift RANTES-LT-Strep towards dimer/monomer fractions an increase of salt concentration was not enough as it was previously stated [370], in our case the protein concentration had to be decreased as well.

9.2.3.3. MBP-PrePro-RANTES-Strep Purification

MBP-PrePro-RANTES-Strep was expressed and purified following the same strategy as MBP-PrePro-RANTES-LT-Strep. Briefly the soluble fraction from one liter of bacterial culture was applied to a Strep-Trap column. The elution fractions were pooled together and digested with PreScission protease overnight. Unfortunately, removal of the MBP fusion led to total precipitation of the protein.

9.2.3.4. MBP-PrePro-SDF1α-Strep Purification

MBP-PrePro-SDF1α-Strep was expressed and purified following the same strategy as MBP-PrePro-RANTES-LT-Strep. Briefly the soluble fraction from one liter of bacterial culture was applied to a Strep-Trap column. The elution fractions pooled together and digested with PreScission protease overnight. Once again, the digestion was complete but led to protein precipitation.

It was surprising and obvious from those experiments that besides enhancing the protein expression and the solubility of the fusion proteins, the LT tag was necessary to maintain the chemokine soluble after MBP cleavage. Therefore, the LT tag was added to the SDF1α construct by PCR resulting in MBP-PrePro-SDF1α-LT-Strep construct.

9.2.3.5. MBP-PrePro-SDF1α-LT-Strep Purification

MBP-PrePro-SDF1α-LT-Strep was expressed and purified following the same strategy as MBP-PrePro-RANTES-LT-Strep chemokine. A first step of purification was performed on a Strep Tactin column. Elution fractions containing the fusion protein were pooled and PreScission protease digestion was carried out (Figure 9.13).

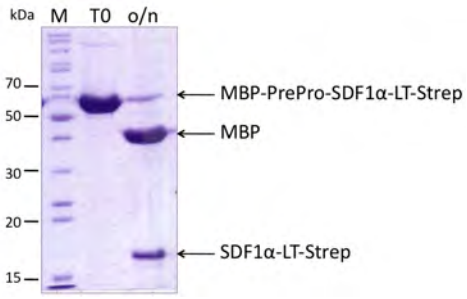

Figure 9.13.: MBP-PrePro-SDF1α-LT-Strep digestion with PreScission protease.
M - marker, T0 - non-digested MBP-PrePro-SDF1α-LT-Strep, o/n - protein after overnight digestion.

As described earlier, the digested sample was applied to the GST column to eliminate the GST tagged PreScission protease. The flow through from the GST column, containing SDF1α-LT-Strep, MBP and uncleaved proteins was applied to the amylose column where MBP and its fusions were retained while the chemokine was collected in the flow through fraction. The flow through from the amylose column was concentrated and applied to a Gel Filtration Superdex 200 column (Figure 9.14).

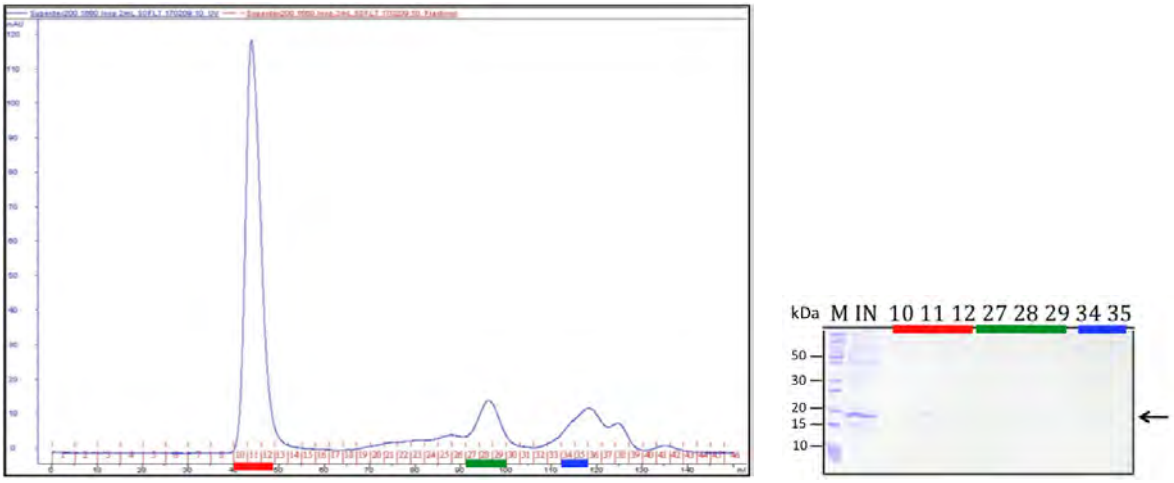

(a) (b)

Figure 9.14.: Purification of SDF1α-LT-Strep on Superdex 200 column.
(a) SDF1α-LT-Strep elution profile from Superdex 200 column. (b) SDS-polyacrylamide gel corresponding to the underlined fractions from the Superdex 200 column. M - Marker, IN - input sample to the Superdex 200 column, 10-35 - elution fraction numbers, the arrow indicates SDF1α-LT-Strep.

The SDF1α-LT-Strep fractions corresponding to the first peak were pooled and concentrated. At the end of the purification we obtained 0.104 mg of SDF1α-LT-Strep from one liter of bacterial culture.

The presence of two disulphide bridges, required for proper protein folding was confirmed by Mass Spectroscopy analysis. The protein was analyzed in oxidized and reduced conditions (in the presence of DTT). A 4 Da mass increase (from 13933 Da to 13937 Da) confirmed the presence of the two awaited disulphide bridges for these chemokines.

9.2.4. Functional assays

9.2.4.1. Chemotaxis

Chemotaxis assays were performed in collaboration with Rabia Sadir (IBS, Grenoble).

In order to finally validate the functionality of our produced chemokines we examined the chemotactic activity of purified SDF1α chemokines and therefore chemotaxis assay was performed. The experiment was carried out using the Boyden chamber-based cell migration assay: a chamber of two medium-filled compartments separated by a microporous membrane. Cells were placed in the upper compartment and were allowed to migrate through the pores of the membrane into the lower compartment, in which chemotactic agents were present. After an appropriate incubation time, the number of cells that have migrated to the lower side of the membrane were determined. Human Jurkat T cells expressing CXCR4 receptors on their surface were used.

As a control for this experiment we used a sample of SDF1α that Rabia Sadir was already using in her experiments (prepared from *E. coli* inclusion bodies) and the functionality of this chemokine was confirmed. Chemokine was added at different concentrations 0,3 nM; 3 nM; 30 nM; 100 nM and 300 nM. The control SDF1α induced chemotaxis of cells with a typically bimodal concentration dependence dose response curve. The maximal response of the cells was obtained for the control SDF1α chemokine at the concentration of 3 nM (Figure 9.15).

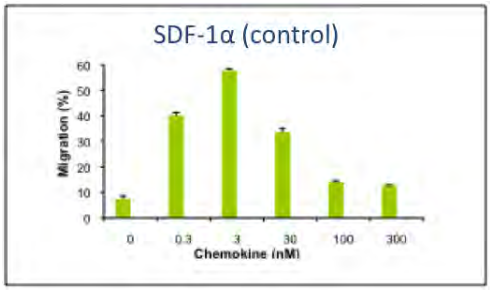

Figure 9.15.: Chemokine induced cell migration.
Control experiment. Mean numbers of migrated cells in triplicate wells are represented.

Two proteins were tested in this assay: the non cleaved MBP-SDF1α-LT and after the SDF1α-LT purified after MBP cleavage (Figure 9.16).

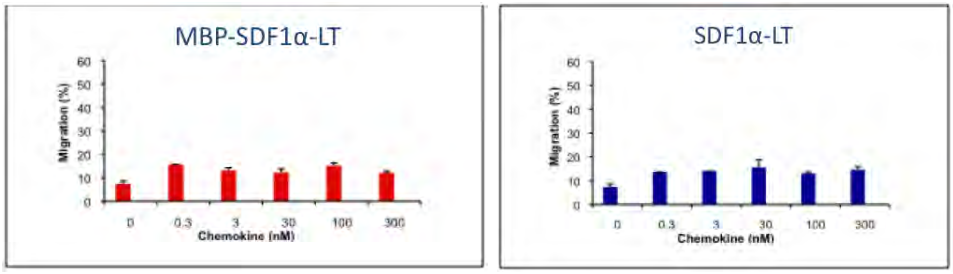

(a) (b)

Figure 9.16.: Chemotaxis assay of MBP-SDF1α-LT and SDF1α-LT.
Mean numbers of migrated cells in triplicate wells are represented.

Unfortunately neither MBP-SDF1α-LT nor SDF1α-LT induced cell migration (Figure 9.16). They had no effect on cell migration within the tested concentration range.

As awaited and contrary to what was published [361] it appears that chemokines that still contained the MBP fusion were not functional in a chemotaxis assay. As expected the MBP-SDF1α-LT was not active, since the N-terminal of chemokines are known to be involved in the interaction with the receptor. Although after MBP cleavage we expected to have a functional chemokine. The disulphide bridge formation is not a conclusive proof of a correct folding; it is necessary but not sufficient. Therefore, it was unexpected to see that SDF1α-LT did not induced cell migration. At the time being the cells used for this chemotaxis assay were expressing only the CXCR4 receptor and for that reason we could not test the functionality of the produced RANTES.

The chemokine production strategy then was changed towards the inclusion body approach.

9.3. Expression in *E. coli* inclusion bodies

9.3.1. Molecular biology

The previous experiments indicated that the addition of the lanthanoid binding tag increased the protein expression and solubility. Thus, for the expression in *E. coli* inclusion bodies chemokines were prepared with and without the LT tag.

New constructs of chemokines were prepared by PCR. The synthetic genes encoding SDF1α and RANTES were cloned into the pET-20b expression vectors. Various constructs of each chemokines were designed for various purposes. On the C-terminal, SDF1α contained either a

Hexahistidine Tag or a Strep-Tag. In another project developed in the group, we had observed that the Strep-Tag could some how reduce the yield of production of another protein that required refolding. Therefore, for the chemokine production from the inclusion bodies additional constructs were designed with a C-terminal His-tag. The two constructs were designed in two versions with and without the LT tag, resulting in 4 constructs: SDF1α-His, SDF1α-LT-His, SDF1α-Strep, SDF1α-LT-Strep. For RANTES three constructs were created, RANTES-Strep, RANTES-LT-Strep and RANTES without of any tag. Those seven versions of chemokines are schematically represented in Figure 9.17.

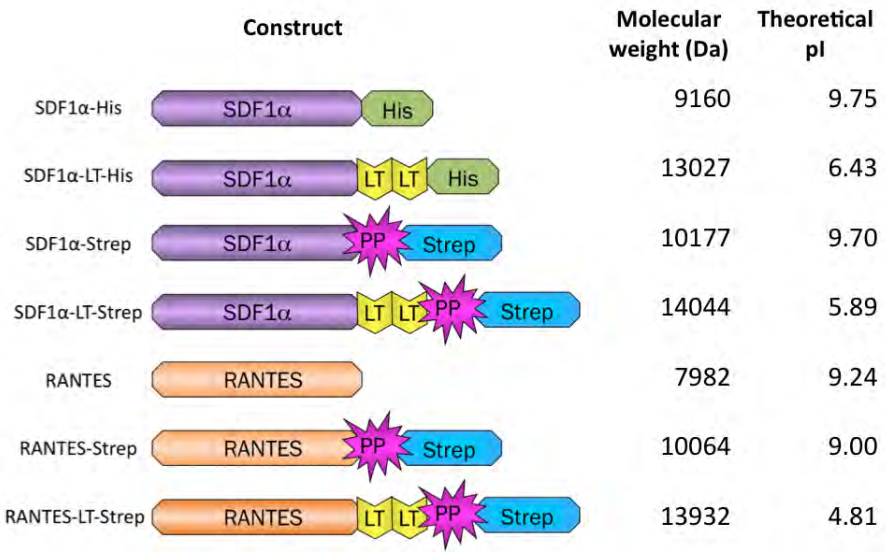

Figure 9.17.: Schematic representation of chemokine constructs for the expression in *E. coli* inclusion bodies.

The first constructs that were prepared were SDF1α-His and SDF1α-LT-His. Once the protocols for the expression and purification were set up, the correct refolding was confirmed and chemotaxis assay showed that the produced chemokines were functional, only then, we carried out with the remaining constructs.

9.3.2. Chemokine expression

The expression of the chemokines was attempted via expression in *E. coli* inclusion bodies [364].

The BL21 (DE3) competent bacteria cells were transformed with various plasmids. The protein expression was carried out in one liter of LB medium with appropriate antibiotic at 37°C. When the culture $OD_{600\,nm}$ reached 0.6-0.8, cultures were induced with 1 mM of IPTG for SDF1α-His and SDF1α-LT-His or 0.5 mM of IPTG for the other constructs. Bacterial culture for the constructs without the LT tag were harvested after 3 hours growth at 37°C. Culture of the constructs with the LT tag were harvested after overnight growth (16 h) at 20°C. Bacterial pellets were resuspended in lysis buffer and lysed with a microfluidizer.

After ultracentrifugation the supernatant containing the soluble proteins (supernatant) were separated from the pellet, where the inclusion bodies remained (pellet) (Figure 9.18).

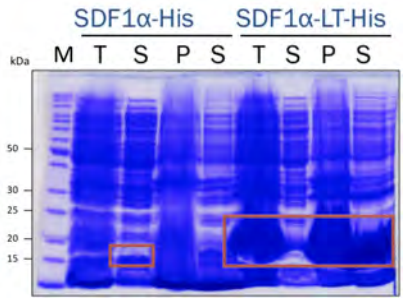

Figure 9.18.: SDS-polyacrylamide gel showing SDF1α-His and SDF1α-LT-His expression in *E. coli* inclusion bodies.
M - marker, T – total extract, S – supernatant, P –pellet.

Once again it was observed that addition of the Lanthanoid binding tag tremendously increased the amount of expressed proteins as well as their solubility.

9.3.3. SDF1α-His and SDF1α-LT-His purification

To solubilize inclusion bodies two conditions were tested for each construct: 7.5 M Guanidine Hydrochloride (GuHCl) and 6 M Urea. The inclusion bodies of the SDF1α-His were solubilized only in the presence of 7.5 M GuHCl and nothing was solubilized in the presence of 6 M Urea. While for the SDF1α-LT-His, the inclusion bodies were solubilized by 6 M Urea but not by 7.5 M GuHCl (Figure 9.19). Refolding took place overnight at 4°C in 50 mM Tris-HCl pH 8.0 buffer.

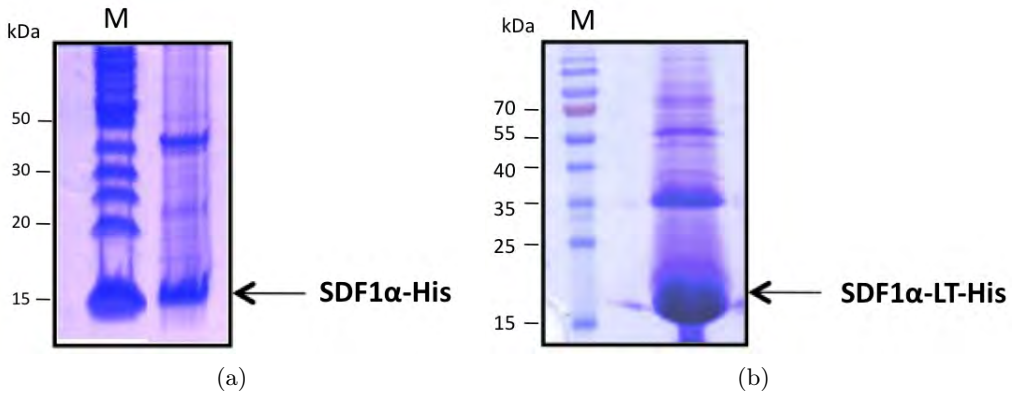

Figure 9.19.: SDS-polyacrylamide gel showing solubilized inclusion bodies.
(a) SDF1α-His solubilized in 7.5 M GuHCl, (b) SDF1α-LT-His solubilized in 6 M Urea. M - marker.

Chemokines have very basic pI, (9.75 for SDF1α-His) (Figure 9.17) and could therefore be purified over a cation exchange column. The addition of the Lanthanoid binding tag changed this

chemokine property, the pI of the SDF1α-LT-His is 6.43. Therefore, the SDF1α-LT-His could be purified on the anion exchange column. After refolding, SDF1α-His was applied to a Capto S column and SDF1α-LT-His was therefore purified over a Q Sepharose column (Figure 9.20).

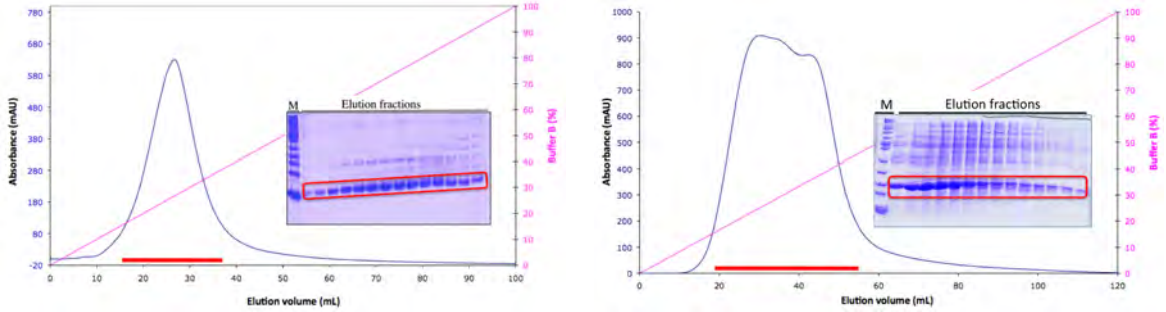

(a) SDF1α-His (b) SDF1α-LT-His

Figure 9.20.: Cation (a) and Anion (b) - exchange chromatography.
Fractions identified by the red line were analyzed on a SDS-polyacrylamide gel. M - marker

Fractions containing chemokines were pooled and concentrated prior injection to a Gel Filtration Superdex 200 column (Figure 9.21).

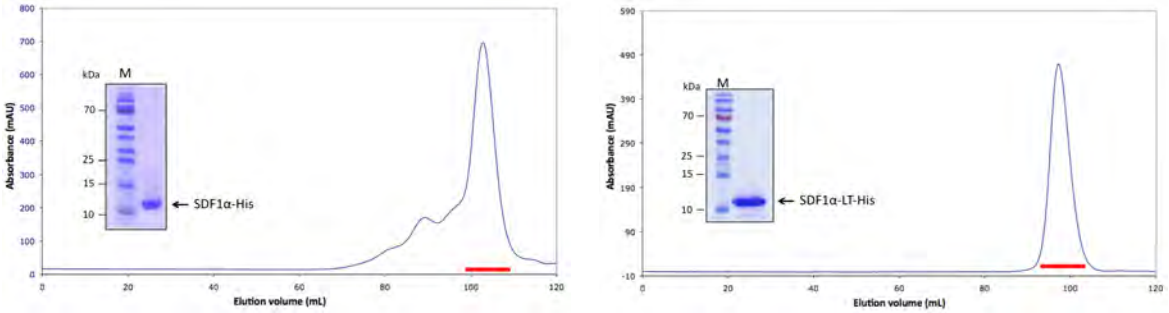

(a) (b)

Figure 9.21.: Gel Filtration elution profiles of SDF1α-His and SDF1α-LT-His.
(a) SDF1α-His elution profile from Superdex 200 column. The protein samples from the main peak were pooled and concentrated. The SDS-polyacrylamide gel indicates the purified SDF1α-His. (b) SDF1α-LT-His elution profile from Superdex 200 column. The protein samples from the peak were pooled and concentrated. The SDS-polyacrylamide gel indicates the purified SDF1α-LT-His. M - marker, the red line indicate protein fractions which were pooled and concentrated.

From one liter of bacterial culture 7.8 mg of pure SDF1α-His and 3 mg of pure SDF1α-LT-His were obtained. The presence of two disulphide bridges, required for proper protein folding was confirmed by Mass Spectroscopy analysis. The protein was analyzed in reducing (in the presence of DTT) and non-reducing conditions. A 4 Da mass increase for SDF1α-His from 9160 Da to 9156 Da and for SDF1α-LT-His from 13023 to 13027 Da confirmed the presence of the two expected disulphide bridges characteristic for these chemokines.

9.3.4. SDF1α-Strep and SDF1α-LT-Strep purification

SDF1α-Strep and SDF1α-LT-Strep were purified form inclusion bodies using the strategy used for SDF1α-His and SDF1α-LT-His. Details of purifications could be found in the Annex 15.1.

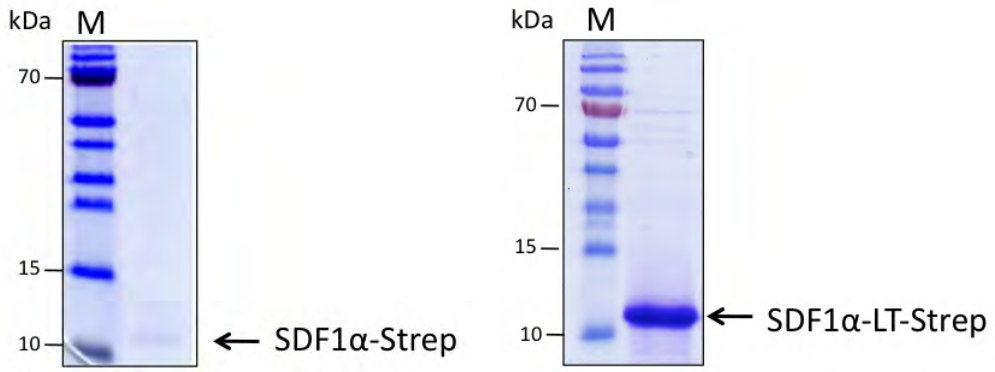

(a) (b)

Figure 9.22.: SDS-polyacrylamide gel showing purified SDF1α-Strep and SDF1α-LT-Strep. (a) Sample of purified SDF1α-Strep. (b) Sample of purified SDF1α-LT-Strep.

The details of purification are placed in Annex 15.1. From one liter of bacterial culture 0.2 mg of SDF1α-STREP and 3.2 mg of SDF1α-LT-Strep were obtained (Figure 9.22).

9.3.5. RANTES-Strep purification

Due to the known RANTES tendency to oligomerize the purification protocol used for SDF1α-His was not optimal and was further improved by referring to some published protocol [371]. Inclusion bodies containing RANTES-Strep were solubilized in 6 M GuHCl, incubated for 30 minutes at 60°C and dialyzed against 1% acetic acid. Due to its very basic pI (9.00) and its particular biochemistry RANTES-Strep resists to the harsh purification conditions while most of other proteins precipitate. The protein sample was then centrifuged and diluted up to 1 mg/ml final concentration in 50 mM Tris-HCl pH 8.0, 6 M GuHCl , 1 mM DTT buffer. Protein was refolded overnight at 4°C in 20 mM Tris-HCl pH 8.8, 0.01 mM oxidized glutathione, 0.1 mM reduced glutathione buffer. The refolded sample was centrifuged, the pH was adjusted to 4.5 and the protein was applied to a Capto S column (Figure 9.23a).

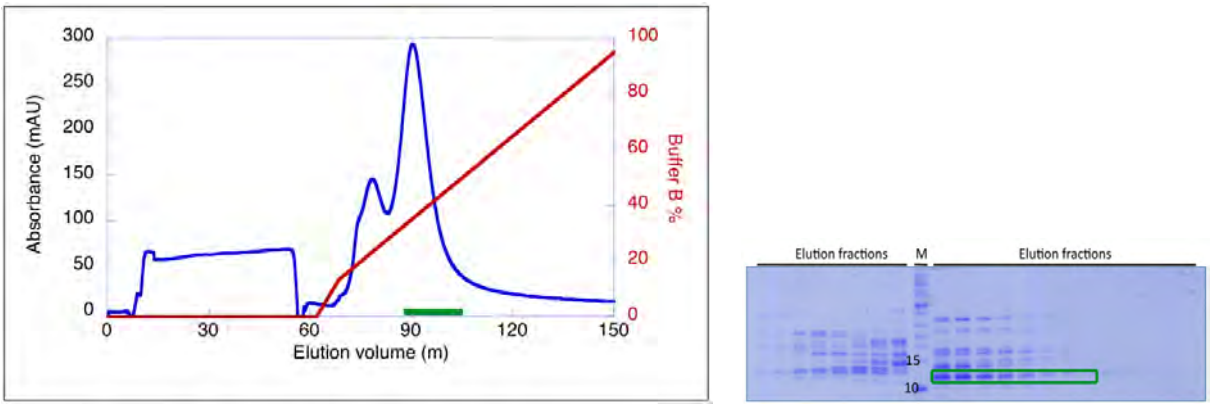

(a) (b)

Figure 9.23.: RANTES-Strep purification on Capto S column.
(a) RANTES-Strep loading (first 50 ml) and elution from Capto S column, (b) Elution fractions form both peaks were analyzed on a SDS-polyacrylamide gel. Fractions identified by the green line on the chromatogram correspond to the indicated RANTES-Strep on the SDS-polyacrylamide gel.

Elution fractions were analyzed on SDS-polyacrylamide gel (Figure 9.23b) which revealed that RANTES-Strep was eluted in the second pick of the Capto S column. Fractions containing the chemokine were pooled and concentrated prior injection to a Superdex 200 Gel Filtration column (Figure 9.24).

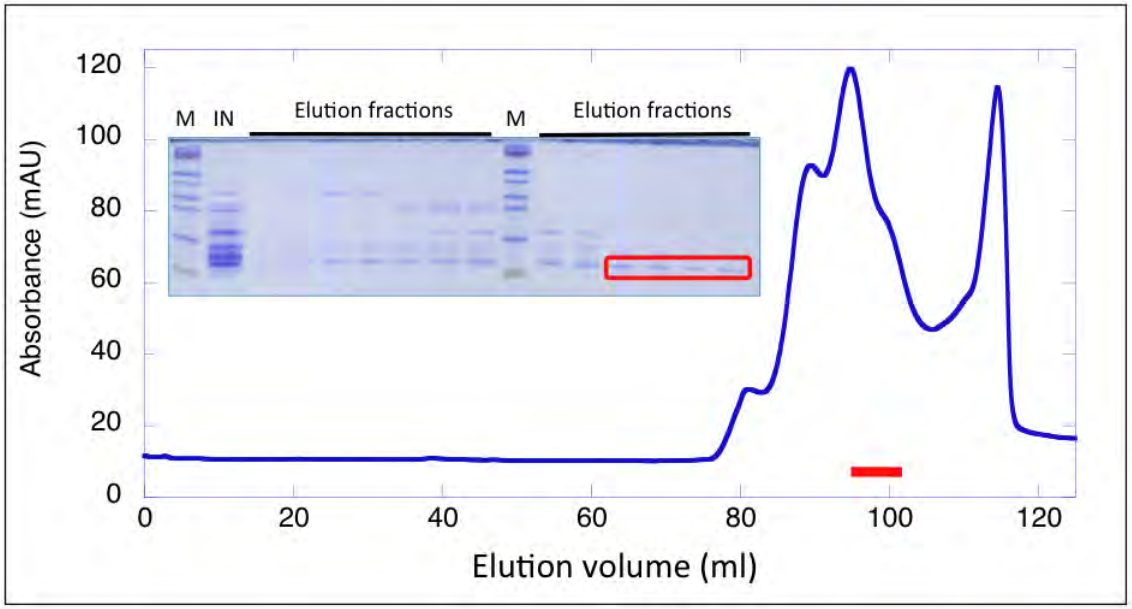

Figure 9.24.: RANTES-Strep elution profile from the Superdex 200 column.
Elution pics were analyzed on a SDS-polyacrylamide gel. The fractions identified by the red line on the chromatogram corresponds to the indicated RANTES-Strep in the SDS-polyacrylamide gel.

The purest fractions containing RANTES-Strep were pooled and concentrated. From one liter

of bacterial culture 0.2 mg of RANTES-Strep were obtained (Figure 9.25).

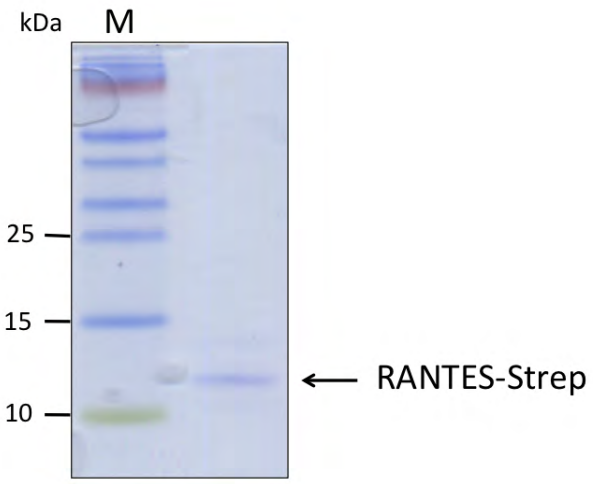

Figure 9.25.: SDS-polyacrylamide gel of purified RANTES-Strep.

9.3.6. RANTES purification

RANTES purification protocol was carried out as previously described for RANTES-Strep. From one liter of bacterial culture 0.22 mg of RANTES were obtained (Figure 9.26).

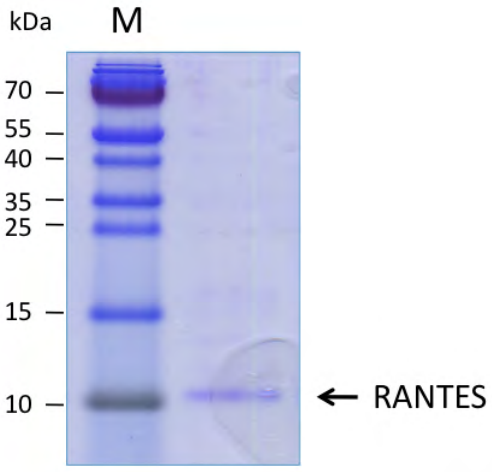

Figure 9.26.: SDS-polyacrylamide gel of purified RANTES.

9.3.7. RANTES-LT-Strep purification

RANTES-LT-Strep was purified as previously described SDF1α-LT-His. Inclusion bodies containing RANTES-LT-Strep were solubilized in 6M Urea and protein was refolded overnight at 4°C by a drop wise dilution in 20 mM Tris-HCl pH 8.8, 0.01 mM oxidized glutathione, 0.1 mM

reduced glutathione buffer. The refolded sample was centrifuged and applied to a Q Sepharose column (Figure 9.27a).

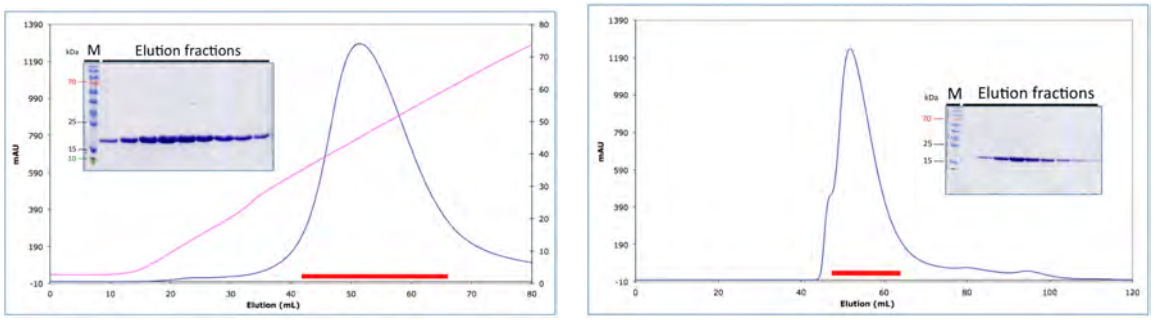

(a) Q Sepharose column (b) Superdex 200 column

Figure 9.27.: RANTES-LT-Strep purification on Q Sepharose (a) and Superdex 200 (b) columns. Fractions identified by the red line were analyzed on a SDS-polyacrylamide gel. M - marker.

Elution fractions from Q Sepharose column containing the protein were pooled and centrifuged prior injection to the Superdex 200 column. RANTES-LT-Strep eluted as oligomers (Figure 9.27b), fraction containing containing RANTES-LT-Strep were pooled and concentrated. From one liter of bacterial culture 6.5 mg of RANTES-LT-Strep were obtained.

All purified chemokines are summarized in the Figure 9.28.

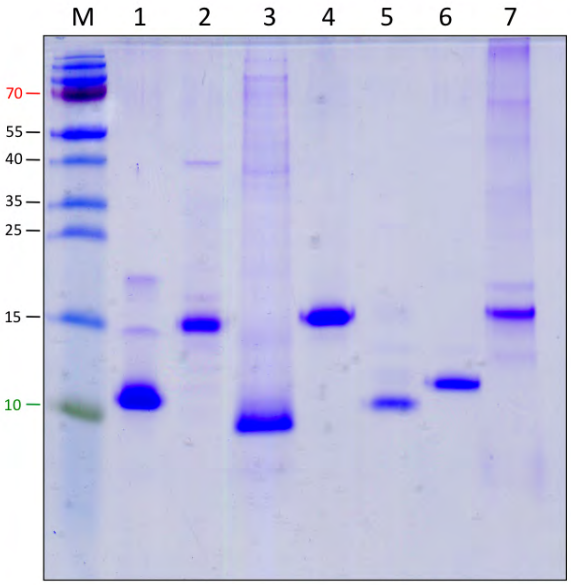

Nr	Construct	Production Yield *
1	SDF1α-His	7.8
2	SDF1α-LT-His	3
3	SDF1α-STREP	0.2
4	SDF1α-LT-STREP	3.2
5	RANTES	0.22
6	RANTES-STREP	0.2
7	RANTES-LT-STREP	6.5

Figure 9.28.: SDS-polyacrylamide gel representing all purified chemokine constructs. M - marker (kDa), * - mg/per liter of culture.

All prepared chemokine constructs were purified although not all of them were obtained in similar quantities. Comparing the C-terminal tags of SDF1α it is clear that the refolding was

working far better for His-tagged chemokines than for Strep-Tagged ones. The LT tag enable a big improvement only for the Strep-Tagged constructs while it did not enhance so much His-tagged constructs. For RANTES purification the LT tag allowed a tremendous (more than 30 times) improvement. The yield of RANTES and RANTES-Strep were very similar. RANTES purification has just been produced once, contrary to the other chemokine construct productions that were always obtained in similar amounts.

9.4. Chemotaxis

In order to examine the chemotactic activity of the purified chemokines a chemotaxis assay was performed. The experiment was performed using the Boyden chamber-based cell migration assay. As before, a control SDF1α from Rabia Sadir was used. The functionality of this control chemokine was first assessed (SDF1α-WT). As before, the chemokine was added at different concentrations ranging from 0.3 nM to 300 nM. Our "home made" chemokines SDF1α-His, SDF1α-LT-His, SDF1α-Strep, SDF1α-LT-Strep, RANTES-Strep and RANTES-LT-Strep were tested using the same concentration range from 0.3 nM to 300 nM (Figure 9.29).

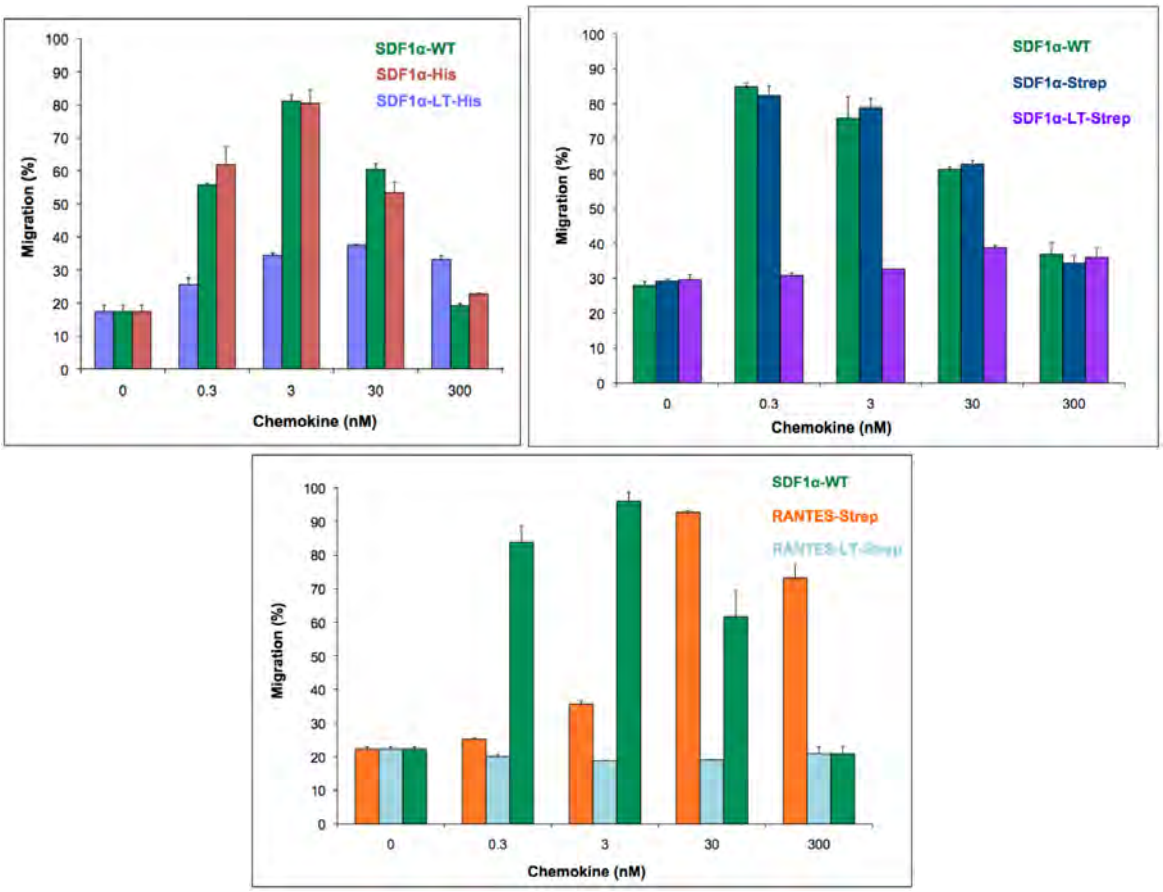

Figure 9.29.: Chemotaxis assay of chemokines.
SDF1α-WT is a control experiment (green histograms). Mean numbers of migrated cells in triplicate wells are represented.

From this chemotaxis assays we can conclude that recombinant SDF1α-His, SDF1α-Strep and RANTES-Strep chemokines are functional. The control SDF1α-WT and our "home made" SDF1α-His induced chemotaxis of cells with a typically bimodal concentration dependence dose response curve. Similar effect could be observed for the SDF1α-Strep. Surprisingly the SDF1α-LT-His showed decreased activity but still followed the same typical bimodal concentration dependence dose response curve. Though, it is hard to conclude if the slight activity of SDF1α-LT-Strep at 30 nM concentration is significant. For some reason the SDF1α-LT-His showed some activity while it is doubtful in the case of SDF1α-LT-Strep. RANTES-Strep induced cell migration but with a lower sensitivity than SDF1α, as the maximal responses of the cells were obtained at 3 nM and 30 nM concentration, respectively. From the obtained results it is quite clear that RANTES-LT-Strep was not active in this chemotaxis assay.

9.5. Luminescence titration

For terbium titration 2 ml of SDF1α-LT-His chemokine at 75 μM concentration were used.

Terbium luminescence was enhanced when metal-protein complex was excited at 280 nm. The indole ring of the Trp present in the Lanthanoid binding tag serves as an antenna for the terbium which then emits at 490 nm and 542 nm. The LT was developed to exclude water from the lanthanide coordination sphere, since coordinated water molecules cause excited terbium to undergo rapid, non-radiative energy transfer to the vibrational states of the water O-H bonds, leading to a decrease in the luminescence intensity and lifetime. When terbium is in buffer (in aqueous environment) the coordination of water leads to non-radiative decay of the lanthanide excited state. Therefore no sharp picks are observed (Figure 9.30 blue graph). Upon peptide binding (LT) to the terbium the water from the inner coordination sphere was excluded and terbium was chelated. When terbium is bound to the protein, long luminescence lifetimes and very sharp emission bands of the complexes were observed (Figure 9.30 red graph).

First the smallest concentration detectable in buffer of terbium was determined: a 2 μM concentration was the smallest terbium concentration detectable (Figure 9.30 blue graph). Then the same concentration of terbium was added to the protein solution (Figure 9.30 red graph). the tremendous increase of the 2 emission peaks clearly indicate that the terbium is bound to the LT.

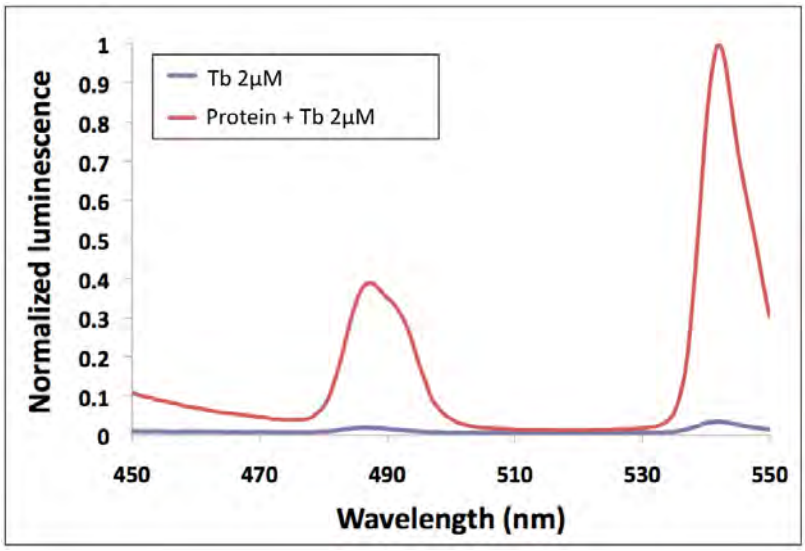

Figure 9.30.: Tryptophane-sensitized Tb^{3+} luminescence emission spectra of buffer and SDF1α-LT-His during 2 µM terbium.
Blue graph - Tb^{3+} in the presence of buffer, red graph - Tb^{3+} in the presence of SDF1α-LT-His.

The terbium binding to the LT was assessed via direct luminescence titration (Figure 9.31).

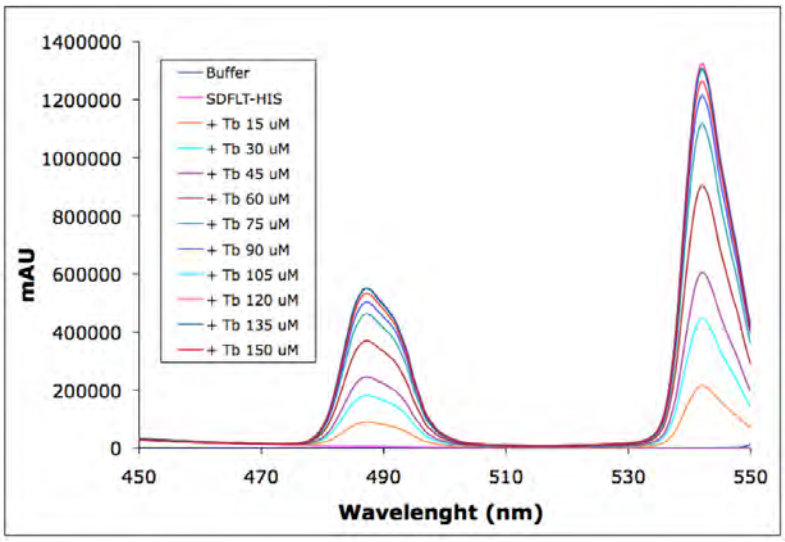

Figure 9.31.: Tryptophane-sensitized Tb^{3+} luminescence emission spectra of SDF1α-LT-His in the presence of terbium titration.

Titration performed on SDF1α-LT-His (monomer) using increasing concentrations, ranging from 15 µM to 150 µM, of terbium indicated an increase of luminescence at 490 nm and 542 nm. Those results indicated that the Lanthanoid binding tag is well structured and thus functional, since it can bind terbium.

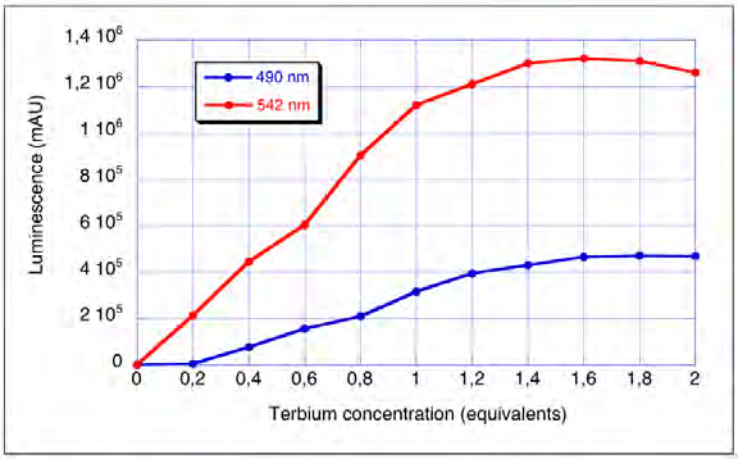

Figure 9.32.: Luminescence at 490 nm and 542 nm as a function of terbium concentration.

In order to determine at what terbium concentration both binding sites in the LT tag were fully occupied the luminescence values from two wavelengths (of each major pick) were plotted (Figure 9.32). That graphic indicated that saturation of the double Lanthanoid binding tag is achieved with two equivalents of terbium per protein as expected.

9.6. Development of an electrophysiology test of chemokine triggered signal transduction

It is known that modifications of the N-terminal chemokine part drastically affect interaction with their receptor. Nothing has been reported so far for C-terminal modifications. To characterize receptor binding and signal transduction triggered by our recombinant chemokines we used the approach set up by C. Moreau and M. Vivaudou (IBS, Grenoble).

Their strategy consists in the expression of the receptor in Xenopus oocytes (eukaryotic system) by relatively simple mRNA transfection. Using the Two-Electrode Voltage Clamp method, the ligand binding to the chemokine receptor triggers it activation and the subsequent activation of G proteins that would affect ion channel gating. Real-time measurement of ion channel activation allows the evaluation of biological chemokine activity both quantitatively and qualitatively.

The data corresponding to the characterization of engineered chemokines using an electrophysiology approach are presented in the following preliminary version of a future manuscript.

Engineering and production of tagged CXCR4/CCR5 chemokines and functional characterization with a Xenopus oocyte electrophysiological assay

Picciocchi Antoine[1235], Šiaučiūnaitė-Gaubard Lina[1235], Petit-Hartlein Isabelle[123], Vivaudou Michel[123], Fieschi Franck[134], Moreau Christophe[1236], Vivès Corinne[1236].

[1]Institut de Biologie Structurale, Université Joseph Fourier-Grenoble, 41 rue Jules Horowitz, 38027 Grenoble, France; [2]CEA, DSV, 38027 Grenoble France; [3]CNRS, UMR 5075, 38027 Grenoble, France; [4]Institut Universitaire de France, 103 boulevard Saint-Michel, 75005 Paris, France; [5]These authors contributed equally to this work; [6]Correspondence and requests for materials should be addressed to christophe.moreau@ibs.fr and corinn.vives@ibs.fr

Introduction

The crucial interest in G protein coupled receptors (GPCRs) does not need to be demonstrated any more. The percentage – over 30 % - of drugs available in the actual pharmaceutical market that target GPCRs is sufficient to rank them as major biological topics Lagerström & Schiöth (2008). However, despite a very recent breakthrough in the resolution of GPCR structures (for a recent review see Katritch *et al.* (2012)), the heavy sequence modifications that were required to overcome expression, purification and crystallization bottlenecks may have introduced bias to apprehend the biological functions of those proteins. The oligomeric status of the class A receptor/ligand complex in its native environment, for instance, has not yet been answered by those structures. Besides, there is still a strong need for "in solution" investigations of the receptor or the receptor/ligand complex. Although the membrane protein production remains the most delicate aspect of such an approach, when the ligand is also a protein, one prerequisite to such studies is as well the set up of a solid and valid ligand production system. Once recombinant ligand has been produced, and in particular if some modifications have been introduced in its sequence, its functionality has to be assessed, and its receptor binding and signaling capacities have to be evaluated prior any further receptor/ligand complex formation. To investigate such molecular recognition events and the consecutive ligand induced signaling cascade, the reconstitution of an environment that resembles the native membrane is often required. Consequently, expression at the cell membrane can be considered but is never straightforward as toxicity problems may be faced. Alternatively, reconstitution in proteoliposomes can be requested. One prerequisite for some of those experiments is the expression of large amount of proteins, which could be a tight obstacle with those receptors that are notoriously known to be reticent to overexpression. Besides, most of the existing methods to determine binding affinity are based on the use of labeled ligands. One of the problems to circumvent in that type of approach is to find the ideal label that does not interfere with ligand binding. Radioactivity can thus appear as a very attractive approach as the introduction of radioactive isotopes does not modify the binding properties but is unavoidably linked to the drawbacks inherent to radioactivity handling and disposal. One alternative is the use of a fluorescent label Briddon *et al.* (2011), there, two difficulties have to be faced: getting a sufficient signal/noise ratio, and introducing the fluorophore to the ligand. Besides, functional tests must ensure GPCR signal transduction cascade. Ligand binding to GPCRs triggers conformational changes within GPCR helices, leading to a coupling with the heterotrimeric G protein. The G protein a subunit undergoes an exchange of GDP to GTP and dissociates from the $\beta\gamma$ subunits. Both elements can then interact with downstream elements (adenylate cyclase, ion channels...) and modulate their activity. Besides various secondary messengers (cAMP, IP3) are produced by the effectors leading to the amplification of the signal. Most of the functional assays on GPCRs are distal from the initial activation event as solely based on the determination of concentration variation of those second messengers. Those include the mesurement of agonist stimulated radioactive GTP binding to the G protein Labrecque *et al.* (2009), the measurement of intracellular Ca^{2+} flux, variation in cAMP concentration... Finally some cellular assays based on GPCR induced cell morphology changes Peters *et al.* (2007) or on ligand triggered receptor translocation Grånäs *et al.* (2005).

We present here the valuable diversion that can be done from a conventional electrophysiology approach to study the transduction path-

way generated by chemokine ligands binding to their respective GPCRs. As regards of their key roles in inflammatory processes and HIV pathology, the two models that are considered in this work (CXCL12/CXCR4 and CCL5/CCR5) do not need to be further advertised as attractive drug targets Sallusto *et al.* (2000); Wyatt & Sodroski (1998). However, although they have been extensively studied since the mid-nineties, crucial questions around their biology remain unanswered and have not found any responses from the recently published structure of CXCR4 Wu *et al.* (2010): those include ligand/receptor complex stoichiometry or the relevance of receptor oligomerisation. Molecular investigation of those chemokines/ receptor interactions could be facilitated by the sequence engineering of the ligands. Affinity tags could be added to facilitate purification (His tag), ligand could be visualised by the incorporation of fluorescent properties (addition of Lanthanoid binding Tag), ligand anchorage to solid support (chromatography matrix, Biacore chips...) could be enabled (addition of Strep Tag). However such modifications could alter their functionality.

Abundant literature can be found concerning N-terminus modifications of those chemokines that have been reported to dramatically modified their functionality including Examples of N-terminal modified chemokines, designed and studied for their potency as HIV inhibitors C1 C5 CCL5, Polo *et al.* (2000), AOP CCL5, Mack *et al.* (1998), NNY-CCL5, Sabbe *et al.* (2001), P2 CCL5, Jin *et al.* (2010)... Therefore sequence engineering was performed on the C-terminus of the chemokines. In order to test the biological activity of our broad range of differentially tagged recombinant chemokines we exploited the ability of CXCL12 and CCL5, to trigger Gi/o protein activation after binding to their respective CXCR4 and CCR5 receptors. Once activated the heterotrimeric Gi/o proteins separates and the G$\beta\gamma$ dimers open the G protein-activated potassium channel Kir3.1* (Fig. 1A).

By co-injecting Kir3.1* mRNA with chemokine receptors mRNA (Fig. 1B), we create an electrophysiological reporter of the chemokine-induced G protein activation. Using the Two-Electrode Voltage-Clamp (TEVC) technique (Fig. 1C), the current generated by all Kir3.1* channels expressed in the plasma membrane are easily recordable. Moreover, the TEVC technique is appropriate for the functional characterization of external ligands, such as the chemokines.

Thus, the Kir3.1* functional assay offers the possibility to easily evaluate the biological activity of chemokines, qualitatively (receptor/channel activation or not, reversibility of the activation) and quantitatively (amplitude of activation, apparent affinity). Besides it reflects a direct recording of the ligand binding without too many secondary messenger intermediates. No overexpression or purification procedure of the GPCR are required.

This article describes the expression and purification of various chemokine constructs designed as new tools to carry out chemokine receptor studies and their functional validation using an electrophysiology approach. This test non only states the receptor binding capacity of the engineered chemokines but also reports the consequences of the modification on signal transduction.

Materials and methods

Engineering of expression vectors

Standard pUC57 plasmids containing optimized synthetic human genes designed for the efficient production of chemokines in *E. coli* were manufactured by GeneCust (Evry, France). After PCR amplifications using suitable primers, cDNAs encoding the full-length chemokines were sub-cloned into the pET-20b (Novagen) (chemokines expres-

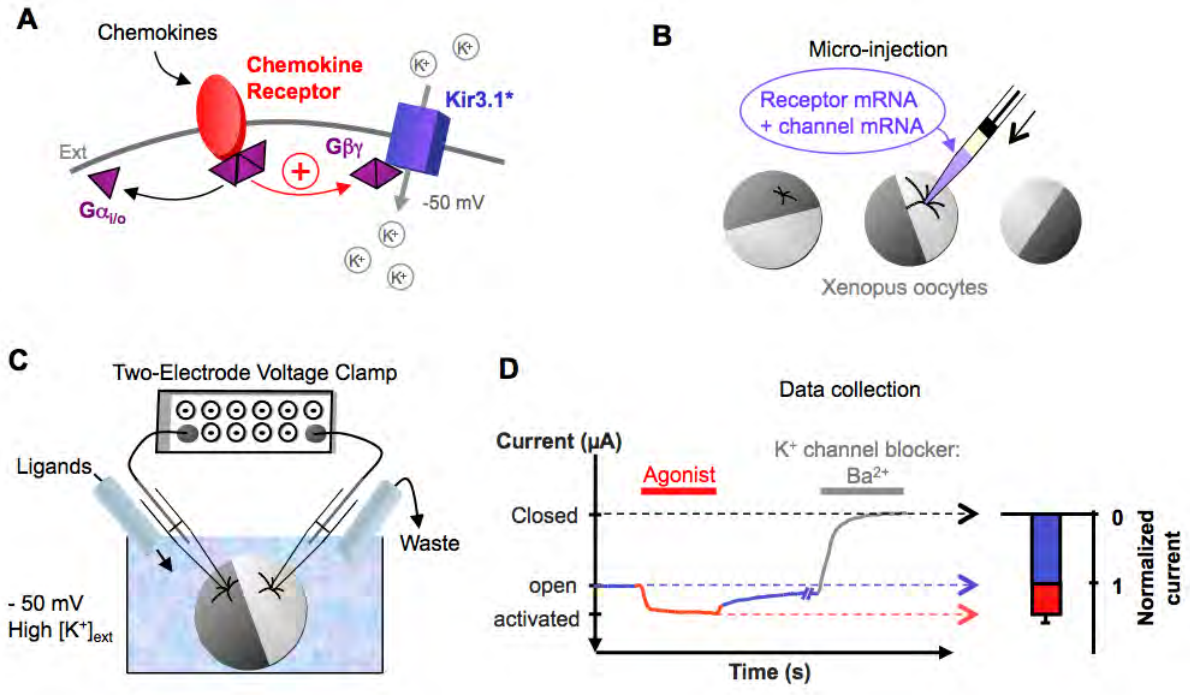

Figure 1: Principle of the electrophysiological characterization of chemokine receptors. **A**. Schematic representation of a plasma membrane containing the heterologously expressed chemokine receptor and the G protein activated Kir3.1* channel. The channel Kir3.1 is mutated (*: F137S) to form homomeric channels. Binding of specific chemokines induces receptor conformational changes and subsequently the activation and scission of the heterotrimeric Go proteins. The Gβγ subunits activates the Kir3.1* channels resulting in an increase of the inward current amplitude generated at -50mV in symmetrical K^+ concentration. **B**. Chemokine receptors and Kir3.1* channels are heterologously expressed in Xenopus laevis oocytes by mRNA micro-injection. After 2 days-incubation, purified chemokines are electrophysiologically characterized. **C**. Schematic representation of the Two-Electrode Voltage Clamp set-up. The oocyte is impaled by 2 glass pipettes containing 3M KCl and a Ag/AgCl electrode. Electrical current recording is performed under continuous flow of buffer +/- ligands or channel blockers. Change of solutions is controlled by a semi-automatic perfusion system. The used TEVC bath has a potassium concentration similar to the intracellular K+ concentration. **D**. Representative TEVC recording of Kir6.2 generated current at -50 mV. The basal current generated by the channels in basal state is determined in the first minute and represented in blue line and bar. This basal current is the reference (100%) for the normalization of ligand-induced effect represented in red line and bar. Barium (Ba^{2+}) is a generic blocker of K^+ channels and positions the barium-sensitive baseline.

sion in *E. coli* inclusion bodies) or pMAL-C4x (New England Biolabs) (chemokines expression with a N-terminal fused maltose binding protein) expression plasmids (Fig. 2). For some constructs, an additional double-lanthanide-binding tag Martin *et al.* (2007) was inserted in the C-terminal part of the proteins. Depending on the construction, this tag is located before a PreScission protease site that can be used for the cleavage of the C-terminal Strep-tag. The sequencing of each construction listed in Fig. 2 was done by Cogenics (Meylan, France).

Expression of recombinant chemokines

The *E. coli* BL21 (DE3) cells transformed with the different expression vectors were grown at 37°C in Luria Bertani medium supplemented with 100 µg.mL-1 of ampicillin until cultures reached an optical density of 0.6 to 0.8 at 600 nm. Then, 1 mM isopropylthio-β-D-galactopyranoside (IPTG) was added to the cultures in order to induce synthesis of recombinant proteins. Cells were further incubated for 3 h at 37°C (CXCL12-His, CXCL12-Strep and CCL5-Strep) or 16 h at 20°C (MBP-CXCL12-Strep, MBP-CCL5-Strep, CXCL12-LT-His, CXCL12-LT-Strep and CCL5-LT-Strep), harvested and centrifuged for 30 min at 5 000 g.

MBP-CXCL12-Strep and MBP-CCL5-Strep purification

Bacterial cells expressing the MBP-fused chemokines were resuspended in buffer A (100 mM Tris-HCl pH 8.0, 150 mM NaCl, 1 mM EDTA) containing 1 tablet of Complete protease inhibitors (Roche) and disrupted as described above. After centrifugation for 45 min at 20 000 g, soluble MBP-chemokines present in the supernatant were purified by an affinity chromatography using a StrepTactin column (5 mL, Amersham Biosciences) previously equilibrated in buffer A. After an extensive washing step, recombinant chemokines were eluted with buffer A supplemented with 2.5 mM of dethiobiotin. After purification, the N-terminal MBP-domain of the fusion proteins was cleaved after an overnight incubation at room temperature with the Pre-Scission protease (1.75 U protease/mg of fusion proteins). Removal of the MBP moiety was performed by purification over an amylose column (BioLabs). The unbound fraction that contained the chemokine was concentrated and run over a Superdex 200 gel filtration column.

Inclusion bodies preparation

Bacterial cells expressing chemokines in inclusion bodies were resuspended in 50 mM Tris-HCl pH 8.0 (buffer B) supplemented with 1 tablet of Complete protease inhibitors (Roche). Each bacterial pellet was disrupted twice using a Microfluidizer M-110P (Microfluidics international, Newton, MA) at 10 000 psi. After centrifugation for 30 min at 20 000 g, inclusion bodies were pelleted and washed with buffer B supplemented with 2M Urea and 5 % Triton X100, then with buffer B containing 2M Urea and finally with the buffer B alone.

CXCL12-His and CXCL12-Strep refolding and purification

Inclusion bodies were solubilised for 20 min at 50°C in buffer B with 7.5 M GdmCl, 5 mM EDTA and 20 mM DTT. Refolding was performed by rapid dilution with buffer B down to 1 M GdmCl. The mixture was gently stirred overnight at 4°C after addition of Complete protease inhibitors (Roche), diluted 4 times with buffer B and loaded onto a CaptoS column (5 mL, Amersham Biosciences) equilibrated in 50 mM Tris-HCl pH 7.5. Chemokines were then eluted with a NaCl gradient (0-1 M), concentrated and further

Constructs	Molecular weight (Da)	Theoretical pI	Expression	Refolding efficiency
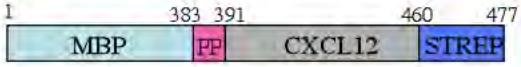	52836	6,64	+	NT
	52724	5,77	+	NT
	9160	9,75	+	+ +
	13027	6,43	+ +	+ +
	10177	9,70	+	-
	14044	5,89	+ +	+ +
	7982	9,24	+	-
	10064	9,00	+	-
	13932	4,81	+ +	+ +

Figure 2: Scheme of the expression pattern and theoretical parameters of the different engineered chemokines.

Schematic representation of each chemokine construction are reported on the left. The numbers represent the position to the sequence in each construction. The theoretical molecular weight and isoelectric point were determined with the Expasy ProtParam tool (http://web.expasy.org/protparam/). The chemokine expression and refolding efficiency are also indicated. MBP: Maltose Binding Protein; PP: PreScission protease site; STREP: Strep-Tag; HIS: His-Tag; LT: Lanthanoid binding tag; (-): low refolding efficiency; (+): good expression level; (++): strong expression level; NT: Not tested.

purified on a Superdex 200 gel filtration column (Amersham Biosciences) previously equilibrated in 20 mM Na_2HPO_4 pH 6.0. Purified proteins were analyzed by ion-spray mass spectrometry and stored at –80°C until use.

CCL5-Strep refolding and purification

Inclusion bodies were solubilised for 30 min at 60°C in buffer B with 6 M GdmCl and 1 mM DTT. After centrifugation for 30 min at 20,000 g, the clear supernatant is dialyzed 4 hours at room temperature against a 1% acetic acid in order to remove impurities. The concentrated, clear supernatant was diluted to obtain 1 mg/mL of protein and refolding was achieved by dropwise dilution in the adequate refolding buffer (20 mM Tris-HCl pH 8.0, 0.01 mM oxidized glutathione and 0.1 mM reduced glutathione). After an overnight incubation at 4°C with mild stirring, the pH of the solution was adjusted to 4.5 and subsequently loaded on a CaptoS column (5 mL, Amersham Biosciences) pre-equilibrated in 50 mM Na-Acetate pH 4.5. The protein was then eluted with a NaCl gradient (0-1 M), concentrated and further purified on a Superdex 200 gel filtration column previously equilibrated in 20 mM Na_2HPO_4 pH 6.0, 150 mM NaCl.

CXCL12-LT-His, CXCL12-LT-Strep and CCL5-LT-Strep refolding and purification

Inclusion bodies were solubilised for 1 h at room temperature in 100 mM Tris-HCl pH 8.0 (buffer C) supplemented with 6 M Urea, 100 mM NaCl, 0.5 mM EDTA and 5 mM DTT. Refolding was achieved by drop wise dilution into a volume 100 times that of the Urea solution of buffer C containing 0.5 mM EDTA, 0.2 mM oxidized glutathione and 1 mM reduced glutathione. The respective refolding solution was stirred overnight at 4°C and loaded onto a 10 mL Q-sepharose column (Amersham Biosciences) pre-equilibrated in buffer B. A linear gradient elution was performed over 100 mL from 0 to 1 M sodium chloride in buffer B and the fractions containing the refolded chemokines were concentrated and further purified on a Superdex 200 gel filtration column equilibrated in buffer B containing 150 mM NaCl. Purified proteins were analyzed as described above.

Terbium titration and PAGE analysis

Titrations were recorded on Photon Technology International Quanta Master I fluorimeter using 1 cm path length quartz cuvette and slit widths of 2 and 4 nm. Tryptophan-sensitized Tb^{3+} luminescence was collected at room temperature by exciting the sample at 280 nm. The purified CXCL12-LT-His protein (2 mL at 75 µM in Hepes 20 mM pH 8.0; NaCl 100 mM) was titrated by adding ten 2 µL aliquots of 15 mM Tb^{3+}. After each addition, the solution was mixed and the luminescence emission spectrum was recorded between 450 and 550 nm. For SDS-PAGE analysis, proteins were loaded on two 15% polyacrylamide gels in denaturing buffer, and subjected to electrophoresis at 220 V for 1 hour. After the migration, one gel is immediately stained with a Blue Coomassie solution whereas the other one is washed twice for 20 minutes in buffer D (100 mM NaCl, 10 mM HEPES pH 7.0), followed by an incubation of 1 hour in buffer C containing 50 µM of $TbCl_3$. Luminescent bands were visualized on a UV-transilluminator (Gel Doc 2000, Bio-Rad).

Co-expression of receptors and channel in Xenopus oocytes

Human CXCR4 and CCR5 genes were subcloned in pGEMHE vector designed for protein overexpression in Xenopus oocytes like the Kir3.1F137S (Kir3.1*) gene. Kir3.1 channels are physiologically associated with Kir3.4 subunits to form functional G protein-activated channels. The muta-

tion Kir3.1F137S, noted Kir3.1*, allows the formation of functional homotetramers simplifying the system by abrogating one subunit. All constructs were linearized in 3' terminus of the polyA sequence and mRNAs synthesized using the T7 mMessage mMachine Kit (Ambion). mRNAs were purified by standard phenol:chloroform extraction, analysed on agarose gel and quantified by spectrophotometry.

Animal handling and experiments fully conformed with French regulations and were approved by local governmental veterinary services (authorization no. 38-08-10 from the Ministère de l'Agriculture, Direction des Services Vétérinaires to Michel Vivaudou). Oocytes were surgically removed from Xenopus laevis and defolliculated by 2h incubations in 2 mg.ml-1 type 1A collagenase solution at 19°C. Stage V and VI oocytes were microinjected with 50 nl of RNase-free water containing one or a mixture of the following quantities of RNA: β2-Kir6.2, 5 ng; Kir6.2ΔC36, 2 ng; TMD0(SUR1)-F195, 1 ng. Microinjected oocytes were incubated for >2 days at 19°C in Barth's solution (in mM: 1 KCl, 0.82 $MgSO_4$, 88 NaCl, 2.4 $NaHCO_3$, 0.41 $CaCl_2$, 16 HEPES, pH 7.4) supplemented with 100 U.ml-1 penicillin, streptomycin and gentamycin. All chemicals were purchased from Sigma-Aldrich.

Electrophysiological recordings

Whole-cell currents were recorded with the two-electrode voltage clamp (TEVC) technique using a GeneClamp 500 amplifier (Molecular Devices). Microelectrodes were filled with 3 M KCl and oocytes were bathed in the following solution (in mM): 91 KCl, 1.8 $CaCl_2$, 1 $MgCl_2$, 5 HEPES, 0.3 Niflumic acid (to block endogenous Cl^- currents), pH 7.4. The TEVC voltage protocol consisted of 500-ms steps to 50, 0 and +50 mV - during which current was measured - separated by 5 s at a holding potential of 0 mV. The values shown in the figures are those recorded at -50 mV. In our TEVC configuration, chemokines are applied in a constant flow over the impaled oocytes, and under the conditions of -50 mV clamped-voltage and high potassium concentration (96 mM), the current generated by Kir3.1* is recorded in real-time (Fig. 1D). By convention, the recorded current is negative in our experimental conditions, and the first seconds of recordings (Fig. 1D, blue line) correspond to the basal current generated by the channel in basal state (in absence of chemokines). Application of agonists (such as chemokines) increases the negative current amplitude (Fig. 1D, red curve) and is consequently normalized using the basal current as a reference (Fig. 1D, right-side bar chart).

Data analysis

Basal current was measured while oocytes were in standard bath solution during the first minute of recording. Ba^{2+} (3 mM) was used as a generic potassium-channel blocker to establish the amount of exogenous current, designated as Ba^{2+}-sensitive current and calculated by subtracting from all measured values the value measured at the end of an experiment after application of 3 mM Ba^{2+}. All values of current reported here refer to Ba^{2+}-sensitive currents. Changes in Ba^{2+}-sensitive currents by effectors were calculated with respect to the value measured before application. Arrows in the figures indicate the points at which the current were measured on the current traces. For the concentration-response data, obtained by sequential application of increasing agonist concentrations, changes in current were calculated only with respect to the current before application of the initial, lowest concentration.

Average values are presented as mean±s.e.m. Non-linear least-square curve-fitting was carried

out with Origin 8 software (OriginLab) using a standard Hill equation:

$$f(x) = \frac{Max}{1+\left(\frac{EC_{50}}{x}\right)h}$$

where x is the concentration of a ligand, Max the asymptotical maximal effect, EC_{50} the concentration for half-maximal effect, and h the Hill coefficient. The fits shown in the figures were performed using average data. For statistical analysis of parameters Max and EC_{50} (using Origin 8 software), individual dose-response data from each oocyte tested were fitted using the above equation with h=1 to obtain a set of values of Max and EC_{50} for each construct and ligand. Statistical significance for these parameters and for other experimental data was established with unpaired two-tailed Student t-tests and is indicated as p-values in the text.

Results and discussion

Different versions of the two chemokines, CCL5 and CXCL12, were designed for diverse purposes; they vary by the tags that have been appended. Two different production approaches were considered.

Expression and purification of chemokines

Soluble expression of MBP fusions

The first production attempt was based on the strategy adopted by Cho and co-workers Cho *et al.* (2008) that promises high level of soluble chemokine expression in *E. coli* thanks to a N-terminal fusion with the Maltose Binding Protein MBP. Synthetic genes encoding for CXCL12 and CCL5, optimised for E.coli expression, were designed to be cloned into the pMal 4x vectors. The final constructs MBP-CCL5-Strep and MBP-CXCL12–Strep displayed from Nterm to Cterm: the MBP sequence, a prescission protease site to enable the subsequent cleavage of the fusion protein, the chemokine synthetic gene, a thrombin cleavage site and a C-terminal Strep Tag. Similar constructs comprising an additional double lanthanoid binding tag (LT) were also designed: MBP-CCL5-LT-Strep and MBP-CXCL12-LT-Strep. This tag specifically binds Terbium (Tb) which fluorescent properties could be used to track the chemokine. All those constructs are represented in Fig. 2.

Protein expression was induced in *E. coli* BL21 (DE3) cells. After cell disruption, and removal of cellular debris, the supernatant was purified over a StrepTactin column. Although all MBP fusion proteins were expressed with satisfactory yields, a remarkable enhancement was provided by the addition of the LT tag. A yield of 7-8 mg / liter of culture were obtained for MBP-CCL5-Strep and MBP-CXCL12–Strep while the presence of the LT boosted the quantities up to 70-80 mg/ liter of culture. The following cleavage of the fusion protein led to the precipitation of the whole protein sample despite attempts to optimize the conditions. Once again the LT tag dramatically affected the protein behavior since its presence maintained the chemokine perfectly soluble after cleavage. Removal of the MBP moiety was performed by purification over an amylose column. The unbound fraction that contained the chemokine was concentrated and run over a Superdex 200 gel filtration column. The proteins eluted as a unique peak corresponding to oligomers but that happened to be inactive in chemotaxis assays (data not shown).

Insoluble expression and refolding

Expression was then attempted via the approach most commonly used for chemokine production: an expression in E.coli under an insoluble form in inclusion bodies [15]. For that purpose, the synthetic genes encoding for CCL5 and CXCL12

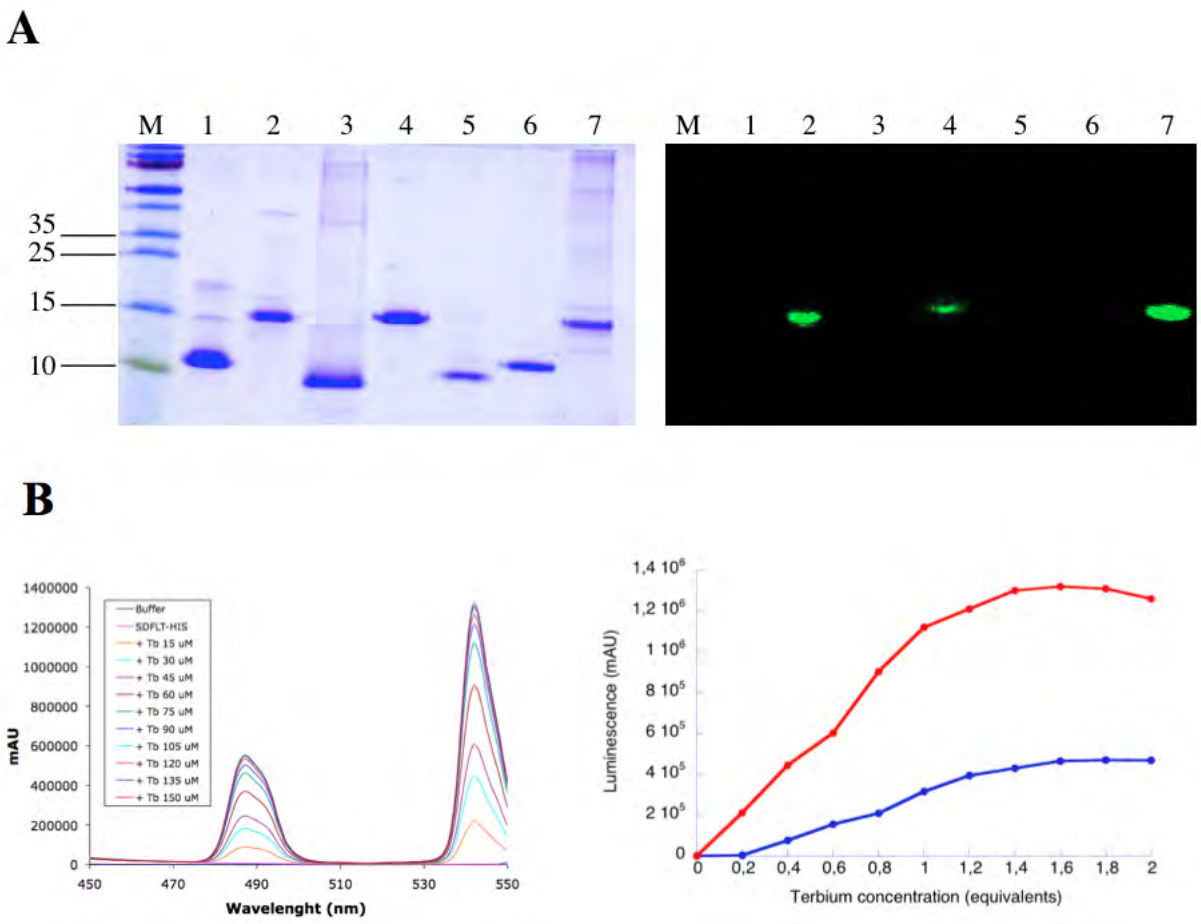

Figure 3: CXCL12-LT-His terbium titration and SDS-PAGE analysis of purified chemokines. **A**. SDS-PAGE analysis of the purified recombinant chemokines. Proteins were loaded onto 15% SDS-PAGE polyacrylamide gels in denaturing buffer, subjected to electrophoresis at 220 V for 1 hour and stained with a Blue Coomassie solution or treated with 50 µM of TbCl3. Luminescent bands associated with the chemokines-LT constructs were visualized on a UV-transilluminator with contrast enhancement. M: Protein mass ladder; lane 1: CXCL12-His; lane2: CXCL12-LT-His; lane 3: CXCL12-Strep; lane 4: CXCL12-LT-Strep; lane 5: CCL5; lane 6: CCL5-Strep; lane 7: CCL5-LT-Strep. **B**. Tryptophan-sensitized Tb^{3+} luminescence was collected as indicated in the materials and methods section. Briefly, the purified CXCL12-LT-His protein (2 mL at 75 µM in 20 mM Hepes pH 8.0; 100 mM NaCl) was titrated by adding ten 2 µL aliquots of 15 mM Tb^{3+} (concentrations ranging from 15 µM to 150 µM). After each addition, the solution was mixed and the luminescence emission spectrum was recorded between 450 and 550 nm. Inset: final terbium concentration after each metal addition in the protein sample. Luminescence at 487 nm (blue graph) and 542 nm (red graph) as a function of terbium concentration is also reported.

mentioned above were cloned into the pET-20b expression vector. Once again, various constructs of each chemokines were designed for various purposes. CXCL12 was C-terminally appended with either a Hexahistidine Tag or a Strep-Tag. The two constructs were declined under two versions with or without an LT Tag, resulting in 4 constructs: CXCL12-His, CXCL12-LT-His, CXCL12-Strep, CXCL12-LT-Strep. For CCL5 solely 3 constructs were created, CCL5-Strep, CCL5-LT-Strep and CCL5 devoid of any tag. Those seven versions of chemokines are schematically represented in Fig.2.

Protein expression was induced in BL21(DE3) cells. Solubilization of inclusion bodies and the subsequent purification steps completely differed between the LT containing constructs and the others. That is mainly explained by the great pI discrepancy between those two sets of proteins, the formers display an acidic pI (below 6.5) while the latter are highly basics with pI values above 9 (see Fig.2). LT bearing proteins were thus solubilized in a 6M Urea buffer, while the others were treated with 7.5 M Guanidine buffer. Solubilized inclusion bodies were loaded on a SDS-PAGE gel (data not shown) and the amount of overexpressed proteins was roughly appreciated (Fig.2). One clear observation from this analysis was the clear increase of expression triggered by the LT addition. Indeed, for all constructs, the LT form was far better expressed (CXCL12-His versus CXCL12-LT-His, CXCL12-Strep versus CXCL12-LT-His, CCL5-Strep versus CCL5-LT-Strep).

Refolding of the non-LT containing chemokines was achieved by a 7.5 fold rapid dilution while LT chemokines were refolded by drop wise dilution into a large volume of refolding solution. Amazing discrepancies were observed during the refolding. Comparison of the same constructs with or without LT Tag showed that while most of the protein remained soluble in the constructs containing a LT tag, apart from CXCL12-His which refolded very well, all the proteins deprived of LT precipitated. Another noticeable observation was the penalty triggered by the Strep Tag. Indeed, comparison of the refolding efficiencies of the CXCL12-His and CXCL12-Strep constructs showed that the presence of the Strep Tag led to the precipitation of a significant amount of protein. After refolding a first step of purification over an ion-exchange chromatography was performed. The basic non-LT containing chemokines, were retained by a Capto S column, while their LT counterpart, with acidic pI were purified over a Q-Sepharose column. After concentration, the proteins were further purified over a Superdex 200 gel filtration. CXCL12 proteins eluted as a nice single monomer peak, while CCL5, which is well known to oligomerize, eluted as bigger complexes of higher molecular weight. The structural integrity of the samples had to be evaluated. First of all, ion-spray mass spectrometry demonstrated that the oxidized proteins had four mass units less than the reduced forms due to the formation of the chemokine characteristic two disulfide bridges. The purity of the prepared protein can be appreciated on Fig 3A and is satisfactory.

The enhancement of the fluorescence triggered by addition of terbium to the CXCL12-LT-His suggested the correct folding of the protein. Besides terbium titration (see Fig. 3B) demonstrated that a 2:1 molar ratio of Tb:protein was necessary to saturate the sites and confirmed that the double Lanthanoid binding tag was fully functionnal. The fluorescent properties of the LT Tag are clearly illustrated on Fig. 3B that displays the visualization of the fluorescent chemokines on a SDS-PAGE gel that was simply bathed into a terbium containing solution.

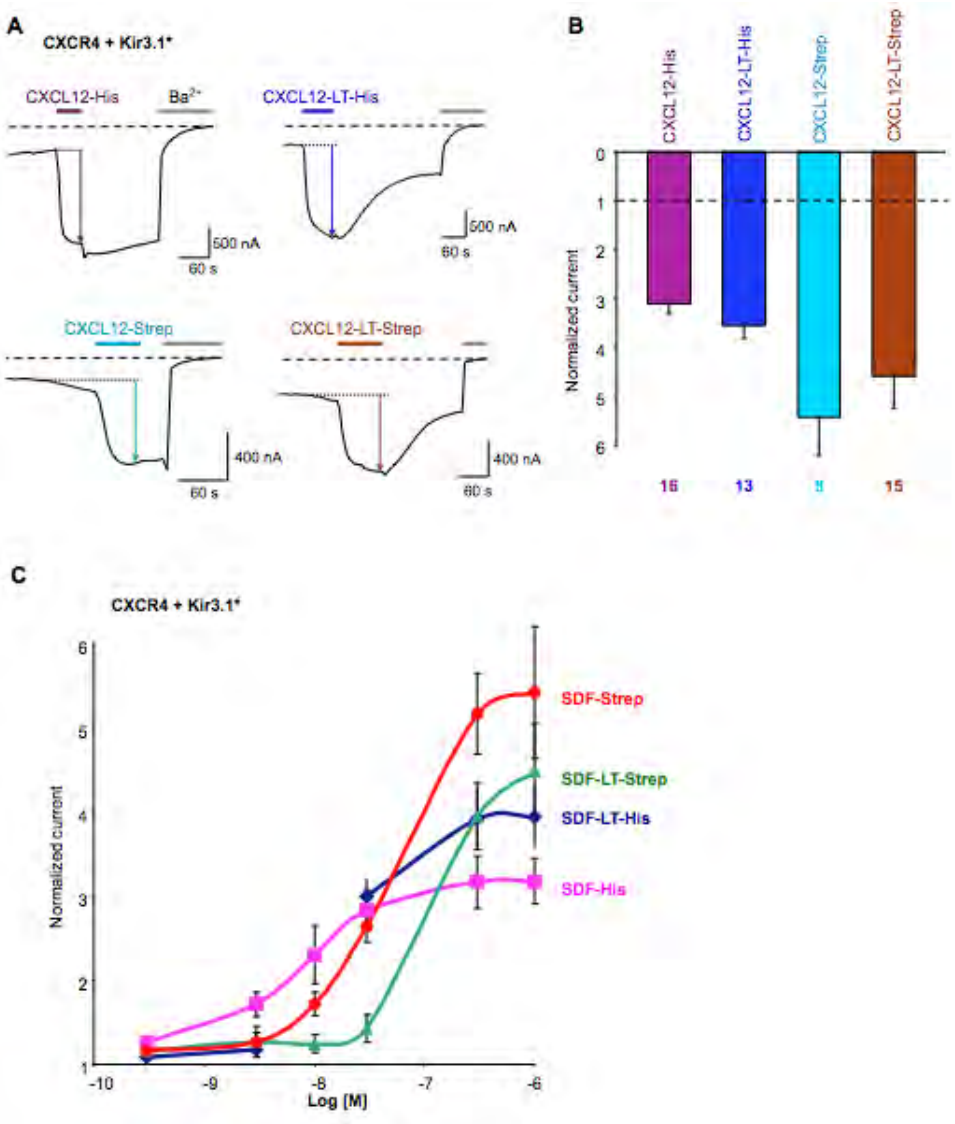

Figure 4: Functional characterization of tagged-CXCL12 chemokines.
A. Representative TEVC recordings performed on Xenopus oocytes co-expressing CXCR4 and Kir3.1*. Different oocytes are used for each recording. The coloured arrows indicate the channel activations induced by chemokine-binding on CXCR4 and subsequent Go protein activation. The chemokines concentration is 1µM. **B**. Average current (+/- s.e.m.) normalized in reference to the basal current (=1) and measured at the end of the ligand application represented by the arrows in the panel A. Numbers below bars are the numbers of recordings. **C**. Dose-response curves of the indicated-chemokines. Chemokine concentrations are applied gradually on the same oocyte and each point of the curves are the mean +/- s.e.m. of different recordings from different oocytes.

Quantitative and qualitative functional characterization of tagged chemokines

Tagged and purified CXCL12 chemokines at a fixed concentration of 1 µM were applied on Xenopus oocytes expressing CXCR4 and Kir3.1*. This concentration far above the Kd (reported to be of the low nM range) ensured to be in saturating conditions and trigger a maximal response. Figure 4A reveals that all tagged CXCL12 are able to activate Kir3.1*, meaning the binding of the modified chemokines on CXCR4 and the subsequent activation of the $G_{i/o}$ proteins. Statistical analysis (Fig. 4B) show a similar amplitude of activation between CXCL12 +/- LT tagged chemokines and a slight but significant higher activation of CXCL12-Strep than CXCL12-His.

The differences of ligand efficacy at 1 µM are also confirmed by dose-response curves (Fig. 4C) performed by increments of chemokine concentrations. Interestingly, the dose-response curves reveal that while insertion of the LT-tag does not significantly affect the CXCL12 efficacy at 1 µM, it decreases the apparent affinity of CXCL12-LT-Strep, but not CXCL12-LT-His. In an opposite way, insertion of the LT tag in CXCL12-His, does not alter the ligand affinity but increases slightly the ligand efficacy (LT-His *vs* His). Thus, analysing the tagged-CXCL12 effect only at the saturating concentration (1 µM) (Fig. 4C) reveals that LT-tag does not modify significantly the CXCL12 efficacy (Emax: Strep *vs* LT-Strep and His vs LT-His), but LT-tag clearly decreases the apparent affinity for Strep-tagged CXCL12 (EC_{50} LT-Strep>Strep).

Another change induced by the LT-tag is the apparition of "reversibility". Reversibility corresponds in our recordings to the rapid loss of the Kir3.1* activation during the post-ligand washing as shown in Fig.4A (right recordings). In order to confirm the apparition of reversibility with LT-tag insertion, we applied non LT-tagged and LT-tagged chemokines sequentially in different orders as shown in Fig. 5B and compare it with the wt CXCL12 (without tags). The wt chemokine displays an absence of reversibility in Fig. 5A even at low concentration (30 nM) and this phenotype is conserved for the His- and Strep-tagged chemokine (Fig. 5A). Insertion of the LT-tag induces reversibility of the chemokine-evoked activation even at the saturating concentration of 1 µM (Fig. 5B). When the CXCL12-LT-His is applied first, the reversibility allows the subsequent, clear and not reversible activation induced by CXCL12-His, while the reciprocal application sequence shows a weak and irreversible CXCL12-LT-His induced-activation due to the long lasting activation of the first-applied CXCL12-His. Thus, application of non LT-tagged and LT-tagged chemokines on the same oocyte during the same recordings demonstrates the specific effect of the LT tag on CXCL12-reversibility.

Similar electrophysiological characterizations were performed on CCL5-tagged chemokines, and Fig. 6A reveals that this chemokine applied on CCR5 has an equivalent behavior than CXCL12-effects on CXCR4. Thus, non-tagged CCL5 (wt CCL5) induces a reversible activation of CCR5, like the Strep-tagged version of this chemokine. Surprisingly, insertion of the LT-tag abolished this reversibility and decreased drastically (~2-fold of the CCL5-evoked activation) the efficacy of the chemokine (Fig. 6B). The only observed similitude between tagged CCL5 and CXCL12 are the increased efficacy of the Strep-tagged chemokines in an about 2-fold amplitude compare to their wt version.

Conclusion

CXCL12 and CCL5 chemokines are precious not only for their physiological role in lymphocytes B

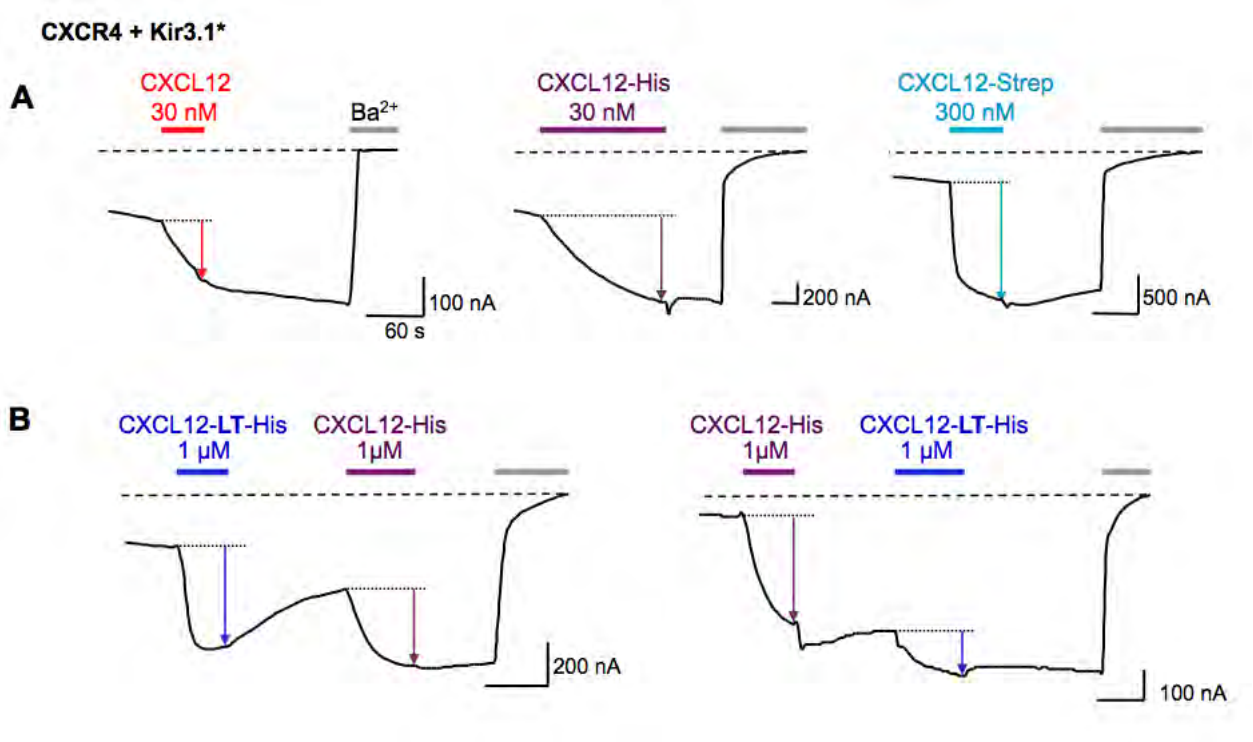

Figure 5: Lanthanid-binding tag affects the long-lasting activation in TEVC recordings. **A**. Representative TEVC recordings showing the non-or weakly-reversible activation of indicated chemokines. The non-tagged CXCL12 chemokine is in red. **B**. Sequential application of CXCL12-His +/- LT tag during the same recording on the same oocyte but in different order show the rapid "reversibility" of the activation induced by the LT-tagged CXCL12 chemokine.

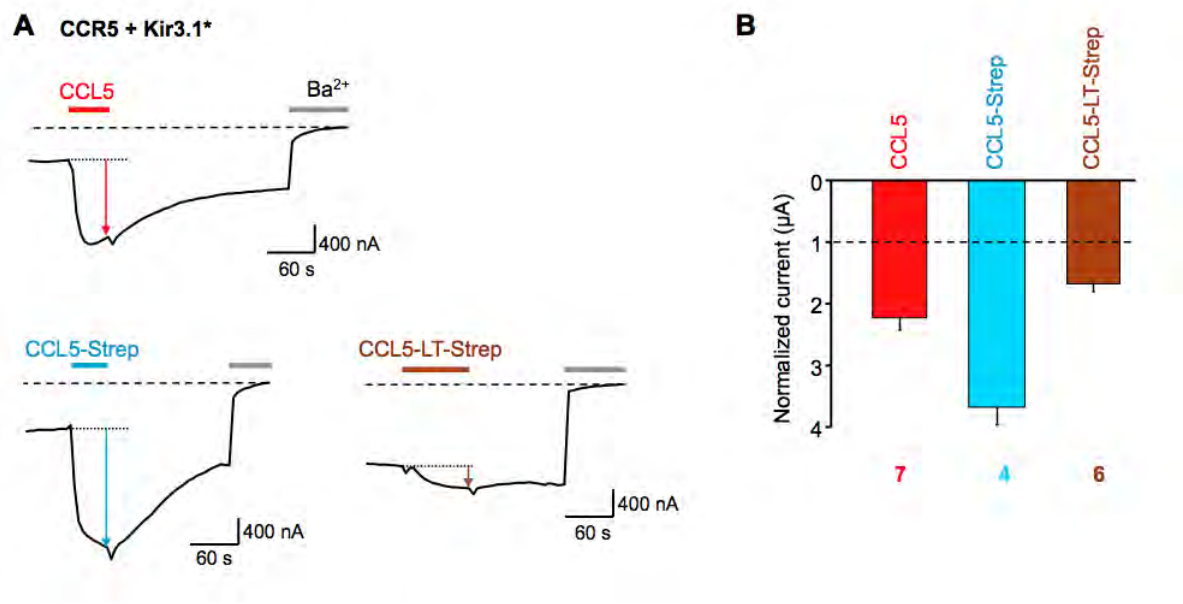

Figure 6: Functional characterization of the tagged-CCL5 chemokines.
A. Representative TEVC recordings performed on Xenopus oocytes co-expressing CCR5 and Kir3.1* and subjected to the indicated CCL5 chemokine applications at 1µM. **B**. Average current (+/- s.e.m.) normalized in reference to the basal current (=1) for each indicated chemokines at 1µM. In red is the non-tagged CCL5 chemokine.

chemotaxis, but also for the molecular characterization and biochemical studies of their related receptors which are notably involved in the HIV entry process. The pecuniary value of the commercially available chemokines makes their affordable quantity too low for long-standing and structural studies of chemokine receptors. Home-made expression and purification of those chemokines appears as a prerequisite for the studies of chemokine receptors at the molecular level. To simplify this step and allow the possibility to undergo various experiments including fluorescent labelling, the set up of a chemokine affinity chromatography, functionalisation of SPR surfaces, several tags have been added (His tag, Strep Tag, lanthanide-binding tag). We demonstrated in this study that the nature of the tag insertion clearly affected the properties of the chemokines.

First of all, we observed that the addition of single tags or of a combination of tags can have unexpected effects on the biochemical properties of the chemokine: insertion of the LT tag dramatically enhanced protein expression and solubility, addition of a Strep tag greatly disfavoured protein refolding. The important modifications linked to addition of LT tag could be attributed to the high negative charges of this sequence, that greatly modify the isoelectric points of those highly basic chemokines and could therefore influence their biochemical behaviour.

It has been reported that modifications of the CXCL12 and CCL5 sequences can highly alter the chemokine functionality and receptor binding properties Simmons *et al.* (1997); Mosier *et al.* (1999); Pastore *et al.* (2003). This has been particularly observed when the N-terminus is affected, which is absolutely coherent with the crucial role played by this region for chemokine/receptor interactions Crump *et al.* (1997); Kofuku *et al.* (2009). Therefore the set up of a method to ensure that the sequence engineering performed on the chemokines did not modify the chemokine capacity to signal

Chemokine	Tag(s)	Recertor activation*	Long-lasting activation	Affinity	Efficacy
CXCL12	Without (wt)	?	+	EC_{50}=1.2 [1]	
	His	+	+	=	=
	Strep	++	+	=	++
	LT-His	+	-	=	=
	LT-Strep	++	-	<	=
CCL5	Without (wt)	+	-	EC_{50}=3.2 [2]	
	Strep	++	-	=	
	LT-Strep	<	+	=	

Table 1: Summary of the tag effect on CXCL12 and CCL5 determine by TEVC.
* - Receptor activation through G proteins; [1] - data from Zhan *et al.* (2007); [2] - data from Blanpain *et al.* (2003)

through its receptor was required. However the hydrophobic nature of those ligands render difficult some straightforward ligand binding experiments such as filter binding assays. To access the consequences of chemokine sequence modifications both on receptor binding capacity and signal transduction, we used here a simple system based on co-expression of chemokine receptors and G protein-activated channels in Xenopus oocytes and Two-Electrode Voltage-Clamp recordings. This method allowed us to record in real-time the receptor activation and dose-response curves are easily executed by sequential applications of increased ligand concentration in constant flow. We could determine the effect of the tag insertion on the apparent affinity, on the efficacy and the "reversibility".

While the effects on the activity of chemokine N-terminus modifications are clearly documented to have rather dramatic effects on their receptor binding activity and signal transduction capacity, the experiments that we carried out indicate that C terminus modifications do not abrogate those functions but rather have a subtle tuning effect. Although the C-terminus of CXCL12 and CCL5 has not been reported to be involved in receptor binding mechanism, modifications of this region could affect the chemokine oligomerisation and therefore its functionality. We first observed that insertion of one tag (Strep or His) did not alter the ability of CXCL12 or CCL5 to activate Gi/o proteins via their respective receptors, however it appears that the Strep-tag increased the efficacy of both chemokines. The consistency of the responses got more confused with the addition of a second tag. This is clearly illustrated by the various and somehow erratic effects attributed to the LT-Tag insertion that can alternatively, decrease the apparent affinity (Strep-tagged CCL12), increase the efficacy (His-tagged CCL12), induce reversibility (Strep and His-tagged CCL12) or even have the opposite consequences, including suppression of reversibility and diminution of efficacy on CCL5 constructs.

We listed here those properties that could be used for new applications (Table 1).

The major strength of the technique is that without having to struggle with membrane protein expression, it gives an easy access to many types of experiments that could be delicate with other approaches such as the determination of an EC_{50} by dose response tests or competition assays. Besides it seems that internalisation processes are rather limited in Xenopus oocytes, which clearly ease the ligand binding assays as it enable the possibility of consecutive perfusions Cox & Crowder (2004).

Besides, one other advantage of this approach that has not been exploited in this study could be to easily undertake structure/function studies from the receptor side. The effects of modifications on the GPCR sequences could be easily addressed by this system both in term of ligand binding or signaling. The interest of such changes has been clearly illustrated by the strategy used to crystallize and solve the high-resolution structure of several GPCR Katritch *et al.* (2012). Indeed, the modifications that have been required to obtain crystallizable forms of the proteins could be easily transferred to the mRNA injected in the Xenopus oocytes. Comparative ligand binding assays with the wild type and the modified GPCR could thus be informative on the impact of such modifications.

This article describes the production of a large range of functional chemokines modified at their C terminus with different tags that could open a broad way to undertake "in solution" chemokine/chemokine receptor complex studies including the possibility to perform pull down experiments and the set up of affinity chromatography column, the functionalisation of Biacore chips (Strep and His tags) or even to track chemokines or receptor/chemokine complex via the fluorescent properties offered by the LT. We also report the convenient use of an electrophysiology test to assess receptor binding and signal transduction of the tagged chemokines, which is a mandatory prerequisite before their utilization. Data obtained by this technique validated that the C-terminus of chemokines could be used to functionalised them without interfering with their major functions.

References

Blanpain, C., Doranz, B. J., Bondue, A., Govaerts, C., Leener, A. D., Vassart, G., Doms, R. W., Proudfoot, A., & Parmentier, M. (2003). *J Biol Chem,* **278** (7), 5179–87.

Briddon, S. J., Kellam, B., & Hill, S. J. (2011). *Methods Mol Biol,* **746**, 211–36.

Cho, H.-J., Lee, Y., Chang, R. S., Hahm, M.-S., Kim, M.-K., Kim, Y. B., & Oh, Y.-K. (2008). *Protein Expression and Purification,* **60** (1), 37–45.

Cox, B. M. & Crowder, A. T. (2004). *Mol Pharmacol,* **65** (3), 492–5.

Crump, M. P., Gong, J. H., Loetscher, P., Rajarathnam, K., Amara, A., Arenzana-Seisdedos, F., Virelizier, J. L., Baggiolini, M., Sykes, B. D., & Clark-Lewis, I. (1997). *EMBO J,* **16** (23), 6996–7007.

Grånäs, C., Lundholt, B. K., Heydorn, A., Linde, V., Pedersen, H.-C., Krog-Jensen, C., Rosenkilde, M. M., & Pagliaro, L. (2005). *Comb Chem High Throughput Screen,* **8** (4), 301–9.

Jin, H., Kagiampakis, I., Li, P., & Liwang, P. J. (2010). *Proteins,* **78** (2), 295–308.

Katritch, V., Cherezov, V., & Stevens, R. C. (2012). *Trends in Pharmacological Sciences,* **33** (1), 17–27.

Kofuku, Y., Yoshiura, C., Ueda, T., Terasawa, H., Hirai, T., Tominaga, S., Hirose, M., Maeda, Y., Takahashi, H., Terashima, Y., Matsushima, K., & Shimada, I. (2009). *J Biol Chem,* **284** (50), 35240–50.

Labrecque, J., Wong, R. S. Y., & Fricker, S. P. (2009). *Methods Mol Biol,* **552**, 153–69.

Lagerström, M. C. & Schiöth, H. B. (2008). *Nat Rev Drug Discov,* **7** (4), 339–57.

Mack, M., Luckow, B., Nelson, P. J., Cihak, J., Simmons, G., Clapham, P. R., Signoret, N.,

Marsh, M., Stangassinger, M., Borlat, F., Wells, T. N., Schlöndorff, D., & Proudfoot, A. E. (1998). *J Exp Med,* **187** (8), 1215–24.

Martin, L. J., Hähnke, M. J., Nitz, M., Wöhnert, J., Silvaggi, N. R., Allen, K. N., Schwalbe, H., & Imperiali, B. (2007). *J. Am. Chem. Soc.* **129** (22), 7106–7113.

Mosier, D. E., Picchio, G. R., Gulizia, R. J., Sabbe, R., Poignard, P., Picard, L., Offord, R. E., Thompson, D. A., & Wilken, J. (1999). *J Virol,* **73** (5), 3544–50.

Pastore, C., Picchio, G. R., Galimi, F., Fish, R., Hartley, O., Offord, R. E., & Mosier, D. E. (2003). *Antimicrob Agents Chemother,* **47** (2), 509–17.

Peters, M. F., Knappenberger, K. S., Wilkins, D., Sygowski, L. A., Lazor, L. A., Liu, J., & Scott, C. W. (2007). *J Biomol Screen,* **12** (3), 312–9.

Polo, S., Nardese, V., Santis, C. D., Arcelloni, C., Paroni, R., Sironi, F., Verani, A., Rizzi, M., Bolognesi, M., & Lusso, P. (2000). *Eur. J. Immunol.* **30** (11), 3190–8.

Sabbe, R., Picchio, G. R., Pastore, C., Chaloin, O., Hartley, O., Offord, R., & Mosier, D. E. (2001). *Journal of Virology,* **75** (2), 661–71.

Sallusto, F., Mackay, C. R., & Lanzavecchia, A. (2000). *Annu Rev Immunol,* **18**, 593–620.

Simmons, G., Clapham, P. R., Picard, L., Offord, R. E., Rosenkilde, M. M., Schwartz, T. W., Buser, R., Wells, T. N., & Proudfoot, A. E. (1997). *Science,* **276** (5310), 276–9.

Wu, B., Chien, E. Y. T., Mol, C. D., Fenalti, G., Liu, W., Katritch, V., Abagyan, R., Brooun, A., Wells, P., Bi, F. C., Hamel, D. J., Kuhn, P., Handel, T. M., Cherezov, V., & Stevens, R. C. (2010). *Science,* **330** (6007), 1066–71.

Wyatt, R. & Sodroski, J. (1998). *Science,* **280** (5371), 1884–8.

Zhan, W., Liang, Z., Zhu, A., Kurtkaya, S., Shim, H., Snyder, J. P., & Liotta, D. C. (2007). *Journal of medicinal chemistry,* **50** (23), 5655–64.

10. Receptor production

10.1. Molecular biology

CCR5 and CXCR4 clonings have been performed before my arrival. To circumvent the limitation due to rare codons the nucleotide sequences of both receptors were optimized for the expression in *E. coli*. Synthetic cDNA were produced in which the codons frequently used by *E. coli* were selected. Receptors were cloned using a fusion strategy developed by Jean-Louis Banères and Bernard Mouillac, targeting the GPCR expression towards *E. coli* inclusion bodies (IB) [104]. This is an alternative approach based on novel original fusion partners, which enable to produce full-length receptors in high amounts, and is already applicable to a dozen of GPCRs. The strategy is based on accumulation of the fusion-GPCR complexes in *E. coli* inclusion bodies followed by a subsequent *in vitro* refolding. To target recombinant proteins to *E. coli* inclusion bodies the combination of charged and β-turn forming residues are critical and have to correspond to a high fraction of the selected protein sequence. Comparing these physicochemical parameters, as a fusion partner, a fragment of the extracellular β-propeller domain of the human α5 integrin (α5I) was chosen [104].

CCR5 had a N-terminal fusion with an α5 Integrin (α5I) fragment (residues from 231 to 514) and a C-terminal His tag. The thrombin cleavage site was added to cleave the α5 Integrin part from the His tagged GPCR. CCR5 construct was cloned into pET-21a(+) expression vector and referred to as α5I-CCR5-His.

For CXCR4 receptor expression one fusion protein was not enough to enable an efficient expression in *E. coli* inclusion bodies, therefore an additional fusion protein was incorporated. A fragment of the hormone arginine-vasopressin V2 receptor (V2) was added to the N-terminal side of CXCR4 resulting in the α5I-V2-CXCR4, which was then cloned into pET-21a(+) expression vector.

10.2. Expression and purification of α5I-CCR5-His

Cultures of Rosetta2 (DE3) competent bacteria were transformed with α5I-CCR5-His and grown at 37°C in LB media to an $OD_{600\ nm}$ of 1. Bacterial cultures where induced with 1 mM IPTG

and glucose was added. Bacteria were grown for another 4 hours until cultures were harvested by centrifugation.

Bacterial pellet containing expressed α5I-CCR5-His was resuspended in lysis buffer and cells where lysed using a microfluidizer. The pellet containing inclusion bodies was extensively washed first with lysis buffer containing 1 M Urea and then twice with lysis buffer containing 2 M Urea. The inclusion body solubilization step was performed overnight using 6 M Urea to completely solubilize the protein of interest. The presence of the His-tag at the C-terminus of the receptor allowed protein purification over a Ni-NTA resin under denaturing conditions (Figure 10.1).

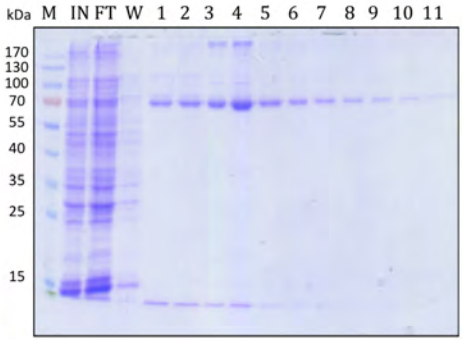

Figure 10.1.: SDS-polyacrylamide gel representing α5I-CCR5-His purification over a Ni-NTA resin.
M - marker, IN - input to the Ni-NTA resin, FT - flow-through, W - wash, 1-11 - elution fractions containing almost pure α5I-CCR5-His.

The protein was recovered by elution with 500 mM Imidazole containing buffer. The elution fractions were pooled and dialyzed against thrombin digestion buffer to eliminate Urea.

Thrombin digestion kinetic was observed by collecting aliquots after 1 and 4 hour digestion (Figure 10.2).

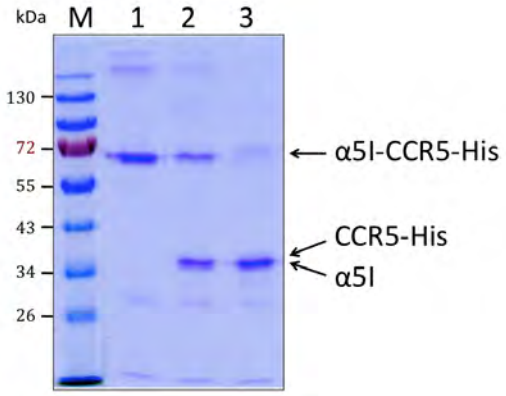

Figure 10.2.: SDS-polyacrylamide gel representing α5I-CCR5-His thrombin digestion.
M - marker, 1 - sample of non-digested α5I-CCR5-His, 2 - sample after 1 hour of thrombin digestion, 3 - sample after 4 hours of thrombin digestion.

After 4 hour incubation the digestion was almost complete. The reaction was stopped by the addition of 6 M Urea and 0.4 % SDS. The cleaved α5I fragment was separated from the CCR5-His by a second Ni-NTA purification (Figure 10.3).

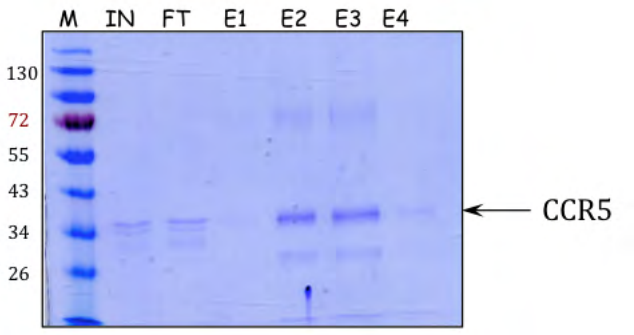

Figure 10.3.: SDS-polyacrylamide gel showing CCR5-His purification on Ni-NTA resin. M - marker, IN - input sample to the Ni-NTA resin, FT - flow-through, E1-4 - elution fractions.

The flow through (FT) and wash (W) fractions contained the α5I protein fragment. The elution fractions containing the CCR5-His were pooled and dialyzed against 0.8% SDS buffer until Urea traces were removed.

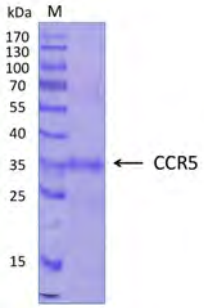

Figure 10.4.: SDS-polyacrylamide gel of purified CCR5-His.

We obtained 0.46 mg of CCR5-His from one liter of bacterial culture (Figure 10.4).

10.3. Expression and purification of α5I-V2-CXCR4-His

Cultures of Rosetta2 (DE3) competent bacteria were transformed with α5I-V2-CXCR4 and grown at 37°C in LB media to an $OD_{600\ nm}$ of 1. Bacterial cultures where induced with 0.1 mM IPTG and glucose was added. Bacteria were grown for another 4 hours until cultures were harvested by centrifugation.

Bacterial pellet was resuspended in lysis buffer and cells where lysed using a microfluidizer. The pellet containing inclusion bodies was extensively washed first with lysis buffer containing 1 M

Urea and then twice with lysis buffer containing 2 M Urea. The inclusion body solubilization step was performed overnight using 6 M Urea to completely solubilize the protein of interest. The presence of the His-tag at the C-terminus of the receptor allowed protein purification over a Ni-NTA resin under denaturing conditions (Figure 10.5).

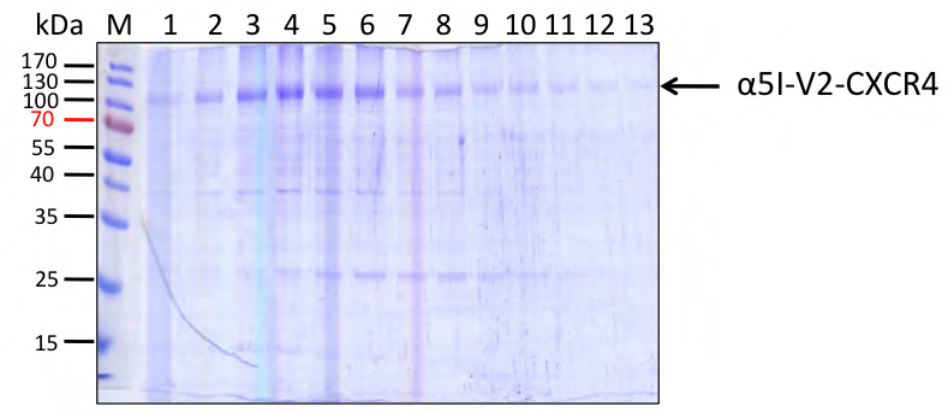

Figure 10.5.: SDS-polyacrylamide gel representing α5I-V2-CXCR4 first step of purification. M - marker, 1 -13 - elution fractions from Ni-NTA resin. The arrow marks the bands of CXCR4 fusion which runs as expected around 110 kDa.

The protein was recovered by elution with a buffer containing 500 mM Imidazole. The elution fractions were pooled and dialyzed against thrombin digestion buffer to eliminate urea.

Thrombin digestion kinetic was observed by collecting aliquots after 1, 3 hour and overnight digestion at 20°C and at 37°C; 20 µl and 200 µl of each sample was loaded into a SDS-polyacrylamide gel (Figure 10.6).

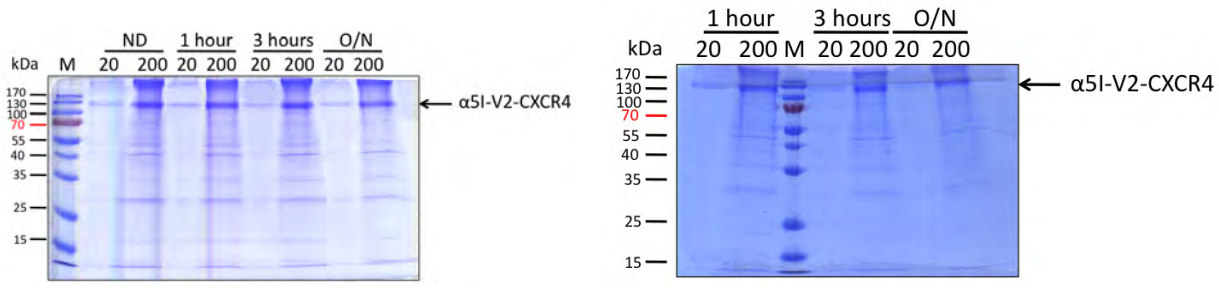

(a) Thrombin digestion at 20°C

(b) Thrombin digestion at 37°C

Figure 10.6.: SDS-polyacrylamide gel representing α5I-V2-CXCR4 thrombin digestion. (a) α5I-V2-CXCR4 digestion with thrombin at 20°C. (b) α5I-V2-CXCR4 digestion with thrombin at 37°C. M - marker, 20 and 200 indicated the amount (µl) of loaded sample, ND - non-digested sample, 1 hour - sample after 1 hour of digestion, 3 hours - sample after 3 hours of digestion, O/N - sample after overnight digestion with thrombin. The arrow marks the bands of CXCR4 fusion proteins.

As observed on the SDS-polyacrylamide gel, thrombin digestion did not work even after extensive

dialysis against digestion buffer to remove traces of urea and SDS. To improve the thrombin digestion a different buffer was used (20 mM Tris HCl pH 8.0, 150 mM NaCl, 1 mM DTT, 5 mM $CaCl_2$) but unfortunately no improvement was observed. Also thrombin was tested at different concentrations, but even an increase up to 13 units of thrombin per milligram of fusion protein did not allow the cleavage. The difficulties of thrombin digestion of CXCR4 fusion protein led us to concentrate our efforts on CCR5 production.

10.4. CCR5 folding - previous works

The first assays of CCR5 folding was assessed before my arrival in a collaboration with J.-L. Banères (Montpellier).

A first set of receptor folding conditions was tested where the denaturing agent (SDS) was replaced by a detergent/lipids mixture that stabilized the native structure of the receptor. To find the best conditions, various detergents were tested, while keeping constant the concentration and nature of the lipids. Only the buffer containing 0.1mg/ml asolectin, 0.02% cholesteryl hemisuccinate and n-Dodecyl-β-D-maltoside (DDM) (1/3 w/w) led to the re-solubilization of a significant amount of receptor.

The ability of the receptor to bind its ligand was evaluated using fluorescence polarization with an agonist, MIP-1β, which was labeled with a fluorophore (Texas-Red).

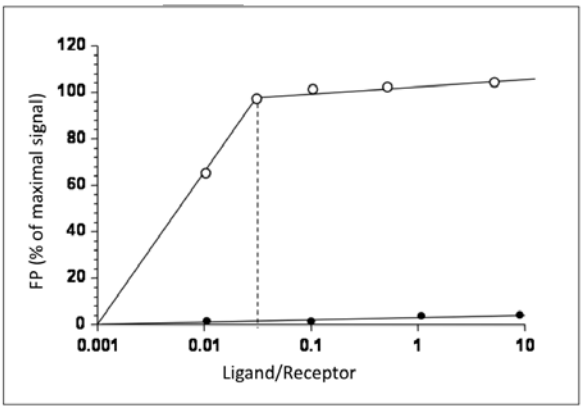

Figure 10.7.: Folded receptor interaction with MIP1β.
Fluorescence polarization measurements were performed with 50 nM MIP1β marked with Texas-Red and folded CCR5 (white circles). The black circles represent polarization measurements with recombinant BLT1 receptor and MIP1β (negative control experiment).

As shown in Figure 10.7, a specific interaction is clearly observed between the receptor and its agonist and is not observed with an irrelevant receptor (leukotriene B4 receptor, BLT1) , taken as a negative control.

The specificity of this interaction is clearly demonstrated by the complete competition assay between a fluorescent ligand and an excess of unlabeled agonist. Displacement is not observed in the presence of SDF1α (ligand of CCR4) demonstrating the specificity of the interaction (Figure 10.8).

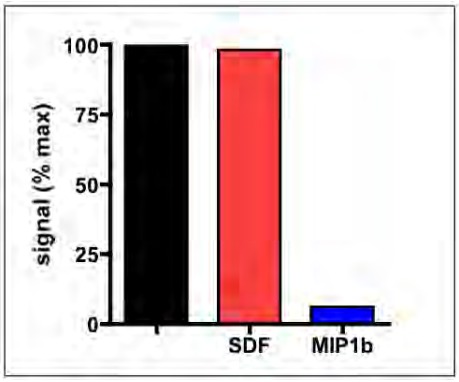

Figure 10.8.: Histograms representing fluorescence polarization signal between MIP1β-Texas Red and the CCR5 receptor.
Interaction between MIP1β-Texas Red and the CCR5 receptor folded in detergents is indicated. Back column - in the absence of competitor, red - in the presence of an excess of SDFα, blue - in the excess of a unlabeled MIP1β.

Polarization tests have been performed at a ligand concentration well above the K_D value of CCR5 interaction with MIP1β (K_D in the range of 0.2-0.5 nM estimated from cellular systems), the amount of functional receptor can be estimated from the titration curve in Figure 10.7 as corresponding to about 4% of the amount of soluble receptor obtained after CCR5 folding.

Several preliminary tests with the receptor in the presence of pMal-B100 a commercial amphipol were performed. This time the receptor refolding yield was significantly higher than obtained in the presence of detergents, about 50% of the protein was recovered in a soluble form in the presence of pMal-B100. The amount of functional receptor was estimated by fluorescence measurements and indicated that 20 to 30% of the total amount of soluble receptor was functional.

Those preliminary experiments suggested better refolding yield in amphipols that detergents. Therefore we orientated our refolding towards Amphipol assisted methods.

10.5. Amphipol-assisted CCR5 folding

Optimal refolding of the receptor was obtained when the receptor was used at concentrations ranging from 0.3 to 0.5 mg/ml.

For a CCR5 folding in A8-35 a protein:amphipol mass ratio of 1:5 was used. Receptor folding was initiated by precipitating dodecyl sulphate as its potassium salt (KDS) by the addition

of KCl followed by extensive dialysis to remove any SDS traces [327]. No significant protein loss through precipitation occurred during amphipol mediated folding. The amount of protein remaining soluble in the buffer was determined by calculating the soluble protein concentration and monitored on SDS-polyacrylamide gel (Figure 10.10).

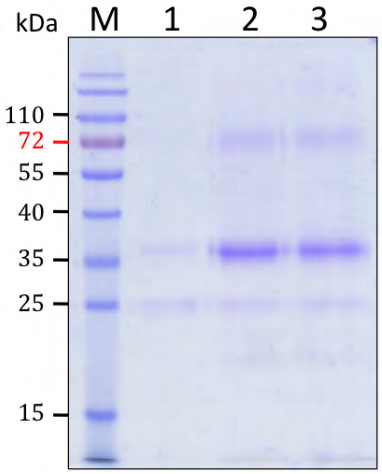

Figure 10.9.: SDS-polyacrylamide gel representing CCR5-His folding in A8-35.
M - marker; 1 - sample of CCR5 alone, no detergent or surfactants were added; 2 - CCR5 refolded with A8-35 at protein/amphipol weight ratio 1:5; 3 - CCR5 refolded in the presence of A8-35 and asolectin at 1:5:1 protein:amphipol:lipid weight ratio.

The effect of lipid addition on the folding process was tested. In the presence of A8-35 with 1:5 protein:A8-35 ratio over 45% of CCR5 remained soluble. Addition of lipids at a 1:5:1 protein:A8-35:lipid weight ratio allowed around 61 % of CCR5 to remain soluble (Figure 10.10).

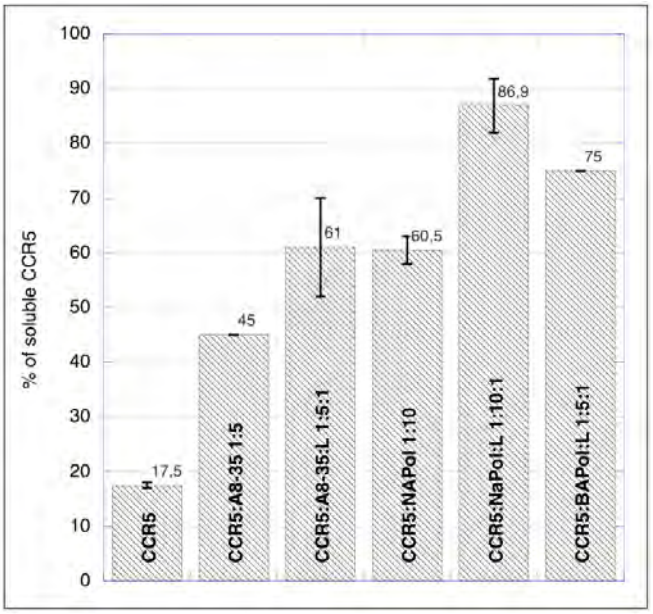

Figure 10.10.: Histograms representing CCR5 folding in different conditions.

Therefore, the amphipol lipid combination slightly improved the amount of receptor maintained soluble after folding showing the positive impact of lipid on the receptor folding procedure.

Folding with non-ionic amphipols NAPols was then tested (Figure 10.10). Higher concentration of amphipols were used for folding in NAPol. Two conditions were tested 1:10 protein:NAPol weight ratio and 1:10:1 protein:NAPol:Lipid weight ratio. In both conditions over 60% of CCR5 remained soluble after folding. However, in the presence of lipids less aggregation was observed. Folding of CCR5 in three different amphipols, A8-35, NAPol and BAPol was tested in the presence of lipids (Figure 10.10).

The best conditions of folding have been obtained in the presence of NAPol in a 1:10:1 protein:NAPol:lipid weight ratio which maintain over 86% of the sample soluble.

The CCR5 folded in NAPols can be stored for months at room temperature (Figure 10.11).

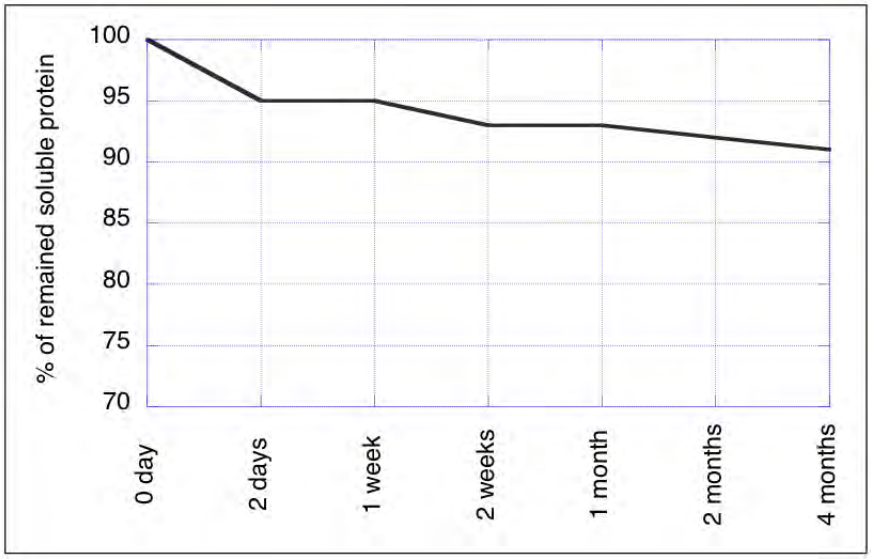

Figure 10.11.: Time-dependent CCR5/NAPol solubility.

Folded CCR5 functionality was assessed by ligand binding assay using Surface Plasmon Resonance (SPR) experiments.

10.6. Improvements

CCR5 over-expression greatly differs from one culture to another. The overall purification scheme being quite tedious, we wanted to be able to assess the initial level of over-expression before undertaking the inclusion body solubilization. The C-terminal His tag initially seemed appropriate. Therefore, before purification the samples were taken from expression cultures and analyzed on a SDS-polyacrylamide gel and Western Blot using an anti-His antibody.

However, for unexplained reasons, anti-His identification of the expressed CCR5 was very weak in the best cases and often undetectable. Even the purified protein could not be visualized in most of the anti-His Western blot. This type of problem has been reported for several other GPCR detection [personal communications]. Therefore, it was impossible to perform a rapid and early screen of the expression prior starting the purification process.

A second construct was thus created for CCR5. A C9 tag, a highly antigenic nine-amino acid sequence of the rhodopsin carboxyl tail (TETSQVAPA), which allows the detection by the anti-rhodopsin 1D4 monoclonal antibody was added on the carboxyl terminus of α5I-CCR5-His resulting in α5I-CCR5-His-C9 construct. The additional C9 tag drastically improved the GPCR detection using 1D4 antibody in Western blots.

10.7. Expression and purification of α5I-CCR5-His-C9

The expression and purification of α5I-CCR5-His-C9 were carried out as described for α5I-CCR5-His.

Bacterial pellet was resuspended in lysis buffer and cells where lysed using a microfluidizer. The inclusion body were solubilized in 6 M Urea and fusion protein was purified using a Ni-NTA resin under denaturing conditions (Figure 10.12).

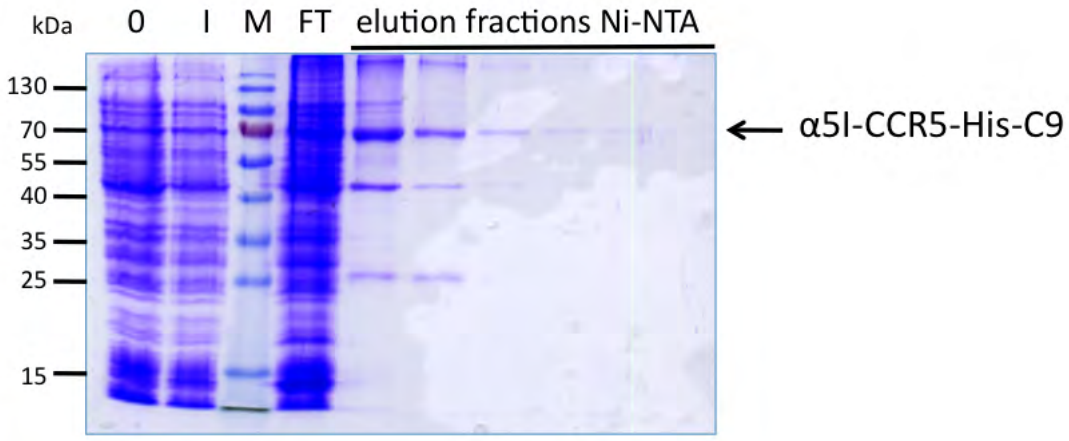

Figure 10.12.: SDS-polyacrylamide gel representing α5I-CCR5-His-C9 purification over a Ni-NTA resin.
M - marker; 0 - sample before induction, I - sample after induction, FT - flow through from the Ni-NTA resin. The arrow indicates α5I-CCR5-His-C9.

A conclusive double Western blot carried out on the same samples identified via an anti-His and a 1D4 antibody can be observed in Figure 10.13. The tremendous improvement of the C9 insertion is obvious.

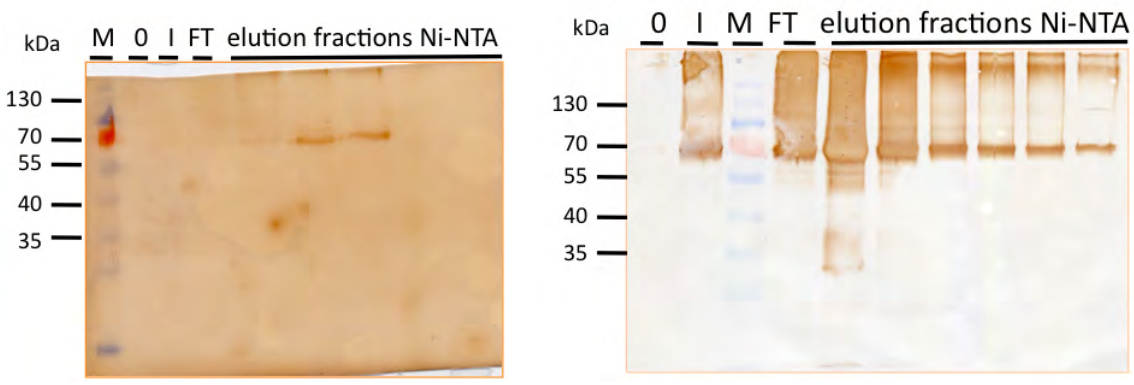

(a) anti-His antibody (b) 1D4 antibody

Figure 10.13.: Western blotting representing α5I-CCR5-His-C9 purification over a Ni-NTA resin. Western blotting of α5I-CCR5-His-C9 purification using Ni-NTA resin using (a) anti His antibody, (b) 1D4 antibody. M - marker, 0 - sample before induction, I - sample after induction, FT - flow through from the Ni-NTA resin.

The elution from the Ni-NTA column were pooled and dialyzed against thrombin digestion buffer to eliminate Urea. Thrombin digestion kinetics was observed by collecting aliquots after 1, 2 and 3 hours of digestion (10.14).

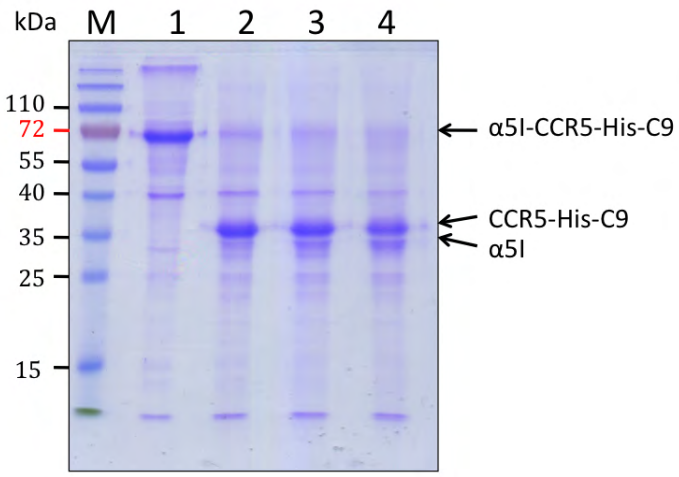

Figure 10.14.: SDS-polyacrylamide gel representing α5I-CCR5-His-C9 digestion with thrombin. M - marker; 1 - non digested sample; 2 - sample after 1 hour of digestion; 3 - sample after 2 hours of digestion; 4 - sample after 3 hours of digestion.

After one hour the digestion was completed. The reaction was stopped by the addition of 6 M Urea and 0.4 % SDS. The cleaved α5I fragment was separated from the CCR5-His-C9 by a second Ni-NTA purification (Figure 10.15).

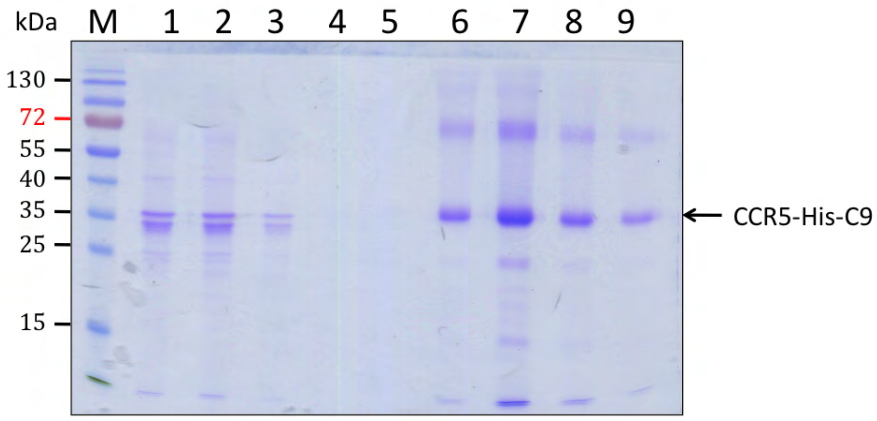

Figure 10.15.: SDS-polyacrylamide gel representing CCR5-His-C9 purification on Ni-NTA resin. M - marker; 1 - input, sample after thrombin digestion; 2-3 - flow-through; 4-5 - wash fractions; 6-9 - elution fractions.

The flow through (FT) and wash (W) fractions contained the α5I protein. The elution fractions containing the CCR5-His-C9 were pooled and dialyzed against 0.8% SDS buffer until Urea traces were removed.

Arround 2.2 mg of CCR5-His-C9 were obtained from one liter of bacterial culture.

CCR5-His-C9 folding was performed in the presence of NAPol and lipids in a 1:1:10 protein:lipid:NAPol weight ratio as previously described and analyzed on a SDS-polyacrylamide gel. As before the amount of protein maintained soluble was determined (82%).

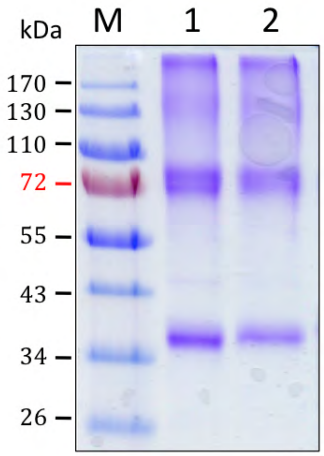

Figure 10.16.: SDS-polyacrylamide gel representing the sulubilized CCR5-His-C9 in NAPol. M - marker, 1 - CCR5-His-C9 before the SDS precipitation, 2 - CCR5-His-C9 after folding in a 1:1:10 protein:lipid:NAPol weight ratio.

Solubilized CCR5-His-C9 was extensively dialyzed against 30 mM Potassium phosphate pH 8.0, 150 mM KCl buffer. Over 1 mg of folded CCR5-His-C9 was obtained form one liter of bacterial culture. This sample was later used for SPR analysis.

11. Analysis of CCR5 - RANTES interaction using SPR

11.1. Introduction on Surface Plasmon Resonance

In 1990, Pharmacia AB, Uppsala, Sweden introduced the Biacore technology, which uses the Surface Plasmon Resonance (SPR) phenomenon that occurs in thin conducting films at an interface between media of different refractive index. In Biacore, the media are the glass of the sensor chip and the sample solution, and the conducting film is the gold layer on the sensor chip surface. The gold layer present on the sensor chip creates the physical conditions required for SPR. The SPR biosensor technology allows the real-time detection and monitoring of biomolecular binding events. This technology is widely used today, due to its high sensitivity and speed of analysis.

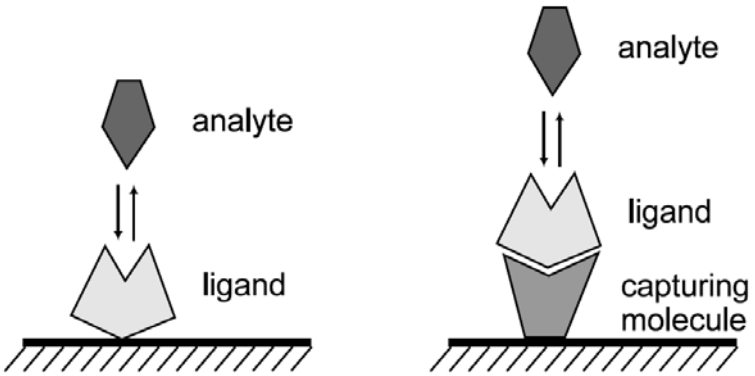

Figure 11.1.: Ligand, analyte and capturing molecule in relation to the sensor surface. Figure from biacore.com.

Biacore monitors the interaction between two molecules, one is the ligand attached to the sensor surface (the sensor chip), the other molecule is free in solution (analyte) delivered to the surface in a continuous flow (Figure 11.1). Ligand attachment to the surface may be covalent or through high affinity binding to another molecule, the capturing molecule, which is covalently attached to the surface.

The changes of refractive index are related to the mass concentration changes at the sensor chip surface (Figure 11.2).

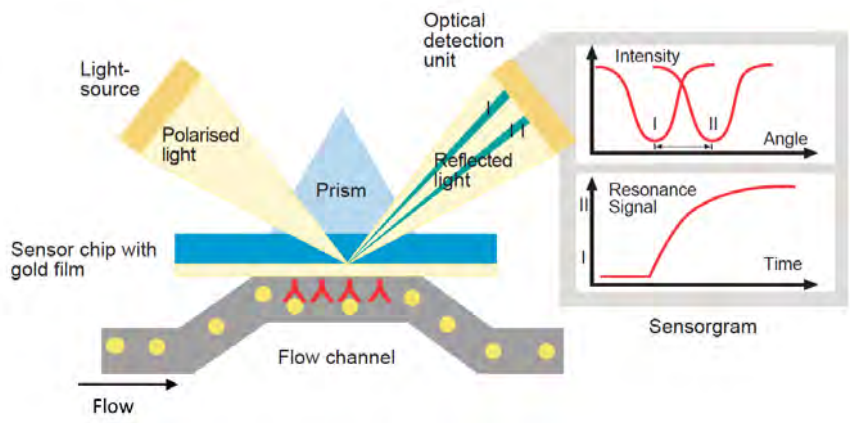

Figure 11.2.: Overview of Biacore SPR technology.
Ligand is represented as red Y-shapes and analyte is seen as yellow spheres. SPR measures changes in the resonance angle in real time. Angle I = no analyte binding. Angle II = analyte binds. Figure from biacore.com.

SPR measures changes in the resonance angle (which are directly related to refractive index and thus to the mass concentration of dissolved material close to the chip surface) in real time. The change in the SPR is directly related to the amount of analytes/biomolecules/molecules bound near the surface of the chip.

SPR follows the binding of analyte to the immobilized ligand and that leads to the detection of mass concentrations at the sensor surface. When analyte binds to a ligand the mass concentration increases, when they dissociate the mass decreases. This simple principle forms the basis of the sensorgram, the data output of the technology is the sensorgram, which is a plot of response units against time, a continuous, real-time monitoring of the association and dissociation of the interacting molecules (Figure 11.3).

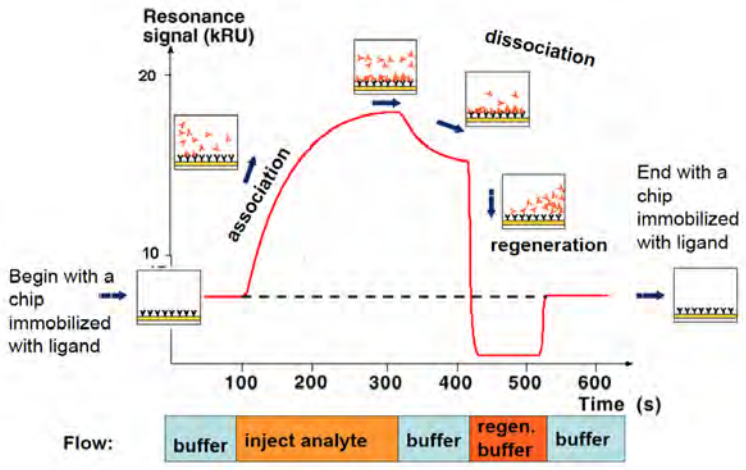

Figure 11.3.: Schematic illustration of a sensorgram.
The bars below the sensorgram curve indicate the solutions that pass over the sensor surface. Figure from biacore.com.

The sensorgram provides both qualitative and quantitative information in real-time on specificity of binding, concentration of active molecules in a sample, kinetics and affinity.

The SPR response is measured in Response (or Resonance) Units (RU) and is proportional to the molecular mass on the surface (Figure 11.4). R_{max} describes the maximum binding capacity of the surface. This means that for a molecule of a given mass the response is proportional to the number of molecules at the surface for sensor chip CM5. 1000 RU typically corresponds to 1 ng of protein bound per 1 mm^2, however the exact conversion from RU to protein amount depends on the sensor surface and the analyte molecule.

$$R_{max} = \frac{MW_A}{MW_L} \times R_L \times n$$

Figure 11.4.: Equation to calculate maximal binding capacity.
MW_A - molecular weight of analyte, MW_L - molecular weight of ligand, R_L- the amount of immobilized ligand in RU, n - stoichiometric coefficient.

SPR technology is used to characterize molecular interactions involving small molecules, proteins, polysaccharides, lipids and nucleic acids. Experiments are performed either with purified analytes or with analytes present in crude media such as cell or bacterial lysates, tissue extracts and biological fluids.

11.1.1. Sensor surface properties

The sensor chip is a glass slide coated with a thin layer of gold, which is commonly functionalized with carboxymethylated dextran matrix (Figure 11.5). Ligands to the dextran matrix can be attached using a variety of methods.

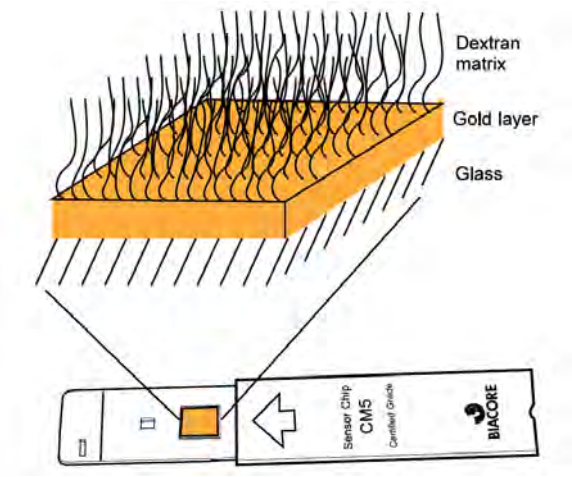

Figure 11.5.: Schematic illustration of the structure of the sensor chip surface.
Figure from biacore.com.

The gold layer and dextran matrix on the sensor surface are stable under a wide range of conditions, including extreme pH (from pH 1.5 to pH 8.5), moderate concentrations of many organic solvents (up to 30% DMSO, 40 % glycerol, 40 % ethylene glycol) or high salt concentrations (up to 2M $MgCl_2$). Once the ligand has been immobilized, the stability of the sensor surface is determined by the stability of the attached ligand.

11.1.2. Ligand immobilization methods

Different strategies exist for the ligand immobilization onto the sensor surface. A range of various sensor chips are available for use in Biacore systems. The discussion below is focused on immobilization strategies based on biomolecule capture by His-tag and biotin-tag as well as covalent immobilization by amine-coupling chemistry which are the techniques used in this thesis (Table 11.1).

Sensor Chip	**Surface type**	**Applications**
CM4 Sensor Chip	CM-dextran with lower carboxymethylation level than CM5	For low immobilization levels and reduced non-specific binding
SA Sensor Chip	CM-dextran with immobilized streptavidin	For capture of biotinylated ligands
NTA Sensor Chip	CM-dextran with immobilized NTA	For capture of poly-histidine tagged ligands

Table 11.1.: Biacore sensor chips used in this study.

11.1.3. Covalent immobilization methods

Molecules can be attached to the chip surface by covalent immobilization. There are wide range of well-defined chemistries but the simplest and the most commonly used is amine coupling.

11.1.3.1. Amine coupling

Amine coupling is the most widely applied approach for covalent immobilization of the biomolecules to the sensor surface. The matrix on CM-series of sensor chips is composed of a linear carboxymethylated dextran, which is covalently attached to a gold surface presents itself as a hydrogel under aqueous conditions. The matrix provides a hydrophilic 3-dimensional environment to biomolecules, the carboxyl groups of the matrix serve for covalent immobilization of ligands by amine coupling chemistry (Figure 11.6).

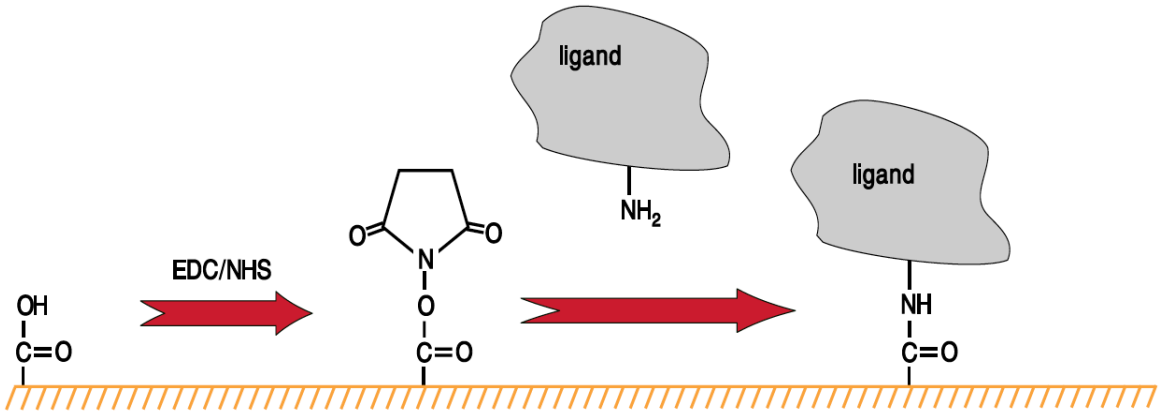

Figure 11.6.: Schematic view of amine coupling of ligands to the sensor surface. An overview of amine-coupling using N-hydroxysuccinimide (NHS) and N'-(3-dimethylaminopropyl) carbodiimide hydrochloride (EDC). Figure from biacore.com.

The dextran matrix on the sensor chip surface is first activated with a mixture of EDC (1-ethyl-3-(3-dimethylaminopropyl)- carbodiimide) and NHS (N-hydroxysuccinimide) to give reactive succinimide esters. Ligand is then passed over the surface and the esters react spontaneously with uncharged amino groups and other nucleophilic groups to link the ligand covalently to the dextran.

Unreacted esters are subsequently blocked with 1 M ethanolamine, which also releases loosely-bound ligand from the surface.

The ligand to be coupled must be as pure as possible and storage buffer free from primary amines such as Tris, glycine or stabilizing proteins. As the carboxymethylated matrix is negatively charged in the running buffer (pH 7.4), the ligand must have a positive charge so that it is not electrostatically repelled from the surface during the coupling reaction. By using coupling buffers with a pH below the isoelectric point of the ligand, the positive net charge of the ligand can be achieved.

In some cases, amine coupling may involve amine groups at or near the active site of the ligand and attachment would lead to the loss of activity. However, it is common that proteins contain several amine groups so that efficient immobilization can be achieved without seriously affecting the biological activity of the ligand.

11.1.3.2. Conditions for ligand immobilization

For an efficient amine coupling method the ligand immobilization conditions should be determined.

This can be investigated quickly and easily using an intact CM surface and injecting ligand diluted in buffers of different pH, a process called pH-scouting or pre-concentration.

Before covalent bonds are formed between ligand and matrix, the ligand molecules are directed to the surface due to electrostatic attraction. The magnitude of this attraction depends on the net charge of the ligand, which in turn depends on pH of the buffer. The stronger the attraction, the more of the ligand will be immobilized. Therefore it is useful to determine the optimal pH of the buffer.

The carboxymethylated surface of the sensor chip carries a net negative charge at pH values above about 3.5, so to achieve efficient pre-concentration the pH of the buffer should be higher than 3.5 and lower than the isoelectric point of the ligand. In some cases the optimal pH is a compromise between efficient pre-concentration and the stability of the ligand. Therefore, a choice of pH can be a critical parameter in determining the success of immobilization (Figure 11.7). The experimental procedure for finding the appropriate immobilization pH consists of several injections of the ligand diluted in buffers of different pH.

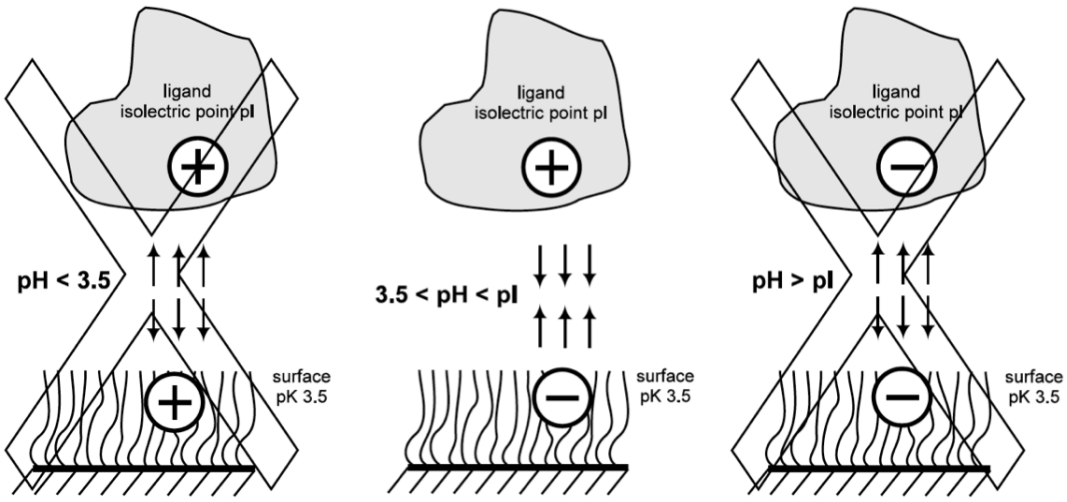

Figure 11.7.: Electrostatic attraction of the ligand to the CM-dextran.
Ligand is concentrated on the surface through electrostatic attraction when the pH lies between the pK_a of the surface and the isoelectric point of the ligand. If the pH is too high or too low, ligand will not be attracted to the surface. Figure from biacore.com.

An additional requirement for efficient pre-concentration is a low ionic strength in the immobilization buffer. In general, a maximum of 10-15 mM monovalent ions is recommended. It is required to use high concentration of the ligand due to the phenomenon of the electrostatic attraction. For most proteins, concentrations of 5–50 µg/ml are sufficient.

Once pre-concentration conditions have been established the surface should be washed with ethanolamine to remove all loosely bound ligand molecules and immobilization can be performed.

11.1.3.3. Results of immobilization

The result of immobilization is the amount of ligand remaining on the surface at the end of the immobilization procedure, measured as the response relative to the baseline after surface activation (Figure 11.8).

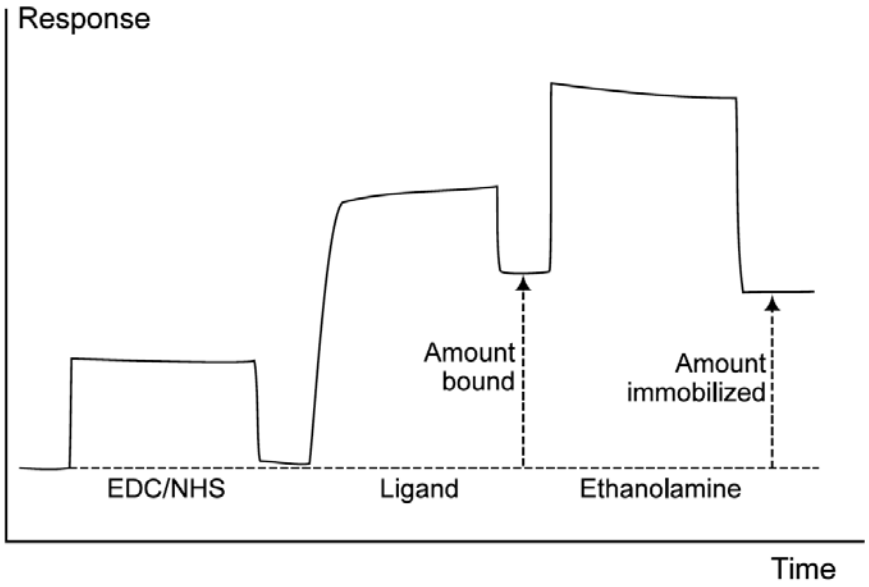

Figure 11.8.: Sensorgram from a typical amine coupling.
The distinction between the amount of ligand bound and the amount immobilized is illustrated. Figure from biacore.com.

11.1.4. Capturing techniques

Several capturing approaches can be considered, they are based on biospecific interaction between ligand and capturing molecule. The capturing molecule is normally covalently immobilized on the surface. The advantage of using capturing techniques is that the ligand orientation is known. The disadvantage is that the ligand surface might be unstable - ligand dissociates from the surface and has to be re-injected. Also, it could be difficult to find regeneration conditions, as in most cases the regeneration of the surface involves ligand removal from the capturing molecule together with bound analyte.

11.1.4.1. Streptavidin-biotin capture

On the surface of SA Sensor Chip streptavidin is covalently attached to a dextran matrix. It is designed to capture biotinylated ligands (Figure 11.9).

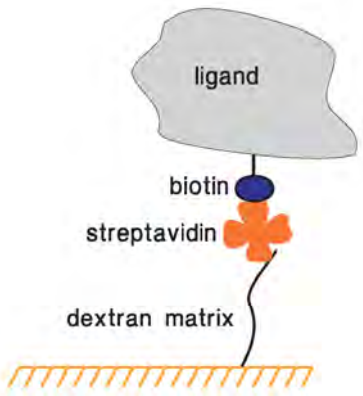

Figure 11.9.: Schematic view of biotinylated ligand capture by high affinity binding to streptavidin on Sensor Chip SA.
Figure from biacore.com.

Biotin may be introduced to a variety of biomolecules including proteins, carbohydrates, lipids and, as in this work, amphipols. The affinity of streptavidin for biotin is very high ($K_D \approx 10^{-15}$ M), the biotinylated ligand cannot be removed from the streptavidin surface, so the ligand is permanently attached to the surface. Therefore, streptavidin-biotin capture is more similar to covalent attachment than to other capturing approaches.

11.1.4.2. Antibody-based capture

Due to their high specificity and affinity monoclonal antibodies can be used as capturing molecules in Biacore. They can be immobilized on the sensor surface using amine-coupling method (Figure 11.10).

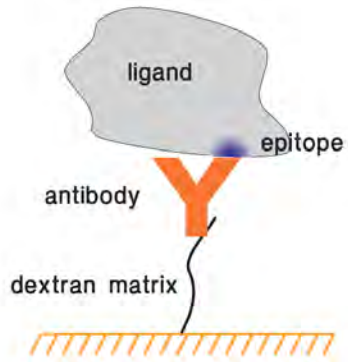

Figure 11.10.: Schematic view of antibody-based capture.
Antibody-based capture relies on the specific binding between an immobilized antibody and the antigenic epitope on the ligand. Figure from biacore.com.

Antibodies designed against chosen epitopes on the ligands enables ligands to be captured in controlled orientations.

11.1.4.3. Capture of histidine-tagged molecules

It is common to include a poly-histidine tag to recombinant proteins for affinity purification purposes and the same principle can be applied to capture recombinant proteins on the sensor surface in Biacore. A commonly used poly-histidine tag can chelate Ni^{2+} ions in complex with nitrilotriacetic acid (NTA), and therefore can be used for capturing his-tagged constructs on NTA Sensor Chip (Figure 11.11). By using NTA Sensor Chip the orientation of the histidine-tagged ligands can be controlled.

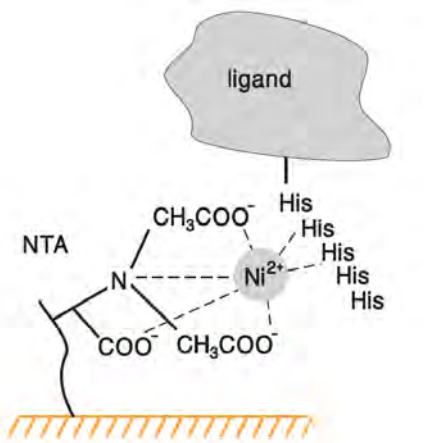

Figure 11.11.: Schematic view of the chip surface of NTA Sensor Chip.
Figure from biacore.com.

The captured His-tagged proteins can be removed from the surface by injecting EDTA, which removes the metal ions and releases the his-tagged ligand. This allows to use the sensor chip for multiple experiments.

11.2. Results

To test CCR5 functionality SPR experiments were performed. CCR5 samples folded in the presence of lipids (L) and amphipols: A8-35 (CCR5/A8-35/L), NAPol (CCR5/NAPol/L) and BAPol (CCR5/BAPol/L) were tested. Two different versions of CCR5, CCR5-His and CCR5-His-C9, were used. Three functionalization approaches were considered. The presence of these two tags allowed non-covalent capture on Ni^{2+}-NTA and on a 1D4 antibody functionalized sensor chip, respectively. On the other hand the use of the biotinylated amphipol (BAPol), provided the possibility of a strong non-covalent capture on SA sensor chip.

11.2.1. CCR5 capture on NTA sensor chip

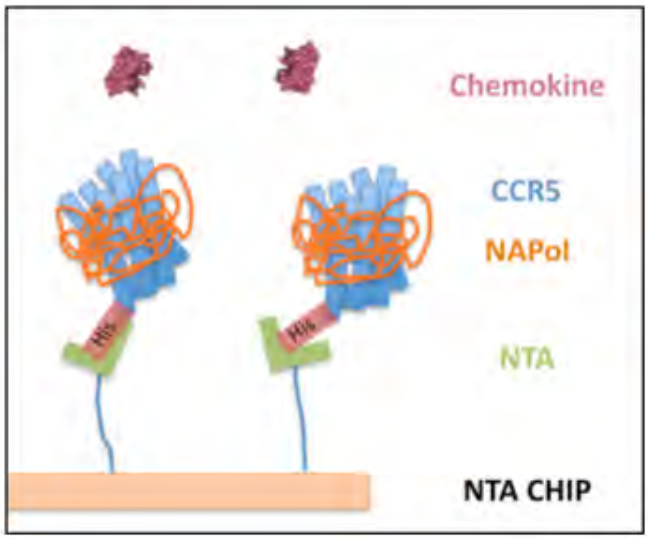

Figure 11.12.: Schematic representation of CCR5/NAPol immobilization on NTA sensor chip.

11.2.1.1. Development of the SPR assay to study CCR5 - chemokine interaction

While working with NTA sensor chip the first step is to load Ni^{2+} on the chosen active flow cell surface. In our case flow cell 2 (Fc2) was chosen for receptor immobilization, therefore it was loaded with Ni^{2+}, while leaving Fc1 intact. The 4 min injection of CCR5-His/NAPol/L (at a 60 µg/ml receptor concentration) gave a final binding response of 643 RU on Fc2 while nothing bound to Fc1.

Binding assays were then performed using an irrelevant ligand SDF1α-Strep (specific for CXCR4) and then a CCR5 specific ligand, RANTES-Strep. SDF1α-Strep (at 500 nM) was injected first over the CCR5-His/NAPol/L surface followed by a RANTES-Strep (at 500 nM) injection (Figure 11.13).

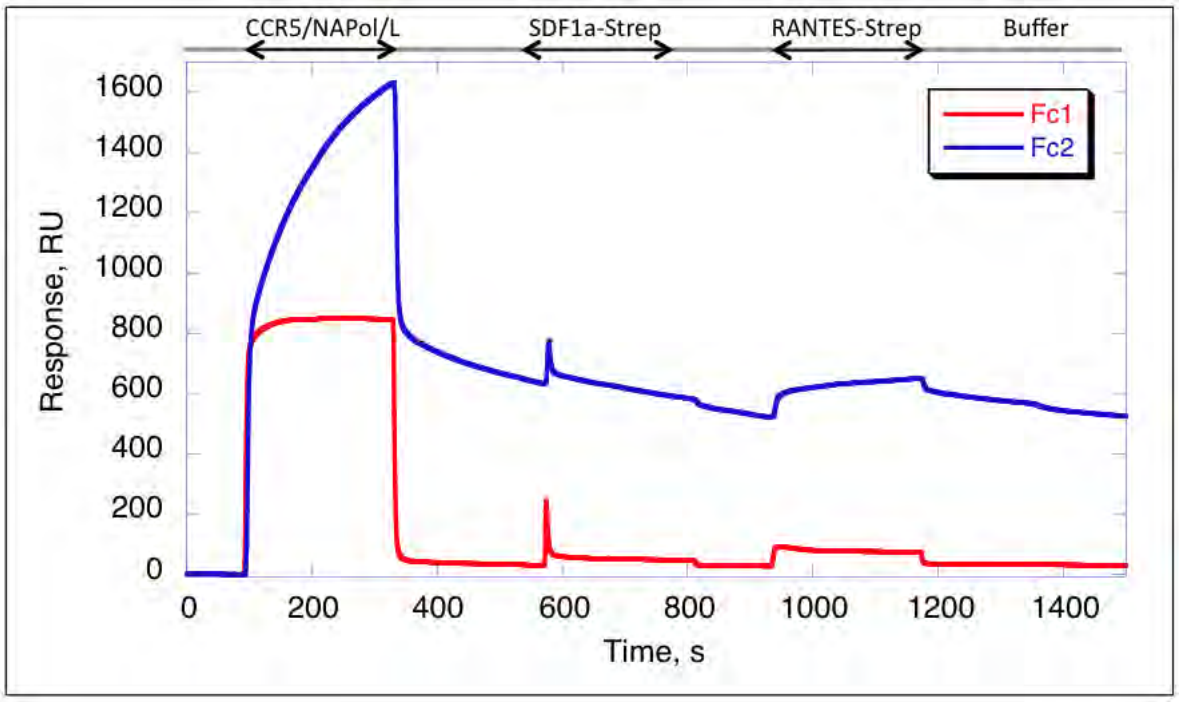

(a)

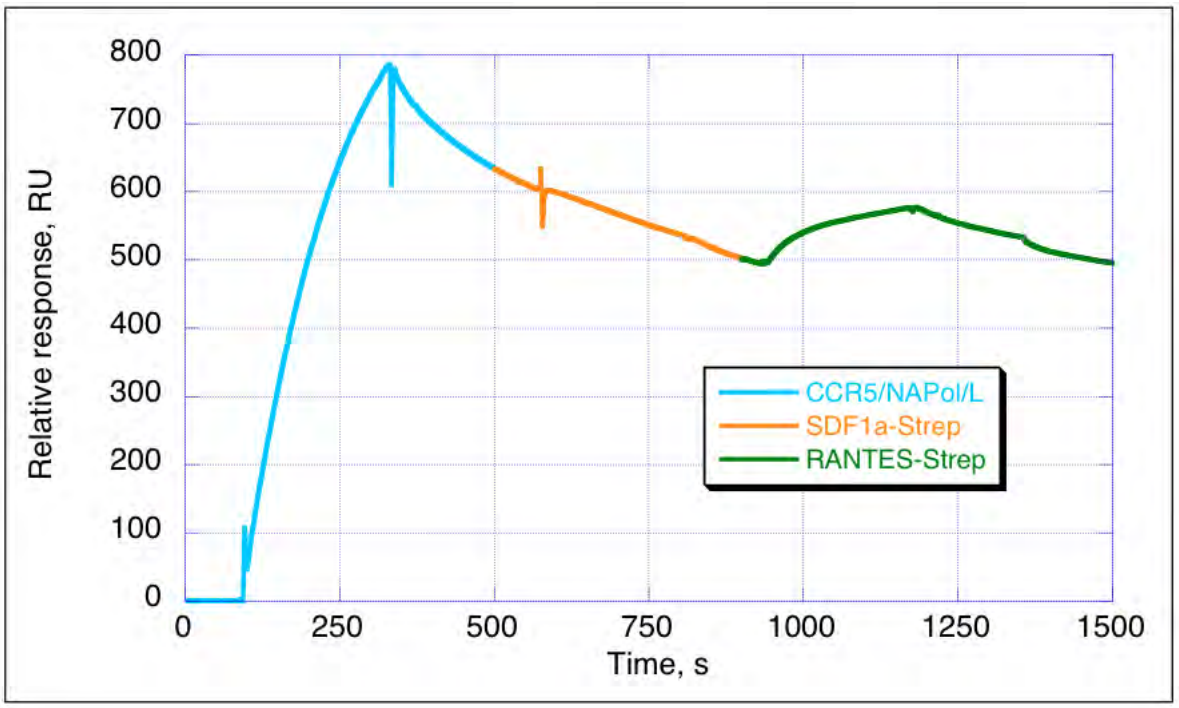

(b)

Figure 11.13.: Normalized sensorgrams representing NTA chip functionalization and chemokine binding test.
(a) The CCR5-His/NAPol/L was injected over the reference surface Fc1 (red) and Ni^{2+} activated surface Fc2 (blue). Subsequently SDF1α-Strep (500 nM) and RANTES-Strep (500 nM) were injected over both reference and receptor functionalized surfaces. (b) Reference surface corrected sensorgrams representing the same injections as panel (a). Reference surface corrected sensorgram refers to a differential sensorgram, where a control surface response is subtracted from the raw active surface sensorgram.

Analysis of the subtracted curve (Figure 11.13b) allows us to eliminate the bulk effects observed in the Figure 11.13a. The absence of SDF1α-Strep binding shows the specificity of the interaction with the receptor. The fact that RANTES-Strep bound to CCR5 captured surface indicates that CCR5/NAPol/L is active and specific. Unfortunately, the baseline was not stable and one hour after CCR5/NAPol/L injection only 368 RU of receptor remained on the surface.

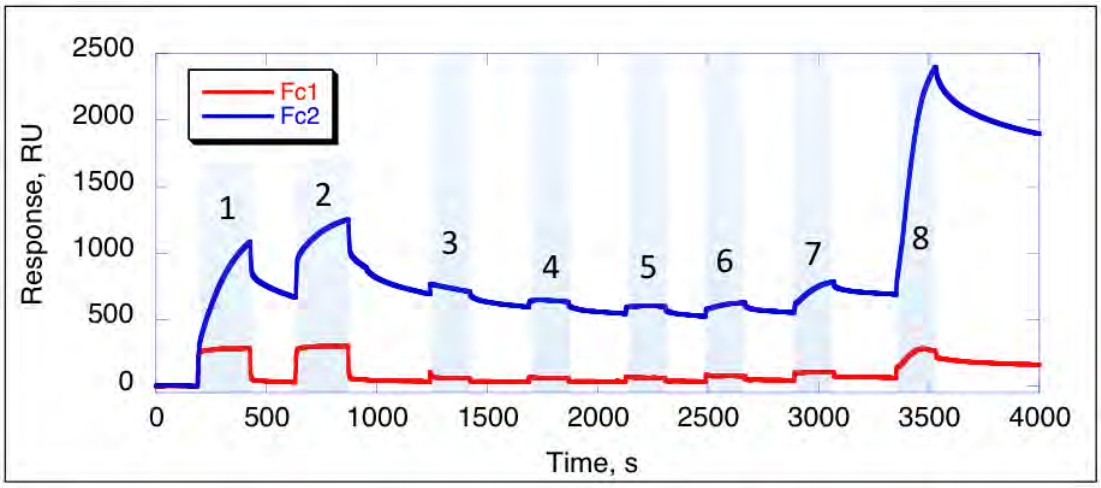

(a)

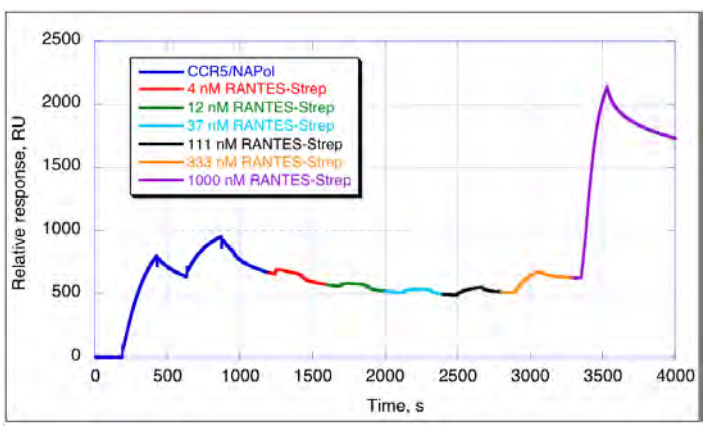

(b)

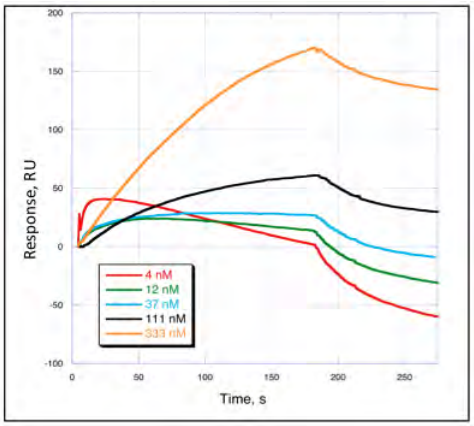

(c)

Figure 11.14.: Normalized sensorgrams showing RANTES-Strep interaction with CCR5-His/NAPol/L surface.
(a) Sensorgrams representing absolute response on reference surface Fc1 (red) and Ni^{2+} activated surface Fc2 (blue) during the following injections: 1, 2 - CCR5-His/NAPol/L, 3 - 8 RANTES-Strep at 4 nM, 12 nM, 37 nM, 111 nM, 333 nM and 1000 nM, respectively. (b) Reference surface corrected sensorgrams representing the same injections as panel (a). (c) Reference surface corrected overlaid sensorgrams showing RANTES-Strep (4 nM - 333 nM) interaction with CCR5-His/NAPol/L.

To evaluate the active receptor amount and to obtain the affinity value (K_D), the titration of RANTES-Strep was performed. Prior to that, the active surface (Fc2) was regenerated and receptor was re-captured up to a final response of 660 RU via two successive injections to increase

the immobilization level. Despite the unstable surface after receptor immobilization the titration of chemokine was performed. The expected affinity of RANTES interaction with CCR5 is at low nM range (0.2 - 6.2 nM) as described in the literature [372]. However, CCR5 being expressed in E. coli, it missed post-translational modifications that may contribute to this high affinity. Therefore, a range of 4 nM - 1000 nM concentrations of RANTES-Strep was chosen for the analysis. The lowest concentration of RANTES-Strep (4 nM) was first injected (Figure 11.14).

It is obvious that there is no non-specific RANTES-Strep interaction with the reference surface except for the last injection of 1000 nM (Figure 11.14a). RANTES-Strep binding responses are concentration dependent, but the continuous decrease of the baseline due to the receptor dissociation from the NTA surface complicates RANTES-Strep binding responses (Figure 11.14c). Nevertheless, we plotted RANTES-Strep binding responses against the used concentrations to see the binding pattern (Figure 11.15).

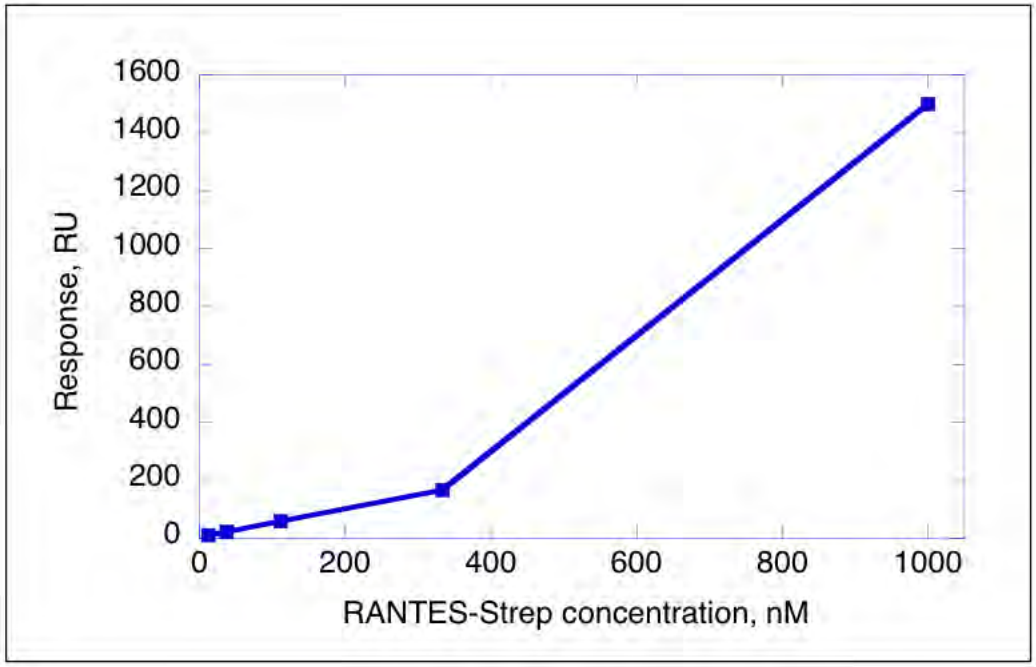

Figure 11.15.: Concentration dependency of RANTES-Strep binding responses.

Obviously the obtained binding curve significantly deviates from the standard Langmuir binding isotherm. We can observe two phases of the curve, the first part being linear and a second part with a tremendous slope increase. To elucidate the reason of this deviation we calculated the theoretical binding capacity of the prepared surface and compared with the observed binding responses.

660 RU of the complex were bound to the sensor chip, the MW of RANTES-Strep equal to 10 kDa, we estimate that we have ~100 kDa of NAPol bound per receptor (43 kDa) monomer [337, 336], then calculated theoretical $R_{max}$is 46 RU (Figure 11.16).

$$R_{max} = \frac{MW_{RANTES-Strep}}{MW_{CCR5/NAPol/L}} \times R_{CCR5/NAPol/L} \times n$$

$$R_{max} = \frac{10\,kDa}{143\,kDa} \times 660\,RU \times n = 46\,RU \times n$$

Figure 11.16.: Calculation of CCR5/NAPol/L maximal binding capacity.
n - stoichiometry index. If the chemokine interacts with the receptor as 1:1, then the stoichiometry index would be equal to 1. If the chemokine interacts with the receptor as 1:2, then the stoichiometry index would be equal to 0.5.

Surprisingly when RANTES-Strep concentration is higher than 37 nM the amount of bound RANTES-Strep significantly exits the expected theoretical R_{max}value. For example, 1000 nM RANTES-Strep injection gives 1500 RU binding response, which is approximately 30 times higher than the expected value. This theoretical $R_{max}$was calculated excluding the lipids that could be present in the receptor complex, if we included the lipids in the calculation, the theoretical R_{max}value would be even lower. These high RANTES-Strep binding responses could be explained by concentration dependent increase of the chemokine MW, i.e. oligomerization. Indeed, it is well known that RANTES oligomerize at high concentrations (1 μM) [277].

Although the interaction data were complicated (due to the unstable baseline) we have tried to extract the rough kinetic parameters for the interaction. The fitting has been performed on two of the conditions tested that fulfilled the following criteria: RANTES-Strep should not be in an oligomeric form (lower than 1000 nM concentration), it should be from a part of the experiment with a reduced surface leaking. For this reason two sensorgrams representing 111 nM and 333 nM RANTES-Strep binding to CCR5/NAPol/L surface were chosen to perform separate fitting of Langmuirian dissociation and association differential rate equations to the last 50 s interval of the dissociation phases and to the early portions of 150 s intervals of the association phases, respectively to calculate the interaction parameters. The determined rate constants and the K_D are listed in Table 11.2.

Ligand	Conc.	k_a, $\times 10^4 M^{-1}s^{-1}$	k_d, $\times 10^{-3}s^{-1}$	K_D, nM
RANTES-Strep	111 nM	7.61	4.03	53
	333 nM	2.05	1.3	63.4

Table 11.2.: Apparent RANTES-Strep - CCR5 interaction parameters.

The obtained $K_D$values are at low nM range which are not far from to the published ones [372] considering the absence of post-translational modifications on *E. coli* expressed CCR5.

11.2.1.2. Chemokine tag influence for the interaction with the receptor

The surface of the NTA sensor chip was prepared as described above. Because of the surface leaking and to start the experiment with the high receptor level on the surface CCR5/NAPol/L was coupled by three successive injections and the final binding response was approximately 500 RU (before injection of RANTES-Strep) (Figure 11.17).

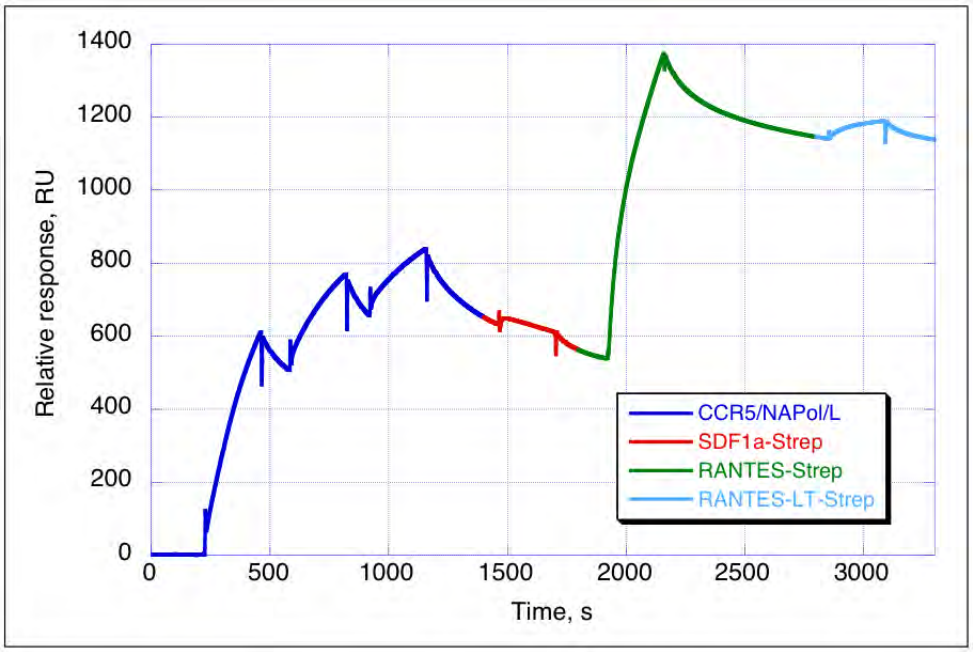

Figure 11.17.: Normalized reference surface corrected sensorgram showing a comparison of different chemokine interaction with the CCR5/NAPol/L surface.
Injections: blue - three successive injections of CCR5/NAPol/L (60µg/ml), red - SDF1α-Strep (500 nM), green - RANTES-Strep (500 nM), cyan - RANTES-LT-Strep (500 nM).

A big difference in binding responses was observed when comparing the responses of RANTES-Strep and RANTES-LT-Strep injections. The calculated theoretical R_{max}value is roughly 35 RU while RANTES-Strep binding clearly exceeds this value by more than 10 times. This might be caused by oligomerization of this chemokine. On the other hand RANTES-LT-Strep binding response is 50 RU, which is in the range of expected binding capacity of the prepared surface. We can conclude that RANTES-LT-Strep is binding as a monomer to CCR5 while RANTES-Strep is clearly oligomeric (500 nM) at concentration lower than what has been published to trigger oligomerization (1µM).

Receptor capturing on the NTA sensor chip was not stable and the surface capacity was decreasing significantly, which does not allow to set up a proper interaction test. Hence, we decided to consider different immobilization approaches to improve the surface stability.

11.2.2. CCR5 immobilization on CM4 sensor chip

From the Ni-NTA sensor chip data to fit kinetic binding data with simple interaction models was a hard task. Therefore the experimental design was improved by means of employing a relatively low-capacity surface (CM4) and orienting the immobilization of the ligand to the flow-cell surface.

Usually the proteins are immobilized covalently on the sensor chips of CM series by amine coupling chemistry, which in most cases results in stable ligand surfaces. In order to keep the receptor oriented the we did not perform the amine coupling directly with the receptor. For this reason the C9 tag was introduces on the C-terminus of the CCR5 (Figure 11.18).

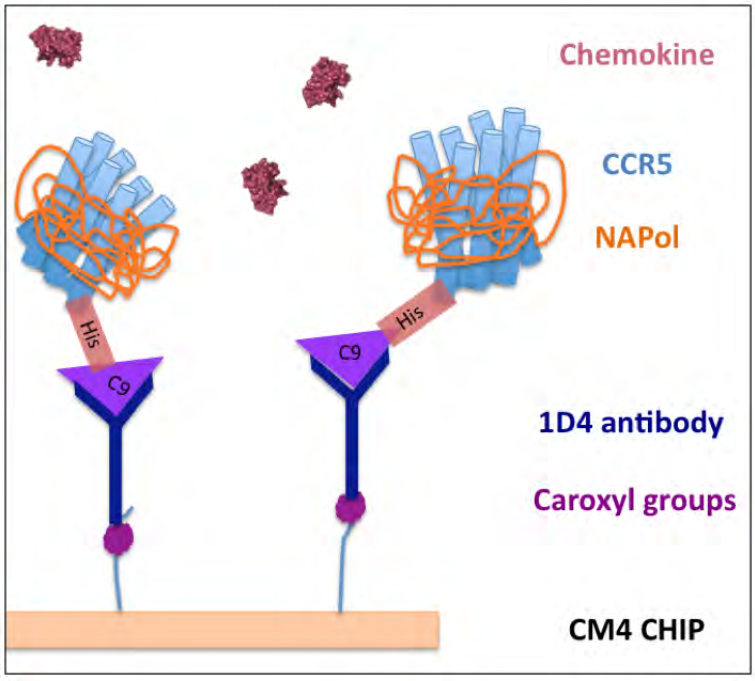

Figure 11.18.: Schematic representation of 1D4 capture on CM4 sensor chip and CCR5/NAPol binding.

A linear C9 peptide tag (TETSQVAPA), located at the C-terminus of the receptor and recognized by the 1D4 monoclonal antibody [373], gives the opportunity of a non-covalent capture of the receptor via the C9 interaction with the latter antibody. Hence, the 1D4 can be covalently immobilized by amine coupling and the prepared surface can be used for biospecific capture of the receptor as it was previously published [372].

11.2.2.1. Optimization of the antibody immobilization conditions

CM4 sensor chip was chosen for SPR measurements because it has a lower carboxylation level of the dextran matrix than CM5 sensor chip, i.e. lower amount of negative charges, which reduces the possibility of non-specific electrostatic interactions.

Amine coupling requires the protein to be prepared in acidic pH so that the molecules would have a positive net charge, which allows electrostatic attraction to negatively charged matrix surface. The optimal buffer pH, which would allow the highest yield of protein immobilization, can be determined by performing pre-concentration tests. For this reason the protein has to be diluted in buffers of different pH and injected on the intact sensor chip surface.

It is necessary to have a sufficient amount of the 1D4 antibody immobilized so that efficient receptor capture can be achieved. We tested 1D4 pre-concentration in four different pH buffers: 4.0, 4.5, 5.0 and 5.5 (Figure 11.19a).

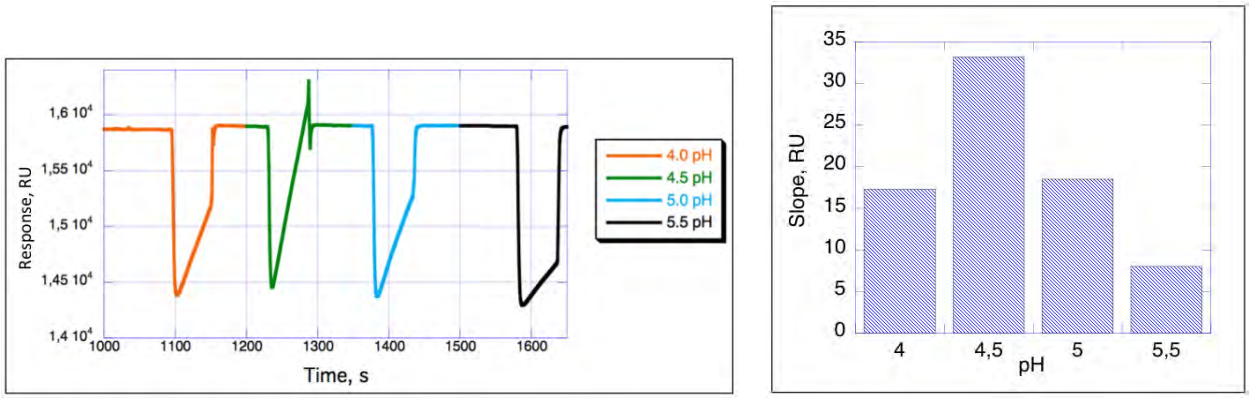

(a) (b)

Figure 11.19.: Test of 1D4 antibody pre-concentration on CM4 sensor chip.
(a) Sensorgram showing injections of 1D4 antibody (5 µg/ml) in 10 mM sodium acetate buffers at different pH: orange - pH 4.0, green - pH 4.5, cyan - pH 5.0, black - pH 5.5. (b) Histogram representation of the slope values of each injection corresponding to different pH.

The pre-concentration efficiency can be evaluated by the slope value of the response during the injection. As can be seen from the Figure 11.19b the highest slope value is achieved at pH 4.5. Hence, this buffer was chosen for 1D4 immobilization.

11.2.2.2. 1D4 antibody immobilization by amine coupling

The monoclonal antibody 1D4 was immobilized on CM4 sensor chip using standard amine-coupling chemistry on the Flow cell 2. The CM-dextran surface was activated by a 10-min injection of EDC/NHS mixture. Then 1D4 antibody was injected to the surface with a 7-min injection in 10 mM sodium acetate pH 4.5. Remaining activated carboxyl groups were blocked by a 10-min injection of ethanolamine (Figure 11.20).

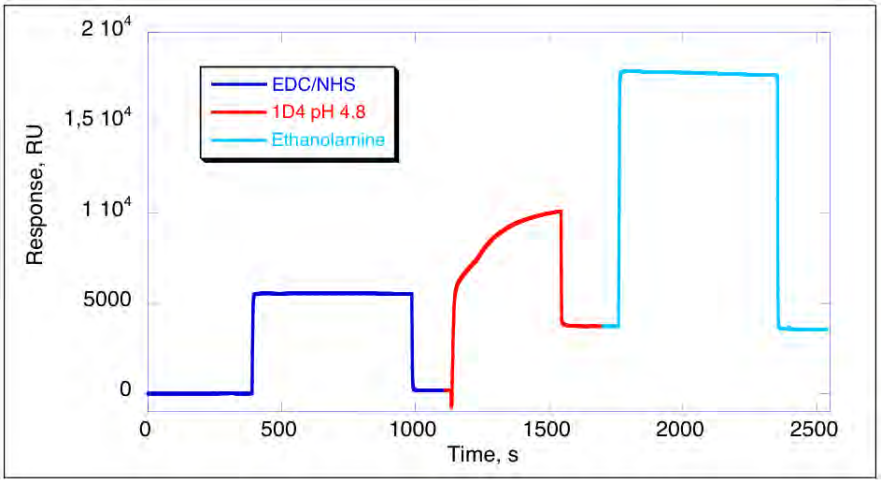

Figure 11.20.: The sensorgram representing 1D4 immobilization by amine coupling. Injections: blue - EDS/NHS, red - 1D4 (5 μg/ml), cyan - ethanolamine.

The final response of immobilized 1D4 antibody on Fc2 was 3400 RU. The reference surface (Fc1) was activated by a 10-min injection of EDC/NHS mixture and blocked by a 10-min injection of ethanolamine.

11.2.2.3. Receptor capture on 1D4 antibody surface

The prepared 1D4 antibody surface on the Fc2 was used to capture the receptor. The mixture of CCR5/NAPol/L (60 μg/ml) was injected over the Fc2 surface (Figure 11.21).

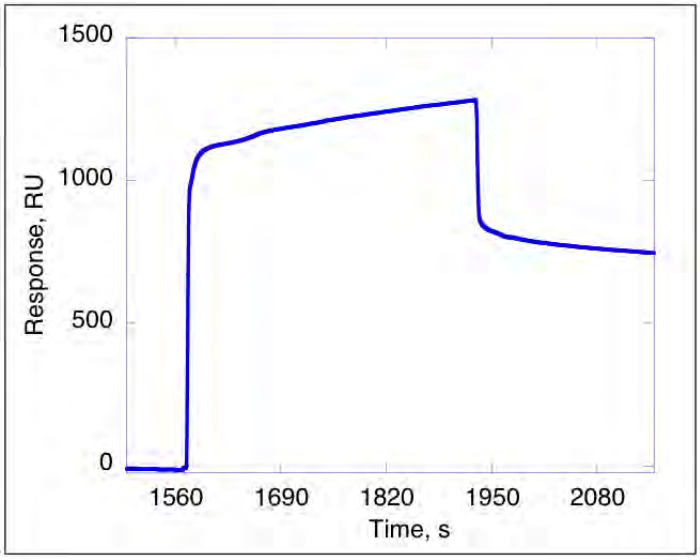

Figure 11.21.: Normalized sensorgram showing CCR5/NAPol/L binding on 1D4 surface.

The final response of captured CCR5/NAPol/L was 700 RU.

11.2.2.4. The CCR5 surface activity test

First we checked whether RANTES-Strep could non-specifically interact with 1D4 antibody surface on Fc1 (Figure 11.22).

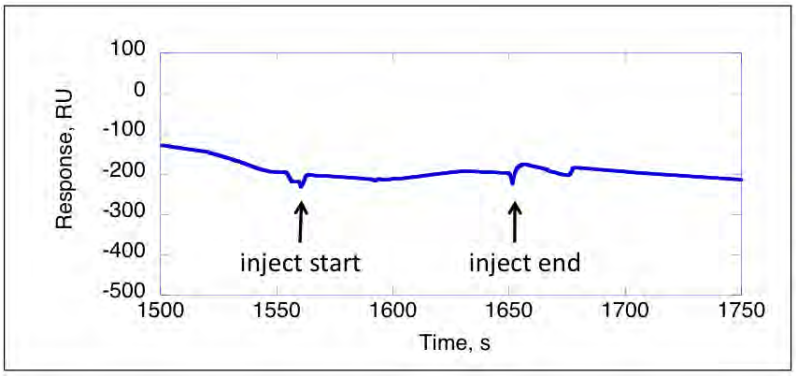

Figure 11.22.: Sensorgram representing RANTES-Strep injection over 1D4 surface.

There was no RANTES-Strep interaction with 1D4 surface observed. Then several injections of chemokines RANTES-Strep and SDF1α-His were performed to test activity and specificity of CCR5/NAPol/L surface (Figure 11.23).

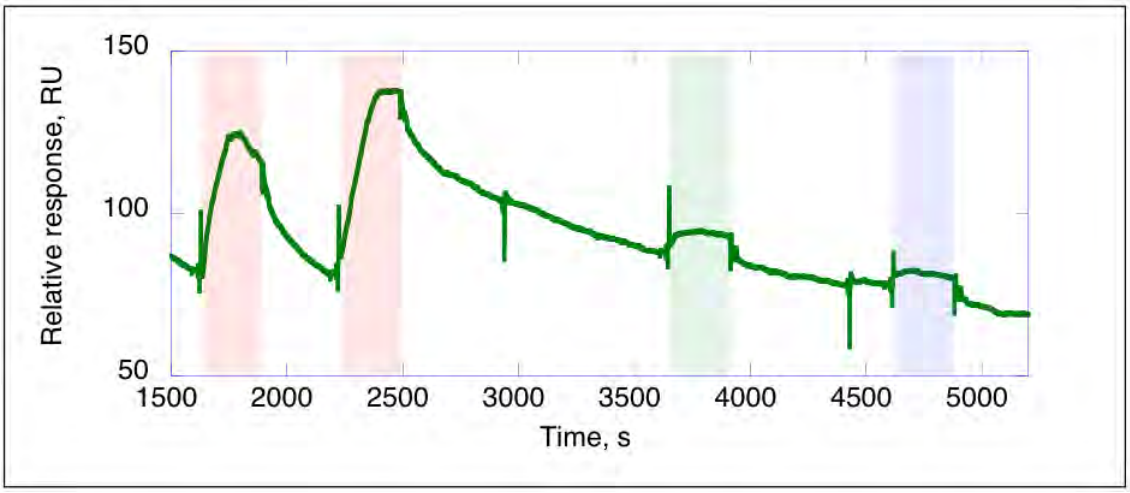

Figure 11.23.: Reference surface corrected sensorgram showing injections of chemokines onto CCR5/NAPol/L surface.
Different color boxes represents the different injections: red background – injection of 200 nM RANTES-Strep, green background – injection of 200 nM SDF1α-His, blue background – injection of buffer HBS-N.

The responses of RANTES-Strep and SDF1α-His were double referenced [374, 375, 376]. While using low-capacity surfaces it intrinsically leads to lower signal-to-noise ratio. However, in SPR analysis there are systematic artifacts arising from the sample application, which can be removed

using a two-step data correction (or double referencing). First, data is subtracted from a reference surface. The systematic artifacts (also called bulk effects) are essentially equal between the reaction and reference flow cells, and can be removed by subtracting the reference surface data (Fc1) from the reaction surface data (Fc2). The second referencing step is subtracting blank injections. The increase of the signal response during the analyte injections could be also observed when running buffer was injected over the ligand surface. Subtracting the running buffer data from all binding responses collected under the same conditions can eliminate this drift and allow us better analysis of chemokine interaction (Figure 11.24).

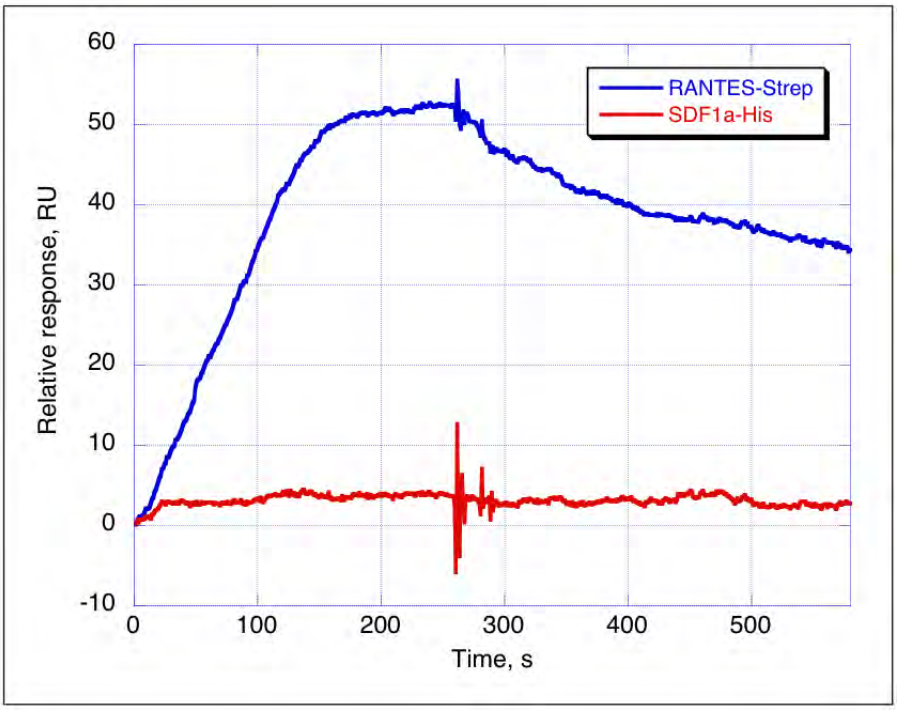

Figure 11.24.: Normalized and double referenced sensorgrams showing the specificity of CCR5 surface.
Injections of chemokines onto CCR5/NAPol/L surface: blue - 200 nM RANTES-Strep, red - 200 nM SDF1α-His.

Due to the double referencing the sensorgram of SDF1α-His becomes flat and we can better evaluate RANTES-Strep specific interaction.

$$R_{max} = \frac{MW_{RANTES-Strep}}{MW_{CCR5/NAPol/L}} \times R_{CCR5/NAPol/L} \times n = \frac{10\,kDa}{143\,kDa} \times 700\,RU \times n = 49\,RU \times n$$

Figure 11.25.: Calculation of CCR5/NAPol/L maximal binding capacity.
n - stoichiometry index. If the chemokine interacts with the receptor as 1:1, then the stoichiometry index would be equal to 1. If the chemokine interacts with the receptor as 1:2, then the stoichiometry index would be equal to 0.5.

Once again, the calculated theoretical R_{max} is 49 RU (Figure 11.25) while we observe a RANTES-

Strep binding of 52 RU (Figure 11.24). From this results it is possible to conclude that at 200 nM concentration RANTES-Strep is monomeric and is interacting with the receptor at 1:1 ratio.

11.2.3. Chemokine interaction with amphipols

To be absolutely sure that the observed binding of RANTES result from a specific interaction with the CCR5 and not from non-specific binding to the amphipols some control experiments were needed. There are two possibilities monitor the RANTES specific binding. The first and best option would be to prepare the control surface with another GPCR, that do not bind RANTES, folded in amphipols. The second option is to prepare a RANTES surface and inject amphipols. This control was prepared. As RANTES supports well acidic pH buffers there was no problem for its covalent immobilization on the CM4 sensor chip by amine coupling chemistry.

For better RANTES-Strep immobilization pre-concentration experiments were performed. RANTES-Strep was prepared in 10 mM NaAcetate buffers at pH 4.0; 4.5; 5.0; 5.5; 6.0. The pre-concentration efficiency can be evaluated by the slope value of the response during injection. As can be seen from the Figure 11.26 the highest slope value is achieved at pH 5. Hence, this buffer was chosen for RANTES-strep immobilization.

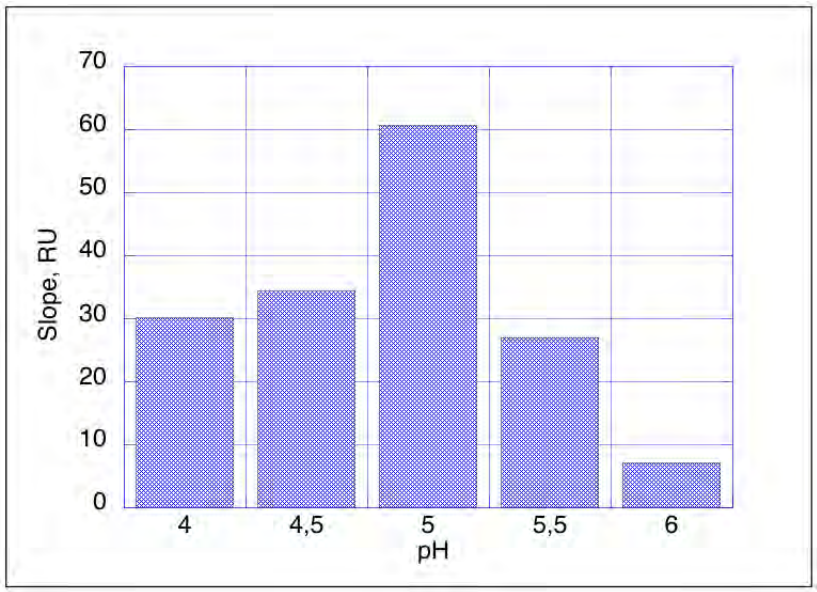

Figure 11.26.: Histograms representing RANTES-Strep pre-concentration.

RANTES-Strep was immobilized on CM4 sensor chip using standard amine-coupling chemistry on the Flow cell 2. The CM-dextran surface was activated by a 10-min injection of EDC/NHS mixture. Then the RANTES-Strep was injected to the surface with a 7-min injection in 10 mM NaAcetate pH 5. Remaining activated carboxyl groups were blocked by a 10-min injection of ethanolamine. The final response of immobilized RANTES-Strep on Fc2 was 437.5 RU. Flow

cell 1, the reference surface, was activated by a 10-min injection of EDC/NHS mixture and blocked by a 10-min injection of ethanolamine. Both amphipols NAPol and A8-35 were tested for nonspecific interaction with RANTES-Strep (Figure 11.27).

The final NAPol concentration in the receptor solution used for the SPR experiments described before, was 1.17 mg/ml. The same concentration and five times less (0.234 mg/ml) of both amphipols were used to test the interaction with RANTES-Strep. Amphipols were injected at two flow rates: 100 µl/min and 20 µl/min.

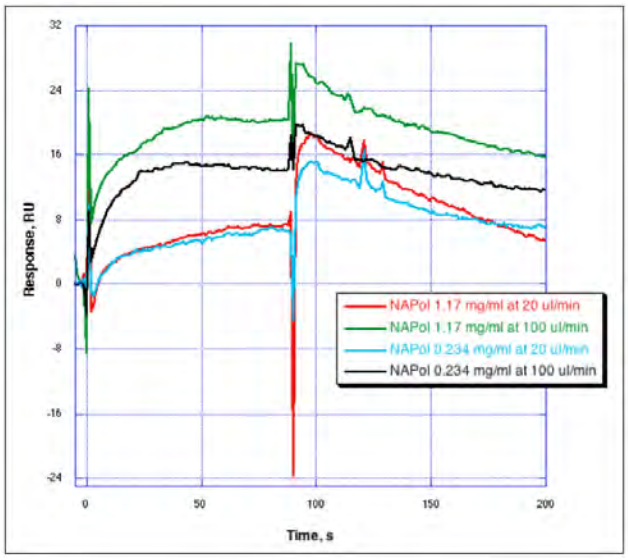

(a) NAPol

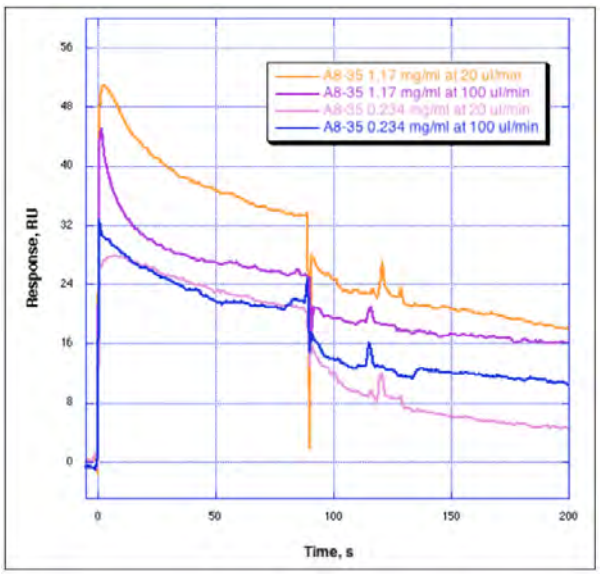

(b) A8-35

Figure 11.27.: Reference surface corrected sensorgrams showing injections of NAPol and A8-35 onto RANTES-Strep surface.
Injections: (a) NAPols, (b) A8-35 over RANTES-Strep surface.

For better evaluation of amphipols interaction with RANTES-Strep the final responses were

plotted in a histogram representation (Figure 11.28).

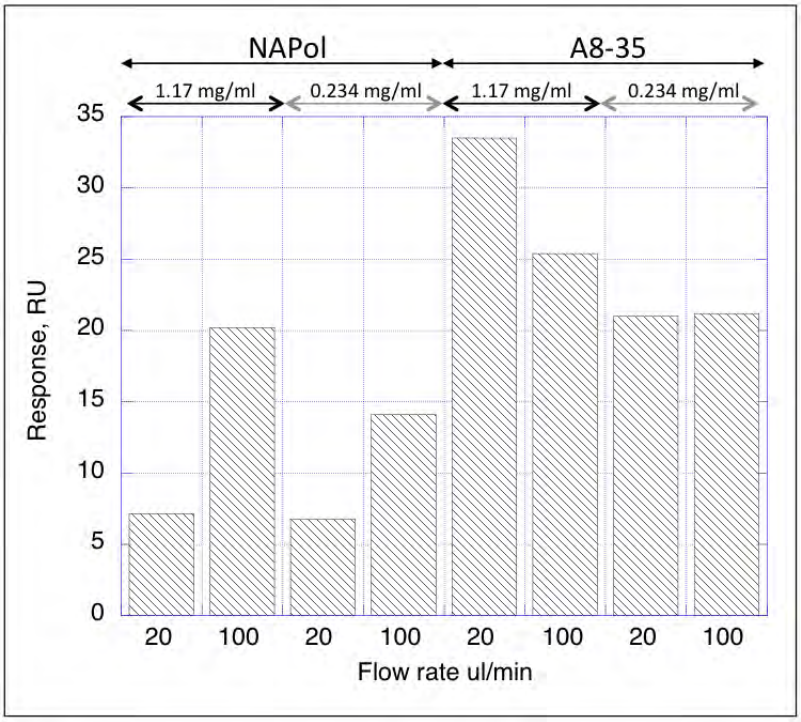

Figure 11.28.: Histograms representing NAPol and A8-35 interaction with RANTES-Strep surface.

Non-specific NAPol interaction with RANTES-Strep is lower when the flow rate is 20 µl/min and that was the flow rate used for CCR5 interaction test. There was no significant difference of concentration of NAPol used at the flow rate 20 µl/min. At high flow rate (100 µl/min) the lower non-specific interaction was observed when the NAPol was injected at smaller concentration (0.234 mg/ml). Using high NAPol concentration at the high flow rate increased non-specific interaction with RANTES-Strep. Therefore, NAPol non-specific interaction to RANTES-Strep is sensitive to the flow rate; at the low flow rate non-specific interaction was reduced. A8-35 non-specific interaction with RANTES-Strep was similar at lower concentrations independent to the flow rate. Whereas using high concentration of A8-35 a higher flow rate (100 µl/min) led to slightly lower non-specific interaction comparing to low flow rate (20 µl/min).

Globally, the amphipol interaction with RANTES-Strep is rather low and non-specific NAPol interaction to RANTES-Strep is lower than with A8-35.

11.2.4. CCR5 immobilization on a SA sensor chip

We also tested the functionalization of a surface via the biotin moiety of CCR5 refolded in BAPol on a SA sensor chip (Figure 11.29).

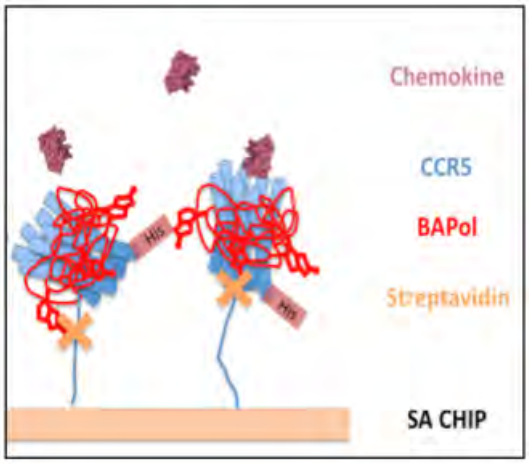

Figure 11.29.: Schematic representation of CCR5/BAPol immobilization on SA sensor chip.

When this experiment was performed we only had access to the Strep tagged version of RANTES and could not investigate ligand binding to the receptor surface.

SA sensor chip with pre-immobilized Streptavidin was used for the capture of CCR5 folded in BAPols. The Fc2 of the SA sensor chip was functionalized with CCR5/BAPol/L mixture at 60 µg/ml concentration up to 818 RU (Figure 11.30).

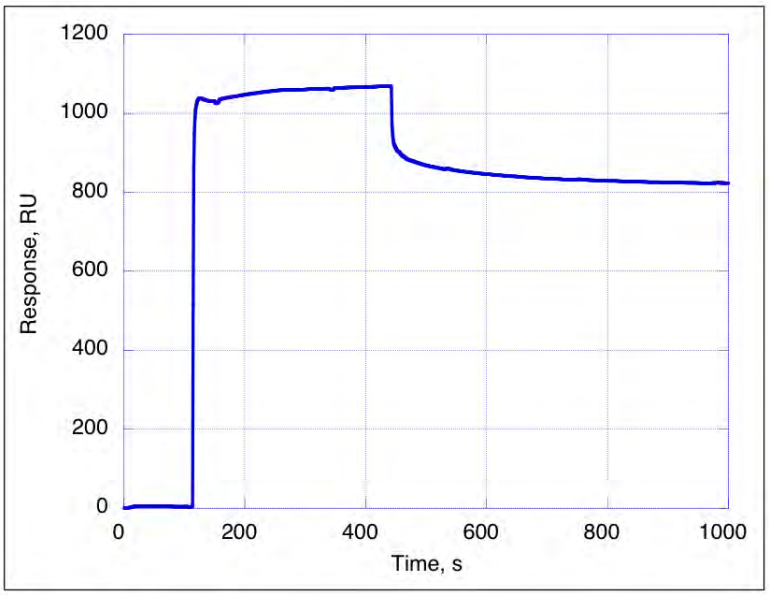

Figure 11.30.: Normalized sensorgram showing CCR5/BAPol/L functionalization on SA sensor chip.

It was observed that this CCR5/BAPol/L prepared surface was stabilizing quite fast and did not display any leaking. At this time, we decided to prepare RANTES without any tag to be able to test its binding to this surface.

11.2.5. CCR5 surface stability

With all available tools the surface stability during SPR experiments was evaluated.

Three different surfaces were prepared and their schematic representation is shown in Figure 11.31.

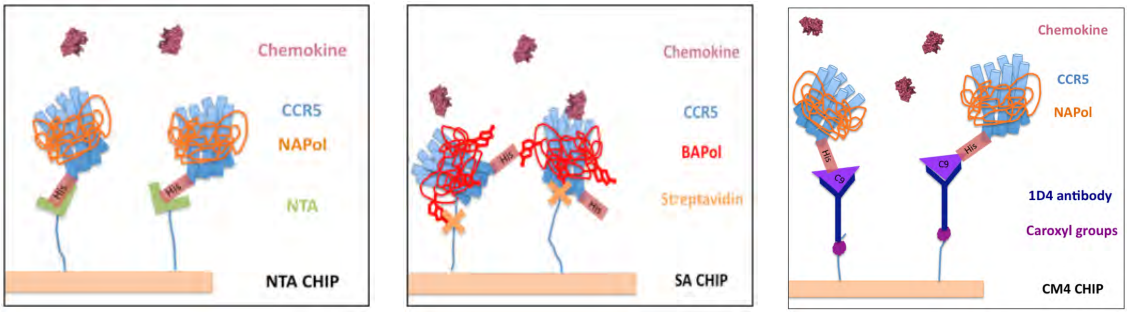

(a) NTA Sensor Chip (b) SA Sensor Chip (c) CM4 Sensor Chip

Figure 11.31.: Schematic representation of the different surfaces prepared for SPR experiments.

The stability of three different surfaces was evaluated by measuring: the amount (in RU) of captured receptor, the slope over the 100 seconds and after 900 seconds from the receptor injection and by calculating the percentage of captured receptor dissociation per second (Table 11.3).

Immobilization	**Amphipols**	**slope**	**Bound receptor RU**	**% of captured ligand dissociation per second**
His tag	CCR5/NAPol	-0,793	897	-0,08
Biotin moiety of BAPol	CCR5/BAPol	-0,161	858	-0,02
via C9 tag	CCR5/NAPol	-0,303	900	-0,03

Table 11.3.: Three different surface stability comparison.

From the calculated values it appeared that a maximal stability was achieved with a CCR5/BAPol surface on the SA sensor chip and was very close to the values observed with functionalization of CCR5/NAPol on the CM4 sensor chip. As observed earlier CCR5/NAPol on the NTA sensor chip was the least stable. Nevertheless we were able to capture similar amount of the receptor onto all surfaces.

12. Résumé des résultats en français

12.1. Production de chimiokines

La première partie des résultats décrira l'ingénierie des différentes versions de deux ligands des co-récepteurs du VIH, RANTES (pour CCR5) et SDF1α (pour CXCR4). Ces chimiokines recombinantes constituent des outils essentiels afin d'évaluer la fonctionnalité du récepteur repliée et par la suite seront utilisées pour étudier les complexes récepteur/ligand. Les chimiokines disponibles dans le commerce sont très chères, la production recombinante a été réalisée dans *E. coli*. Nous avons profité d'une approche d'expression recombinant pour introduire des étiquettes différentes avec des objectifs divers. Plusieurs modifications ont été introduites à l'extrémité C-terminal telles que des étiquettes Strep, His et un site de liaison des Lanthanides. L'étiquette Strep a été introduite afin de à constituer une chromatographie d'affinité. L'étiquette « Lanthanide » a été introduite pour des expériences de luminescence. Afin de mettre en place des protocoles de production de chimiokines les stratégies déjà publiées dans la littérature ont été examinées. Deux approches différentes ont été envisagées.

La première méthode consistait à fusionner la protéine liant le maltose (MBP) à la partie N-terminale des chimiokines [361]. Il a été démontré que la fusion MBP améliore la solubilité des protéines, un repliement approprié, une purification globale via une chromatographie d'affinité et qu'elle protège de la protéolyse [363, 362, 361]. Selon les auteurs cette stratégie de fusion a entraîné de haut rendement d'expression des chimiokines fonctionnelles. Il a été indiqué que l'aide d'un système de double fusion comprenant une étiquette et une fusion avec la MBP augmentait la pureté des chimiokines. Les activités de liaison des chimiokines recombinantes, MBP-RANTES et MBP-SDF1α, à leur récepteur a été confirmée par cytométrie en flux en utilisant des cellules exprimant des récepteurs CCR5 et CXCR4 sur leur surface [361].

La deuxième approche a consisté en la production de chimiokines dans les corps d'inclusion chez *E. coli* [364]. Cette méthode exige la lyse des cellules et l'isolement des corps d'inclusion suivie de la solubilisation des protéines et de leur renaturation.

Au début de ma thèse la première approche semblait plus prometteuse puisque des chimiokines fonctionnelles étaient directement produites, en évitant l'étape délicate de repliement. Par conséquent, les chimiokines ont d'abord été produites en utilisant cette stratégie.

Les chimiokines RANTES et SDF1α ont été commandées sous forme de gènes synthétiques, où tous les nucléotides ont été optimisés pour l'expression dans *E. coli*. La construction de la chimiokine contenait plusieurs éléments. Un site de clivage par le facteur Xa (Xa) permet le clivage de la MBP de la chimiokine. Les chimiokines ont également une étiquette Strep à leur extrémité C-terminale (Strep), ceci facilite l'étape de purification et permettra la création ultérieure d'une colonne d'affinité. Nous avons ajouté l'étiquette de fixation des Lanthanides (LT) à l'une des constructions. Cette étiquette spécifique lie le terbium (Tb). Le but de cette étiquette était de faciliter le suivi de la chimiokine par fluorescence et aussi de résoudre une future structure du complexe entre la chimiokine et le récepteur.

Nous avons cloné les chimiokines SDF1α et SDF1α-LT afin d'étudier l'interaction avec le récepteur CXCR4 et les chimiokines RANTES et RANTES-LT pour l'interaction avec le récepteur CCR5. Toutes les constructions ont été vérifiées par séquençage.

Plusieurs purifications des chimiokines ont été réalisées et il a été conclu que des optimisations étaient nécessaires pour améliorer la purification. Tout d'abord le facteur Xa clivait de manière non spécifique et imprévisible la protéine donc nous avons dû changer le site de clivage par celui de la protéase PreScission.

Finalement nous avons été confrontés à de nombreux problèmes avec fusion à la MBP. Après clivage de la MBP des étapes de purification supplémentaires ont été nécessaires afin d'éliminer la protéine de fusion. Le clivage était incomplet, les contaminations de l'échantillon par MBP étaient toujours présentes et les protéines agrégeaient.

La production de chimiokines avec la fusion MBP a été remplacée par une expression dans les corps d'inclusion d' *E. coli* [364]. Les premières constructions essayées ont été SDF1α-His et SDF1α-LT-His. Après optimisation des protocoles d'expression, la purification de 3 mg de SDF1α-LT-His a été obtenue à partir de un litre de culture bactérienne. La production de SDF1α-His a était plus efficace et environ 7.8 mg de SDF1α-His ont été obtenus par litre de culture bactérienne.

Des constructions similaires ont été produites avec une étiquette Strep C-terminale pour la production ultérieur d'une colonne d'affinité pour les récepteurs de chimiokines. Étonnamment ce changement d'étiquette d'affinité a considérablement réduit le rendement de la production de chimiokines, en particulier pour les constructions sans étiquette LT que pour RANTES-Strep et SDF1α-Strep, 0.2 mg ont été obtenus par litre de culture bactérienne pour deux chimiokines.

Pour évaluer la fonctionnalité de ces chimiokines, des expériences de contrôle ont été effectuées. Pour la caractérisation structurale (uniquement la formation de ponts disulfures a été évaluée) une analyse par spectrométrie de masse a été réalisée utilisés. Pour chacune des constructions, deux conditions ont été testées, l'une sans DTT (agent réducteur) et une avec DTT. L'augmentation de la masse de 4 Dalton dans l'échantillon avec DTT a confirmé la formation de deux ponts disulfure caractéristiques de cette famille de chimiokines.

Il est connu que les modifications sur la partie N-terminale des chimiokines affectent considérablement l'interaction avec leur récepteur. Rien n'a été jusqu'ici signalé pour des modifications en C-terminales. Afin de caractériser la liaison au récepteur et la transduction du signal déclenché par les chimiokines recombinantes une méthode originale de double électrode (Two-Electrode Voltage Clamp (TEVC)) a été utilisée. Les récepteurs de chimiokines et des canaux potassiques activés par les protéines G ont été co-exprimés dans des ovocytes de Xenope. La liaison du ligand au récepteur de chimiokine provoque l'activation des protéines G qui aurait une incidence sur l'ouverture du canal ionique. Des mesure en temps réel de l'activation des canaux ioniques permet l'évaluation de l'activité biologique des chimiokines à la fois quantitativement et qualitativement.

Pour cette expérience des ovocytes de Xenope ont été transfectés avec deux ARNs: le GPCR (CXCR4) et Kir3.1* un canal potassique activé par les protéines G. Les chimiokines SDF1α-His et SDF1α-LT-His ont été testées. Lors de la liaison des chimiokines à CXCR4 les protéines G ont été activées qui ont agi sur les canaux Kir3.1*. Avec cette expérience, nous démontrons la capacité de notre chimiokines modifiées en C-terminale à lier leurs récepteurs et à déclencher la signalisation via les protéines G.

Il a été observé que la présence de l'étiquette LT augmente la dissociation de SDF1α-LT-His (activation est réversible) de son récepteur, tandis que la présence de l'étiquette LT pour RANTES-Strep aboli la réversibilité et considérablement diminue l'efficacité de la chimiokine. À cette étape, nous pouvons conclure que la partie C-terminale de la chimiokine peut accueillir des modifications sans abroger la liaison au récepteur. Cependant, la combinaison des étiquettes, His ou Strep avec le LT, a un effet de « réglage » subtil sur l'affinité, l'efficacité, et la réversibilité de liaison au récepteur.

Le troisième contrôle de la fonctionnalité chimiokine était un essai de chimiotactisme. Le chimiotactisme est le mouvement caractéristique des cellules le long d'un gradient de concentration chimique soit en direction soit loin du stimulus chimique. Ce mécanisme permet aux lymphocytes de se mouvoir selon un gradient de chimiokines. Pour cette expérience des cellules exprimant CXCR4 et CCR5 à leur membrane ont été utilisés. Des expériences ont été effectuées en utilisant la stratégie de la chambre de Boyden. Celle ci présente deux compartiments: le compartiment inférieur contient les chimiokines et le compartiment supérieur les cellules. La membrane filtrante sépare les deux compartiments, les cellules peuvent passer au travers. Dans le compartiment inférieur différentes concentrations de la chimiokine ont été ajoutés, tandis que dans le compartiment supérieur du même concentration de cellules a été maintenue. Après incubation, la quantité de cellules dans le compartiment inférieur a été déterminée. Les résultats ont montré que les chimiokines SDF1α-His, SDF1α-Strep, RANTES-Strep induisent un chimiotactisme. Pour les chimiokines portant l'étiquette LT les résultats étaient différents, SDF1α-LT-His a montré une baisse d'activité par rapport aux autres chimiokines, le chimiotactisme était douteux dans le cas de SDF1α-LT-Strep et il était assez clair que RANTES-LT-Strep n'est pas actif.

Les chimiokines repliées étaient fonctionnelless et adaptées pour les essais de liaison aux récepteurs. L'étiquette lanthanide supplémentaire permet d'améliorer les niveaux d'expression des

chimiokines et de la solubilité des protéines. Toutefois, la présence de l'étiquette LT perturbe le chimiotactisme: certaines chimiokines portant une étiquette LT étaient moins efficaces et certaines n'ont pas induit du tout la migration des cellules. Néanmoins, les chimiokines portant l'étiquette LT étaient capables de se lier à leur récepteur et de transduire un signal comme il a été indiqué par la méthode TEVC.

12.2. La production des récepteurs

Nous avons exprimé le récepteur CCR5 fusionné au domaine extracellulaire d'une sous-unité de l'integine α5β1 dans les corps d'inclusion de *E. coli*, comme décrit précédemment [104]. La stratégie est basée sur l'accumulation des complexes protéine fusion/RCPG dans les corps inclusion, leur purification suivi d'un repliement in vitro. Pour cibler les protéines recombinantes vers les corps d'inclusion de E. coli la combinaison de charge et de résidus formant des β-tour sont critiques et doivent correspondre à une fraction élevée de la séquence protéique. C'est sur ces paramètres physico-chimiques qu'un fragment du domaine extracellulaire de β-hélice de l'intégrine humaine α5 (α5I) a été choisi [104].

Les corps d'inclusion ont été recueillis après lyse des cellules en utilisant un microfluidiseur. Après de longs lavages les culots ont été solubilisés dans un tampon contenant de l'urée. L'étiquette His à l'extrémité C-terminale des co-récepteurs a permis la purification des protéines sur une résine Ni-NTA en conditions dénaturantes. Nous avons obtenu plusieurs mg de protéine de fusion à partir d'un litre de culture bactérienne. La dialyse et digestion par la thrombine ont été réalisées pour éliminer la protéine de fusion. Le co-récepteur a ensuite été sélectivement purifié sur résine Ni-NTA.

L'expression de récepteur CXCR4 a été plus compliquée que CCR5. Même la fusion avec le domaine extracellulaire d'une sous-unité de l'integine α5β1 n'était pas suffisante pour permettre l'expression. Nos collaborateurs J.-L. Banères et B. Mouillac (Montpellier) ont observé l'expression de CXCR4 pour une triple fusion formée du domaine extracellulaire de l' integine et d'un fragment du récepteur V2 de la vasopressine. Nous essayons actuellement de déterminer les meilleures conditions de culture en changeant les paramètres classiques tels que la température d'expression, ou les milieux.

La production du récepteur est la partie la plus difficile du projet. De nombreux problèmes ont été rencontrés lors des différentes étapes de l'expression et la purification. Résoudre ces problèmes a nécessité beaucoup de temps. Une fois que le récepteur a été exprimé et purifié le repliement a été réalisé. Cette étape est très délicate. De nombreux laboratoires rencontrent des problèmes pour obtenir des récepteurs repliés et fonctionnels. Une approche alternative au repliement en détergent a été entreprise grâce à notre collaborateur Jean-Luc Popot (IBPC, Paris) qui nous a fourni différents types d'amphipoles. Les amphipoles (APols) sont de courts polymères amphipatiques qui peuvent maintenir les protéines membranaires intégrales solubles

dans l'eau. Plusieurs types de d'APols ont été conçus, synthétisés et testés. Pour cette étude l'A8-35 a été utilisé, il s'agit du premier amphipole a avoir été validé, sa solubilité est due à la présence d'hydrates de carbone. Le second APol utilisé est à base de glucose, il s'agit d'un amphipole non ionique (NAPol). Une version biotinylé de l'A8-35, le BAPol a également été considéré.

Différentes conditions ont été testées pour le repliement. Pour évaluer ces conditions, le pourcentage de récepteurs solubles restant après la procédure de repliement a été estimé. Depuis les premiers essais il a été observé qu'une combinaison d'A8-35 et de lipides a permis à environ 61% de CCR5 de rester soluble (Figure 10.10). Les meilleures conditions de repliement ont été obtenues en présence d'une protéine dans ratio de poids de 1:10:1 protéines:NAPol:lipide, ces conditions maintiennent plus de 86% de l'échantillon soluble.

Une deuxième construction de CCR5 a été créé, un nouvelle épitope, l'étiquette C9, a été ajouté à l'extrémité C-terminale de la construction CCR5-His. L'étiquette C9 est une séquence hautement antigénique de neuf d'acides aminés de la rhodopsine bovine (TETSQVAPA), elle permet une détection par l'anticorps monoclonal anti-rhodopsine 1D4. Cette séquence a été ajoutée à la terminaison C-terminale de α5I-CCR5-His résultant en α5I-CCR5-His-C9.

L'étiquette supplémentaire C9 a considérablement amélioré la détection en Western blot en utilisant l'anticorps 1D4. Les rendements de production sont les suivants: 0.5 mg de CCR5-His et 2.2 mg de CCR5-His-C9 ont été obtenus à partir d'un litre de culture bactérienne. Le repliement de CCR5 en présence de trois amphipoles différentes, l'A8-35, l' amphipole non-ionique (NAPol) et la version de biotinylé de l'A8-35 (BAPol) ont été testés en présence ou non de lipides (Fig. 10.10). Les meilleures conditions de repliement ont été obtenus en présence d'NAPol dans un rapport massique 1:10:1 protéines: NAPol: lipide Cette condition maintient plus de 80% de CCR5 soluble.

12.3. Analyse de l'interaction CCR5 – RANTES par SPR

Pour tester la fonctionnalité de CCR5 des expériences de SPR ont été réalisées. Les échantillons de CCR5 replié en présence de lipides (L) et amphipoles: A8-35 (CCR5/A8-35/L), NAPol (CCR5/NAPol/L) et BAPol (CCR5/BAPol/L) ont été testés. Deux versions différentes de CCR5, CCR5-His et CCR5-His-C9, ont été utilisées. Trois approches de fonctionnalisation ont été considérées (Fig. 11.31). La présence de deux étiquettes C-terminales différentes sur CCR5 a permis soit une capture non covalente sur le biocapteur NTA via l'étiquette His soit une liaison sur la pice CM4 fonctionalisée avec l'anticorps 1D4 via l'étiquette C9. L'utilisation de l'amphipol biotinylé (BAPol) a également permis une autre méthode de capture non-covalente de capture sur un biocapteur SA. Avec tous ces outils, trois différentes surfaces de CCR5 ont été préparées pour des expériences de liaison de ligand en utilisant l'analyse SPR. Il a été montré que notre

récepteur produit est fonctionnel et peut lier spécifiquement son ligand - RANTES et n'interagit pas avec SDF1α (un ligand non spécifique) (Fig 11.24).

Pour évaluer la quantité de récepteur fonctionnel et d'obtenir le K_{D} , le titrage de RANTES-Strep a été effectué. L'affinité attendue pour l'interaction de RANTES avec CCR5 est de l'ordre de quelques nanomomolaire (0.2 à 6.2 nM) telle qu'énoncée dans la littérature [372]. Toutefois, CCR5 étant exprimé dans *E. coli*, les modifications post-traductionnelles qui peuvent contribuer à cette grande affinité ne sont pas présente. Par conséquent, une gamme de concentration de RANTES-Strep allant de 4 nM à 1000 nM a été choisie pour l'analyse. Bien que les données d'interaction aient été difficiles à analyser (en raison de la ligne de base instable), nous avons essayé d'extraire les paramètres cinétiques bruts pour l'interaction. Malgré la baisse de ligne de base, deux lots de données avec différentes concentrations de RANTES (111 nM et 333 nM) nous ont permis de calculer des paramètres cinétiques bruts pour l'interaction. Les K_{D} calculés, 53 nM et 63 nM, présentent 1 à 2 log de différence avec les valeurs publiées dans la littérature (0.2 à 6.2 nM) [372].

Le récepteur CCR5 a été produit et purifié dans les corps d'inclusion chez *E. coli*, son repliement a été évaluée en utilisant trois différents amphipoles: l'A8-35, le NAPol et le BAPol. La stabilité des trois différentes surfaces pour les mesures de SPR a été évaluée. A partir des valeurs calculées il est apparu qu'une stabilité maximale était obtenue avec une surface CCR5/BAPol sur la puce SA et était très proche des valeurs observées avec fonctionnalisation de CCR5/NAPol sur la puce CM4. Comme indiqué précédemment, la surface NTA fonctionnalisé avec CCR5 en NAPol était la moins stable. Néanmoins nous avons pu fixer les quantités similaires de récepteur sur toutes les surfaces.

Part IV.

Discussions, conclusions and future perspectives

13. Discussions, conclusions and future perspectives

13.1. State of the art at the beginning of my Ph.D.

Every single step while working with GPCRs is delicate. Indeed, their over-expression, purification, stabilization and crystallization are always difficult. Different expression systems have been tested for GPCR production such as *Escherichia coli* (*E. coli*) [117], *Saccharomyces cerevisiae* (*S. cerevisiae*), *Pichia pastoris* (*P. pastoris*) [115, 377], insect cells [378], mammalian cell lines [379], as well as expression in photoreceptor cells of *Drosophila* [380], *Xenopus* [381], mouse [382] and cell free synthesis [383]. Most of the GPCRs for which structure has been solved were produced in insect cells expression system. In every case, variety of different protein modifications were required, their sequences were often heavily engineered and most of them contained a T4L fusion. Besides insect cell expression is an expensive system and is not affordable for many laboratories. Moreover, the quantities of produced receptors are limited. Therefore, the development of alternative strategies for functional GPCR production in large amounts is still of great interest.

Our team has been part of a network funded by the ANRS that undertook the survey of a large panel of recombinant over-expression systems (*E. coli*, *H. polymorpha*, insect cells, mammalian cells). However, after three years of investigations all the approaches were abandoned except for the *E. coli* expression system. In contrary to the expensive eukaryotic expression system, *E. coli* can be an interesting alternative for GPCR expression. This system is inexpensive and affordable for many laboratories. Attempts to express GPCR in *E. coli* inner membrane generally led to high toxicity and limited expression. An alternative approach consists in GPCR expression as insoluble inclusion bodies (IBs) that accumulates in the *E. coli* cytoplasm. This strategy presents several advantages: IB expression is not toxic; it allows high expression levels and enable a first step of purification. Therefore, targeting GPCRs to IBs via a protein fusion strategy has been considered.

In the laboratory different N-terminal fusions have been tested, such as GST, the carbohydrate-binding domain of a Lectin (DC-SIGN), which was highly expressed in *E. coli* inclusion bodies. These strategies did not trigger a huge GPCR expression improvement (only a slight enhancement was observed with the Lectin fusion). Collaboration with Jean-Louis Banères (Institut des Biomolécules Max Mousseron (IBMM), Montpellier) and Bernard Mouillac (Institut

de Génomique Fonctionnelle, Montpellier) was established and they have developed a rather generic fusion strategy with an α5 Integrin fragment to target GPCR expression towards IBs. This approach initially developed with BLT1 receptor was further applied to serotonin receptor [384, 104, 385, 342, 386]. More recently this strategy was extended to several other GPCRs including: the catecholamine β3AR, the hormone arginine-vasopressin V2 receptor, oxytocin (OT) receptor (OTR), the chemokine-like ChemR23 receptor, the cannabinoid CB1 receptor, the bioactive lipid leukotriene BLT2, CysLT1 and CysLT2 receptors [104]. They have attempted the α5I fusion to CCR5 and CXCR4 but although the former was efficiently expressed, a double fusion with α5I and a fragment of vasopressin receptor for CXCR4 receptor was necessary to enable CXCR4 expression. The GPCR genes were optimized for *E. coli* expression system to circumvent the limitation due to rare codons. The fusion protein was recovered from the inclusion bodies under denaturing conditions, i.e. in the presence of Urea, and purified by immobilized metal affinity chromatography on a Ni^{2+} -NTA column. The fusion constructs contained a C-terminal His tag, which facilitates purification in denaturing conditions. Once the fusion partner was cleaved off, the GPCR was re-purified. Then the GPCR was available for further folding approaches.

Preliminary tests were performed by Jean-Louis Banères and clearly indicated a folding far more efficient in amphipols than in detergents. Therefore amphipol assisted folding was considered. Development along these methods have been started in the group in the context of an ANR contract (coordinated by J.-L. Popot) and of FP7, Marie Curie, Initial Training Network, SBMP, supporting me for my Ph.D. studies.

The use of amphipols presents many potential advantages. Amphipols do not compete with protein-protein interaction, they do not disrupt protein complexes allowing them to be in the required stoichiometry [328, 313]. The protein/amphipol complex could easily accommodate lipids, and co-factors, which could be necessary for protein stabilization and/or activation. To validate the receptor folding strategy in amphipols we need to set up a molecular interaction test using both folded receptor and its ligand – chemokine.

In order to be able to access the functionality of the folded receptors, their ligands were required. Therefore a "home made" chemokine production needed to be established. At this stage I joined the project and I was in charge of a chemokine production strategy set up. This allowed us to produce "functionalized" chemokines carrying different tags such as His tag, Strep tag or Lanthanoid binding tag (LT), which could be used for different applications such as affinity purification, anchorage on solid support or chemokine visualization.

13.2. Chemokine production and functional validation

13.2.1. Achievements

In order to set up a chemokine production strategy, protocols already published in the literature were examined. Two different approaches were considered. The first method was based on fusing the Maltose Binding Protein (MBP) to the N-terminal part of chemokines [361]. The second method consisted in chemokine production in *E. coli* inclusion bodies [364]. Having already to produce the receptor in *E. coli* inclusion bodies we initially wanted to avoid the refolding step for the chemokine production, therefore, the MBP fusion strategy was attempted first.

Unfortunately many problems were faced with the fused MBP constructs. First of all, the Factor Xa protease was not specific. Additional search for other suitable proteases was performed. After the MBP cleavage, extra purification steps were necessary to remove the cleaved fusion protein. The MBP itself was highly contaminating following purifications and it was not always easy to eliminate it. Nevertheless, after MBP cleavage chemokines precipitated and only the ones with the LT remained soluble. The additional LT unpredictably improved chemokine expression and solubility. That was probably due to its charges; chemokines are basic proteins (pI around 9) and the additional LT shifted the pI below 7. Using the MBP fusion strategy we could obtain very little amounts of proteins, though they were not able to induce chemotaxis. Consequently, the chemokine production strategy was changed.

The second approach consisted in chemokine production in *E. coli* inclusion bodies [364]. First, two SDF1α versions, SDF1α-His and SDF1α-LT-His, were produced. The correct folding was confirmed by the presence of two disulfide bridges revealed by Mass Spectroscopy analysis. Functional activity was confirmed by chemotaxis assay. Receptor binding and signaling was assessed using an electrophysiology recording strategy. Using the Two-Electrode Voltage Clamp method, ligand binding to the chemokine receptor was recorded in real-time by measuring ion channel activation (Figure 13.1).

From that point, other chemokine constructs were designed. Considering the advantages in the production steps of the additional Lanthanoid Binding Tag, all chemokine versions were produced with and without the LT resulting in: SDF1α-Strep, SDF1α-LT-Strep, RANTES-Strep, RANTES-LT-Strep. The additional LT drastically changed the chemokine properties. Their pI, very basic (RANTES-Strep – 9.00; SDF1α-Strep – 9.7) was changed with the LT addition (RANTES-LT-Strep – 4.81; SDF1α-LT-Strep – 5.89). As before, the LT tremendously increased chemokine expression and solubility levels. Differences were observed in SDF1α production for the various affinity tag addition: His tagged chemokines were produced with higher yield than Strep tagged chemokine, that might be due to the tryptophan present in the Strep tag, as tryptophan, due to its amphipathy, is more sensitive during the protein folding procedure. The functionality of the new produced chemokines was equally assessed. Electrophysiology recording data enabled

to follow receptor binding and signal transduction, demonstrated that the addition of His or Strep tag on the C-terminus of chemokines did not alter their ability to activate $G_{i/o}$ proteins via their receptors. These observations validate our initial approach to functionalize chemokines via their C-terminus. However, the combination of tags, His or Strep with the LT, had some "tuning" effect on chemokine affinity to their receptor, efficiency, and binding reversibility.

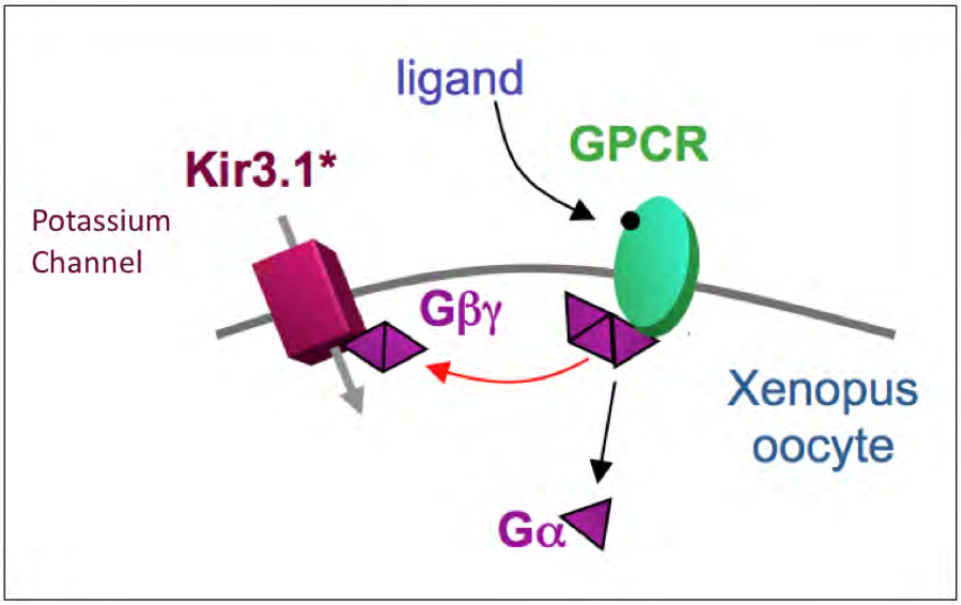

Figure 13.1.: Schematic representation of channel gating through G proteins. Upon binding of its ligand at an extracellular site, a transmembrane GPCR adopts a new conformation that triggers gating changes of Kir 3.1* channel through intracellular G-protein activation reporting GPCR ligand binding. Figure adapted from [387].

Overall, chemokine production from *E. coli* inclusion bodies was satisfactory. Refolded chemokines were functional and suitable for the receptor binding assays. The additional LT improved chemokine expression levels and protein solubility. However, the presence of LT disturbed the chemotaxis assay: some chemokines bearing a LT were less efficient and some were not inducing cell migration at all. Chemokines bearing LT were able to bind their receptor. Up to this stage, all tests in electrophysiology were performed where LT was not loaded with terbium. Although, the chemokine production was not the main goal of my thesis, one year and a half were necessary to establish functional chemokine production strategy.

13.2.2. Perspectives

Chemokine production strategy being set up now, different chemokine mutants that are unable to oligomerize or cannot interact with heparan sulfate could be produced and characterized using the various tests that were set up or available in the institute: electrophysiology recordings and chemotaxis assay.

The introduced Lanthanoid Binding Tag could introduce some fluorescent properties usable for the study of receptor-ligand interaction. Recently the use of lanthanoids was highlighted in a study where the ligands of GPCRs were labeled with lanthanoids and were used to study their receptor dimer/oligomeric nature in live cells using time-resolved FRET strategy [369]. In addition, the production of functionalized chemokines would open the way to useful techniques such as affinity chromatography, pull-down experiments or SPR measurements.

Finally, we have also developed a functional expression system, in collaboration with M. Vivaudou group, that will enable us to perform structure/function studies [387]. This system is based on ion channels heterologously expressed in Xenopus oocytes. The Kir6.2, inward rectifier potassium channel is not regulated by G proteins, but has the particularity to be regulated by another membrane protein SUR (Sulfonylurea receptor). Inspired by this rather unique design, our collaborators C. Moreau and M. Vivaudou (Grenoble, IBS) postulated that, if SUR could be replaced by another receptor such as a G-protein-coupled receptor (GPCR), an ion channel sensitive to GPCR ligands could be created and utilized to convert chemical information into a direct electrical signal (Figure 13.2) [387]. They created an Ion-Channel-Coupled Receptor (ICCR) between a GPCR and Kir6.2 channel. Upon binding of its ligand at an extracellular site, a transmembrane GPCR adopts a new conformation that triggers gating changes of the fused Kir6.2 reporting GPCR ligand binding. The strategy was validated using muscarinic M2 receptor and later on applied to dopaminergic D2 receptors. To create functional ICCRs with CXCR4 and CCR5 we are actually trying to determine the optimal linker sequence between those two components since the communication between the GPCR and the ion channel has to be optimal for each new construct.

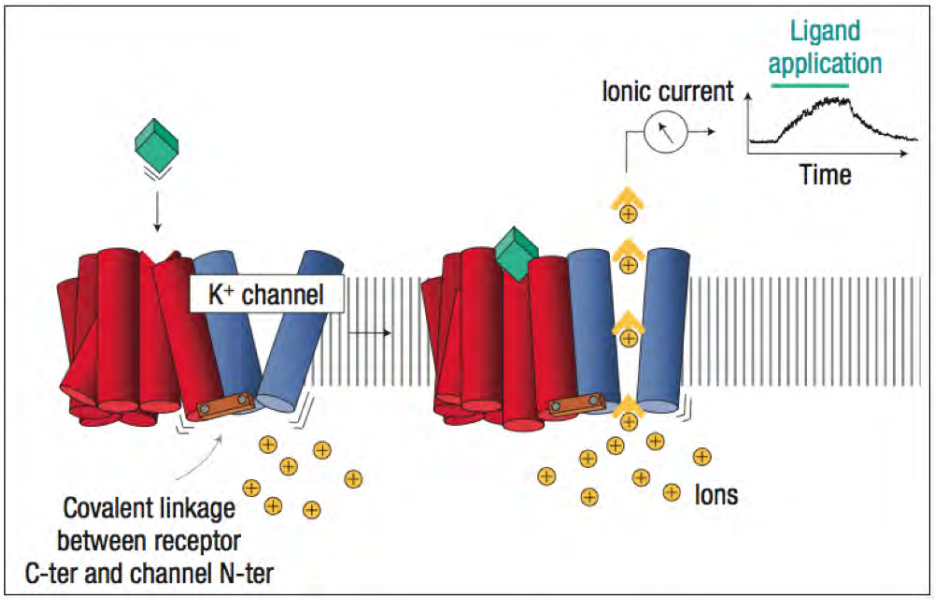

Figure 13.2.: Schematic representation of ion-channel-coupled receptors (ICCR) principle. In an ICCR, the GPCR is mechanically coupled to an ion channel. When the GPCR binds a ligand and changes conformation, this change is directly transmitted to the channel and results in a change in channel gating and in the ionic current of the channel. Figure adapted from [387].

This strategy opens the ways to the study of structure/function relationship as the consequences of sequence modification could be directly evaluated in term of signal transduction. This could be of great interest to determine modified functional form favorable to crystallogenesis.

13.3. Receptor production

13.3.1. Achievements

Before my arrival, CCR5 production strategy had been developed and CCR5 folding had been carried out in A8-35. The functionality of the amphipol folded receptor had to be assessed. Gel Filtration experiments were set up on one hand, with CCR5 folded in A8-35 and on the other, with CCR5 folded in A8-35 and in complex with some chemically produced fluorescently labeled chemokines. Unfortunately, although a clear co-elution of the GPCR and the chemokine was observed, the possibility of a non-specific interaction between the hydrophobic and cationic chemokine and the charged A8-35 could not be ruled out, as it was also observed that the fluorescently labeled chemokine was co-eluting with free amphipol. Therefore, the uncharged NAPol appeared at this point as a promising alternative to carry out the receptor folding. At this step I joined the group.

Handling membrane proteins is never an easy task. Even thought the expression strategy was established earlier, it was not always working as expected. First of all, it was not always reproducible. The level of expressed protein was varying from nothing to moderate levels. The problems in Western Blots with anti-His antibody complicated the detection. At that time, a new epitope, the C9 tag, was added to the C-terminus of the CCR5-His constructs. Fortunately, the additional C9 tag improved the protein detection in Western Blotting using 1D4 antibody, which was shown to be more specific and more reliable than the anti-His antibody. From this point improvement of the receptor production has been possible, we have now access to a satisfactory level of receptor produced in a reproducible way.

Once the receptor was produced and purified, its folding was tested. Receptor folding was assessed using three different amphipols: A8-35, NAPol and BAPol. It was shown that the mix of lipids and amphipols improved CCR5 solubility and stability.

In vitro synthesis of CCR5 and CXCR4 was also attempted. Not all prepared constructs were equally expressed.

13.3.2. Perspectives

The purification of the CXCR4 still needs to be optimized, the conditions of the thrombin cleavage need to be determined and the receptor purification should be undertaken. Subsequently, CXCR4 folding strategies could be established with protocols similar to those applied to CCR5.

Now, that functional receptor and chemokine are available, their complex should be formed and characterized by several techniques including BN-PAGE gels, MALS (Multi Angle Light Scattering), Gel Filtration methods, analytical ultracentrifugation in order to assess its homogeneity and stoichiometry status. Having access to the purified GPCR would even allow the reconstitution of complexes with CD4-gp120 or with G proteins for future characterization at the molecular level.

The introduced Strep tag for the chemokine allows the subsequent creation of affinity column (Figure 13.3), where the chemokine bound to the Strep-Trap column could be use to trap the receptor correctly folded in amphipols.

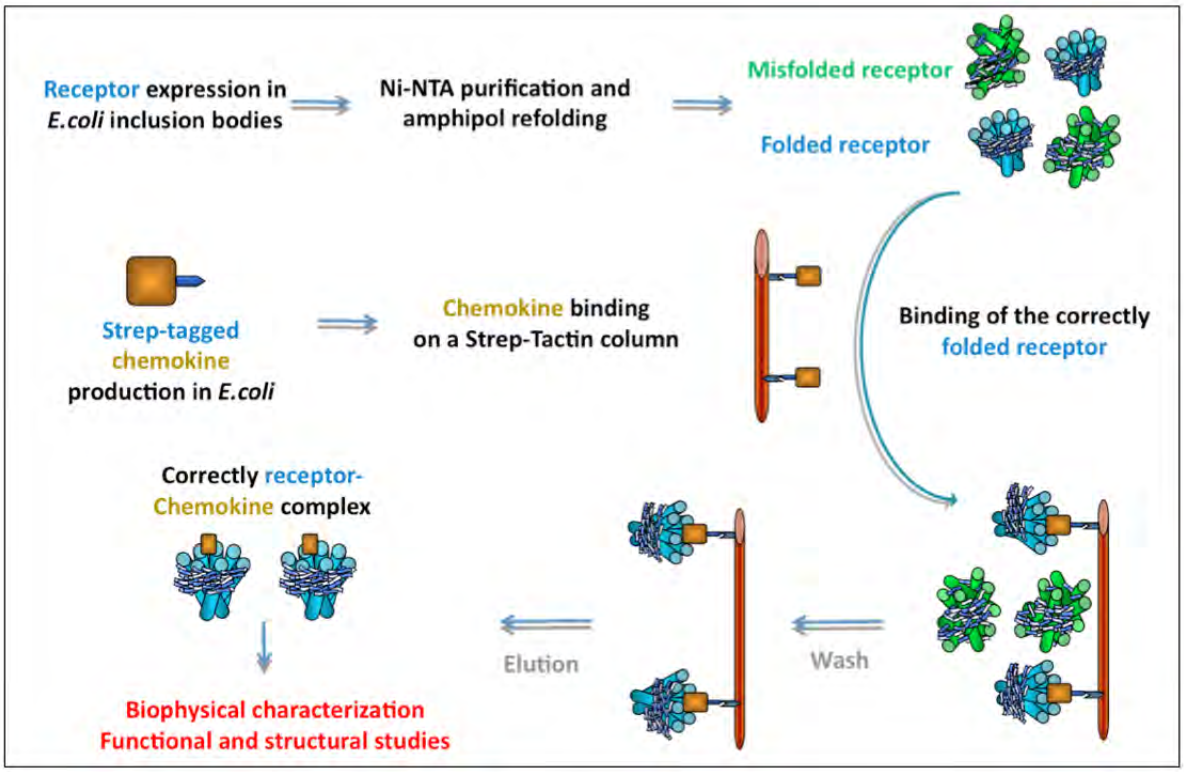

Figure 13.3.: Schematic representation of chemokine affinity column.

This experiment would allow us to estimate the folding yield of the receptor by ligand binding experiments. These tools will also be convenient and necessary to sort out correctly folded receptor molecules from the mix of functional and non-functional receptors that will result from the folding steps.

13.4. Surface Plasmon Resonance

13.4.1. Achievements

To evaluate the functionality of the produced CCR5, SPR experiments were performed. The advantage of using a receptor folded in amphipols for the SPR experiments is that there is no need to add the amphipols to all used buffers.

The presence of two different C-terminal tags on the CCR5 allowed a non-covalent capture on NTA sensor chip through the His tag and on 1D4 antibody functionalized CM4 sensor chip to capture receptor through the C9 tag. The use of biotinylated amphipol BAPol provides the means to use another strong non-covalent capture on SA sensor chip. With all these tools three different CCR5 surfaces were prepared for ligand binding experiments using SPR analysis.

Our first choice was to functionalize the NTA sensor chip with the CCR5 folded in NAPols through the C-terminal His tag. Using this approach, the receptor is orientated. However the baseline was not stable, which complicated the ligand binding assays. This is a common problem while working with His-tagged receptors on NTA sensor chips [376]. Nevertheless, it was clear that our produced receptor is functional and could specifically bind its ligand - RANTES and was not interacting with SDF1α (non specific ligand). Despite the dropping baseline, two data sets with different RANTES concentrations (111 nM and 333 nM) allowed us to calculate rough kinetic parameters for the interaction. Separate fitting of Langmuirian dissociation and association differential rate equations were performed. The calculated K_{D} values, 53 nM and 63 nM, were in 1 to 2 log difference comparing to what was published in the literature (0.2 - 6.2 nM) [372].

The N-terminus of CCR5, when produced in eucaryotic systems, undergoes post-translational modifications. In particular, the addition of sulfate groups to tyrosine 3, 10, 14 and 15 is required for high affinity interaction with its ligand [388]. Some studies have been shown, that lack of sulfation lowers the affinity between the receptor and its ligand [389]. Indeed, the difference we observe between our receptor and natural receptor (containing post-translational modifications) could be explained by this fact and is understandable.

To improve the baseline stability we used the strategy described by Navratilova and co-workers [372]. For this approach we used CM4 sensor chip where the 1D4-capturing antibody was immobilized on the carboxydextran matrix that coats the CM4 sensor chip surface. CCR5 expressed with a C-terminal C9 tag trapped in NAPol was captured. CCR5 specificity was confirmed using SDF1α as a negative control, which does not bind the receptor and RANTES, the specific ligand, interacting with the CCR5 surface. The calculated theoretical receptor maximal binding capacity was 49 RU and the obtained RANTES binding value was 52 RU. These two values are very close and it is possible to conclude that RANTES at used concentration (200 nM) is

monomeric. It is possible to extrapolate that RANTES interacts with its receptor as a 1:1 receptor:chemokine ratio. At this step it is also possible to estimate that most of the captured NAPOL folded receptor is functional.

The third CCR5 surface was prepared using SA sensor chips, where CCR5 folded in BAPols was immobilized via its biotin moiety. At that time, only RANTES-Strep was available so we could not perform ligand-binding assay. This experiment was only performed to test the surface baseline stability. From our observations and calculations, CCR5/BAPol surface on SA sensor chip was slightly more stable than the 1D4 functionalized CM4 surface.

Within the first SPR experiments, the difference between RANTES-Strep and RANTES-LT-Strep was observed in terms of oligomerization. It was observed that RANTES-LT-Strep binding response was close to the calculated possible maximal response for the prepared CCR5 surface, while RANTES-Strep clearly exceeds this value by more than 10 times suggesting a possible chemokine oligomerization. The impact of the C-terminal chemokine tag to the oligomerization effect could be better evaluated. Now, having a stable CCR5 surface concentration titrations could be performed and the affinity K_{D} could be calculated for each chemokine construct.

At this stage, further optimization of SPR surface, were required to better characterize the interactions. Unfortunately, at the end of my Ph.D. the access to NAPol (through J.-L. Popot lab) was limited by the difficulty of its chemical synthesis. Further development will have to wait the new campaign of NAPol synthesis.

13.4.2. Perspectives

With prepared stable CCR5 surface more accurate kinetic parameters could be calculated. The impact of the lacking sulfations on the N-terminal part of CCR5 could be better investigated.

The prepared CCR5/BAPol stable surface where anchorage occurs via the amphipol belt that surrounds the protein leaves both the extracellular and intracellular parts of the receptor available. Different complex reconstitution studies could now take place, ligand binding studies together with the G protein interaction or any other GPCR partner could be characterized in the future.

However, for future SPR experiments a control that could rule out the non-specific interaction between the chemokine and the amphipol is still required. Another GPCR folded in NAPol or BNAPol could be used to confirm that it does not interact with the chemokine.

14. Discussions, conclusions et perspectives en français

14.1. Etat de l'art au début de ma thèse de doctorat

Lorsque l'on travaille avec des RCPGs, chaque étape est délicate. En effet, leur surexpression, purification, stabilisation et cristallisation sont toujours difficiles. Différents systèmes d'expression ont été testés pour la production de RCPGs tels que *Escherichia coli* (*E. coli*) [117], *Saccharomyces cerevisiae* (*S. cerevisiae*), *Pichia pastoris* (*P. pastoris*) [115, 377], les cellules d'insectes [378], des lignées cellulaires de mammifères [379], ainsi que l'expression dans les cellules photoréceptrices de la drosophile [380], Xenopus [381], la souris [382] et la synthèse acellulaire [383]. La plupart des RCPGs dont la structure a été résolue ont été produites en cellules d'insecte. Dans tous les cas, des modifications des protéines ont été nécessaires, leur séquence ont été souvent fortement modifiées et la plupart d'entre elle contenait une fusion T4L. En outre l'expression en cellules d'insecte est un système coûteux et n'est pas abordable pour de nombreux laboratoires. De plus, les quantités de récepteurs produits sont limitées. Par conséquent, le développement de stratégies alternatives pour la production de RCPGs fonctionnels en grande quantité est encore d'un grand intérêt.

Notre équipe a fait partie d'un réseau financé par l'ANRS qui a testé un large panel de systèmes d'expression recombinante (*E. coli*, *H. polymorpha*, des cellules d'insectes, des cellules de mammifères) pour la production des RCPGs, CCR5 et CXCR4. Cependant, après trois ans d'investigations toutes les approches ont été abandonnées, sauf le système d'expression chez *E. coli*. Au contraire du coûteux système d'expression eucaryote, l'expression chez *E. coli* peut être une alternative intéressante pour l'expression des RCPGs. Les tentatives pour exprimer RCPG dans la membrane interne de *E. coli* conduisent généralement à une toxicité élevée et une expression limitée. Une approche alternative consiste en l'expression des RCPGs sous forme de corps d'inclusion qui s'accumulent dans le cytoplasme de E. coli. Cette stratégie présente plusieurs avantages: l'expression dans les corps d'inclusion n'est pas toxique, elle permet des niveaux d'expression élevés et constitue une première étape de purification. Par conséquent, le ciblage des RCPG dans les corps d'inclusion en utilisant une stratégie de protéine fusion a été pris en considération.

Différentes fusions N-terminales ont été testées, comme la GST, ou encore le domaine de fixation des sucres d'une lectine (DC-SIGN), qui dans le laboratoire s'exprimaient fortement sous

forme de corps d'inclusion. Ces stratégies n'ont pas permis de nette amélioration des quantité exprimées (seule une légère augmentation a été observée avec la fusion à la séquence de la lectine). Une collaboration avec Jean-Louis Banères (Institut des Biomolécules Max Mousseron (IBMM), Montpellier) et Bernard Mouillac (Institut de Génomique Fonctionnelle, Montpellier) a été établie. Nos collaborateurs ont développé une stratégie de fusion plutôt générique avec un fragment de l'ntégrine α5 permettant de cibler l'expression des RCPGs vers les corps d'inclusion. Cette approche initialement développée avec le récepteur BLT1 a également été appliquée au récepteur de la sérotonine [384, 104, 385, 342, 386]. Plus récemment, cette stratégie a été étendue à plusieurs autres RCPG, y compris: le récepteur β3 adrénergique, le récepteur V2 de la vasopressine récepteur, OTR le récepteur de l'ocytocine (OT), le récepteur cannabinoïde CB1, BLT2 le récepteur des leucotriènes [104]. Ils ont tenté la fusion α5I avec récepteurs CCR5 et CXCR4, mais bien que le premier ait été exprimé de manière efficace, une fusion double avec α5I et un fragment du récepteur de la vasopressine a été nécessaire pour permettre l'expression de CXCR4. Les gènes de CCR5 et CXCR4 ont été optimisés pour l'expression chez E. coli pour contourner la limitation due à la présence de codons rares. La protéine de fusion a été extraite des corps d'inclusion par des conditions dénaturantes, c'est à dire en présence d'urée, et purifiée par chromatographie d'affinité sur une colonne Ni^{2+}-NTA grâce à une étiquette polyhistidine présence à l'extrémité C-terminale de la protéine de fusion. Une fois le partenaire de fusion clivé, le RCPG a été re-purifié

Des tests préliminaires de repliement ont été réalisées par Jean-Louis Bañeres et ont clairement suggérés un repliement beaucoup plus efficace en amphipoles qu'en présence de détergents. Le développement de méthodes de repliement en amphipoles de RCPGs a été initiés dans le groupe dans le cadre d'un contrat ANR (coordonné par J.-L. Popot) et soutenu par le réseau de formation Marie Curie FP7, (SBMP), qui a financé mon doctorat focalisé sur le repliement de CCR5 et CXCR4.

L'utilisation d' amphipoles présente de nombreux avantages potentiels. Les amphipoles n'entrent pas en compétition avec les interactions protéine-protéine, ils ne perturbent pas les complexes protéiques leur permettant d'être dans la stoechiométrie nécessaire [328, 313]. Les complexes protéine/amphipole sont également succeptibles d'accueillir facilement des lipides, et des cofacteurs, qui pourraient être nécessaires à la stabilisation des protéines et/ou à leur activation. Afin de valider la fonctionalité des récepteurs repliés en amphipoles nous avions besoin de mettre en place un test d'interaction moléculaire entre le récepteur et son ligand naturel, la chimiokine.

Par conséquent, la production de chimiokines "faites maison" était nécessaire. À cette étape, j'ai rejoint le projet et j'ai eu en charge de mettre en place une stratégie de production de chimiokines. Nous avons profité de cette occasion pour produire des chimiokines "fonctionnalisées" c'est à dire qui portent différentes étiquettes, telles que une étiquette His, une étiquette Strep ou encore un site de fixation des lanthanide (LT), qui pourraient être utilisées pour différentes applications telles que la purification par affinité, l'ancrage sur un support solide ou la visualisation de la chimiokine.

14.2. La production de chimiokines et de validation de leur fonctionalité

14.2.1. Travaux accomplis

Afin de mettre en place une stratégie de production des chimiokines, des protocoles déjà publiés dans la littérature ont été examinés. Deux approches différentes ont été envisagées pour la production en *E. coli.* La première méthode était basée sur une fusion avec la protéine fixant le Maltose (MBP) en partie N-terminale des chimiokines [361]. La deuxième méthode a consisté en la production de chimiokines sous forme de corps d'inclusion [364]. Ne pouvant nous affranchir de la production des récepteurs en corps d'inclusion nous avons d'abord voulu éviter l'étape de repliement pour la production des chimiokines, par conséquent, la stratégie de fusion MBP a été tentée en premier lieu.

Malheureusement, de nombreux problèmes ont été rencontrés avec les constructions fusionnées à la MBP. Tout d'abord, la protéase (Facteur Xa) n'était pas spécifique. Une recherche supplémentaire afin d'identifier une protéase appropriée a été réalisée. Après le clivage de la MBP, des étapes de purification supplémentaires étaient nécessaires pour éliminer la protéine de fusion clivée. Cette étape s'est avérée assez compliquée, des contaminations par la MBP étaient observées. Néanmoins, après coupure de la MBP, les chimiokines précipitaient, seules celles qui portaient l'étiquette LT restaient solubles. De plus, nous avons observé que l'ajout de l'étiquette LT améliorait de manière de manière inattendue l'expression des chimiokines et leur solubilité. Ceci était probablement dû aux charges portées par cette étiquette; les chimiokines sont des protéines basiques (pI d'environ 9) et le LT supplémentaire déplace leur pI en dessous de 7. Au final, la stratégie de fusion avec la MBP nous a permis d'obtenir de petites quantités de protéines, qui n'étaient pas capables d'induire de chimiotactisme. En conséquence, la stratégie de la production des chimiokines a été changée.

La deuxième approche a consisté en la production de chimiokines dans *E. coli* sous forme de corps d'inclusion [364]. Tout d'abord, deux versions de SDF1α ont été produites: SDF1α-His et SDF1α-LT-His. Leur repliement correct a été confirmé par la présence de deux ponts disulfures révélés par l'analyse en spectroscopie de masse. Leur activité a, quant à elle, été confirmée d'une part par un test de chimiotactisme et d'autre par en étudiant la liaison au récepteur et la signalisation à l'aide d'une stratégie d'enregistrement d'électrophysiologique. En utilisant la méthode de double électrode, la fixation du ligand au récepteur de chimiokine a été enregistré en temps réel en mesurant l'activation des canaux ioniques (Figure 13.1).

A partir de là, d'autres constructions de chimiokine ont été conçues. Considérant les avantages dans les étapes de production de l'étiquette LT, toutes les versions de chimiokines ont été produites avec et sans le LT résultant en : SDF1α-Strep, SDF1α-LT-Strep, RANTES-Strep, RANTES-LT-Strep. L'étiquette LT supplémentaire a radicalement changé les propriétés des

chimiokines. Leur pI, très basique (RANTES-Strep – 9.00; SDF1α-Strep – 9.7) a été modifié avec l'ajout LT (RANTES-LT-Strep – 4.81; SDF1α-LT-Strep – 5.89). Comme auparavant, le LT a énormément augmenté l'expression des chimiokines et les taux de solubilité. Les différences ont été observées dans la production de SDF1α en fonction de l'étiquette d'affinité utilisée: les chimiokines marquées avec une étiquette Histidine ont été produites avec un rendement plus élevé que les chimiokines possédant une étiquette Strep. La fonctionnalité de ces nouvelles chimiokines a également été évaluée. L'enregistrement des données d'électrophysiologie ont permis de suivre la liaison au récepteur et transduction du signal, elles ont démontré que l'ajout des étiquettes His ou Strep du côté C-terminal des chimiokines ne modifie pas leur capacité à activer les protéines Gi/o via leurs récepteurs. Ces observations valident notre approche initiale consistant en fonctionnaliser les chimiokines par leur extrémité C-terminale. Cependant, nous avons observé que la combinaison des étiquettes, His ou Strep avec le LT, avait résultait en des modulations fine de l'affinité des chimiokines pour leur récepteur, sur leur efficacité, et sur la réversibilité de liaison.

Dans l'ensemble, la production de chimiokines en corps d'inclusion dans *E. coli* a été satisfaisante. Les chimiokines repliées étaient fonctionnelles et adaptées aux essais de liaison aux récepteurs. Bien que la production de chimiokines n'ait pas été le but principal de ma thèse, un an et demi ont été nécessaires pour mettre en place une stratégie production fonctionnelle.

14.2.2. Perspectives

Maintenant que la stratégie de production des chimiokines a été mise en place, différents mutants incapables d'oligomériser ou ne pouvant pas interagir avec les héparanes sulfate pourraient être produits et caractérisés à l'aide des différents tests disponibles: enregistrements électrophysiologiques et essai de chimiotactisme.

L'étiquette LT pourrait introduire certaines propriétés fluorescentes utilisables pour l'étude de l'interaction récepteur-ligand. Récemment, l'utilisation des lanthanides a été utilisés dans une étude où les ligands de RCPG ont été marqués avec des lanthanides et utilisés pour étudier la dimérisation des récepteurs dans des cellules vivantes en utilisant la stratégie de FRET en temps résolu [369]. De plus, la production de chimiokines fonctionnalisées ouvrent la voie à des expériences de précipitation ou des mesures de SPR.

Enfin, nous avons également développé un système d'expression fonctionnelle, en collaboration avec le group de M. Vivaudou, qui va nous permettre d'effectuer des études structure/fonction [387]. Ce système est basé l'expression hétérologue de canaux ioniques dans des ovocytes de Xenopus. Kir6.2, un canal potassique rectifiant entrant n'est pas régulé par des protéines G, mais a la particularité d'être régulé par SUR une autre protéine membranaire (récepteur des sulfonylurées). Inspiré par ce design assez unique, nos collaborateurs C. Moreau et M. Vivaudou (Grenoble, IBS) ont postulé que, si SUR pourrait être remplacé par un autre récepteur tel qu'un

GPCR, un canal ionique sensible aux ligands des RCPG pourrait être créé et utilisé pour convertir l'information chimique en un signal électrique direct (Figure 13.2) [387]. Ils ont créé un récepteur couplé aux canaux ioniques (ICCR) entre un RCPG et le canal Kir6.2. Lors de la liaison de son ligand sur un site extracellulaire, un RCPG transmembranaire adopte une conformation nouvelle qui déclenche des changements d'ouverture de la protéine Kir6.2 qui lui est fusionnée reportant ainsi la fixation du ligand sur le RCPG. La stratégie a été validée en utilisant des récepteurs muscariniques M2 et a plus tard été appliquée aux récepteurs dopaminergiques D2. Afin de créer des ICCR fonctionnels avec CXCR4 et CCR5 nous tentons de déterminer la séquence optimale de liaison entre ces deux composantes, puisque la communication entre le GPCR et le canal ionique doit être optimale pour chaque nouvelle construction.

Cette stratégie ouvre les voies à l'étude des relations structure/fonction puisque les conséquences des modifications de séquence peuvent être directement évaluées en terme de transduction du signal. Cela pourrait être d'un grand intérêt pour déterminer des constructions fonctionnelles modifiées favorables à la cristallogenèse.

14.3. La production des récepteurs

14.3.1. Travaux accomplis

Avant mon arrivée, la stratégie de production de CCR5 a été mise au point et le repliement a été réalisée en présence d'A8-35. La fonctionnalité du récepteur replié en amphipole devait être évaluée. Des expériences de filtration de gel avaient été mis en place, avec d'une part CCR5 replié en A8-35 et d'autre part avec CCR5 replié en A8-35 en complexe avec des chimiokines produites chimiquement et marquées par fluorescence. Malheureusement, même si une claire co-élution de la GPCR et la chimiokine a été observée, la possibilité d'une interaction non spécifique entre la chimiokine, hydrophobe et cationique, et l'A8-35 chargé ne pouvait pas être exclue, puisqu'il avait également été observé que la chimiokine fluorescente co-éluait avec l'amphipol libre. Par conséquent, le NAPol, amphipole non chargé est apparu à ce moment comme une alternative prometteuse pour effectuer le repliement des récepteurs. C'est cette étape que j'ai rejoint le groupe.

La manipulation de protéines membranaires n'est jamais une tâche facile. Bien que la stratégie d'expression ait été mise au point, la production n'était pas toujours satisfaisante. Tout d'abord le niveau d'expression variait de rien à des niveaux modérés. Les problèmes rencontrés avec la révélation par des anticorps anti-His en Western Blot ont compliqué la détection. A cette époque, un nouvelle épitope, l'étiquette C9, a été ajouté à l'extrémité C-terminale des constructions CCR5-His. Cette nouvelle étiquette a permis d'améliorer la détection de la protéine en Western blot grâce à l'utilisation de l'anticorps 1D4, qui s'est avéré beaucoup plus sensible et fiable que l'anticorps anti-His. A partir de là, la production de récepteur a pu être améliorées, nous avons maintenant accès à une production de récepteur satisfaisante et reproductible.

Une fois que le récepteur a été produit et purifié, son repliement a été testé. Le repliement des récepteurs a été évaluée en utilisant trois amphipols différents: l'A8-35, le NAPol et le BAPol. Il a été montré qu'un mélange de lipides et d'amphipoles améliore la solubilité et la stabilité de CCR5.

La synthèse in vitro de CCR5 et CXCR4 a également été tentée. Toutes les constructions ont été préparées et s'expriment de manière comparable.

14.3.2. Perspectives

La purification de CXCR4 doit encore être optimisée, les conditions de clivage par la thrombine doivent être déterminées et la purification du récepteur doit être entreprise. Par la suite, le protocole de repliement CXCR4 devra être établi avec des protocoles similaires à ceux utilisé pour CCR5.

Les récepteurs fonctionnels et les chimiokines étant disponibles, leur complexe peut maintenant être formé et caractériser par plusieurs techniques, gels BN-PAGE, MALS (Multi Angle Light Scattering), filtration sur gel, ultracentrifugation analytique afin d'en évaluer l'homogénéité et la stœchiométrie. L'accès au RCPG purifié pourrait également permettre la reconstitution de complexes avec CD4/gp120 ou avec des protéines G et leur caractérisation au niveau moléculaire.

L'étiquette Strep qui a été ajoutée à la chimiokine, permettra la création ultérieure d'une colonne d'affinité (Figure 13.3), La chimiokine liée à la colonne Strep-Trap pourra être utilisée pour piéger les récepteurs correctement repliés en amphipoles.

Cette expérience nous permettrait d'estimer le rendement de repliement du récepteur par des expériences de liaison de ligand. Ces outils seront également pratiques et nécessaires de séparer les récepteurs correctement repliés à partir mélange de récepteurs fonctionnels et non fonctionnels qui resulteront des étapes de repliement.

14.4. Resonance des plasmon de surface

14.4.1. Travaux accomplis

Afin d'évaluer la fonctionnalité du CCR5 produit, des expériences de SPR ont été réalisées. L'utilisation de récepteurs repliés en amphipole pour les expériences SPR présente l'avantage de ne pas avoir à ajouter d' amphipole tous les tampons utilisés.

Le premier choix a été de fonctionnaliser le biocapteur NTA avec CCR5 replié en NAPols via l'étiquette His C-terminale. En utilisant cette approche, le récepteur est orienté. Cependant la

ligne de base n'était pas stable, ce qui a compliqué les dosages de liaison au ligand. Il s'agit d'un problème courant lorsqu'on fixe des protéines avec des étiquettes His sur des biocapteurs NTA [376]. Néanmoins, il est clair que notre récepteur produit est fonctionnel, peut lier spécifiquement son ligand RANTES et n'a pas d'interaction avec SDF1α (ligand non spécifique).

L'extrémité N-terminale de CCR5, lorsqu'elle est produite dans des systèmes eucaryotes, comportent des modifications post-traductionnelles. En particulier, l'addition de sulfate sur les tyrosines 3, 10, 14 et 15 est requise pour une interaction de forte affinité avec le ligand [388]. Certaines études ont montré que le manque de sulfatation diminue l'affinité entre le récepteur et son ligand [389]. Les différences d'affinité pour le ligand que nous avons observé entre notre récepteur et le récepteur naturel (contenant des modifications post-traductionnelles) pourraient être expliquées par ce fait.

Afin d'améliorer la stabilité de la ligne de base, nous avons utilisé la stratégie décrite par Navratilova et ses collègues [372]. Pour cette approche, nous avons utilisé le biocapteur CM4 où l'anticorps 1D4 a été immobilisé sur la matrice de carboxydextran qui recouvre la surface. CCR5 possédant une extrémité C-terminale C9 replié en NAPOL a été capturé. La spécificité de CCR5 a été confirmée en utilisant SDF1α comme contrôle négatif (pas de liaison au récepteur), et RANTES, ligand spécifique, qui interagit avec la surface CCR5. La capacité maximale de liaison au récepteur théorique calculée était de 49 RU et la valeur obtenue pour la liaison de RANTES était de 52 RU. Ces deux valeurs sont très proches et il est possible de conclure que RANTES à la concentration utilisée (200 nM) est monomérique. Il est possible d'extrapoler que RANTES interagit avec son récepteur avec un ratio de 1:1. À cette étape, il est également possible d'estimer que la plupart des récepteurs capturés et repliés en NAPol sont fonctionnels.

La troisième surface de CCR5 a été préparé en utilisant des biocapteur SA, sur lesquels CCR5 replié en BAPols a été immobilisé par l'intermédiaire de son groupement biotine. A cette époque, seulement RANTES-Strep était disponible ainsi, nous ne pouvions pas effectuer de test de liaison de ligand. Cette expérience a été exécutée uniquement pour tester la stabilité de la ligne de base de la surface. D'après nos observations et les calculs, la surface CCR5/BAPol sur biocapteur SA est légèrement plus stable que la surface CM4 fonctionnalisé avec 1D4.

Dans les premières expériences de SPR, des différences ont été observées entre RANTES-Strep et RANTES-LT-Strep en terme d'oligomérie. Il a été constaté que la liaison RANTES-LT-Strep sur la surface de CCR5 était proche de la réponse théorique maximale alors que la liaison de RANTES-Strep dépasse clairement cette valeur de plus de 10 fois suggérant une oligomérisation de la chimiokine. L'impact des étiquette C-terminale sur l'oligomérie pourrait être mieux caractérisés. Maintenant que des surfaces de CCR5 stables sont disponibles, des titrations pourraient être effectuées et les constantes de dissociation pourraient être calculées pour chaque construction de chimiokine.

A ce stade, l'optimisation de la surface de SPR était nécessaire afin de mieux caractériser les interactions. Malheureusement, à la fin de ma thèse de doctorat l'accès aux NAPol (via le

laboratoire de J.-L. Popot) a été limitée par la difficulté de leur synthèse chimique. La suite de ces travaux devra attendre les nouvelles synthèses de NAPol.

14.4.2. Perspectives

Avec des surfaces de CCR5 stables des paramètres cinétiques plus précis pourraient être calculés. L'impact du manque des sulfations la partie N-terminale de CCR5 pourrait être mieux étudié.

La surface stable CCR5/BAPol où l'ancrage se fait par l'intermédiaire de la ceinture d'amphipole qui entoure la protéine laisse les deux parties extracellulaire et intracellulaire du récepteur disponible. Différentes études de reconstitution de complexes pourraient maintenant avoir lieu, des études de liaison de ligand avec les protéines G ou tout autre partenaire de RCPG pourrait être menées dans le futur.

Néanmoins, pour des expériences futures de SPR un contrôle qui pourrait exclure l'interaction non spécifique entre la chimiokine et l' amphipoel est toujours nécessaire. Un autre RCPG replié en NAPol ou en BNAPol pourrait être utilisé afin de confirmer qu'il n'interagit pas avec la chimiokine.

Part V.

References

Bibliography

[1] Fredriksson, R, Lagerström, M. C, Lundin, L.-G, & Schiöth, H. B. (2003) The g-protein-coupled receptors in the human genome form five main families. phylogenetic analysis, paralogon groups, and fingerprints. *Molecular Pharmacology* **63**, 1256–72.

[2] Bockaert, J & Pin, J. P. (1999) Molecular tinkering of g protein-coupled receptors: an evolutionary success. *EMBO J* **18**, 1723–9.

[3] Bridges, T. M & Lindsley, C. W. (2008) G-protein-coupled receptors: from classical modes of modulation to allosteric mechanisms. *ACS Chem Biol* **3**, 530–41.

[4] Tuteja, N. (2009) Signaling through g protein coupled receptors. *Plant Signal Behav* **4**, 942–7.

[5] Dorsam, R. T & Gutkind, J. S. (2007) G-protein-coupled receptors and cancer. *Nat Rev Cancer* **7**, 79–94.

[6] Gasparini, F, Kuhn, R, & Pin, J.-P. (2002) Allosteric modulators of group i metabotropic glutamate receptors: novel subtype-selective ligands and therapeutic perspectives. *Current Opinion in Pharmacology* **2**, 43–9.

[7] May, L. T & Christopoulos, A. (2003) Allosteric modulators of g-protein-coupled receptors. *Current Opinion in Pharmacology* **3**, 551–6.

[8] Foord, S. M, Bonner, T. I, Neubig, R. R, Rosser, E. M, Pin, J.-P, Davenport, A. P, Spedding, M, & Harmar, A. J. (2005) International union of pharmacology. xlvi. g protein-coupled receptor list. *Pharmacol Rev* **57**, 279–88.

[9] Bjarnadóttir, T. K, Gloriam, D. E, Hellstrand, S. H, Kristiansson, H, Fredriksson, R, & Schiöth, H. B. (2006) Comprehensive repertoire and phylogenetic analysis of the g protein-coupled receptors in human and mouse. *Genomics* **88**, 263–73.

[10] George, S. R, O'Dowd, B. F, & Lee, S. P. (2002) G-protein-coupled receptor oligomerization and its potential for drug discovery. *Nat Rev Drug Discov* **1**, 808–20.

[11] Rondard, P, Liu, J, Huang, S, Malhaire, F, Vol, C, Pinault, A, Labesse, G, & Pin, J.-P. (2006) Coupling of agonist binding to effector domain activation in metabotropic glutamate-like receptors. *J Biol Chem* **281**, 24653–61.

[12] Pin, J.-P, Kniazeff, J, Liu, J, Binet, V, Goudet, C, Rondard, P, & Prézeau, L. (2005) Allosteric functioning of dimeric class c g-protein-coupled receptors. *FEBS J* **272**, 2947–55.

[13] Millar, R. P & Newton, C. L. (2010) The year in g protein-coupled receptor research. *Mol Endocrinol* **24**, 261–74.

[14] Hofmann, K. P, Scheerer, P, Hildebrand, P. W, Choe, H.-W, Park, J. H, Heck, M, & Ernst, O. P. (2009) A g protein-coupled receptor at work: the rhodopsin model. *Trends Biochem Sci* **34**, 540–52.

[15] Palczewski, K, Kumasaka, T, Hori, T, Behnke, C. A, Motoshima, H, Fox, B. A, Trong, I. L, Teller, D. C, Okada, T, Stenkamp, R. E, Yamamoto, M, & Miyano, M. (2000) Crystal structure of rhodopsin: A g protein-coupled receptor. *Science* **289**, 739–45.

[16] Krasnoperov, V, Lu, Y, Buryanovsky, L, Neubert, T. A, Ichtchenko, K, & Petrenko, A. G. (2002) Post-translational proteolytic processing of the calcium-independent receptor of alpha-latrotoxin (cirl), a natural chimera of the cell adhesion protein and the g protein-coupled receptor. role of the g protein-coupled receptor proteolysis site (gps) motif. *J Biol Chem* **277**, 46518–26.

[17] Langley, J. N. (1905) On the reaction of cells and of nerve-endings to certain poisons, chiefly as regards the reaction of striated muscle to nicotine and to curari. *J Physiol (Lond)* **33**, 374–413.

[18] Kenakin, T. (2002) Efficacy at g-protein-coupled receptors. *Nat Rev Drug Discov* **1**, 103–10.

[19] Lean, A. D, Stadel, J. M, & Lefkowitz, R. J. (1980) A ternary complex model explains the agonist-specific binding properties of the adenylate cyclase-coupled beta-adrenergic receptor. *J Biol Chem* **255**, 7108–17.

[20] Samama, P, Cotecchia, S, Costa, T, & Lefkowitz, R. J. (1993) A mutation-induced activated state of the beta 2-adrenergic receptor. extending the ternary complex model. *J Biol Chem* **268**, 4625–36.

[21] Leff, P. (1995) The two-state model of receptor activation. *Trends in Pharmacological Sciences* **16**, 89–97.

[22] Weiss, J. M, Morgan, P. H, Lutz, M. W, & Kenakin, T. P. (1996) The cubic ternary complex receptor-occupancy model. iii. resurrecting efficacy. *J Theor Biol* **181**, 381–97.

[23] Devi, L. A. (2001) Heterodimerization of g-protein-coupled receptors: pharmacology, signaling and trafficking. *Trends in Pharmacological Sciences* **22**, 532–7.

[24] Milligan, G. (2004) G protein-coupled receptor dimerization: function and ligand pharmacology. *Molecular Pharmacology* **66**, 1–7.

[25] Park, P. S.-H, Filipek, S, Wells, J. W, & Palczewski, K. (2004) Oligomerization of g protein-coupled receptors: past, present, and future. *Biochemistry* **43**, 15643–56.

[26] Durroux, T. (2005) Principles: a model for the allosteric interactions between ligand binding sites within a dimeric gpcr. *Trends in Pharmacological Sciences* **26**, 376–84.

[27] Panetta, R & Greenwood, M. T. (2008) Physiological relevance of gpcr oligomerization and its impact on drug discovery. *Drug Discov Today* **13**, 1059–66.

[28] Lavine, N, Ethier, N, Oak, J. N, Pei, L, Liu, F, Trieu, P, Rebois, R. V, Bouvier, M, Hebert, T. E, & Tol, H. H. M. V. (2002) G protein-coupled receptors form stable complexes with inwardly rectifying potassium channels and adenylyl cyclase. *J Biol Chem* **277**, 46010–9.

[29] Koski, G, Streaty, R. A, & Klee, W. A. (1982) Modulation of sodium-sensitive gtpase by partial opiate agonists. an explanation for the dual requirement for na+ and gtp in inhibitory regulation of adenylate cyclase. *J Biol Chem* **257**, 14035–40.

[30] Cerione, R. A, Codina, J, Benovic, J. L, Lefkowitz, R. J, Birnbaumer, L, & Caron, M. G. (1984) The mammalian beta 2-adrenergic receptor: reconstitution of functional interactions between pure receptor and pure stimulatory nucleotide binding protein of the adenylate cyclase system. *Biochemistry* **23**, 4519–25.

[31] Kjelsberg, M. A, Cotecchia, S, Ostrowski, J, Caron, M. G, & Lefkowitz, R. J. (1992) Constitutive activation of the alpha 1b-adrenergic receptor by all amino acid substitutions at a single site. evidence for a region which constrains receptor activation. *J Biol Chem* **267**, 1430–3.

[32] Samama, P, Pei, G, Costa, T, Cotecchia, S, & Lefkowitz, R. J. (1994) Negative antagonists promote an inactive conformation of the beta 2-adrenergic receptor. *Molecular Pharmacology* **45**, 390–4.

[33] Spalding, T. A, Burstein, E. S, Wells, J. W, & Brann, M. R. (1997) Constitutive activation of the m5 muscarinic receptor by a series of mutations at the extracellular end of transmembrane 6. *Biochemistry* **36**, 10109–16.

[34] Pauwels, P. J & Wurch, T. (1999) Review: amino acid domains involved in constitutive activation of g-protein-coupled receptors. *Mol Neurobiol* **17**, 109–35.

[35] Seifert, R & Wenzel-Seifert, K. (2002) Constitutive activity of g-protein-coupled receptors: cause of disease and common property of wild-type receptors. *Naunyn Schmiedebergs Arch Pharmacol* **366**, 381–416.

[36] Wettschureck, N & Offermanns, S. (2005) Mammalian g proteins and their cell type specific functions. *Physiological Reviews* **85**, 1159–204.

[37] Hamm, H. E. (1998) The many faces of g protein signaling. *J Biol Chem* **273**, 669–72.

[38] Ford, C. E, Skiba, N. P, Bae, H, Daaka, Y, Reuveny, E, Shekter, L. R, Rosal, R, Weng, G, Yang, C. S, Iyengar, R, Miller, R. J, Jan, L. Y, Lefkowitz, R. J, & Hamm, H. E. (1998) Molecular basis for interactions of g protein betagamma subunits with effectors. *Science* **280**, 1271–4.

[39] Li, Y, Sternweis, P. M, Charnecki, S, Smith, T. F, Gilman, A. G, Neer, E. J, & Kozasa, T. (1998) Sites for galpha binding on the g protein beta subunit overlap with sites for regulation of phospholipase cbeta and adenylyl cyclase. *J Biol Chem* **273**, 16265–72.

[40] Juno, J. A & Fowke, K. R. (2010) Clarifying the role of g protein signaling in hiv infection: new approaches to an old question. *AIDS Rev* **12**, 164–76.

[41] Downes, G. B & Gautam, N. (1999) The g protein subunit gene families. *Genomics* **62**, 544–52.

[42] Lambright, D. G, Sondek, J, Bohm, A, Skiba, N. P, Hamm, H. E, & Sigler, P. B. (1996) The 2.0 a crystal structure of a heterotrimeric g protein. *Nature* **379**, 311–9.

[43] Lambright, D. G, Noel, J. P, Hamm, H. E, & Sigler, P. B. (1994) Structural determinants for activation of the alpha-subunit of a heterotrimeric g protein. *Nature* **369**, 621–8.

[44] Mixon, M. B, Lee, E, Coleman, D. E, Berghuis, A. M, Gilman, A. G, & Sprang, S. R. (1995) Tertiary and quaternary structural changes in gi alpha 1 induced by gtp hydrolysis. *Science* **270**, 954–60.

[45] Noel, J. P, Hamm, H. E, & Sigler, P. B. (1993) The 2.2 a crystal structure of transducin-alpha complexed with gtp gamma s. *Nature* **366**, 654–63.

[46] Coleman, D. E, Berghuis, A. M, Lee, E, Linder, M. E, Gilman, A. G, & Sprang, S. R. (1994) Structures of active conformations of gi alpha 1 and the mechanism of gtp hydrolysis. *Science* **265**, 1405–12.

[47] OLDHAM, W. M & HAMM, H. E. (2008) Heterotrimeric g protein activation by g-protein-coupled receptors. *Nat Rev Mol Cell Biol* **9**, 60–71.

[48] Strathmann, M & Simon, M. I. (1990) G protein diversity: a distinct class of alpha subunits is present in vertebrates and invertebrates. *Proc Natl Acad Sci USA* **87**, 9113–7.

[49] Smotrys, J. E & Linder, M. E. (2004) Palmitoylation of intracellular signaling proteins: regulation and function. *Annu Rev Biochem* **73**, 559–87.

[50] Murakami, Y, Kohsaka, H, Kitasato, H, & Akahoshi, T. (2007) Lipopolysaccharide-induced up-regulation of triggering receptor expressed on myeloid cells-1 expression on macrophages is regulated by endogenous prostaglandin e2. *J Immunol* **178**, 1144–50.

[51] Conti, M. (2000) Phosphodiesterases and cyclic nucleotide signaling in endocrine cells. *Mol Endocrinol* **14**, 1317–27.

[52] Taussig, R, Iñiguez-Lluhi, J. A, & Gilman, A. G. (1993) Inhibition of adenylyl cyclase by gi alpha. *Science* **261**, 218–21.

[53] Hofstra, C. L, Desai, P. J, Thurmond, R. L, & Fung-Leung, W.-P. (2003) Histamine h4 receptor mediates chemotaxis and calcium mobilization of mast cells. *J Pharmacol Exp Ther* **305**, 1212–21.

[54] Medkova, M & Cho, W. (1999) Interplay of c1 and c2 domains of protein kinase c-alpha in its membrane binding and activation. *J Biol Chem* **274**, 19852–61.

[55] Kuner, R, Swiercz, J. M, Zywietz, A, Tappe, A, & Offermanns, S. (2002) Characterization of the expression of pdz-rhogef, larg and g(alpha)12/g(alpha)13 proteins in the murine nervous system. *Eur J Neurosci* **16**, 2333–41.

[56] Holinstat, M, Mehta, D, Kozasa, T, Minshall, R. D, & Malik, A. B. (2003) Protein kinase calpha-induced p115rhogef phosphorylation signals endothelial cytoskeletal rearrangement. *J Biol Chem* **278**, 28793–8.

[57] Hurowitz, E. H, Melnyk, J. M, Chen, Y. J, Kouros-Mehr, H, Simon, M. I, & Shizuya, H. (2000) Genomic characterization of the human heterotrimeric g protein alpha, beta, and gamma subunit genes. *DNA Res* **7**, 111–20.

[58] Wall, M. A, Coleman, D. E, Lee, E, Iñiguez-Lluhi, J. A, Posner, B. A, Gilman, A. G, & Sprang, S. R. (1995) The structure of the g protein heterotrimer gi alpha 1 beta 1 gamma 2. *Cell* **83**, 1047–58.

[59] Matsuda, T, Takao, T, Shimonishi, Y, Murata, M, Asano, T, Yoshizawa, T, & Fukada, Y. (1994) Characterization of interactions between transducin alpha/beta gamma-subunits and lipid membranes. *J Biol Chem* **269**, 30358–63.

[60] Cuello, F, Schulze, R. A, Heemeyer, F, Meyer, H. E, Lutz, S, Jakobs, K. H, Niroomand, F, & Wieland, T. (2003) Activation of heterotrimeric g proteins by a high energy phosphate transfer via nucleoside diphosphate kinase (ndpk) b and gbeta subunits. complex formation of ndpk b with gbeta gamma dimers and phosphorylation of his-266 in gbeta. *J Biol Chem* **278**, 7220–6.

[61] Casey, P. J. (1995) Protein lipidation in cell signaling. *Science* **268**, 221–5.

[62] Wedegaertner, P. B, Wilson, P. T, & Bourne, H. R. (1995) Lipid modifications of trimeric g proteins. *J Biol Chem* **270**, 503–6.

[63] Lane, K. T & Beese, L. S. (2006) Thematic review series: lipid posttranslational modifications. structural biology of protein farnesyltransferase and geranylgeranyltransferase type i. *J Lipid Res* **47**, 681–99.

[64] McIntire, W. E. (2009) Structural determinants involved in the formation and activation of g protein betagamma dimers. *Neurosignals* **17**, 82–99.

[65] Yang, W & Xia, S.-H. (2006) Mechanisms of regulation and function of g-protein-coupled receptor kinases. *World J Gastroenterol* **12**, 7753–7.

[66] Ritter, S. L & Hall, R. A. (2009) Fine-tuning of gpcr activity by receptor-interacting proteins. *Nat Rev Mol Cell Biol* **10**, 819–830.

[67] Penela, P, Elorza, A, Sarnago, S, & Mayor, F. (2001) Beta-arrestin- and c-src-dependent degradation of g-protein-coupled receptor kinase 2. *EMBO J* **20**, 5129–38.

[68] Luttrell, L. M, Ferguson, S. S, Daaka, Y, Miller, W. E, Maudsley, S, Rocca, G. J. D, Lin, F, Kawakatsu, H, Owada, K, Luttrell, D. K, Caron, M. G, & Lefkowitz, R. J. (1999) Beta-arrestin-dependent formation of beta2 adrenergic receptor-src protein kinase complexes. *Science* **283**, 655–61.

[69] Hall, R. A, Premont, R. T, & Lefkowitz, R. J. (1999) Heptahelical receptor signaling: beyond the g protein paradigm. *J Cell Biol* **145**, 927–32.

[70] Marrero, M. B, Schieffer, B, Paxton, W. G, Schieffer, E, & Bernstein, K. E. (1995) Electroporation of pp60c-src antibodies inhibits the angiotensin ii activation of phospholipase c-gamma 1 in rat aortic smooth muscle cells. *J Biol Chem* **270**, 15734–8.

[71] Mitchell, R, McCulloch, D, Lutz, E, Johnson, M, MacKenzie, C, Fennell, M, Fink, G, Zhou, W, & Sealfon, S. C. (1998) Rhodopsin-family receptors associate with small g proteins to activate phospholipase d. *Nature* **392**, 411–4.

[72] Hall, R. A, Ostedgaard, L. S, Premont, R. T, Blitzer, J. T, Rahman, N, Welsh, M. J, & Lefkowitz, R. J. (1998) A c-terminal motif found in the beta2-adrenergic receptor, p2y1 receptor and cystic fibrosis transmembrane conductance regulator determines binding to the na+/h+ exchanger regulatory factor family of pdz proteins. *Proc Natl Acad Sci USA* **95**, 8496–501.

[73] Hall, R. A, Spurney, R. F, Premont, R. T, Rahman, N, Blitzer, J. T, Pitcher, J. A, & Lefkowitz, R. J. (1999) G protein-coupled receptor kinase 6a phosphorylates the na(+)/h(+) exchanger regulatory factor via a pdz domain-mediated interaction. *J Biol Chem* **274**, 24328–34.

[74] Pawson, T & Scott, J. D. (1997) Signaling through scaffold, anchoring, and adaptor proteins. *Science* **278**, 2075–80.

[75] Brakeman, P. R, Lanahan, A. A, O'Brien, R, Roche, K, Barnes, C. A, Huganir, R. L, & Worley, P. F. (1997) Homer: a protein that selectively binds metabotropic glutamate receptors. *Nature* **386**, 284–8.

[76] Tu, J. C, Xiao, B, Yuan, J. P, Lanahan, A. A, Leoffert, K, Li, M, Linden, D. J, & Worley, P. F. (1998) Homer binds a novel proline-rich motif and links group 1 metabotropic glutamate receptors with ip3 receptors. *Neuron* **21**, 717–26.

[77] Xiao, B, Tu, J. C, Petralia, R. S, Yuan, J. P, Doan, A, Breder, C. D, Ruggiero, A, Lanahan, A. A, Wenthold, R. J, & Worley, P. F. (1998) Homer regulates the association of group 1 metabotropic glutamate receptors with multivalent complexes of homer-related, synaptic proteins. *Neuron* **21**, 707–16.

[78] Klaasse, E. C, Ijzerman, A. P, de Grip, W. J, & Beukers, M. W. (2008) Internalization and desensitization of adenosine receptors. *Purinergic Signal* **4**, 21–37.

[79] Premont, R. T, Inglese, J, & Lefkowitz, R. J. (1995) Protein kinases that phosphorylate activated g protein-coupled receptors. *FASEB J* **9**, 175–82.

[80] Luttrell, L. M & Lefkowitz, R. J. (2002) The role of beta-arrestins in the termination and transduction of g-protein-coupled receptor signals. *J Cell Sci* **115**, 455–65.

[81] Parsons, W. J & Stiles, G. L. (1987) Heterologous desensitization of the inhibitory a1 adenosine receptor-adenylate cyclase system in rat adipocytes. regulation of both ns and ni. *J Biol Chem* **262**, 841–7.

[82] Pierce, K. L, Premont, R. T, & Lefkowitz, R. J. (2002) Seven-transmembrane receptors. *Nat Rev Mol Cell Biol* **3**, 639–50.

[83] Ferguson, S. S. (2001) Evolving concepts in g protein-coupled receptor endocytosis: the role in receptor desensitization and signaling. *Pharmacol Rev* **53**, 1–24.

[84] Reiter, E & Lefkowitz, R. J. (2006) Grks and beta-arrestins: roles in receptor silencing, trafficking and signaling. *Trends Endocrinol Metab* **17**, 159–65.

[85] Bai, M. (2004) Dimerization of g-protein-coupled receptors: roles in signal transduction. *Cellular Signalling* **16**, 175–86.

[86] Terrillon, S & Bouvier, M. (2004) Roles of g-protein-coupled receptor dimerization. *EMBO Rep* **5**, 30–4.

[87] Lohse, M. J. (2010) Dimerization in gpcr mobility and signaling. *Current Opinion in Pharmacology* **10**, 53–8.

[88] Rozenfeld, R & Devi, L. A. (2010) Exploring a role for heteromerization in gpcr signalling specificity. *Biochem. J.* **433**, 11–8.

[89] Salahpour, A, Angers, S, & Bouvier, M. (2000) Functional significance of oligomerization of g-protein-coupled receptors. *Trends Endocrinol Metab* **11**, 163–8.

[90] Galvez, T, Duthey, B, Kniazeff, J, Blahos, J, Rovelli, G, Bettler, B, Prézeau, L, & Pin, J. P. (2001) Allosteric interactions between gb1 and gb2 subunits are required for optimal gaba(b) receptor function. *EMBO J* **20**, 2152–9.

[91] Margeta-Mitrovic, M, Jan, Y. N, & Jan, L. Y. (2000) A trafficking checkpoint controls gaba(b) receptor heterodimerization. *Neuron* **27**, 97–106.

[92] Marshall, F. H, White, J, Main, M, Green, A, & Wise, A. (1999) Gaba(b) receptors function as heterodimers. *Biochem. Soc. Trans* **27**, 530–5.

[93] White, J. H, Wise, A, Main, M. J, Green, A, Fraser, N. J, Disney, G. H, Barnes, A. A, Emson, P, Foord, S. M, & Marshall, F. H. (1998) Heterodimerization is required for the formation of a functional gaba(b) receptor. *Nature* **396**, 679–82.

[94] Kaupmann, K, Malitschek, B, Schuler, V, Heid, J, Froestl, W, Beck, P, Mosbacher, J, Bischoff, S, Kulik, A, Shigemoto, R, Karschin, A, & Bettler, B. (1998) Gaba(b)-receptor subtypes assemble into functional heteromeric complexes. *Nature* **396**, 683–7.

[95] Benkirane, M, Jin, D. Y, Chun, R. F, Koup, R. A, & Jeang, K. T. (1997) Mechanism of transdominant inhibition of ccr5-mediated hiv-1 infection by ccr5delta32. *J Biol Chem* **272**, 30603–6.

[96] Jordan, B. A & Devi, L. A. (1999) G-protein-coupled receptor heterodimerization modulates receptor function. *Nature* **399**, 697–700.

[97] George, S. R, Fan, T, Xie, Z, Tse, R, Tam, V, Varghese, G, & O'Dowd, B. F. (2000) Oligomerization of mu- and delta-opioid receptors. generation of novel functional properties. *J Biol Chem* **275**, 26128–35.

[98] Vila-Coro, A. J, Rodríguez-Frade, J. M, de Ana, A. M, Moreno-Ortíz, M. C, Martínez-A, C, & Mellado, M. (1999) The chemokine sdf-1alpha triggers cxcr4 receptor dimerization and activates the jak/stat pathway. *FASEB J* **13**, 1699–710.

[99] Rodríguez-Frade, J. M, Vila-Coro, A. J, de Ana, A. M, Albar, J. P, Martínez-A, C, & Mellado, M. (1999) The chemokine monocyte chemoattractant protein-1 induces functional responses through dimerization of its receptor ccr2. *Proc Natl Acad Sci USA* **96**, 3628–33.

[100] Vila-Coro, A. J, Mellado, M, de Ana, A. M, Lucas, P, del Real, G, Martínez-A, C, & Rodríguez-Frade, J. M. (2000) Hiv-1 infection through the ccr5 receptor is blocked by receptor dimerization. *Proc Natl Acad Sci USA* **97**, 3388–93.

[101] Albizu, L, Moreno, J. L, González-Maeso, J, & Sealfon, S. C. (2010) Heteromerization of g protein-coupled receptors: relevance to neurological disorders and neurotherapeutics. *CNS Neurol Disord Drug Targets* **9**, 636–50.

[102] Mellado, M, Rodríguez-Frade, J. M, Vila-Coro, A. J, Fernández, S, de Ana, A. M, Jones, D. R, Torán, J. L, & Martínez-A, C. (2001) Chemokine receptor homo- or heterodimerization activates distinct signaling pathways. *EMBO J* **20**, 2497–507.

[103] Pellissier, L. P, Barthet, G, Gaven, F, Cassier, E, Trinquet, E, Pin, J.-P, Marin, P, Dumuis, A, Bockaert, J, Banères, J.-L, & Claeysen, S. (2011) G protein activation by serotonin type 4 receptor dimers: evidence that turning on two protomers is more efficient. *J Biol Chem* **286**, 9985–97.

[104] Arcemisbéhère, L, Sen, T, Boudier, L, Balestre, M.-N, Gaibelet, G, Detouillon, E, Orcel, H, Mendre, C, Rahmeh, R, Granier, S, Vivès, C, Fieschi, F, Damian, M, Durroux, T, Banères, J.-L, & Mouillac, B. (2010) Leukotriene blt2 receptor monomers activate the g(i2) gtp-binding protein more efficiently than dimers. *J Biol Chem* **285**, 6337–47.

[105] Hopkins, A. L & Groom, C. R. (2002) The druggable genome. *Nat Rev Drug Discov* **1**, 727–30.

[106] Booth, B & Zemmel, R. (2004) Prospects for productivity. *Nat Rev Drug Discov* **3**, 451–6.

[107] Christopoulos, A. (2002) Allosteric binding sites on cell-surface receptors: novel targets for drug discovery. *Nat Rev Drug Discov* **1**, 198–210.

[108] Christopoulos, A & Kenakin, T. (2002) G protein-coupled receptor allosterism and complexing. *Pharmacol Rev* **54**, 323–74.

[109] May, L. T, Leach, K, Sexton, P. M, & Christopoulos, A. (2007) Allosteric modulation of g protein-coupled receptors. *Annu. Rev. Pharmacol. Toxicol.* **47**, 1–51.

[110] Keov, P, Sexton, P. M, & Christopoulos, A. (2011) Allosteric modulation of g protein-coupled receptors: a pharmacological perspective. *Neuropharmacology* **60**, 24–35.

[111] Milligan, G. (2006) G-protein-coupled receptor heterodimers: pharmacology, function and relevance to drug discovery. *Drug Discov Today* **11**, 541–9.

[112] Kent, T, McAlpine, C, Sabetnia, S, & Presland, J. (2007) G-protein-coupled receptor heterodimerization: assay technologies to clinical significance. *Curr Opin Drug Discov Devel* **10**, 580–9.

[113] Dalrymple, M. B, Pfleger, K. D. G, & Eidne, K. A. (2008) G protein-coupled receptor dimers: functional consequences, disease states and drug targets. *Pharmacol Ther* **118**, 359–71.

[114] Shukla, A. K, Haase, W, Reinhart, C, & Michel, H. (2007) Heterologous expression and characterization of the recombinant bradykinin b2 receptor using the methylotrophic yeast pichia pastoris. *Protein Expression and Purification* **55**, 1–8.

[115] André, N, Cherouati, N, Prual, C, Steffan, T, Zeder-Lutz, G, Magnin, T, Pattus, F, Michel, H, Wagner, R, & Reinhart, C. (2006) Enhancing functional production of g protein-coupled receptors in pichia pastoris to levels required for structural studies via a single expression screen. *Protein Sci* **15**, 1115–26.

[116] Zeder-Lutz, G, Cherouati, N, Reinhart, C, Pattus, F, & Wagner, R. (2006) Dot-blot immunodetection as a versatile and high-throughput assay to evaluate recombinant gpcrs produced in the yeast pichia pastoris. *Protein Expression and Purification* **50**, 118–27.

[117] Lundstrom, K, Wagner, R, Reinhart, C, Desmyter, A, Cherouati, N, Magnin, T, Zeder-Lutz, G, Courtot, M, Prual, C, André, N, Hassaine, G, Michel, H, Cambillau, C, & Pattus, F. (2006) Structural genomics on membrane proteins: comparison of more than 100 gpcrs in 3 expression systems. *J Struct Funct Genomics* **7**, 77–91.

[118] Perret, B. G, Wagner, R, Lecat, S, Brillet, K, Rabut, G, Bucher, B, & Pattus, F. (2003) Expression of egfp-amino-tagged human mu opioid receptor in drosophila schneider 2 cells: a potential expression system for large-scale production of g-protein coupled receptors. *Protein Expression and Purification* **31**, 123–32.

[119] Rasmussen, S. G. F, Choi, H.-J, Rosenbaum, D. M, Kobilka, T. S, Thian, F. S, Edwards, P. C, Burghammer, M, Ratnala, V. R. P, Sanishvili, R, Fischetti, R. F, Schertler, G. F. X, Weis, W. I, & Kobilka, B. K. (2007) Crystal structure of the human beta2 adrenergic g-protein-coupled receptor. *Nature* **450**, 383–7.

[120] Hassaine, G, Wagner, R, Kempf, J, Cherouati, N, Hassaine, N, Prual, C, André, N, Reinhart, C, Pattus, F, & Lundstrom, K. (2006) Semliki forest virus vectors for overexpression of 101 g protein-coupled receptors in mammalian host cells. *Protein Expression and Purification* **45**, 343–51.

[121] Ott, D, Frischknecht, R, & Plückthun, A. (2004) Construction and characterization of a kappa opioid receptor devoid of all free cysteines. *Protein Eng Des Sel* **17**, 37–48.

[122] Ott, D, Neldner, Y, Cèbe, R, Dodevski, I, & Plückthun, A. (2005) Engineering and functional immobilization of opioid receptors. *Protein Eng Des Sel* **18**, 153–60.

[123] Rosenbaum, D. M, Cherezov, V, Hanson, M. A, Rasmussen, S. G. F, Thian, F. S, Kobilka, T. S, Choi, H.-J, Yao, X.-J, Weis, W. I, Stevens, R. C, & Kobilka, B. K. (2007) Gpcr engineering yields high-resolution structural insights into beta2-adrenergic receptor function. *Science* **318**, 1266–73.

[124] Cherezov, V, Rosenbaum, D. M, Hanson, M. A, Rasmussen, S. G. F, Thian, F. S, Kobilka, T. S, Choi, H.-J, Kuhn, P, Weis, W. I, Kobilka, B. K, & Stevens, R. C. (2007) High-resolution crystal structure of an engineered human 2-adrenergic g protein coupled receptor. *Science* **318**, 1258–1265.

[125] Warne, T, Serrano-Vega, M. J, Baker, J. G, Moukhametzianov, R, Edwards, P. C, Henderson, R, Leslie, A. G. W, Tate, C. G, & Schertler, G. F. X. (2008) Structure of a beta1-adrenergic g-protein-coupled receptor. *Nature* **454**, 486–91.

[126] Jaakola, V.-P, Griffith, M. T, Hanson, M. A, Cherezov, V, Chien, E. Y. T, Lane, J. R, Ijzerman, A. P, & Stevens, R. C. (2008) The 2.6 angstrom crystal structure of a human a2a adenosine receptor bound to an antagonist. *Science* **322**, 1211–1217.

[127] Wu, B, Chien, E. Y. T, Mol, C. D, Fenalti, G, Liu, W, Katritch, V, Abagyan, R, Brooun, A, Wells, P, Bi, F. C, Hamel, D. J, Kuhn, P, Handel, T. M, Cherezov, V, & Stevens, R. C. (2010) Structures of the cxcr4 chemokine gpcr with small-molecule and cyclic peptide antagonists. *Science* **330**, 1066–71.

[128] Chien, E. Y. T, Liu, W, Zhao, Q, Katritch, V, Han, G. W, Hanson, M. A, Shi, L, Newman, A. H, Javitch, J. A, Cherezov, V, & Stevens, R. C. (2010) Structure of the human dopamine d3 receptor in complex with a d2/d3 selective antagonist. *Science* **330**, 1091–5.

[129] Shimamura, T, Shiroishi, M, Weyand, S, Tsujimoto, H, Winter, G, Katritch, V, Abagyan, R, Cherezov, V, Liu, W, Han, G. W, Kobayashi, T, Stevens, R. C, & Iwata, S. (2011) Structure of the human histamine h1 receptor complex with doxepin. *Nature* **475**, 65–70.

[130] Katritch, V, Cherezov, V, & Stevens, R. C. (2012) Diversity and modularity of g protein-coupled receptor structures. *Trends in Pharmacological Sciences*.

[131] Rasmussen, S. G. F, Choi, H.-J, Fung, J. J, Pardon, E, Casarosa, P, Chae, P. S, DeVree, B. T, Rosenbaum, D. M, Thian, F. S, Kobilka, T. S, Schnapp, A, Konetzki, I, Sunahara, R. K, Gellman, S. H, Pautsch, A, Steyaert, J, Weis, W. I, & Kobilka, B. K. (2011) Structure of a nanobody-stabilized active state of the beta(2) adrenoceptor. *Nature* **469**, 175–80.

[132] Rasmussen, S. G. F, DeVree, B. T, Zou, Y, Kruse, A. C, Chung, K. Y, Kobilka, T. S, Thian, F. S, Chae, P. S, Pardon, E, Calinski, D, Mathiesen, J. M, Shah, S. T. A, Lyons, J. A, Caffrey, M, Gellman, S. H, Steyaert, J, Skiniotis, G, Weis, W. I, Sunahara, R. K, & Kobilka, B. K. (2011) Crystal structure of the beta (2) adrenergic receptor-gs protein complex. *Nature* **477**, 549–557.

[133] Lebon, G, Warne, T, Edwards, P. C, Bennett, K, Langmead, C. J, Leslie, A. G. W, & Tate, C. G. (2011) Agonist-bound adenosine a(2a) receptor structures reveal common features of gpcr activation. *Nature*.

[134] Dror, R. O, Arlow, D. H, Maragakis, P, Mildorf, T. J, Pan, A. C, Xu, H, Borhani, D. W, & Shaw, D. E. (2011) Activation mechanism of the beta 2-adrenergic receptor. *Proc Natl Acad Sci USA*.

[135] Iglesias, P. A & Devreotes, P. N. (2008) Navigating through models of chemotaxis. *Curr Opin Cell Biol* **20**, 35–40.

[136] Roussos, E. T, Condeelis, J. S, & Patsialou, A. (2011) Chemotaxis in cancer. *Nat Rev Cancer* **11**, 573–87.

[137] Jin, T, Xu, X, & Hereld, D. (2008) Chemotaxis, chemokine receptors and human disease. *Cytokine* **44**, 1–8.

[138] Luster, A. D. (1998) Chemokines–chemotactic cytokines that mediate inflammation. *N Engl J Med* **338**, 436–45.

[139] Horuk, R, Chitnis, C. E, Darbonne, W. C, Colby, T. J, Rybicki, A, Hadley, T. J, & Miller, L. H. (1993) A receptor for the malarial parasite plasmodium vivax: the erythrocyte chemokine receptor. *Science* **261**, 1182–4.

[140] Hosking, M. P & Lane, T. E. (2010) The role of chemokines during viral infection of the cns. *PLoS Pathog* **6**, e1000937.

[141] Parish, C. R. (2006) The role of heparan sulphate in inflammation. *Nat. Rev. Immunol.* **6**, 633–43.

[142] Nibbs, R, Graham, G, & Rot, A. (2003) Chemokines on the move: control by the chemokine "interceptors" duffy blood group antigen and d6. *Semin Immunol* **15**, 287–94.

[143] Murphy, P. M, Baggiolini, M, Charo, I. F, Hébert, C. A, Horuk, R, Matsushima, K, Miller, L. H, Oppenheim, J. J, & Power, C. A. (2000) International union of pharmacology. xxii. nomenclature for chemokine receptors. *Pharmacol Rev* **52**, 145–76.

[144] Salanga, C. L, O'Hayre, M, & Handel, T. (2009) Modulation of chemokine receptor activity through dimerization and crosstalk. *Cellular and Molecular Life Sciences (CMLS)* **66**, 1370–86.

[145] Wilson, S, Wilkinson, G, & Milligan, G. (2005) The cxcr1 and cxcr2 receptors form constitutive homo- and heterodimers selectively and with equal apparent affinities. *J Biol Chem* **280**, 28663–74.

[146] Issafras, H, Angers, S, Bulenger, S, Blanpain, C, Parmentier, M, Labbé-Jullié, C, Bouvier, M, & Marullo, S. (2002) Constitutive agonist-independent ccr5 oligomerization and antibody-mediated clustering occurring at physiological levels of receptors. *J Biol Chem* **277**, 34666–73.

[147] Pello, O, Martínez-Muñoz, L, Parrillas, V, Serrano, A, Rodríguez-Frade, J, Toro, M, Lucas, P, Monterrubio, M, Martínez-A, C, & Mellado, M. (2008) Ligand stabilization of cxcr4/ÎŽ-opioid receptor heterodimers reveals a mechanism for immune response regulation. *Eur. J. Immunol.* **38**, 537–549.

[148] Hereld, D & Jin, T. (2008) Slamming the dor on chemokine receptor signaling: heterodimerization silences ligand-occupied cxcr4 and delta-opioid receptors. *Eur. J. Immunol.* **38**, 334–7.

[149] Dejucq, N, Simmons, G, & Clapham, P. R. (1999) Expanded tropism of primary human immunodeficiency virus type 1 r5 strains to cd4(+) t-cell lines determined by the capacity to exploit low concentrations of ccr5. *J Virol* **73**, 7842–7.

[150] Zhong, M. X, Kuziel, W. A, Pamer, E. G, & Serbina, N. V. (2004) Chemokine receptor 5 is dispensable for innate and adaptive immune responses to listeria monocytogenes infection. *Infect Immun* **72**, 1057–64.

[151] Dean, M, Carrington, M, Winkler, C, Huttley, G. A, Smith, M. W, Allikmets, R, Goedert, J. J, Buchbinder, S. P, Vittinghoff, E, Gomperts, E, Donfield, S, Vlahov, D, Kaslow, R, Saah, A, Rinaldo, C, Detels, R, & O'Brien, S. J. (1996) Genetic restriction of hiv-1 infection and progression to aids by a deletion allele of the ckr5 structural gene. hemophilia growth and development study, multicenter aids cohort study, multicenter hemophilia cohort study, san francisco city cohort, alive study. *Science* **273**, 1856–62.

[152] Liu, R, Paxton, W. A, Choe, S, Ceradini, D, Martin, S. R, Horuk, R, MacDonald, M. E, Stuhlmann, H, Koup, R. A, & Landau, N. R. (1996) Homozygous defect in hiv-1 coreceptor accounts for resistance of some multiply-exposed individuals to hiv-1 infection. *Cell* **86**, 367–77.

[153] Samson, M, Libert, F, Doranz, B. J, Rucker, J, Liesnard, C, Farber, C. M, Saragosti, S, Lapoumeroulie, C, Cognaux, J, Forceille, C, Muyldermans, G, Verhofstede, C, Burtonboy, G, Georges, M, Imai, T, Rana, S, Yi, Y, Smyth, R. J, Collman, R. G, Doms, R. W, Vassart, G, & Parmentier, M. (1996) Resistance to hiv-1 infection in caucasian individuals bearing mutant alleles of the ccr-5 chemokine receptor gene. *Nature* **382**, 722–5.

[154] Sabeti, P. C, Walsh, E, Schaffner, S. F, Varilly, P, Fry, B, Hutcheson, H. B, Cullen, M, Mikkelsen, T. S, Roy, J, Patterson, N, Cooper, R, Reich, D, Altshuler, D, O'Brien, S, & Lander, E. S. (2005) The case for selection at ccr5-delta32. *PLoS Biol* **3**, e378.

[155] Hedrick, P. W & Verrelli, B. C. (2006) "ground truth" for selection on ccr5-delta32. *Trends Genet* **22**, 293–6.

[156] Stephens, J. C, Reich, D. E, Goldstein, D. B, Shin, H. D, Smith, M. W, Carrington, M, Winkler, C, Huttley, G. A, Allikmets, R, Schriml, L, Gerrard, B, Malasky, M, Ramos,

M. D, Morlot, S, Tzetis, M, Oddoux, C, di Giovine, F. S, Nasioulas, G, Chandler, D, Aseev, M, Hanson, M, Kalaydjieva, L, Glavac, D, Gasparini, P, Kanavakis, E, Claustres, M, Kambouris, M, Ostrer, H, Duff, G, Baranov, V, Sibul, H, Metspalu, A, Goldman, D, Martin, N, Duffy, D, Schmidtke, J, Estivill, X, O'Brien, S. J, & Dean, M. (1998) Dating the origin of the ccr5-delta32 aids-resistance allele by the coalescence of haplotypes. *Am J Hum Genet* **62**, 1507–15.

[157] Galvani, A. P & Slatkin, M. (2003) Evaluating plague and smallpox as historical selective pressures for the ccr5-delta 32 hiv-resistance allele. *Proc Natl Acad Sci USA* **100**, 15276–9.

[158] Glass, W. G, McDermott, D. H, Lim, J. K, Lekhong, S, Yu, S. F, Frank, W. A, Pape, J, Cheshier, R. C, & Murphy, P. M. (2006) Ccr5 deficiency increases risk of symptomatic west nile virus infection. *J Exp Med* **203**, 35–40.

[159] Wells, T. N, Power, C. A, Lusti-Narasimhan, M, Hoogewerf, A. J, Cooke, R. M, Chung, C. W, Peitsch, M. C, & Proudfoot, A. E. (1996) Selectivity and antagonism of chemokine receptors. *Journal of Leukocyte Biology* **59**, 53–60.

[160] Dorr, P, Westby, M, Dobbs, S, Griffin, P, Irvine, B, Macartney, M, Mori, J, Rickett, G, Smith-Burchnell, C, Napier, C, Webster, R, Armour, D, Price, D, Stammen, B, Wood, A, & Perros, M. (2005) Maraviroc (uk-427,857), a potent, orally bioavailable, and selective small-molecule inhibitor of chemokine receptor ccr5 with broad-spectrum anti-human immunodeficiency virus type 1 activity. *Antimicrob Agents Chemother* **49**, 4721–32.

[161] Ray, N. (2009) Maraviroc in the treatment of hiv infection. *Drug Des Devel Ther* **2**, 151–61.

[162] Garcia-Perez, J, Rueda, P, Alcami, J, Rognan, D, Arenzana-Seisdedos, F, Lagane, B, & Kellenberger, E. (2011) An allosteric model of maraviroc binding to ccr5. *J Biol Chem*.

[163] Choi, W.-T & An, J. (2011) Biology and clinical relevance of chemokines and chemokine receptors cxcr4 and ccr5 in human diseases. *Experimental biology and medicine (Maywood, NJ)*.

[164] Teicher, B. A & Fricker, S. P. (2010) Cxcl12 (sdf-1)/cxcr4 pathway in cancer. *Clin Cancer Res* **16**, 2927–31.

[165] Kim, R. H, Li, B. D. L, & Chu, Q. D. (2011) The role of chemokine receptor cxcr4 in the biologic behavior of human soft tissue sarcoma. *Sarcoma* **2011**, 593708.

[166] Premack, B. A & Schall, T. J. (1996) Chemokine receptors: gateways to inflammation and infection. *Nature Medicine* **2**, 1174–8.

[167] Moore, P. S, Boshoff, C, Weiss, R. A, & Chang, Y. (1996) Molecular mimicry of human cytokine and cytokine response pathway genes by kshv. *Science* **274**, 1739–44.

[168] Ma, Q, Jones, D, Borghesani, P. R, Segal, R. A, Nagasawa, T, Kishimoto, T, Bronson, R. T, & Springer, T. A. (1998) Impaired b-lymphopoiesis, myelopoiesis, and derailed cerebellar neuron migration in cxcr4- and sdf-1-deficient mice. *Proc Natl Acad Sci USA* **95**, 9448–53.

[169] Ratajczak, M. Z, Zuba-Surma, E, Kucia, M, Reca, R, Wojakowski, W, & Ratajczak, J. (2006) The pleiotropic effects of the sdf-1-cxcr4 axis in organogenesis, regeneration and tumorigenesis. *Leukemia* **20**, 1915–24.

[170] Nagasawa, T, Hirota, S, Tachibana, K, Takakura, N, Nishikawa, S, Kitamura, Y, Yoshida, N, Kikutani, H, & Kishimoto, T. (1996) Defects of b-cell lymphopoiesis and bone-marrow myelopoiesis in mice lacking the cxc chemokine pbsf/sdf-1. *Nature* **382**, 635–8.

[171] Zou, Y. R, Kottmann, A. H, Kuroda, M, Taniuchi, I, & Littman, D. R. (1998) Function of the chemokine receptor cxcr4 in haematopoiesis and in cerebellar development. *Nature* **393**, 595–9.

[172] Tachibana, K, Hirota, S, Iizasa, H, Yoshida, H, Kawabata, K, Kataoka, Y, Kitamura, Y, Matsushima, K, Yoshida, N, Nishikawa, S, Kishimoto, T, & Nagasawa, T. (1998) The chemokine receptor cxcr4 is essential for vascularization of the gastrointestinal tract. *Nature* **393**, 591–4.

[173] Roth, C. B, Hanson, M. A, & Stevens, R. C. (2008) Stabilization of the human beta2-adrenergic receptor tm4-tm3-tm5 helix interface by mutagenesis of glu122(3.41), a critical residue in gpcr structure. *Journal of Molecular Biology* **376**, 1305–19.

[174] Crump, M. P, Gong, J. H, Loetscher, P, Rajarathnam, K, Amara, A, Arenzana-Seisdedos, F, Virelizier, J. L, Baggiolini, M, Sykes, B. D, & Clark-Lewis, I. (1997) Solution structure and basis for functional activity of stromal cell-derived factor-1; dissociation of cxcr4 activation from binding and inhibition of hiv-1. *EMBO J* **16**, 6996–7007.

[175] Kofuku, Y, Yoshiura, C, Ueda, T, Terasawa, H, Hirai, T, Tominaga, S, Hirose, M, Maeda, Y, Takahashi, H, Terashima, Y, Matsushima, K, & Shimada, I. (2009) Structural basis of the interaction between chemokine stromal cell-derived factor-1/cxcl12 and its g-protein-coupled receptor cxcr4. *J Biol Chem* **284**, 35240–50.

[176] Gouwy, M, Struyf, S, Berghmans, N, Vanormelingen, C, Schols, D, & Damme, J. V. (2011) Cxcr4 and ccr5 ligands cooperate in monocyte and lymphocyte migration and in inhibition of dual-tropic (r5/x4) hiv-1 infection. *Eur. J. Immunol.* **41**, 963–73.

[177] Gorry, P. R & Ancuta, P. (2011) Coreceptors and hiv-1 pathogenesis. *Curr HIV/AIDS Rep* **8**, 45–53.

[178] Sterjovski, J, Roche, M, Churchill, M. J, Ellett, A, Farrugia, W, Gray, L. R, Cowley, D, Poumbourios, P, Lee, B, Wesselingh, S. L, Cunningham, A. L, Ramsland, P. A, & Gorry,

P. R. (2010) An altered and more efficient mechanism of ccr5 engagement contributes to macrophage tropism of ccr5-using hiv-1 envelopes. *Virology* **404**, 269–78.

[179] Ugurel, S, Schrama, D, Keller, G, Schadendorf, D, Bröcker, E.-B, Houben, R, Zapatka, M, Fink, W, Kaufman, H. L, & Becker, J. C. (2008) Impact of the ccr5 gene polymorphism on the survival of metastatic melanoma patients receiving immunotherapy. *Cancer Immunol Immunother* **57**, 685–91.

[180] Tang, C.-H, Yamamoto, A, Lin, Y.-T, Fong, Y.-C, & Tan, T.-W. (2010) Involvement of matrix metalloproteinase-3 in ccl5/ccr5 pathway of chondrosarcomas metastasis. *Biochem Pharmacol* **79**, 209–17.

[181] Cao, Z, Xu, X, Luo, X, Li, L, Huang, B, Li, X, Tao, D, Hu, J, & Gong, J. (2011) Role of rantes and its receptor in gastric cancer metastasis. *J Huazhong Univ Sci Technol Med Sci* **31**, 342–7.

[182] Qin, Y, Verdegaal, E. M. E, Siderius, M, Bebelman, J. P, Smit, M. J, Leurs, R, Willemze, R, Tensen, C. P, & Osanto, S. (2011) Quantitative expression profiling of g-protein-coupled receptors (gpcrs) in metastatic melanoma: the constitutively active orphan gpcr gpr18 as novel drug target. *Pigment Cell Melanoma Res* **24**, 207–18.

[183] Alkhatib, G, Combadiere, C, Broder, C. C, Feng, Y, Kennedy, P. E, Murphy, P. M, & Berger, E. A. (1996) Cc ckr5: a rantes, mip-1alpha, mip-1beta receptor as a fusion cofactor for macrophage-tropic hiv-1. *Science* **272**, 1955–8.

[184] Oberlin, E, Amara, A, Bachelerie, F, Bessia, C, Virelizier, J. L, Arenzana-Seisdedos, F, Schwartz, O, Heard, J. M, Clark-Lewis, I, Legler, D. F, Loetscher, M, Baggiolini, M, & Moser, B. (1996) The cxc chemokine sdf-1 is the ligand for lestr/fusin and prevents infection by t-cell-line-adapted hiv-1. *Nature* **382**, 833–5.

[185] Feng, Y, Broder, C. C, Kennedy, P. E, & Berger, E. A. (1996) Hiv-1 entry cofactor: functional cdna cloning of a seven-transmembrane, g protein-coupled receptor. *Science* **272**, 872–7.

[186] Deng, H, Liu, R, Ellmeier, W, Choe, S, Unutmaz, D, Burkhart, M, Marzio, P. D, Marmon, S, Sutton, R. E, Hill, C. M, Davis, C. B, Peiper, S. C, Schall, T. J, Littman, D. R, & Landau, N. R. (1996) Identification of a major co-receptor for primary isolates of hiv-1. *Nature* **381**, 661–6.

[187] Connor, R. I, Sheridan, K. E, Ceradini, D, Choe, S, & Landau, N. R. (1997) Change in coreceptor use correlates with disease progression in hiv-1–infected individuals. *J Exp Med* **185**, 621–8.

[188] Glushakova, S, Yi, Y, Grivel, J. C, Singh, A, Schols, D, Clercq, E. D, Collman, R. G, & Margolis, L. (1999) Preferential coreceptor utilization and cytopathicity by dual-tropic hiv-1 in human lymphoid tissue ex vivo. *J Clin Invest* **104**, R7–R11.

[189] Doranz, B. J, Rucker, J, Yi, Y, Smyth, R. J, Samson, M, Peiper, S. C, Parmentier, M, Collman, R. G, & Doms, R. W. (1996) A dual-tropic primary hiv-1 isolate that uses fusin and the beta-chemokine receptors ckr-5, ckr-3, and ckr-2b as fusion cofactors. *Cell* **85**, 1149–58.

[190] Schols, D, Struyf, S, Damme, J. V, Esté, J. A, Henson, G, & Clercq, E. D. (1997) Inhibition of t-tropic hiv strains by selective antagonization of the chemokine receptor cxcr4. *J Exp Med* **186**, 1383–8.

[191] Doms, R. W & Moore, J. P. (2000) Hiv-1 membrane fusion: targets of opportunity. *J Cell Biol* **151**, F9–14.

[192] Doms, R. W & Trono, D. (2000) The plasma membrane as a combat zone in the hiv battlefield. *Genes & Development* **14**, 2677–88.

[193] Chabot, D. J & Broder, C. C. (2000) Substitutions in a homologous region of extracellular loop 2 of cxcr4 and ccr5 alter coreceptor activities for hiv-1 membrane fusion and virus entry. *J Biol Chem* **275**, 23774–82.

[194] Weissman, D, Rabin, R. L, Arthos, J, Rubbert, A, Dybul, M, Swofford, R, Venkatesan, S, Farber, J. M, & Fauci, A. S. (1997) Macrophage-tropic hiv and siv envelope proteins induce a signal through the ccr5 chemokine receptor. *Nature* **389**, 981.

[195] Davis, C. B, Dikic, I, Unutmaz, D, Hill, C. M, Arthos, J, Siani, M. A, Thompson, D. A, Schlessinger, J, & Littman, D. R. (1997) Signal transduction due to hiv-1 envelope interactions with chemokine receptors cxcr4 or ccr5. *J Exp Med* **186**, 1793.

[196] Zaitseva, M, Peden, K, & Golding, H. (2003) Hiv coreceptors: role of structure, post-translational modifications, and internalization in viral-cell fusion and as targets for entry inhibitors. *Biochim Biophys Acta* **1614**, 51–61.

[197] Oppermann, M. (2004) Chemokine receptor ccr5: insights into structure, function, and regulation. *Cellular Signalling* **16**, 1201–10.

[198] Wang, J, Babcock, G. J, Choe, H, Farzan, M, Sodroski, J, & Gabuzda, D. (2004) N-linked glycosylation in the cxcr4 n-terminus inhibits binding to hiv-1 envelope glycoproteins. *Virology* **324**, 140–150.

[199] Sloane, A. J, Raso, V, Dimitrov, D. S, Xiao, X, Deo, S, Muljadi, N, Restuccia, D, Turville, S, Kearney, C, Broder, C. C, Zoellner, H, Cunningham, A. L, Bendall, L, & Lynch, G. W. (2005) Marked structural and functional heterogeneity in cxcr4: Separation of hiv-1 and sdf-1alpha responses. *Immunol Cell Biol* **83**, 129–143.

[200] Vicari, A. P & Caux, C. (2002) Chemokines in cancer. *Cytokine Growth Factor Rev* **13**, 143–54.

[201] Tanaka, T, Bai, Z, Srinoulprasert, Y, Yang, B.-G, Yang, B, Hayasaka, H, & Miyasaka, M. (2005) Chemokines in tumor progression and metastasis. *Cancer Science* **96**, 317–22.

[202] Kryczek, I, Wei, S, Keller, E, Liu, R, & Zou, W. (2007) Stroma-derived factor (sdf-1/cxcl12) and human tumor pathogenesis. *Am J Physiol, Cell Physiol* **292**, C987–95.

[203] Kim, H. K, Sierra, M. D. L. L, Williams, C. K, Gulino, A. V, & Tosato, G. (2006) G-csf down-regulation of cxcr4 expression identified as a mechanism for mobilization of myeloid cells. *Blood* **108**, 812–20.

[204] Burger, J. A & Kipps, T. J. (2006) Cxcr4: a key receptor in the crosstalk between tumor cells and their microenvironment. *Blood* **107**, 1761–7.

[205] Balkwill, F. (2004) The significance of cancer cell expression of the chemokine receptor cxcr4. *Semin Cancer Biol* **14**, 171–9.

[206] Karnoub, A. E, Dash, A. B, Vo, A. P, Sullivan, A, Brooks, M. W, Bell, G. W, Richardson, A. L, Polyak, K, Tubo, R, & Weinberg, R. A. (2007) Mesenchymal stem cells within tumour stroma promote breast cancer metastasis. *Nature* **449**, 557–63.

[207] Borczuk, A. C, Papanikolaou, N, Toonkel, R. L, Sole, M, Gorenstein, L. A, Ginsburg, M. E, Sonett, J. R, Friedman, R. A, & Powell, C. A. (2008) Lung adenocarcinoma invasion in tgfbetarii-deficient cells is mediated by ccl5/rantes. *Oncogene* **27**, 557–64.

[208] Clark-Lewis, I, Kim, K. S, Rajarathnam, K, Gong, J. H, Dewald, B, Moser, B, Baggiolini, M, & Sykes, B. D. (1995) Structure-activity relationships of chemokines. *Journal of Leukocyte Biology* **57**, 703–11.

[209] Clore, G. M & Gronenborn, A. M. (1995) Three-dimensional structures of alpha and beta chemokines. *FASEB J* **9**, 57–62.

[210] Rollins, B. J. (1997) Chemokines. *Blood* **90**, 909–28.

[211] Suratt, B. T, Petty, J. M, Young, S. K, Malcolm, K. C, Lieber, J. G, Nick, J. A, Gonzalo, J.-A, Henson, P. M, & Worthen, G. S. (2004) Role of the cxcr4/sdf-1 chemokine axis in circulating neutrophil homeostasis. *Blood* **104**, 565–71.

[212] Bizzarri, C, Beccari, A. R, Bertini, R, Cavicchia, M. R, Giorgini, S, & Allegretti, M. (2006) Elr+ cxc chemokines and their receptors (cxc chemokine receptor 1 and cxc chemokine receptor 2) as new therapeutic targets. *Pharmacol Ther* **112**, 139–49.

[213] Constantin, G, Majeed, M, Giagulli, C, Piccio, L, Kim, J. Y, Butcher, E. C, & Laudanna, C. (2000) Chemokines trigger immediate beta2 integrin affinity and mobility changes: differential regulation and roles in lymphocyte arrest under flow. *Immunity* **13**, 759–69.

[214] Le, Y, Zhou, Y, Iribarren, P, & Wang, J. (2004) Chemokines and chemokine receptors: their manifold roles in homeostasis and disease. *Cell Mol Immunol* **1**, 95–104.

[215] Zlotnik, A, Yoshie, O, & Nomiyama, H. (2006) The chemokine and chemokine receptor superfamilies and their molecular evolution. *Genome Biol* **7**, 243.

[216] Balestrieri, M. L, Balestrieri, A, Mancini, F. P, & Napoli, C. (2008) Understanding the immunoangiostatic cxc chemokine network. *Cardiovasc Res* **78**, 250–6.

[217] Bazan, J. F, Bacon, K. B, Hardiman, G, Wang, W, Soo, K, Rossi, D, Greaves, D. R, Zlotnik, A, & Schall, T. J. (1997) A new class of membrane-bound chemokine with a cx3c motif. *Nature* **385**, 640–4.

[218] Laing, K. J & Secombes, C. J. (2004) Chemokines. *Dev Comp Immunol* **28**, 443–60.

[219] Brandes, M, Legler, D. F, Spoerri, B, Schaerli, P, & Moser, B. (2000) Activation-dependent modulation of b lymphocyte migration to chemokines. *Int Immunol* **12**, 1285–92.

[220] Zlotnik, A & Yoshie, O. (2000) Chemokines: a new classification system and their role in immunity. *Immunity* **12**, 121–7.

[221] Cyster, J. G. (1999) Chemokines and cell migration in secondary lymphoid organs. *Science* **286**, 2098–102.

[222] Ngo, V. N, Korner, H, Gunn, M. D, Schmidt, K. N, Riminton, D. S, Cooper, M. D, Browning, J. L, Sedgwick, J. D, & Cyster, J. G. (1999) Lymphotoxin alpha/beta and tumor necrosis factor are required for stromal cell expression of homing chemokines in b and t cell areas of the spleen. *J Exp Med* **189**, 403–12.

[223] Gozansky, E. K, Louis, J. M, Caffrey, M, & Clore, G. M. (2005) Mapping the binding of the n-terminal extracellular tail of the cxcr4 receptor to stromal cell-derived factor-1alpha. *Journal of Molecular Biology* **345**, 651–8.

[224] Hoover, D. M, Mizoue, L. S, Handel, T. M, & Lubkowski, J. (2000) The crystal structure of the chemokine domain of fractalkine shows a novel quaternary arrangement. *J Biol Chem* **275**, 23187–93.

[225] Laurence, J. S, Blanpain, C, Burgner, J. W, Parmentier, M, & LiWang, P. J. (2000) Cc chemokine mip-1 beta can function as a monomer and depends on phe13 for receptor binding. *Biochemistry* **39**, 3401–9.

[226] Paavola, C. D, Hemmerich, S, Grunberger, D, Polsky, I, Bloom, A, Freedman, R, Mulkins, M, Bhakta, S, McCarley, D, Wiesent, L, Wong, B, Jarnagin, K, & Handel, T. M. (1998) Monomeric monocyte chemoattractant protein-1 (mcp-1) binds and activates the mcp-1 receptor ccr2b. *J Biol Chem* **273**, 33157–65.

[227] Salanga, C. L & Handel, T. M. (2011) Chemokine oligomerization and interactions with receptors and glycosaminoglycans: the role of structural dynamics in function. *Exp Cell Res* **317**, 590–601.

[228] Nesmelova, I. V, Sham, Y, Gao, J, & Mayo, K. H. (2008) Cxc and cc chemokines form mixed heterodimers: association free energies from molecular dynamics simulations and experimental correlations. *J Biol Chem* **283**, 24155–66.

[229] Mayo, K. H & Chen, M. J. (1989) Human platelet factor 4 monomer-dimer-tetramer equilibria investigated by 1h nmr spectroscopy. *Biochemistry* **28**, 9469–78.

[230] Nesmelova, I. V, Sham, Y, Dudek, A. Z, van Eijk, L. I, Wu, G, Slungaard, A, Mortari, F, Griffioen, A. W, & Mayo, K. H. (2005) Platelet factor 4 and interleukin-8 cxc chemokine heterodimer formation modulates function at the quaternary structural level. *J Biol Chem* **280**, 4948–58.

[231] Ryu, E. K, Kim, T. G, Kwon, T. H, Jung, I. D, Ryu, D, Park, Y.-M, Kim, J, Ahn, K. H, & Ban, C. (2007) Crystal structure of recombinant human stromal cell-derived factor-1alpha. *Proteins* **67**, 1193–7.

[232] Lodi, P. J, Garrett, D. S, Kuszewski, J, Tsang, M. L, Weatherbee, J. A, Leonard, W. J, Gronenborn, A. M, & Clore, G. M. (1994) High-resolution solution structure of the beta chemokine hmip-1 beta by multidimensional nmr. *Science* **263**, 1762–7.

[233] Proudfoot, A. E. I, Handel, T. M, Johnson, Z, Lau, E. K, LiWang, P, Clark-Lewis, I, Borlat, F, Wells, T. N. C, & Kosco-Vilbois, M. H. (2003) Glycosaminoglycan binding and oligomerization are essential for the in vivo activity of certain chemokines. *Proc Natl Acad Sci USA* **100**, 1885–90.

[234] Hoogewerf, A. J, Kuschert, G. S, Proudfoot, A. E, Borlat, F, Clark-Lewis, I, Power, C. A, & Wells, T. N. (1997) Glycosaminoglycans mediate cell surface oligomerization of chemokines. *Biochemistry* **36**, 13570–8.

[235] Jin, H, Shen, X, Baggett, B. R, Kong, X, & Liwang, P. J. (2007) The human cc chemokine mip-1beta dimer is not competent to bind to the ccr5 receptor. *J Biol Chem* **282**, 27976–83.

[236] Johnson, Z, Proudfoot, A. E, & Handel, T. M. (2005) Interaction of chemokines and glycosaminoglycans: a new twist in the regulation of chemokine function with opportunities for therapeutic intervention. *Cytokine Growth Factor Rev* **16**, 625–36.

[237] Koenen, R. R, von Hundelshausen, P, Nesmelova, I. V, Zernecke, A, Liehn, E. A, Sarabi, A, Kramp, B. K, Piccinini, A. M, Paludan, S. R, Kowalska, M. A, Kungl, A. J, Hackeng, T. M, Mayo, K. H, & Weber, C. (2009) Disrupting functional interactions between platelet chemokines inhibits atherosclerosis in hyperlipidemic mice. *Nature Medicine* **15**, 97–103.

[238] von Hundelshausen, P, Weber, K. S, Huo, Y, Proudfoot, A. E, Nelson, P. J, Ley, K, & Weber, C. (2001) Rantes deposition by platelets triggers monocyte arrest on inflamed and atherosclerotic endothelium. *Circulation* **103**, 1772–7.

[239] Mackay, C. R. (2001) Chemokines: immunology's high impact factors. *Nat Immunol* **2**, 95–101.

[240] Luther, S. A & Cyster, J. G. (2001) Chemokines as regulators of t cell differentiation. *Nat Immunol* **2**, 102–7.

[241] Mellado, M, Rodríguez-Frade, J. M, Mañes, S, & Martínez-A, C. (2001) Chemokine signaling and functional responses: the role of receptor dimerization and tk pathway activation. *Annu Rev Immunol* **19**, 397–421.

[242] Mellado, M, Rodríguez-Frade, J. M, Aragay, A, del Real, G, Martín, A. M, Vila-Coro, A. J, Serrano, A, Mayor, F, & Martínez-A, C. (1998) The chemokine monocyte chemotactic protein 1 triggers janus kinase 2 activation and tyrosine phosphorylation of the ccr2b receptor. *J Immunol* **161**, 805–13.

[243] Cardin, A. D & Weintraub, H. J. (1989) Molecular modeling of protein-glycosaminoglycan interactions. *Arteriosclerosis* **9**, 21–32.

[244] Gerard, C & Rollins, B. J. (2001) Chemokines and disease. *Nat Immunol* **2**, 108–15.

[245] Moser, B & Loetscher, P. (2001) Lymphocyte traffic control by chemokines. *Nat Immunol* **2**, 123–8.

[246] Witt, D. P & Lander, A. D. (1994) Differential binding of chemokines to glycosaminoglycan subpopulations. *Curr Biol* **4**, 394–400.

[247] Weber, K. S, von Hundelshausen, P, Clark-Lewis, I, Weber, P. C, & Weber, C. (1999) Differential immobilization and hierarchical involvement of chemokines in monocyte arrest and transmigration on inflamed endothelium in shear flow. *Eur J Immunol* **29**, 700–12.

[248] Colditz, I. G, Schneider, M. A, Pruenster, M, & Rot, A. (2007) Chemokines at large: in-vivo mechanisms of their transport, presentation and clearance. *Thromb Haemost* **97**, 688–93.

[249] Maghazachi, A. A, Al-Aoukaty, A, & Schall, T. J. (1996) Cc chemokines induce the generation of killer cells from cd56+ cells. *Eur. J. Immunol.* **26**, 315–9.

[250] Dorner, B. G, Scheffold, A, Rolph, M. S, Huser, M. B, Kaufmann, S. H. E, Radbruch, A, Flesch, I. E. A, & Kroczek, R. A. (2002) Mip-1alpha, mip-1beta, rantes, and atac/lymphotactin function together with ifn-gamma as type 1 cytokines. *Proc Natl Acad Sci USA* **99**, 6181–6.

[251] Godiska, R, Chantry, D, Dietsch, G. N, & Gray, P. W. (1995) Chemokine expression in murine experimental allergic encephalomyelitis. *J Neuroimmunol* **58**, 167–76.

[252] Robinson, E, Keystone, E. C, Schall, T. J, Gillett, N, & Fish, E. N. (1995) Chemokine expression in rheumatoid arthritis (ra): evidence of rantes and macrophage inflammatory protein (mip)-1 beta production by synovial t cells. *Clin Exp Immunol* **101**, 398–407.

[253] Kurashima, K, Mukaida, N, Fujimura, M, Schröder, J. M, Matsuda, T, & Matsushima, K. (1996) Increase of chemokine levels in sputum precedes exacerbation of acute asthma attacks. *Journal of Leukocyte Biology* **59**, 313–6.

[254] Cocchi, F, DeVico, A. L, Garzino-Demo, A, Arya, S. K, Gallo, R. C, & Lusso, P. (1995) Identification of rantes, mip-1 alpha, and mip-1 beta as the major hiv-suppressive factors produced by cd8+ t cells. *Science* **270**, 1811–5.

[255] Gordon, C. J, Muesing, M. A, Proudfoot, A. E, Power, C. A, Moore, J. P, & Trkola, A. (1999) Enhancement of human immunodeficiency virus type 1 infection by the cc-chemokine rantes is independent of the mechanism of virus-cell fusion. *Journal of Virology* **73**, 684–94.

[256] Czaplewski, L. G, McKeating, J, Craven, C. J, Higgins, L. D, Appay, V, Brown, A, Dudgeon, T, Howard, L. A, Meyers, T, Owen, J, Palan, S. R, Tan, P, Wilson, G, Woods, N. R, Heyworth, C. M, Lord, B. I, Brotherton, D, Christison, R, Craig, S, Cribbes, S, Edwards, R. M, Evans, S. J, Gilbert, R, Morgan, P, Randle, E, Schofield, N, Varley, P. G, Fisher, J, Waltho, J. P, & Hunter, M. G. (1999) Identification of amino acid residues critical for aggregation of human cc chemokines macrophage inflammatory protein (mip)-1alpha, mip-1beta, and rantes. characterization of active disaggregated chemokine variants. *J Biol Chem* **274**, 16077–84.

[257] Daugherty, B. L, Siciliano, S. J, DeMartino, J. A, Malkowitz, L, Sirotina, A, & Springer, M. S. (1996) Cloning, expression, and characterization of the human eosinophil eotaxin receptor. *J Exp Med* **183**, 2349–54.

[258] Struyf, S, Menten, P, Lenaerts, J. P, Put, W, D'Haese, A, Clercq, E. D, Schols, D, Proost, P, & Damme, J. V. (2001) Diverging binding capacities of natural ld78beta isoforms of macrophage inflammatory protein-1alpha to the cc chemokine receptors 1, 3 and 5 affect their anti-hiv-1 activity and chemotactic potencies for neutrophils and eosinophils. *Eur. J. Immunol.* **31**, 2170–8.

[259] Slimani, H, Charnaux, N, Mbemba, E, Saffar, L, Vassy, R, Vita, C, & Gattegno, L. (2003) Interaction of rantes with syndecan-1 and syndecan-4 expressed by human primary macrophages. *Biochim Biophys Acta* **1617**, 80–8.

[260] Proudfoot, A. E, Fritchley, S, Borlat, F, Shaw, J. P, Vilbois, F, Zwahlen, C, Trkola, A, Marchant, D, Clapham, P. R, & Wells, T. N. (2001) The bbxb motif of rantes is the principal site for heparin binding and controls receptor selectivity. *J Biol Chem* **276**, 10620–6.

[261] Ignatov, A, Robert, J, Gregory-Evans, C, & Schaller, H. C. (2006) Rantes stimulates ca2+ mobilization and inositol trisphosphate (ip3) formation in cells transfected with g protein-coupled receptor 75. *British Journal of Pharmacology* **149**, 490–7.

[262] Proudfoot, A. E, Power, C. A, Hoogewerf, A. J, Montjovent, M. O, Borlat, F, Offord, R. E, & Wells, T. N. (1996) Extension of recombinant human rantes by the retention of the initiating methionine produces a potent antagonist. *J Biol Chem* **271**, 2599–603.

[263] Kinter, A, Catanzaro, A, Monaco, J, Ruiz, M, Justement, J, Moir, S, Arthos, J, Oliva, A, Ehler, L, Mizell, S, Jackson, R, Ostrowski, M, Hoxie, J, Offord, R, & Fauci, A. S. (1998) Cc-chemokines enhance the replication of t-tropic strains of hiv-1 in cd4(+) t cells: role of signal transduction. *Proc Natl Acad Sci USA* **95**, 11880–5.

[264] Kelly, M. D, Naif, H. M, Adams, S. L, Cunningham, A. L, & Lloyd, A. R. (1998) Dichotomous effects of beta-chemokines on hiv replication in monocytes and monocyte-derived macrophages. *J Immunol* **160**, 3091–5.

[265] Proost, P, Meester, I. D, Schols, D, Struyf, S, Lambeir, A. M, Wuyts, A, Opdenakker, G, Clercq, E. D, Scharpé, S, & Damme, J. V. (1998) Amino-terminal truncation of chemokines by cd26/dipeptidyl-peptidase iv. conversion of rantes into a potent inhibitor of monocyte chemotaxis and hiv-1-infection. *J Biol Chem* **273**, 7222–7.

[266] Oravecz, T, Pall, M, Roderiquez, G, Gorrell, M. D, Ditto, M, Nguyen, N. Y, Boykins, R, Unsworth, E, & Norcross, M. A. (1997) Regulation of the receptor specificity and function of the chemokine rantes (regulated on activation, normal t cell expressed and secreted) by dipeptidyl peptidase iv (cd26)-mediated cleavage. *J Exp Med* **186**, 1865–72.

[267] Gong, J. H & Clark-Lewis, I. (1995) Antagonists of monocyte chemoattractant protein 1 identified by modification of functionally critical nh2-terminal residues. *J Exp Med* **181**, 631–40.

[268] Polo, S, Nardese, V, Santis, C. D, Arcelloni, C, Paroni, R, Sironi, F, Verani, A, Rizzi, M, Bolognesi, M, & Lusso, P. (2000) Enhancement of the hiv-1 inhibitory activity of rantes by modification of the n-terminal region: dissociation from ccr5 activation. *Eur. J. Immunol.* **30**, 3190–8.

[269] Amara, A, Gall, S. L, Schwartz, O, Salamero, J, Montes, M, Loetscher, P, Baggiolini, M, Virelizier, J. L, & Arenzana-Seisdedos, F. (1997) Hiv coreceptor downregulation as antiviral principle: Sdf-1alpha-dependent internalization of the chemokine receptor cxcr4 contributes to inhibition of hiv replication. *J Exp Med* **186**, 139–46.

[270] Simmons, G, Clapham, P. R, Picard, L, Offord, R. E, Rosenkilde, M. M, Schwartz, T. W, Buser, R, Wells, T. N, & Proudfoot, A. E. (1997) Potent inhibition of hiv-1 infectivity in macrophages and lymphocytes by a novel ccr5 antagonist. *Science* **276**, 276–9.

[271] Mosier, D. E, Picchio, G. R, Gulizia, R. J, Sabbe, R, Poignard, P, Picard, L, Offord, R. E, Thompson, D. A, & Wilken, J. (1999) Highly potent rantes analogues either prevent ccr5-using human immunodeficiency virus type 1 infection in vivo or rapidly select for cxcr4-using variants. *J Virol* **73**, 3544–50.

[272] Pastore, C, Picchio, G. R, Galimi, F, Fish, R, Hartley, O, Offord, R. E, & Mosier, D. E. (2003) Two mechanisms for human immunodeficiency virus type 1 inhibition by n-terminal modifications of rantes. *Antimicrob Agents Chemother* **47**, 509–17.

[273] Gaertner, H, Cerini, F, Escola, J.-M, Kuenzi, G, Melotti, A, Offord, R, Rossitto-Borlat, I, Nedellec, R, Salkowitz, J, Gorochov, G, Mosier, D, & Hartley, O. (2008) Highly potent, fully recombinant anti-hiv chemokines: reengineering a low-cost microbicide. *Proceedings of the National Academy of Sciences* **105**, 17706–11.

[274] Hartley, O, Gaertner, H, Wilken, J, Thompson, D, Fish, R, Ramos, A, Pastore, C, Dufour, B, Cerini, F, Melotti, A, Heveker, N, Picard, L, Alizon, M, Mosier, D, Kent, S, & Offord, R. (2004) Medicinal chemistry applied to a synthetic protein: development of highly potent hiv entry inhibitors. *Proc Natl Acad Sci USA* **101**, 16460–5.

[275] Kawamura, T, Bruse, S. E, Abraha, A, Sugaya, M, Hartley, O, Offord, R. E, Arts, E. J, Zimmerman, P. A, Blauvelt, A, & Bruce, S. E. (2004) Psc-rantes blocks r5 human immunodeficiency virus infection of langerhans cells isolated from individuals with a variety of ccr5 diplotypes. *J Virol* **78**, 7602–9.

[276] Skelton, N. J, Aspiras, F, Ogez, J, & Schall, T. J. (1995) Proton nmr assignments and solution conformation of rantes, a chemokine of the c-c type. *Biochemistry* **34**, 5329–42.

[277] Appay, V, Brown, A, Cribbes, S, Randle, E, & Czaplewski, L. G. (1999) Aggregation of rantes is responsible for its inflammatory properties. characterization of nonaggregating, noninflammatory rantes mutants. *J Biol Chem* **274**, 27505–12.

[278] Wang, X, Watson, C, Sharp, J. S, Handel, T. M, & Prestegard, J. H. (2011) Oligomeric structure of the chemokine ccl5/rantes from nmr, ms, and saxs data. *Structure* **19**, 1138–48.

[279] Lau, E. K, Paavola, C. D, Johnson, Z, Gaudry, J.-P, Geretti, E, Borlat, F, Kungl, A. J, Proudfoot, A. E, & Handel, T. M. (2004) Identification of the glycosaminoglycan binding site of the cc chemokine, mcp-1: implications for structure and function in vivo. *J Biol Chem* **279**, 22294–305.

[280] Swaminathan, G. J, Holloway, D. E, Colvin, R. A, Campanella, G. K, Papageorgiou, A. C, Luster, A. D, & Acharya, K. R. (2003) Crystal structures of oligomeric forms of the ip-10/cxcl10 chemokine. *Structure* **11**, 521–32.

[281] Ward, S. G & Westwick, J. (1998) Chemokines: understanding their role in t-lymphocyte biology. *Biochem J* **333 (Pt 3)**, 457–70.

[282] Bacon, K. B, Premack, B. A, Gardner, P, & Schall, T. J. (1995) Activation of dual t cell signaling pathways by the chemokine rantes. *Science* **269**, 1727–30.

[283] Bacon, K. B, Szabo, M. C, Yssel, H, Bolen, J. B, & Schall, T. J. (1996) Rantes induces tyrosine kinase activity of stably complexed p125fak and zap-70 in human t cells. *J Exp Med* **184**, 873–82.

[284] Kuang, Y, Wu, Y, Jiang, H, & Wu, D. (1996) Selective g protein coupling by c-c chemokine receptors. *J Biol Chem* **271**, 3975–8.

[285] Murooka, T. T, Wong, M. M, Rahbar, R, Majchrzak-Kita, B, Proudfoot, A. E. I, & Fish, E. N. (2006) Ccl5-ccr5-mediated apoptosis in t cells: Requirement for glycosaminoglycan binding and ccl5 aggregation. *J Biol Chem* **281**, 25184–94.

[286] Bennett, L. D, Fox, J. M, & Signoret, N. (2011) Mechanisms regulating chemokine receptor activity. *Immunology* **134**, 246–56.

[287] Yu, L, Cecil, J, Peng, S.-B, Schrementi, J, Kovacevic, S, Paul, D, Su, E. W, & Wang, J. (2006) Identification and expression of novel isoforms of human stromal cell-derived factor 1. *Gene* **374**, 174–9.

[288] Balabanian, K, Lagane, B, Infantino, S, Chow, K. Y. C, Harriague, J, Moepps, B, Arenzana-Seisdedos, F, Thelen, M, & Bachelerie, F. (2005) The chemokine sdf-1/cxcl12 binds to and signals through the orphan receptor rdc1 in t lymphocytes. *J Biol Chem* **280**, 35760–6.

[289] Veldkamp, C. T, Seibert, C, Peterson, F. C, Sakmar, T. P, & Volkman, B. F. (2006) Recognition of a cxcr4 sulfotyrosine by the chemokine stromal cell-derived factor-1alpha (sdf-1alpha/cxcl12). *Journal of Molecular Biology* **359**, 1400–9.

[290] Veldkamp, C. T, Seibert, C, Peterson, F. C, Cruz, N. B. D. L, Haugner, J. C, Basnet, H, Sakmar, T. P, & Volkman, B. F. (2008) Structural basis of cxcr4 sulfotyrosine recognition by the chemokine sdf-1/cxcl12. *Science Signaling* **1**, ra4–ra4.

[291] Amara, A, Lorthioir, O, Valenzuela, A, Magerus, A, Thelen, M, Montes, M, Virelizier, J. L, Delepierre, M, Baleux, F, Lortat-Jacob, H, & Arenzana-Seisdedos, F. (1999) Stromal cell-derived factor-1alpha associates with heparan sulfates through the first beta-strand of the chemokine. *J Biol Chem* **274**, 23916–25.

[292] Sadir, R, Baleux, F, Grosdidier, A, Imberty, A, & Lortat-Jacob, H. (2001) Characterization of the stromal cell-derived factor-1alpha-heparin complex. *J Biol Chem* **276**, 8288–96.

[293] Sadir, R, Imberty, A, Baleux, F, & Lortat-Jacob, H. (2004) Heparan sulfate/heparin oligosaccharides protect stromal cell-derived factor-1 (sdf-1)/cxcl12 against proteolysis induced by cd26/dipeptidyl peptidase iv. *J Biol Chem* **279**, 43854–60.

[294] Sierra, M. D. L. L, Yang, F, Narazaki, M, Salvucci, O, Davis, D, Yarchoan, R, Zhang, H. H, Fales, H, & Tosato, G. (2004) Differential processing of stromal-derived factor-1alpha and stromal-derived factor-1beta explains functional diversity. *Blood* **103**, 2452–9.

[295] Wiener, M. C. (2004) A pedestrian guide to membrane protein crystallization. *Methods* **34**, 364–72.

[296] Privé, G. G. (2007) Detergents for the stabilization and crystallization of membrane proteins. *Methods* **41**, 388–97.

[297] Newby, Z. E. R, O'Connell, J. D, Gruswitz, F, Hays, F. A, Harries, W. E. C, Harwood, I. M, Ho, J. D, Lee, J. K, Savage, D. F, Miercke, L. J. W, & Stroud, R. M. (2009) A general protocol for the crystallization of membrane proteins for x-ray structural investigation. *Nat Protoc* **4**, 619–37.

[298] le Maire, M, Champeil, P, & Moller, J. V. (2000) Interaction of membrane proteins and lipids with solubilizing detergents. *Biochim Biophys Acta* **1508**, 86–111.

[299] Heerklotz, H & Seelig, J. (2000) Titration calorimetry of surfactant-membrane partitioning and membrane solubilization. *Biochim Biophys Acta* **1508**, 69–85.

[300] Kragh-Hansen, U, le Maire, M, & Møller, J. V. (1998) The mechanism of detergent solubilization of liposomes and protein-containing membranes. *Biophys J* **75**, 2932–46.

[301] Seddon, A. M, Curnow, P, & Booth, P. J. (2004) Membrane proteins, lipids and detergents: not just a soap opera. *Biochim Biophys Acta* **1666**, 105–17.

[302] Nath, A, Atkins, W. M, & Sligar, S. G. (2007) Applications of phospholipid bilayer nanodiscs in the study of membranes and membrane proteins. *Biochemistry* **46**, 2059–69.

[303] Bayburt, T. H & Sligar, S. G. (2010) Membrane protein assembly into nanodiscs. *FEBS Letters* **584**, 1721–7.

[304] Denisov, I. G, Grinkova, Y. V, Lazarides, A. A, & Sligar, S. G. (2004) Directed self-assembly of monodisperse phospholipid bilayer nanodiscs with controlled size. *J Am Chem Soc* **126**, 3477–87.

[305] Bayburt, T. H & Sligar, S. G. (2002) Single-molecule height measurements on microsomal cytochrome p450 in nanometer-scale phospholipid bilayer disks. *Proc Natl Acad Sci USA* **99**, 6725–30.

[306] Rajesh, S, Knowles, T, & Overduin, M. (2011) Production of membrane proteins without cells or detergents. *New BIOTECHNOLOGY* **28**, 250–4.

[307] Leitz, A. J, Bayburt, T. H, Barnakov, A. N, Springer, B. A, & Sligar, S. G. (2006) Functional reconstitution of beta2-adrenergic receptors utilizing self-assembling nanodisc technology. *BioTechniques* **40**, 601–2, 604, 606, passim.

[308] Breyton, C, Pucci, B, & Popot, J.-L. (2010) Amphipols and fluorinated surfactants: Two alternatives to detergents for studying membrane proteins in vitro. *Methods Mol Biol* **601**, 219–45.

[309] Peyre, V, Patil, S, Durand, G, & Pucci, B. (2007) Mixtures of hydrogenated and fluorinated lactobionamide surfactants with cationic surfactants: study of hydrogenated and fluorinated chains miscibility through potentiometric techniques. *Langmuir* **23**, 11465–74.

[310] Barthélémy, P, Ameduri, B, Chabaud, E, Popot, J. L, & Pucci, B. (1999) Synthesis and preliminary assessments of ethyl-terminated perfluoroalkyl nonionic surfactants derived from tris(hydroxymethyl)acrylamidomethane. *Org Lett* **1**, 1689–92.

[311] Chabaud, E, Barthélémy, P, Mora, N, Popot, J. L, & Pucci, B. (1998) Stabilization of integral membrane proteins in aqueous solution using fluorinated surfactants. *Biochimie* **80**, 515–30.

[312] Breyton, C, Chabaud, E, Chaudier, Y, Pucci, B, & Popot, J.-L. (2004) Hemifluorinated surfactants: a non-dissociating environment for handling membrane proteins in aqueous solutions? *FEBS Letters* **564**, 312–8.

[313] Popot, J.-L. (2010) Amphipols, nanodiscs, and fluorinated surfactants: three nonconventional approaches to studying membrane proteins in aqueous solutions. *Annu Rev Biochem* **79**, 737–75.

[314] Park, K.-H, Berrier, C, Lebaupain, F, Pucci, B, Popot, J.-L, Ghazi, A, & Zito, F. (2007) Fluorinated and hemifluorinated surfactants as alternatives to detergents for membrane protein cell-free synthesis. *Biochem J* **403**, 183–7.

[315] Park, K.-H, Billon-Denis, E, Dahmane, T, Lebaupain, F, Pucci, B, Breyton, C, & Zito, F. (2011) In the cauldron of cell-free synthesis of membrane proteins: playing with new surfactants. *New BIOTECHNOLOGY* **28**, 255–61.

[316] Kyrychenko, A, Rodnin, M. V, Vargas-Uribe, M, Sharma, S. K, Durand, G, Pucci, B, Popot, J.-L, & Ladokhin, A. S. (2011) Folding of diphtheria toxin t-domain in the presence of amphipols and fluorinated surfactants: Toward thermodynamic measurements of membrane protein folding. *Biochim Biophys Acta*.

[317] Tribet, C, Audebert, R, & Popot, J. L. (1996) Amphipols: polymers that keep membrane proteins soluble in aqueous solutions. *Proc Natl Acad Sci USA* **93**, 15047–50.

[318] Champeil, P, Menguy, T, Tribet, C, Popot, J. L, & le Maire, M. (2000) Interaction of amphipols with sarcoplasmic reticulum ca2+-atpase. *J Biol Chem* **275**, 18623–37.

[319] Picard, M, Duval-Terrié, C, Dé, E, & Champeil, P. (2004) Stabilization of membranes upon interaction of amphipathic polymers with membrane proteins. *Protein Sci* **13**, 3056–8.

[320] Popot, J.-L, Berry, E. A, Charvolin, D, Creuzenet, C, Ebel, C, Engelman, D. M, Flötenmeyer, M, Giusti, F, Gohon, Y, Hong, Q, Lakey, J. H, Leonard, K, Shuman, H. A, Timmins, P, Warschawski, D. E, Zito, F, Zoonens, M, Pucci, B, & Tribet, C. (2003) Amphipols: polymeric surfactants for membrane biology research. *Cell Mol Life Sci* **60**, 1559–74.

[321] Gohon, Y, Dahmane, T, Ruigrok, R. W. H, Schuck, P, Charvolin, D, Rappaport, F, Timmins, P, Engelman, D. M, Tribet, C, Popot, J.-L, & Ebel, C. (2008) Bacteriorhodopsin/amphipol complexes: structural and functional properties. *Biophys J* **94**, 3523–37.

[322] Pocanschi, C. L, Dahmane, T, Gohon, Y, Rappaport, F, Apell, H.-J, Kleinschmidt, J. H, & Popot, J.-L. (2006) Amphipathic polymers: tools to fold integral membrane proteins to their active form. *Biochemistry* **45**, 13954–61.

[323] Picard, M, Dahmane, T, Garrigos, M, Gauron, C, Giusti, F, le Maire, M, Popot, J.-L, & Champeil, P. (2006) Protective and inhibitory effects of various types of amphipols on the ca2+-atpase from sarcoplasmic reticulum: a comparative study. *Biochemistry* **45**, 1861–9.

[324] Martinez, K. L, Gohon, Y, Corringer, P.-J, Tribet, C, Mérola, F, Changeux, J.-P, & Popot, J.-L. (2002) Allosteric transitions of torpedo acetylcholine receptor in lipids, detergent and amphipols: molecular interactions vs. physical constraints. *FEBS Letters* **528**, 251–6.

[325] Charvolin, D, Perez, J.-B, Rouvière, F, Giusti, F, Bazzacco, P, Abdine, A, Rappaport, F, Martinez, K. L, & Popot, J.-L. (2009) The use of amphipols as universal molecular adapters to immobilize membrane proteins onto solid supports. *Proceedings of the National Academy of Sciences* **106**, 405–10.

[326] Catoire, L. J, Damian, M, Giusti, F, Martin, A, van Heijenoort, C, Popot, J.-L, Guittet, E, & Banères, J.-L. (2010) Structure of a gpcr ligand in its receptor-bound state: leukotriene b4 adopts a highly constrained conformation when associated to human blt2. *J. Am. Chem. Soc.* **132**, 9049–57.

[327] Dahmane, T, Damian, M, Mary, S, Popot, J.-L, & Banères, J.-L. (2009) Amphipol-assisted in vitro folding of g protein-coupled receptors. *Biochemistry* **48**, 6516–21.

[328] Popot, J.-L, Althoff, T, Bagnard, D, Banères, J.-L, Bazzacco, P, Billon-Denis, E, Catoire, L. J, Champeil, P, Charvolin, D, Cocco, M. J, Crémel, G, Dahmane, T, de la Maza, L. M, Ebel, C, Gabel, F, Giusti, F, Gohon, Y, Goormaghtigh, E, Guittet, E, Kleinschmidt, J. H, Kühlbrandt, W, Bon, C. L, Martinez, K. L, Picard, M, Pucci, B, Sachs, J. N, Tribet, C, van Heijenoort, C, Wien, F, Zito, F, & Zoonens, M. (2011) Amphipols from a to z. *Annu Rev Biophys* **40**, 379–408.

[329] Gohon, Y, Pavlov, G, Timmins, P, Tribet, C, Popot, J.-L, & Ebel, C. (2004) Partial specific volume and solvent interactions of amphipol a8-35. *Analytical Biochemistry* **334**, 318–34.

[330] Gohon, Y, Giusti, F, Prata, C, Charvolin, D, Timmins, P, Ebel, C, Tribet, C, & Popot, J.-L. (2006) Well-defined nanoparticles formed by hydrophobic assembly of a short and polydisperse random terpolymer, amphipol a8-35. *Langmuir* **22**, 1281–90.

[331] Diab, C, Tribet, C, Gohon, Y, Popot, J.-L, & Winnik, F. M. (2007) Complexation of integral membrane proteins by phosphorylcholine-based amphipols. *Biochim Biophys Acta* **1768**, 2737–47.

[332] Dahmane, T, Giusti, F, Catoire, L. J, & Popot, J.-L. (2011) Sulfonated amphipols: Synthesis, properties, and applications. *Biopolymers* **95**, 811–823.

[333] Prata, C, Giusti, F, Gohon, Y, Pucci, B, Popot, J. L, & Tribet, C. (2000) Nonionic amphiphilic polymers derived from tris(hydroxymethyl)-acrylamidomethane keep membrane proteins soluble and native in the absence of detergent. *Biopolymers* **56**, 77–84.

[334] Bazzacco, P, Sharma, K. S, Durand, G, Giusti, F, Ebel, C, Popot, J.-L, & Pucci, B. (2009) Trapping and stabilization of integral membrane proteins by hydrophobically grafted glucose-based telomers. *Biomacromolecules* **10**, 3317–26.

[335] Sharma, K. S, Durand, G, Giusti, F, Olivier, B, Fabiano, A.-S, Bazzacco, P, Dahmane, T, Ebel, C, Popot, J.-L, & Pucci, B. (2008) Glucose-based amphiphilic telomers designed to keep membrane proteins soluble in aqueous solutions: synthesis and physicochemical characterization. *Langmuir* **24**, 13581–90.

[336] Sharma, K. S, Durand, G, Gabel, F, Bazzacco, P, Bon, C. L, Billon-Denis, E, Catoire, L. J, Popot, J.-L, Ebel, C, & Pucci, B. (2012) Non-ionic amphiphilic homopolymers: Synthesis, solution properties, and biochemical validation. *Langmuir : the ACS journal of surfaces and colloids*.

[337] Bazzacco, P, Billon-Denis, E, Sharma, K. S, Catoire, L. J, Mary, S, Bon, C. L, Point, E, Baneres, J.-L, Durand, G, Zito, F, Pucci, B, & Popot, J.-L. (2012) Non-ionic homopolymeric amphipols: Application to membrane protein folding, cell-free synthesis, and solution nmr. *Biochemistry*.

[338] Zoonens, M, Giusti, F, Zito, F, & Popot, J.-L. (2007) Dynamics of membrane protein/amphipol association studied by förster resonance energy transfer: implications for in vitro studies of amphipol-stabilized membrane proteins. *Biochemistry* **46**, 10392–404.

[339] Tribet, C, Audebert, R, & Popot, J.-L. (1997) Stabilization of hydrophobic colloidal dispersions in water with amphiphilic polymers: Application to integral membrane proteins. *Langmuir* **13**, 5570–5576.

[340] Catoire, L. J, Zoonens, M, van Heijenoort, C, Giusti, F, Popot, J.-L, & Guittet, E. (2009) Inter- and intramolecular contacts in a membrane protein/surfactant complex observed by heteronuclear dipole-to-dipole cross-relaxation. *Journal of Magnetic Resonance* **197**, 91–95.

[341] Zoonens, M, Catoire, L. J, Giusti, F, & Popot, J.-L. (2005) Nmr study of a membrane protein in detergent-free aqueous solution. *Proc Natl Acad Sci USA* **102**, 8893–8.

[342] Baneres, J.-L, Martin, A, Hullot, P, Girard, J.-P, Rossi, J.-C, & Parello, J. (2003) Structure-based analysis of gpcr function: conformational adaptation of both agonist and receptor upon leukotriene b4 binding to recombinant blt1. *Journal of Molecular Biology* **329**, 801–14.

[343] Althoff, T, Mills, D. J, Popot, J.-L, & Kühlbrandt, W. (2011) Arrangement of electron transport chain components in bovine mitochondrial supercomplex i(1)iii(2)iv(1). *EMBO J* **30**, 4652–4664.

[344] Flötenmeyer, M, Weiss, H, Tribet, C, Popot, J.-L, & Leonard, K. (2007) The use of amphipathic polymers for cryo electron microscopy of nadh:ubiquinone oxidoreductase (complex i). *J Microsc* **227**, 229–35.

[345] Cvetkov, T. L, Huynh, K. W, Cohen, M. R, & Moiseenkova-Bell, V. Y. (2011) Molecular architecture and subunit organization of trpa1 ion channel revealed by electron microscopy. *J Biol Chem* **286**, 38168–76.

[346] Nagy, J. K, Hoffmann, A. K, Keyes, M. H, Gray, D. N, Oxenoid, K, & Sanders, C. R. (2001) Use of amphipathic polymers to deliver a membrane protein to lipid bilayers. *FEBS Letters* **501**, 115–20.

[347] Catoire, L. J, Zoonens, M, van Heijenoort, C, Giusti, F, Guittet, E, & Popot, J.-L. (2010) Solution nmr mapping of water-accessible residues in the transmembrane beta-barrel of ompx. *Eur Biophys J* **39**, 623–30.

[348] Catoire, L. J, Damian, M, Baaden, M, Guittet, E, & Banères, J.-L. (2011) Electrostatically-driven fast association and perdeuteration allow detection of transferred cross-relaxation for g protein-coupled receptor ligands with equilibrium dissociation constants in the high-to-low nanomolar range. *J Biomol NMR* **50**, 191–5.

[349] Raschle, T, Hiller, S, Etzkorn, M, & Wagner, G. (2010) Nonmicellar systems for solution nmr spectroscopy of membrane proteins. *Current Opinion in Structural Biology* **20**, 471–479.

[350] Warschawski, D. E, Arnold, A. A, Beaugrand, M, Gravel, A, Chartrand, E, & Marcotte, I. (2011) Choosing membrane mimetics for nmr structural studies of transmembrane proteins. *Biochim Biophys Acta*.

[351] Wu, L, LaRosa, G, Kassam, N, Gordon, C. J, Heath, H, Ruffing, N, Chen, H, Humblias, J, Samson, M, Parmentier, M, Moore, J. P, & Mackay, C. R. (1997) Interaction of chemokine receptor ccr5 with its ligands: multiple domains for hiv-1 gp120 binding and a single domain for chemokine binding. *J Exp Med* **186**, 1373–81.

[352] Martin, L. J, Hähnke, M. J, Nitz, M, Wöhnert, J, Silvaggi, N. R, Allen, K. N, Schwalbe, H, & Imperiali, B. (2007) Double-lanthanide-binding tags: Design, photophysical properties, and nmr applications. *J. Am. Chem. Soc.* **129**, 7106–7113.

[353] Evans, W. J. (2007) The importance of questioning scientific assumptions: some lessons from f element chemistry. *Inorg Chem* **46**, 3435–49.

[354] Silvaggi, N. R, Martin, L. J, Schwalbe, H, Imperiali, B, & Allen, K. N. (2007) Double-lanthanide-binding tags for macromolecular crystallographic structure determination. *J. Am. Chem. Soc.* **129**, 7114–7120.

[355] Franz, K. J, Nitz, M, & Imperiali, B. (2003) Lanthanide-binding tags as versatile protein coexpression probes. *ChemBioChem* **4**, 265–71.

[356] Wöhnert, J, Franz, K. J, Nitz, M, Imperiali, B, & Schwalbe, H. (2003) Protein alignment by a coexpressed lanthanide-binding tag for the measurement of residual dipolar couplings. *J. Am. Chem. Soc.* **125**, 13338–9.

[357] Su, X.-C, Huber, T, Dixon, N. E, & Otting, G. (2006) Site-specific labelling of proteins with a rigid lanthanide-binding tag. *ChemBioChem* **7**, 1599–1604.

[358] Goda, N, Tenno, T, Inomata, K, Iwaya, N, Sasaki, Y, Shirakawa, M, & Hiroaki, H. (2007) Lbt/ptd dual tagged vector for purification, cellular protein delivery and visualization in living cells. *Biochim Biophys Acta* **1773**, 141–6.

[359] Sculimbrene, B. R & Imperiali, B. (2006) Lanthanide-binding tags as luminescent probes for studying protein interactions. *J. Am. Chem. Soc.* **128**, 7346–52.

[360] Leyris, J.-P, Roux, T, Trinquet, E, Verdié, P, Fehrentz, J.-A, Oueslati, N, Douzon, S, Bourrier, E, Lamarque, L, Gagne, D, Galleyrand, J.-C, M'kadmi, C, Martinez, J, Mary, S, Banères, J.-L, & Marie, J. (2011) Homogeneous time-resolved fluorescence-based assay to screen for ligands targeting the growth hormone secretagogue receptor type 1a. *Analytical Biochemistry* **408**, 253–62.

[361] Cho, H.-J, Lee, Y, Chang, R. S, Hahm, M.-S, Kim, M.-K, Kim, Y. B, & Oh, Y.-K. (2008) Maltose binding protein facilitates high-level expression and functional purification of the chemokines rantes and sdf-1alpha from escherichia coli. *Protein Expression and Purification* **60**, 37–45.

[362] Tolia, N. H & Joshua-Tor, L. (2006) Strategies for protein coexpression in escherichia coli. *Nat Methods* **3**, 55–64.

[363] Fox, J. D & Waugh, D. S. (2003) Maltose-binding protein as a solubility enhancer. *Methods Mol Biol* **205**, 99–117.

[364] Proudfoot, A. E. I & Borlat, F. (2000) Purification of recombinant chemokines from e. coli. *Methods in Molecular Biology* **138**, 75–87.

[365] Hammarström, M, Hellgren, N, van Den Berg, S, Berglund, H, & Härd, T. (2002) Rapid screening for improved solubility of small human proteins produced as fusion proteins in escherichia coli. *Protein Sci* **11**, 313–21.

[366] Kapust, R. B & Waugh, D. S. (1999) Escherichia coli maltose-binding protein is uncommonly effective at promoting the solubility of polypeptides to which it is fused. *Protein Sci* **8**, 1668–74.

[367] Shih, Y.-P, Kung, W.-M, Chen, J.-C, Yeh, C.-H, Wang, A. H.-J, & Wang, T.-F. (2002) High-throughput screening of soluble recombinant proteins. *Protein Sci* **11**, 1714–9.

[368] Allen, K. N & Imperiali, B. (2010) Lanthanide-tagged proteins–an illuminating partnership. *Current Opinion in Chemical Biology* **14**, 247–54.

[369] Albizu, L, Cottet, M, Kralikova, M, Stoev, S, Seyer, R, Brabet, I, Roux, T, Bazin, H, Bourrier, E, Lamarque, L, Breton, C, Rives, M.-L, Newman, A, Javitch, J, Trinquet, E, Manning, M, Pin, J.-P, Mouillac, B, & Durroux, T. (2010) Time-resolved fret between gpcr ligands reveals oligomers in native tissues. *Nat Chem Biol* **6**, 587–94.

[370] Martin, L, Blanpain, C, Garnier, P, Wittamer, V, Parmentier, M, & Vita, C. (2001) Structural and functional analysis of the rantes-glycosaminoglycans interactions. *Biochemistry* **40**, 6303–18.

[371] Proudfoot, A. E & Borlat, F. (2000) Purification of recombinant chemokines from e. coli. *Methods Mol Biol* **138**, 75–87.

[372] Navratilova, I, Dioszegi, M, & Myszka, D. G. (2006) Analyzing ligand and small molecule binding activity of solubilized gpcrs using biosensor technology. *Analytical Biochemistry* **355**, 132–9.

[373] Oprian, D. D, Molday, R. S, Kaufman, R. J, & Khorana, H. G. (1987) Expression of a synthetic bovine rhodopsin gene in monkey kidney cells. *Proc Natl Acad Sci USA* **84**, 8874–8.

[374] Myszka, D. G. (1999) Improving biosensor analysis. *J Mol Recognit* **12**, 279–84.

[375] Rich, R. L & Myszka, D. G. (2000) Advances in surface plasmon resonance biosensor analysis. *Curr Opin Biotechnol* **11**, 54–61.

[376] Rich, R. L, Errey, J, Marshall, F, & Myszka, D. G. (2011) Biacore analysis with stabilized g-protein-coupled receptors. *Analytical Biochemistry* **409**, 267–72.

[377] Sarramegna, V, Muller, I, Mousseau, G, Froment, C, Monsarrat, B, Milon, A, & Talmont, F. (2005) Solubilization, purification, and mass spectrometry analysis of the human mu-opioid receptor expressed in pichia pastoris. *Protein Expr Purif* **43**, 85–93.

[378] Mouillac, B, Caron, M, Bonin, H, Dennis, M, & Bouvier, M. (1992) Agonist-modulated palmitoylation of beta 2-adrenergic receptor in sf9 cells. *J Biol Chem* **267**, 21733–7.

[379] Reeves, P. J, Kim, J.-M, & Khorana, H. G. (2002) Structure and function in rhodopsin: a tetracycline-inducible system in stable mammalian cell lines for high-level expression of opsin mutants. *Proc Natl Acad Sci USA* **99**, 13413–8.

[380] Panneels, V, Kock, I, Krijnse-Locker, J, Rezgaoui, M, & Sinning, I. (2011) Drosophila photoreceptor cells exploited for the production of eukaryotic membrane proteins: receptors, transporters and channels. *PLoS ONE* **6**, e18478.

[381] Zhang, L, Salom, D, He, J, Okun, A, Ballesteros, J, Palczewski, K, & Li, N. (2005) Expression of functional g protein-coupled receptors in photoreceptors of transgenic xenopus laevis. *Biochemistry* **44**, 14509–18.

[382] Li, N, Salom, D, Zhang, L, Harris, T, Ballesteros, J. A, Golczak, M, Jastrzebska, B, Palczewski, K, Kurahara, C, Juan, T, Jordan, S, & Salon, J. A. (2007) Heterologous expression of the adenosine a1 receptor in transgenic mouse retina. *Biochemistry* **46**, 8350–9.

[383] Klammt, C, Schwarz, D, Eifler, N, Engel, A, Piehler, J, Haase, W, Hahn, S, Dötsch, V, & Bernhard, F. (2007) Cell-free production of g protein-coupled receptors for functional and structural studies. *Journal of Structural Biology* **158**, 482–93.

[384] Banères, J. L, Roquet, F, Green, M, LeCalvez, H, & Parello, J. (1998) The cation-binding domain from the alpha subunit of integrin alpha5 beta1 is a minimal domain for fibronectin recognition. *J Biol Chem* **273**, 24744–53.

[385] Michalke, K, Gravière, M.-E, Huyghe, C, Vincentelli, R, Wagner, R, Pattus, F, Schroeder, K, Oschmann, J, Rudolph, R, Cambillau, C, & Desmyter, A. (2009) Mammalian g-protein-coupled receptor expression in escherichia coli: I. high-throughput large-scale production as inclusion bodies. *Analytical Biochemistry* **386**, 147–55.

[386] Banères, J.-L, Mesnier, D, Martin, A, Joubert, L, Dumuis, A, & Bockaert, J. (2005) Molecular characterization of a purified 5-ht4 receptor: a structural basis for drug efficacy. *J Biol Chem* **280**, 20253–60.

[387] Moreau, C. J, Dupuis, J. P, Revilloud, J, Arumugam, K, & Vivaudou, M. (2008) Coupling ion channels to receptors for biomolecule sensing. *Nature Nanotech* **3**, 620–625.

[388] Farzan, M, Mirzabekov, T, Kolchinsky, P, Wyatt, R, Cayabyab, M, Gerard, N. P, Gerard, C, Sodroski, J, & Choe, H. (1999) Tyrosine sulfation of the amino terminus of ccr5 facilitates hiv-1 entry. *Cell* **96**, 667–676.

[389] Duma, L, Häussinger, D, Rogowski, M, Lusso, P, & Grzesiek, S. (2007) Recognition of rantes by extracellular parts of the ccr5 receptor. *Journal of Molecular Biology* **365**, 1063–75.

Part VI.

Appendix

15. Experiments

15.1. Chemokine purification

15.1.1. SDF1α-Strep purification

Inclusion bodies containing SDF1α-Strep were solubilized in 7.5 M Guanidine HCl and protein was refolded overnight at 4°C in 50 mM Tris-HCl buffer. Refolded sample was centrifuged and applied to the Capto S column (pI 9.70). Elution fractions from a Capto S column were analyzed by the SDS-PAGE gel (Figure 15.1).

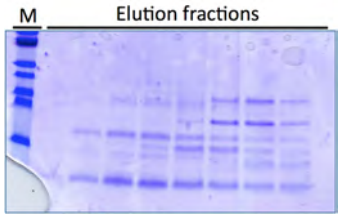

Figure 15.1.: SDF1α-Strep elution from Capto S column.

All elution fractions shown on the SDS-PAGE gel contained SDF1α-Strep and were pooled, concentrated and injected to the Superdex 200 column. Elution fractions were analyzed on the gel (Figure 15.2).

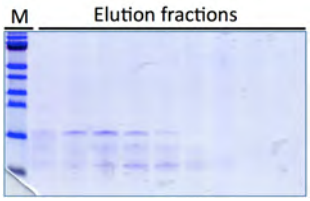

Figure 15.2.: SDF1α-Strep elution from Superdex 200 column.

Fractions containing SDF1α-Strep were pooled and concentrated. From one liter of bacterial culture 0.2 mg of SDF1α-Strep were obtained.

15.1.2. SDF1α-LT-Strep purification

Inclusion bodies containing SDF1α-LT-Strep were solubilized in 6M Urea and protein was refolded overnight at 4°C. The refolded sample was centrifuged and applied to the Q sepharose column (Figure 15.3).

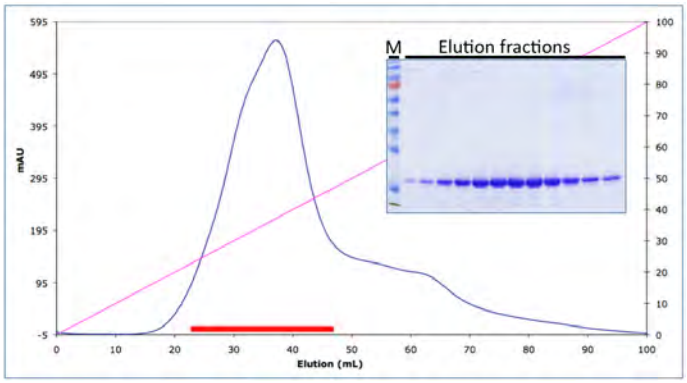

Figure 15.3.: SDF1α-LT-Strep elution profile from Q sepharose column.

Elution fractions were analyzed on the gel. Fractions containing SDF1α-LT-Strep were pooled and concentrated prior injection to a Superdex 200 gel filtration column (Figure 15.4).

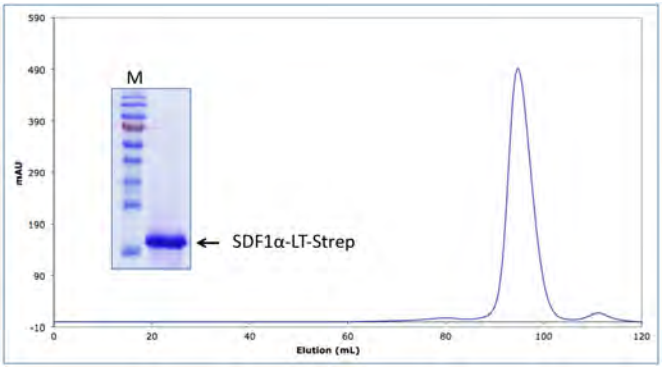

Figure 15.4.: SDF1α-LT-Strep running profile in Superdex 200 column.

Elution fractions were analyzed on the gel. Fractions containing SDF1α-LT-Strep were pooled and concentrated. From one liter of bacterial culture 3.2 mg of SDF1α-LT-Strep were obtained.

15.2. *In vitro* synthesis

Clones of CCR5 and CXCR4 receptors were prepared for cell-free synthesis. Wild type sequences as well as *E. coli* codon optimized sequences were cloned into two types of vectors pIVEX2.3d and pIVEX2.4d optimized for *in vitro* expression. The vector pIVEX2.4d possesses a N-terminal His tag while the vector pIVEX2.3d contains a C-terminal His tag. Seven clones were prepared (Table 15.1).

Nr	Construct name
1	pIVEX 2.3d CCR5 wt
2	pIVEX 2.3d CCR5 optimized
3	pIVEX 2.4d CCR5 optimized
4	pIVEX 2.3d CXCR4 optimized
5	pIVEX 2.4d CXCR4 optimized
6	pIVEX 2.4d CCR5 wt
7	pIVEX 2.3d CXCR4 wt

Table 15.1.: Clones for cell-free synthesis.

Synthesis was performed in 50 µl volume using commercial RTS 100 *E. coli* HY Kit. As a control the vector encoding bacteriorhodopsin was used (sample 8 in both gels). The reactions were carried out for 6 hours at 21°C. Samples were taken from each reaction and centrifuged to separate the soluble proteins from the precipitants. All samples were analyzed on SDS-polyacrylamide gel (Figure 15.5) and western blot using an anti-His antibody (Figure 15.6).

All constructs tested were expressed except sample 7 (CCR5 wt in pIVEX 2.4d vector). The best expression was observed for the samples: 1 - pIVEX 2.3d CCR5 wt, 2 - pIVEX 2.3d CCR5 optimized, 4 - pIVEX 2.3d CXCR4 optimized and 6 - pIVEX 2.4d CCR5 wt.

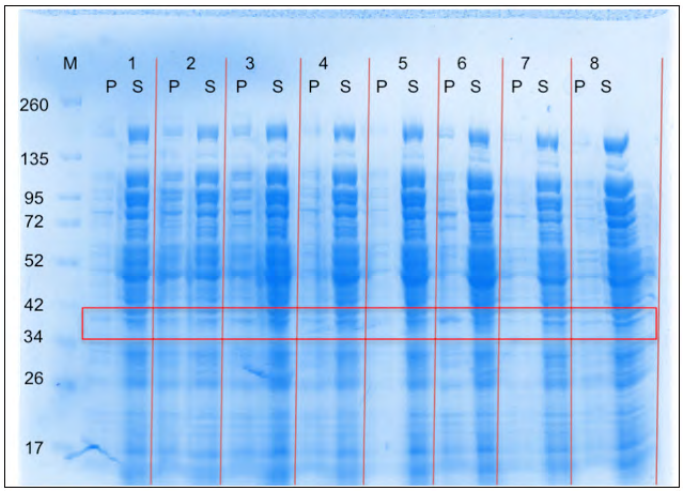

Figure 15.5.: SDS-polyacrylamide gel analysis of chemokine receptors in cell-free synthesis. M - marker, P - pellet, S - soluble fraction, 1-8 - numbers indicating the used constructs.

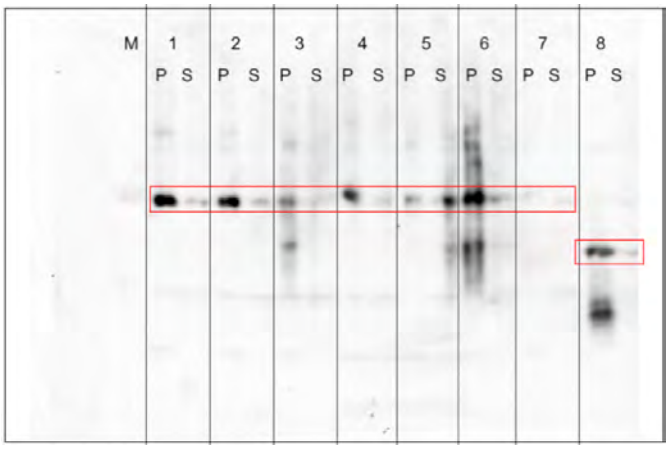

Figure 15.6.: Western Blot of chemokine receptors expression in cell-free synthesis.
M - marker, P - pellet, S - soluble fraction, 1-8 - numbers indicating the used constructs.

As there were no amphipols or detergent in the reaction mix all expressed protein were found in the pellet fraction.

16. Molecular biology

Fragment amplification by PCR

The PCR reaction mix was prepared as follows:

- 1 µl of DNA template at 100 ng/ml
- 2.5 µl of primer 1 at 100 ng/ml
- 2.5 µl of primer 2 at 100 ng/ml
- 2 µl of dNTP at 10 mM
- 10 µl Pfu polymerase buffer
- 2 µl of Pfu polymerase
- add miliQ H_2O up to 100 µl final volume

PCR amplification program:

Denaturation - 95°C – 2 min

Denaturation - 95°C – 1 min

Hybridization - 60°C – 1 min *25 cycles,*

Elongation - 68°C – 3 min

Elongation - 68°C – 5 min

Cloning of DNA

The ligation reaction mix was prepared as follows:

- 1 µl of previously digested vector
- 5 µl of previously digested insert
- 4 µl of 5x ligase buffer (Fermentas)
- 9 µl of miliQ H_2O
- 1 µl of ligase

The mix was incubated for 30 min at room temperature.

Transformation to *E. coli* competent cells

- 5 µl of ligation reaction (or 1 µl of DNA plasmid [0.1 µg]) was added to 50 µl of competent cells
- The reaction mix was incubated for 30 min on ice
- Heat shock at 42°C for 90 seconds
- Addition of 150 µl of SOC medium
- Incubation at 37°C with 220 rpm for 1 hour
- Plate the cells on LB + agar plates containing 100 ng/ml of ampicilin

17. Used primers

Name	Sequence 5'→3'
SDF-NdeI	ggt act att tca gca tat gaa acc ggt gag cct gag c
SDF-XhoI	gct gcc gcg gca cca gct cga gtt tgt tca ggg c
SDFLT-XhoI	gct ggc gcg cgg cac cag ctc gag cgc cag cag ttc
SDF-LT-fw	gcg ctg aac aaa ggc ccg ggc tat att gat acc
SDF-LT-rv	ggt atc aat ata gcc cgg gcc ttt gtt cag cgc
SDF1aLTBF	ctg gaa aaa gcg ctg aac aaa ggc ccg ggc tat att gat acc
SDF1aLTBR	cgc gcg gca cca ggc cgc tcg cca gca gtt cat cgc ctt c
MALE-Fw	ggt cgt cag act gtc gat gaa gcc
M13RV	tgt aaa acg acg gcc agt
SDF1apc4xLTPreProF	caa taa caa taa caa caa cct cgg gct cga ggt act att tca ggg acc caa acc ggt gag cct gag cta tcg ctg ccc gtg
SDF1apc4xLTPreProR	cac ggg cag cga tag ctc agg ctc acc ggt ttg ggt ccc tga aat agt acc tcg agc ccg agg ttg ttg tta ttg tta ttg
RANTESXaPreProR	c aat aac aac aac ctc ggg ctg gaa gtt ctg ttc cag ggg ccc att tca gaa ttc agc ccg tat agc agc gat acc acc
RANTESXaPreProF	c aat aac aac aac ctc ggg ctg gaa gtt ctg ttc cag ggg ccc agc ccg tat agc agc gat acc acc
SDFStrepF	ctg gaa aaa gcg ctg aac aaa ctc gag gta cta ttt cag gga ccc agc gct tgg agc cac ccg cag ttc gaa aaa tag ggc gga tcc gaa ttc gag
SDFStrepR	ctc gaa ttc gga tcc gcc cta ttt ttc gaa ctg cgg gtg gct cca agc gct ggg tcc ctg aaa tag tac ctc gag ttt gtt cag cgc ttt ttc cag
SDFLTStrepF	ggc gat gaa ctg ctg gcg ctc gag gta cta ttt cag gga ccc agc gct tgg agc cac ccg cag ttc gaa aaa tag ctc gag cac cac cac cac
SDFLTStrepR	gtg gtg gtg gtg ctc gag cta ttt ttc gaa ctg cgg gtg gct cca agc gct ggg tcc ctg aaa tag tac ctc gag cgc cag cag ttc atc gcc
RANTESStrepF	gat ata cat atg agc ccg tat agc agc gat acc
RANTESStrepR	att aac agc ctg gaa atg agc ctc gag gta cta ttt cag gga ccc agc gct tgg agc cac ccg cag ttc gaa aaa tag gga tcc gaa ttc
RANTESLTStrepR	gaa ggc gat gaa ctg ctg gcg ctc gag gta cta ttt cag gga ccc agc gct tgg agc cac ccg cag ttc gaa aaa tag gga tcc gaa ttc

Table 17.1.: Primers used for PCR.

Name	Sequence 5'→3'
PivexR5optF	cgt tgc atc cat gga tta tca ggt gag cag ccc
PivexR5optR	atg caa cgc ccg ggc agg ccc acg cta att tcc
PivexR5optstopR	atg caa cgc ccg ggt tac agg ccc acg cta att tcc
PivexR5wtF	cgt tgc atc cat gga tta tca agt gtc aag tcc
PivexR5wtR	atg caa cgc ccg ggc aag ccc aca gat att tcc
PivexR5wtstopR	atg caa cgc ccg ggt tac aag ccc aca gat att tcc
PivexX4optF	cgt tgc atc cat gga agg cat tag cat tta tac c
PivexX4optR	atg caa cgc ccg ggg ctg cta tga aag ctg ctg
PivexX4optstopR	atg caa cgc ccg ggt tag ctg cta tga aag ctg ctg
PivexX4wtF	cgt tgc atc cat gga ggg gat cag tat ata cac
PivexX4wtR	atg caa cgc ccg ggg ctg gag tga aaa ctt gaa g
PivexX4wtstopR	atg caa cgc ccg ggt tag ctg gag tga aaa ctt gaa g

Table 17.2.: Primers used for cell free constructs.

18. Sequences

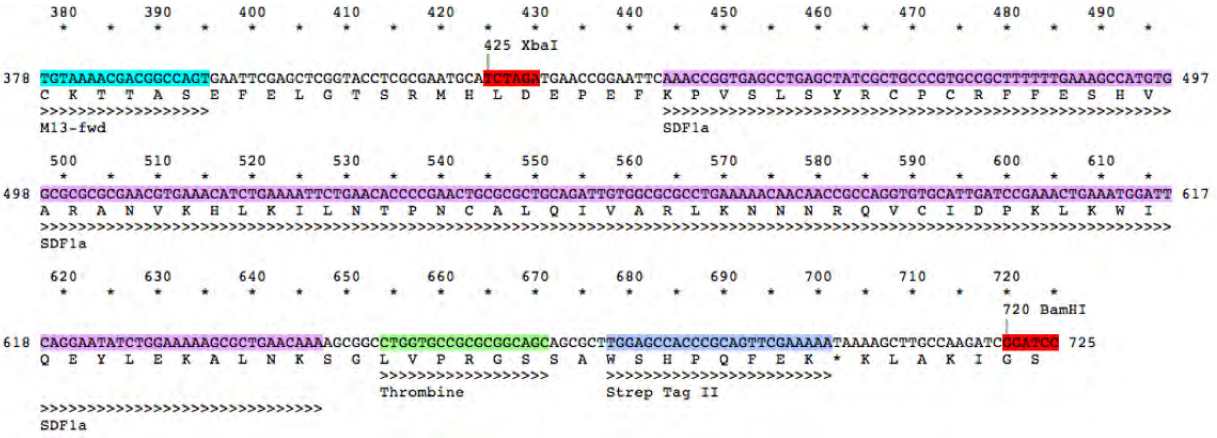

Figure 18.1.: SDF1α DNA sequence in pUC57 vector and protein sequence.

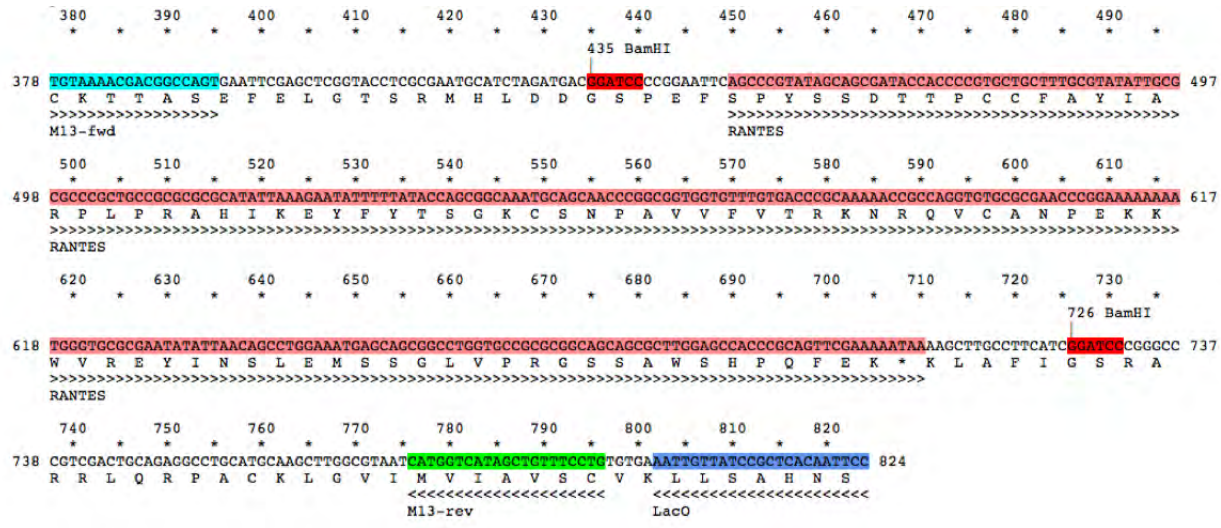

Figure 18.2.: RANTES DNA sequence in pUC57 vector and protein sequence.

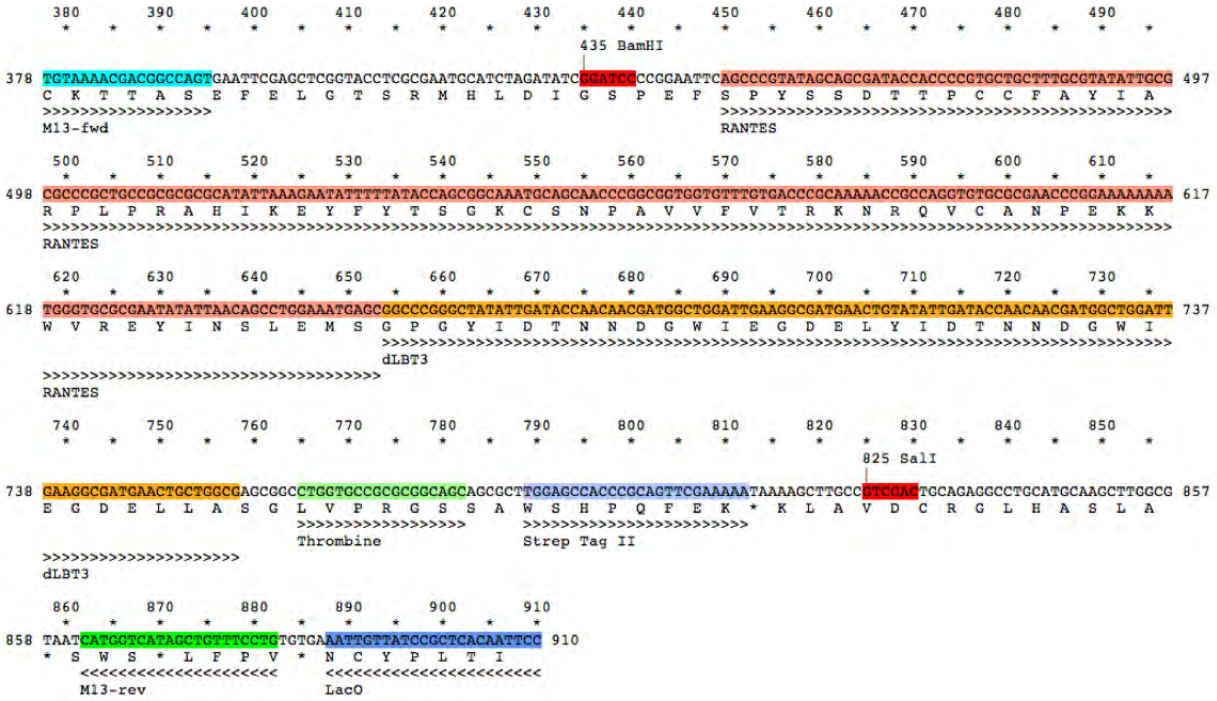

Figure 18.3.: RANTES-LT DNA sequence in pUC57 vector and protein sequence.

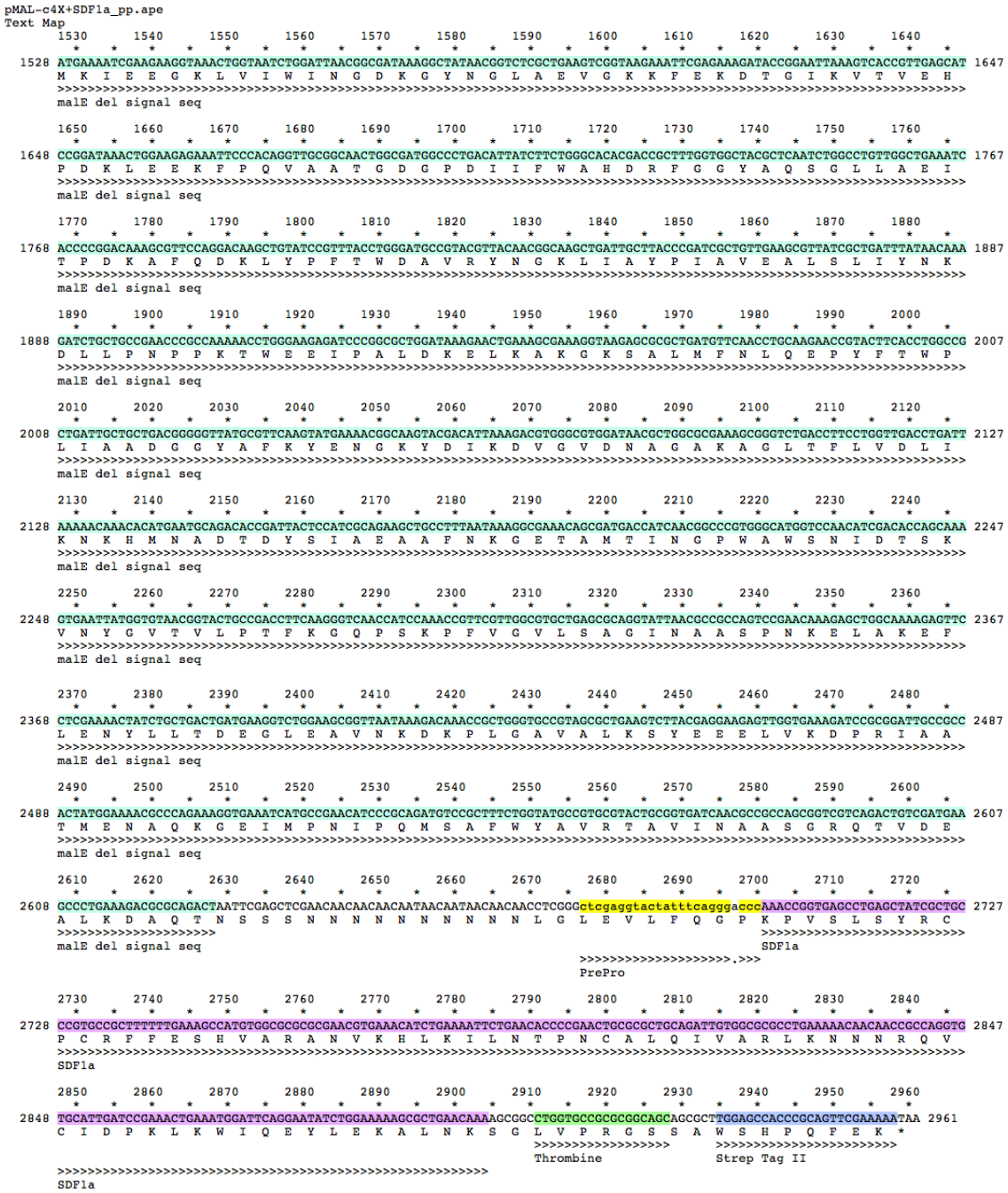

Figure 18.4.: DNA and protein MBP-PrePro-SDF1α-Strep sequence.

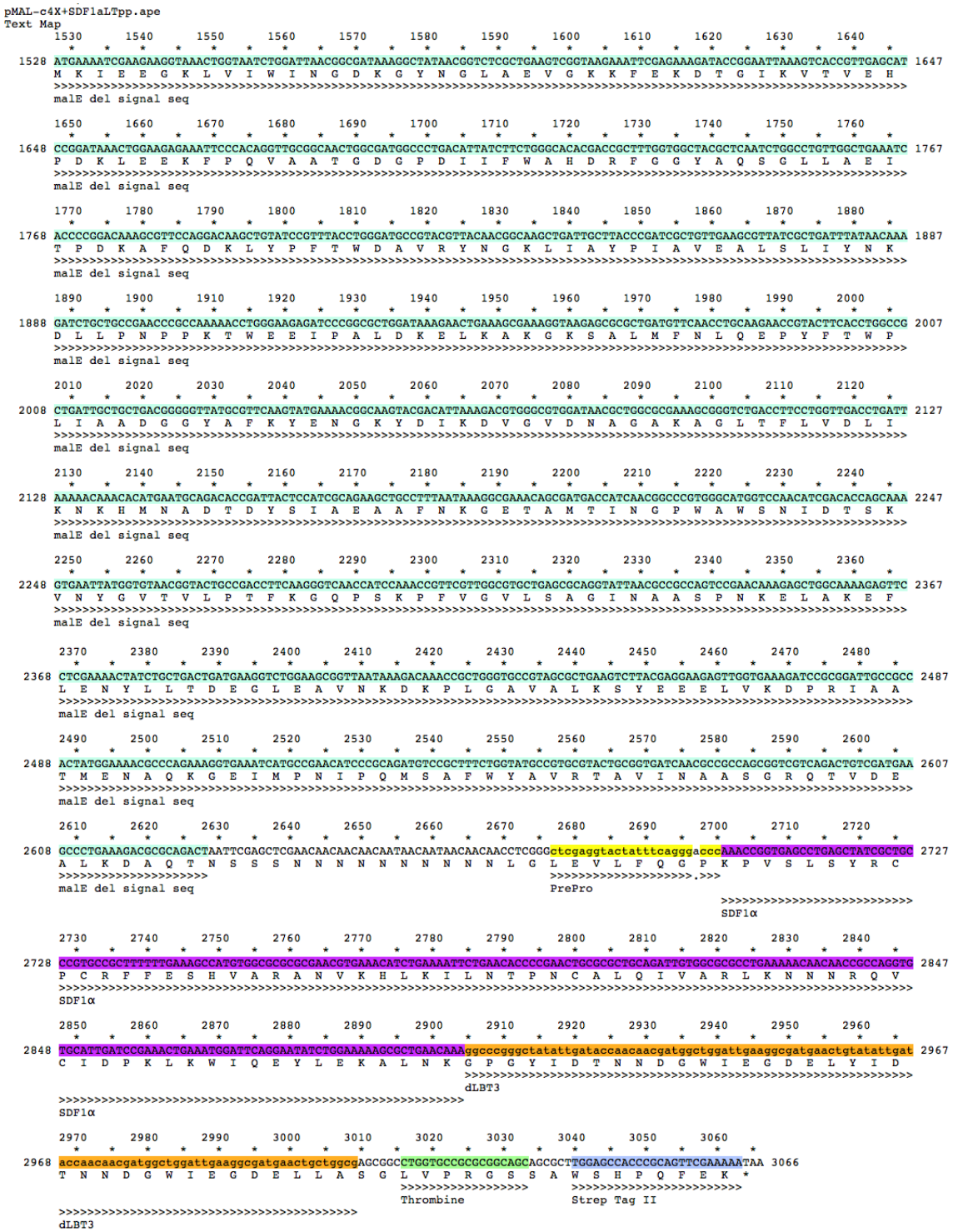

Figure 18.5.: DNA and protein MBP-PrePro-SDF1α-LT-Strep sequence.

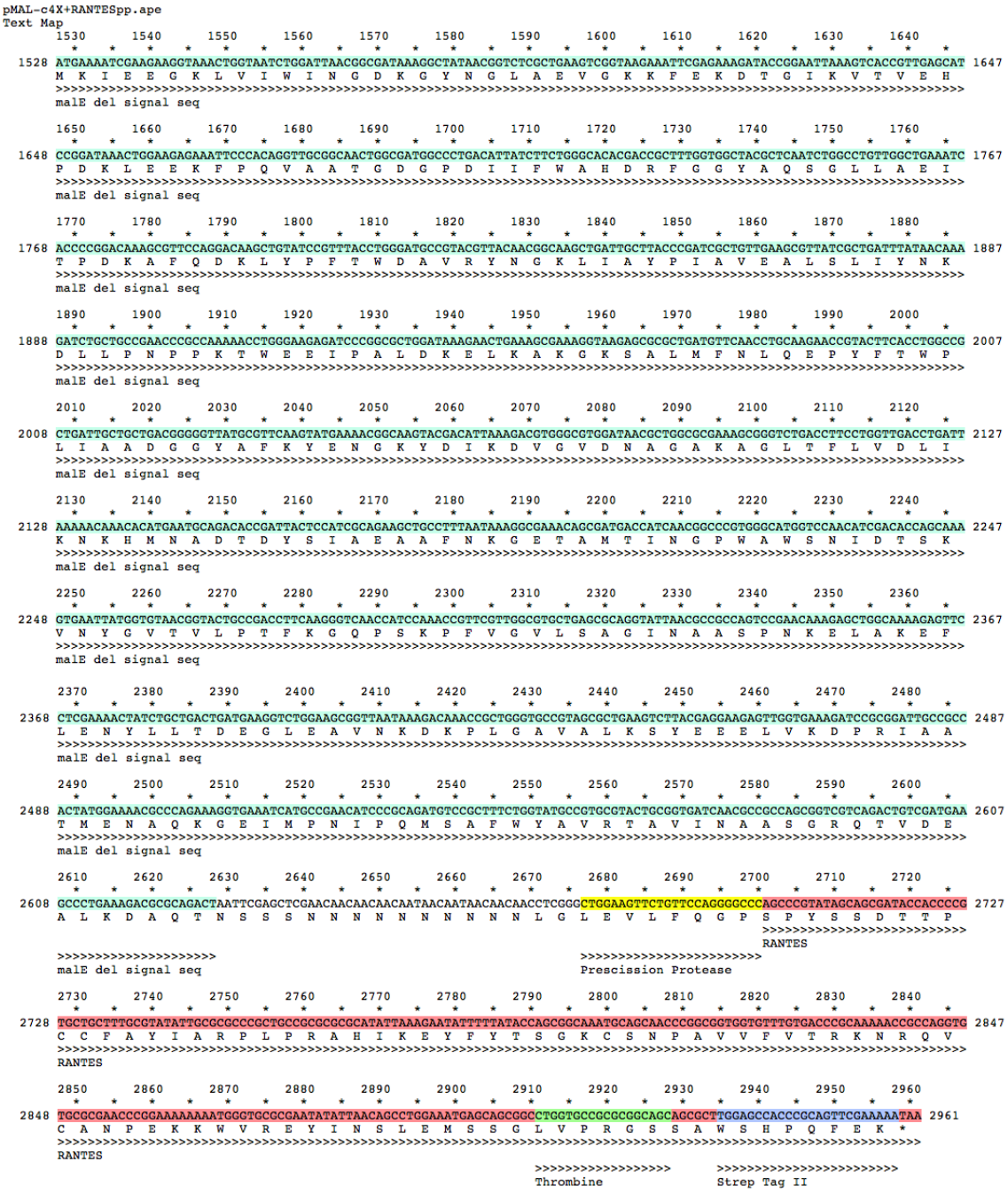

Figure 18.6.: DNA and protein MBP-PrePro-RANTES-Strep sequence.

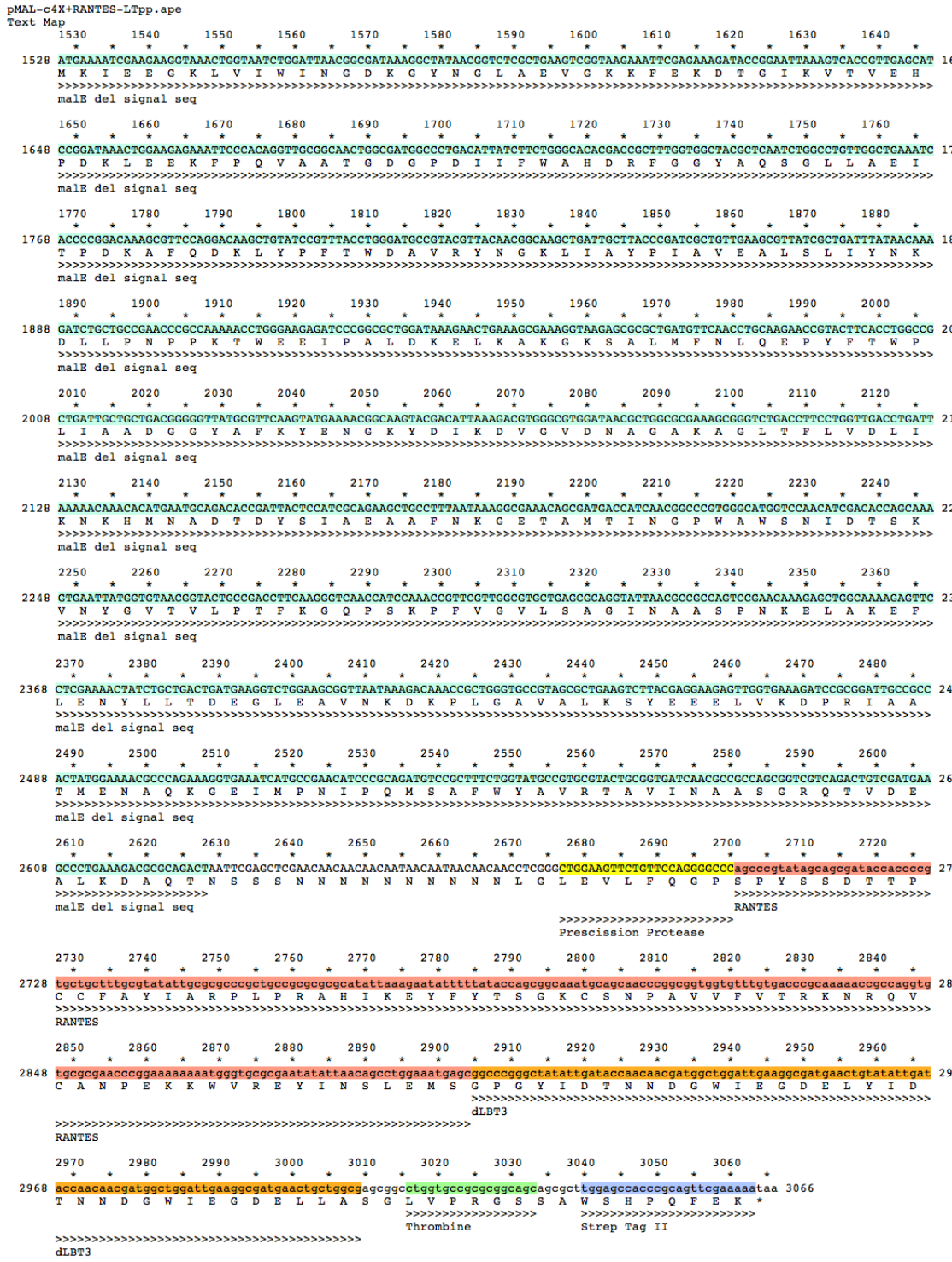

Figure 18.7.: DNA and protein MBP-PrePro-RANTES-LT-Strep sequence.

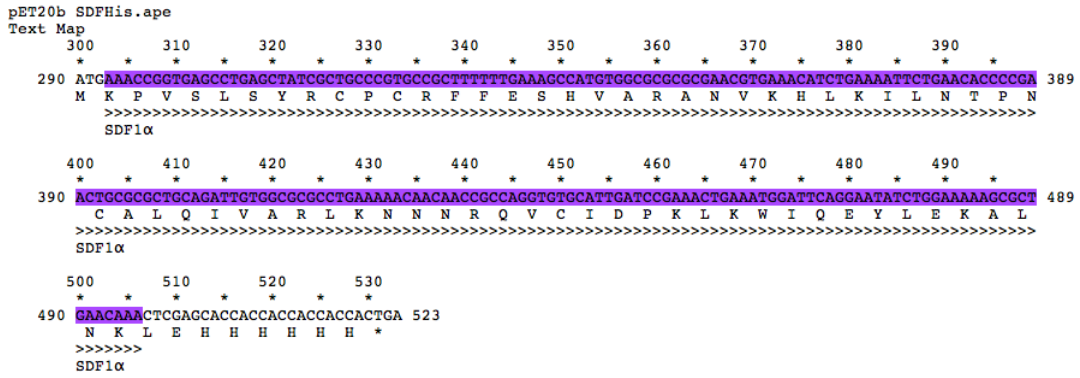

Figure 18.8.: DNA and protein SDF1α-His sequence.

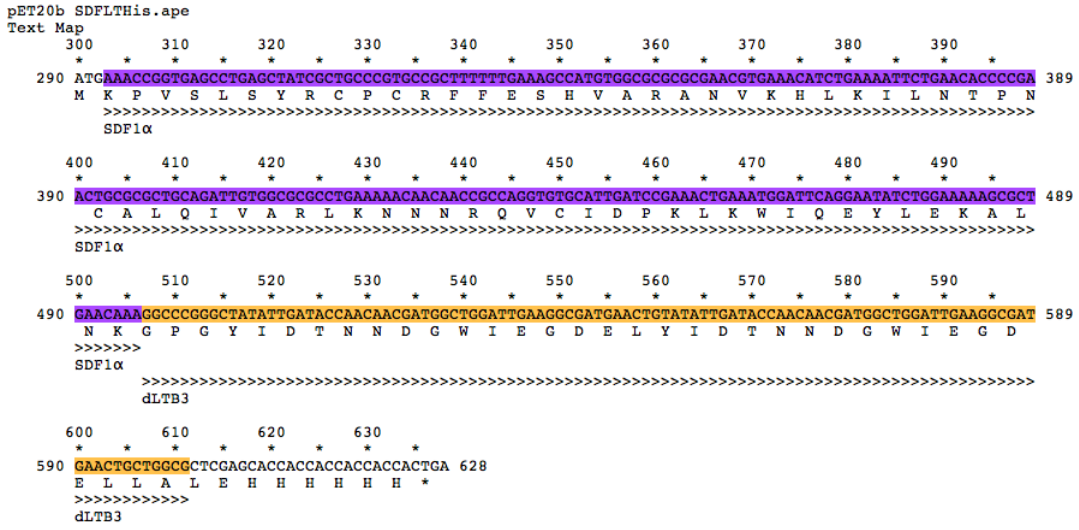

Figure 18.9.: DNA and protein SDF1α-LT-His sequence.

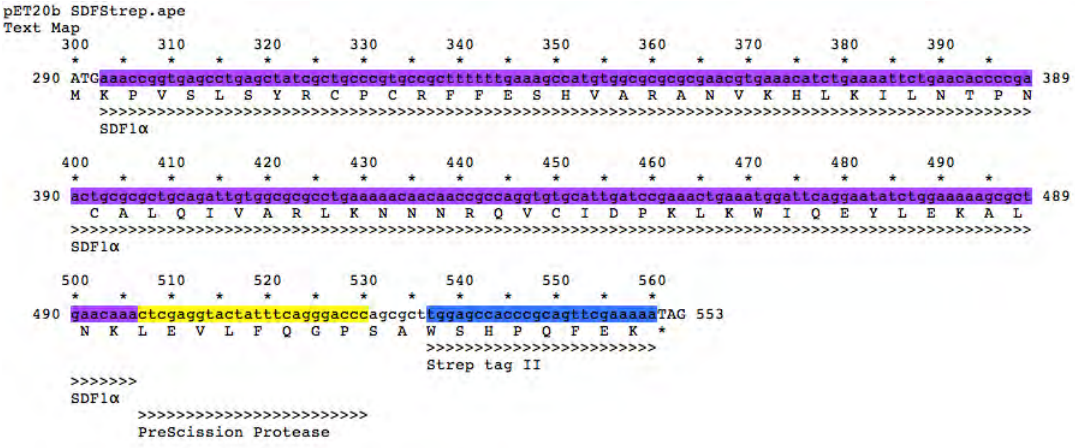

Figure 18.10.: DNA and protein SDF1α-Strep sequence.

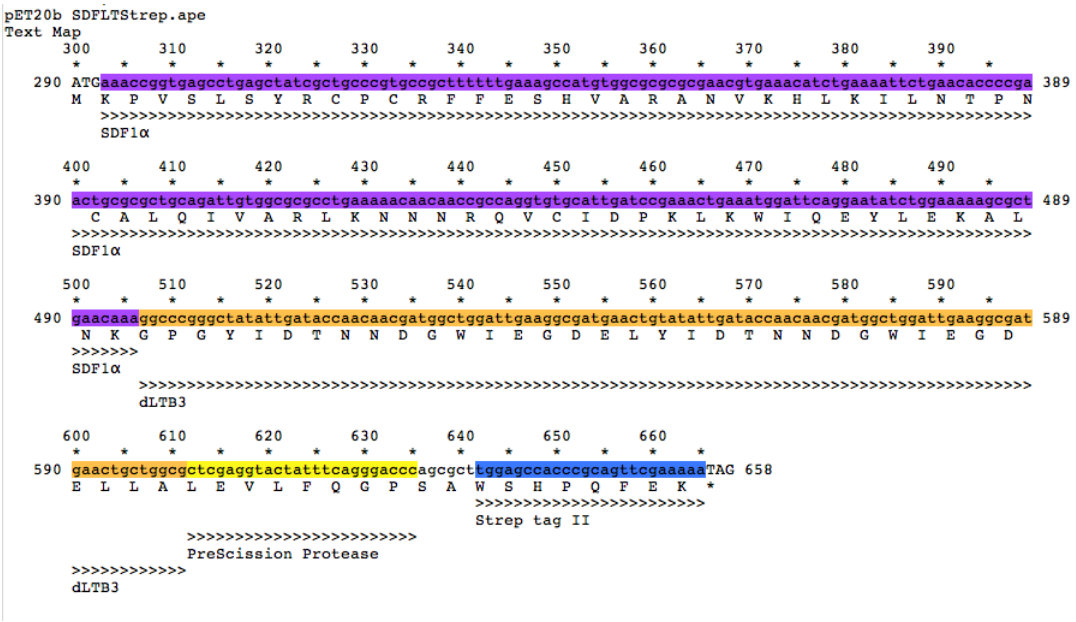

Figure 18.11.: DNA and protein SDF1α-LT-Strep sequence.

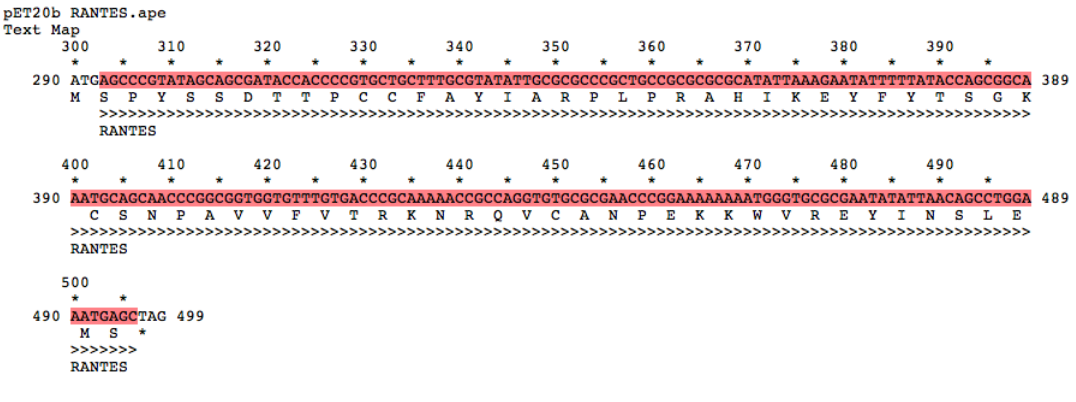

Figure 18.12.: DNA and protein RANTES sequence.

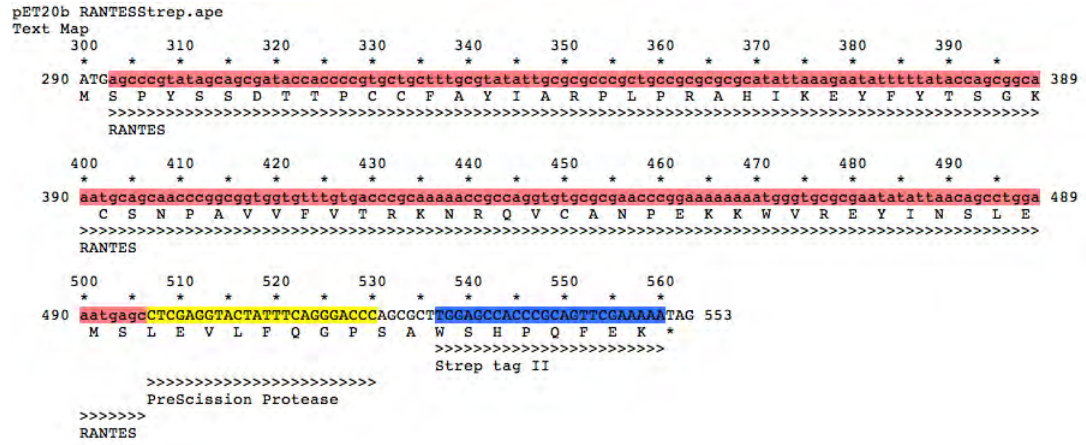

Figure 18.13.: DNA and protein RANTES-Strep sequence.

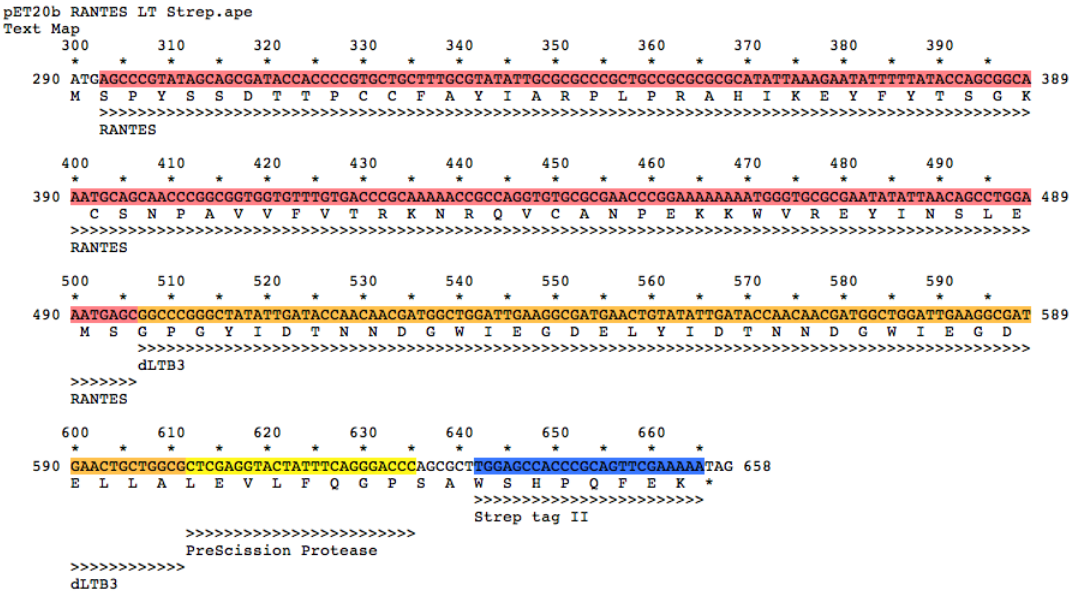

Figure 18.14.: DNA and protein RANTES-LT-Strep sequence.

Figure 18.15.: DNA and protein α5I-CCR5-His sequence.

Figure 18.16.: DNA and protein α5I-CCR5-His-C9 sequence.

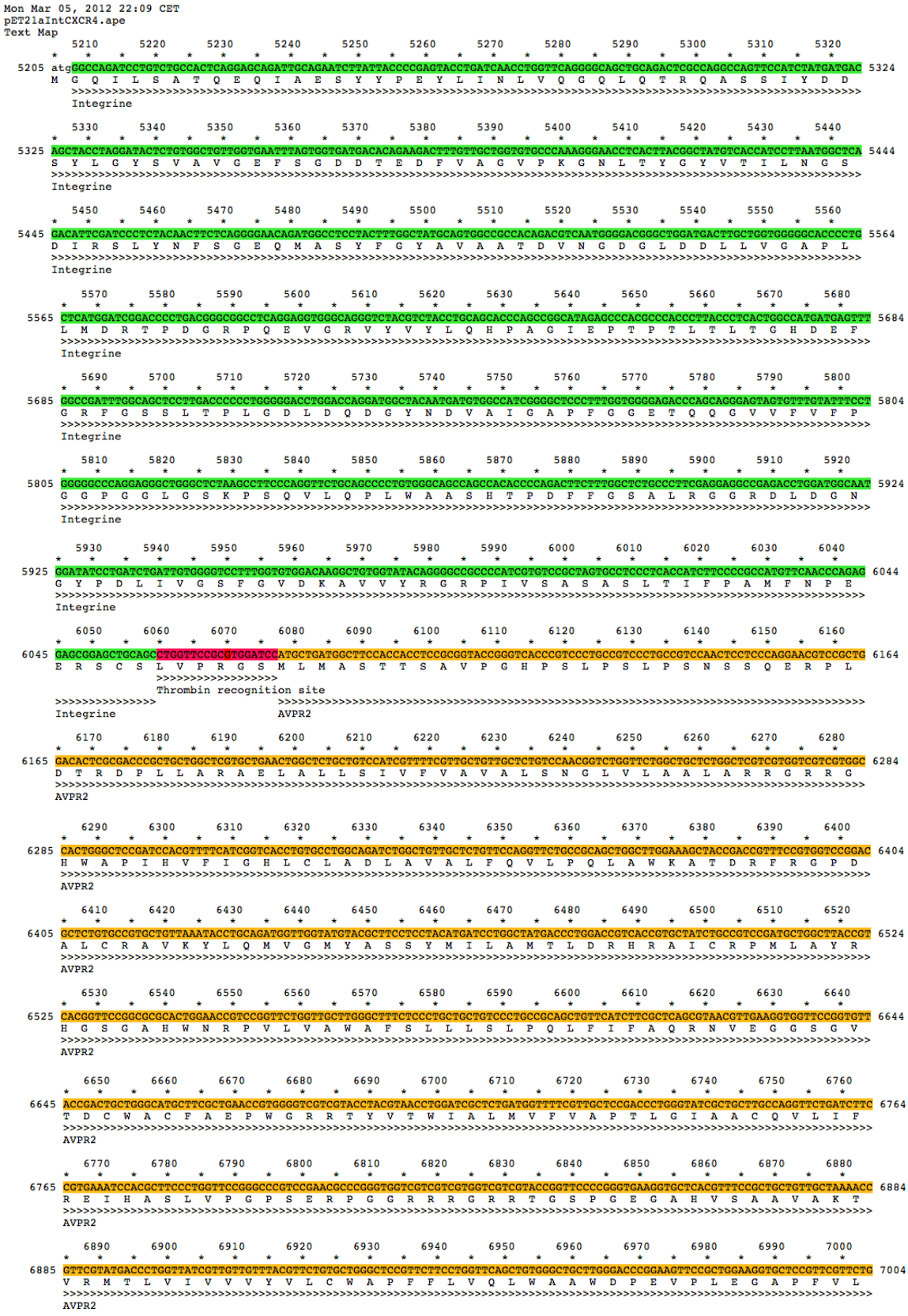

Figure 18.17.: Part I. DNA and protein α5I-V2-CXCR4-His sequence.

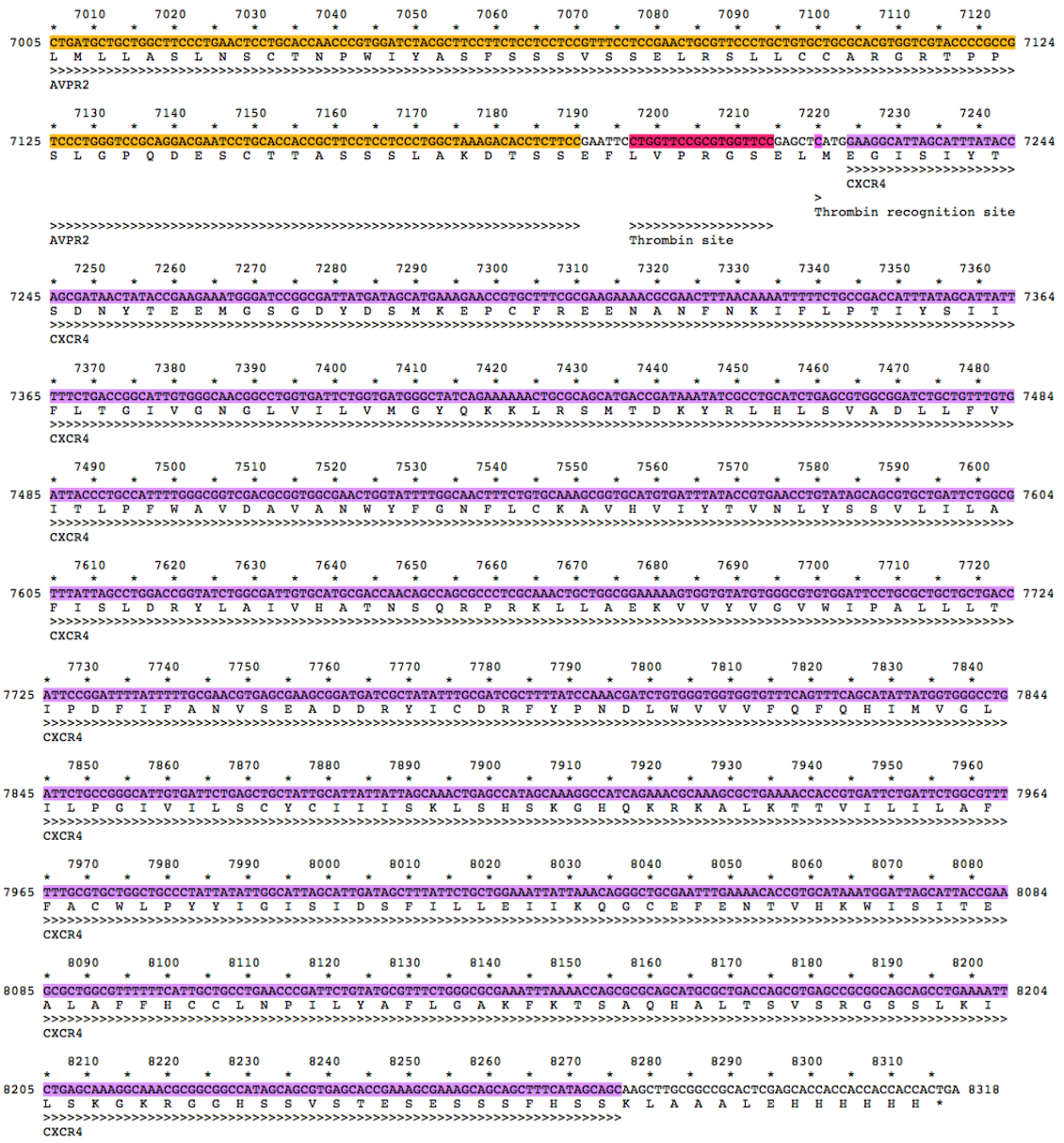

Figure 18.18.: Part II. DNA and protein α5I-V2-CXCR4-His sequence.

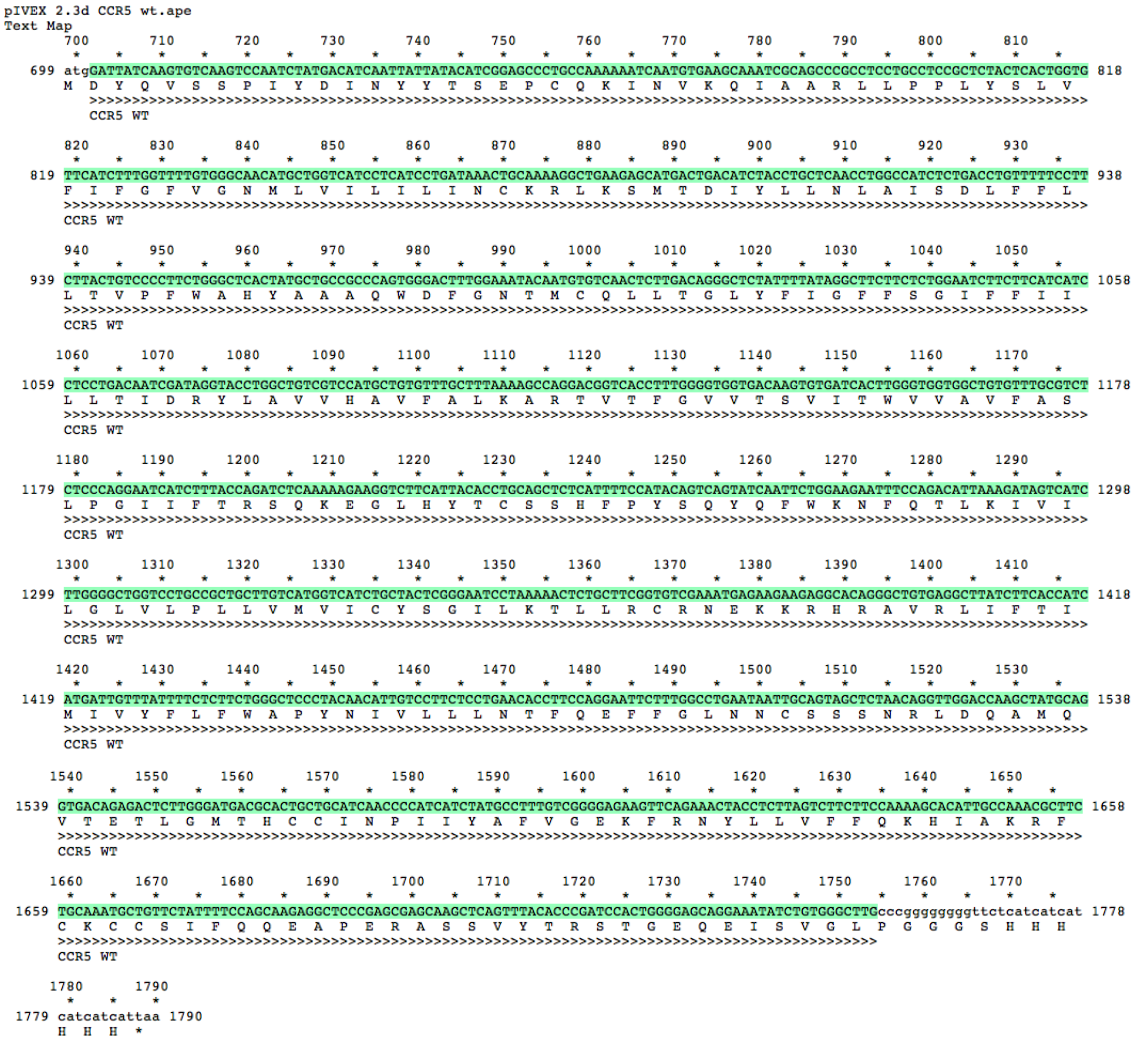

Figure 18.19.: DNA and protein pIVEX 2.3d CCR5 WT sequence.

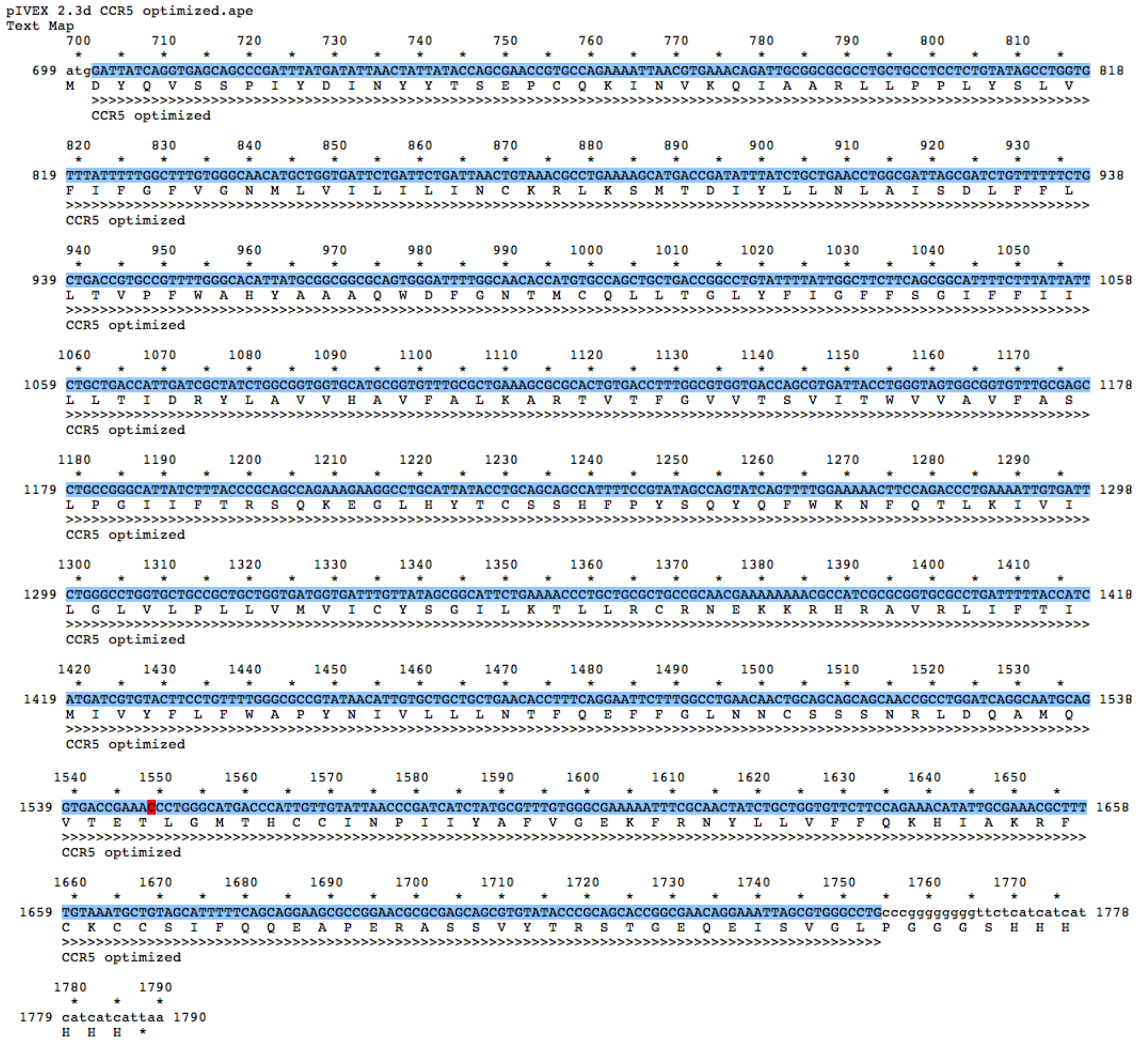

Figure 18.20.: DNA and protein pIVEX 2.3d CCR5 optimized sequence.

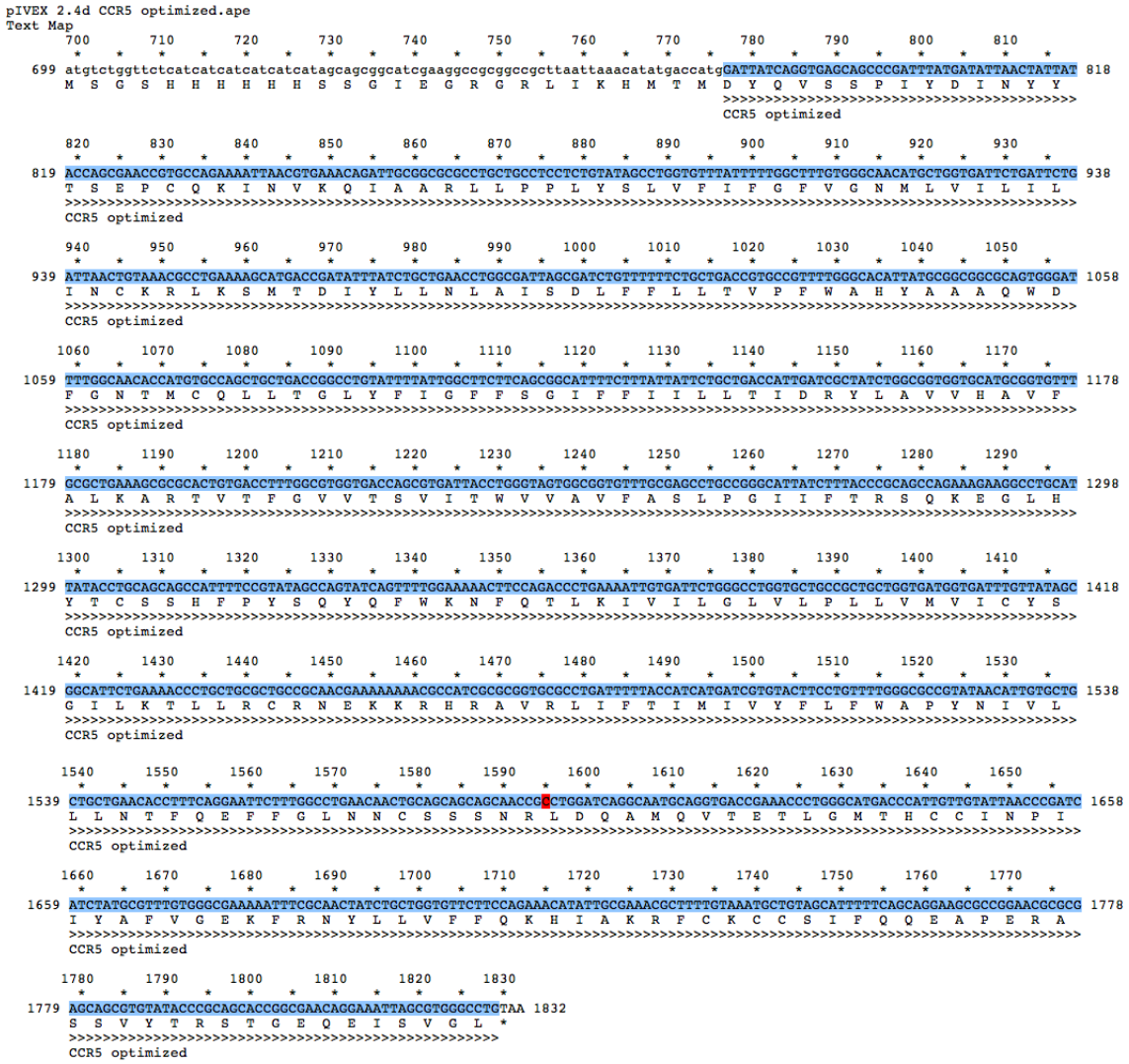

Figure 18.21.: DNA and protein pIVEX 2.4d CCR5 optimized sequence.

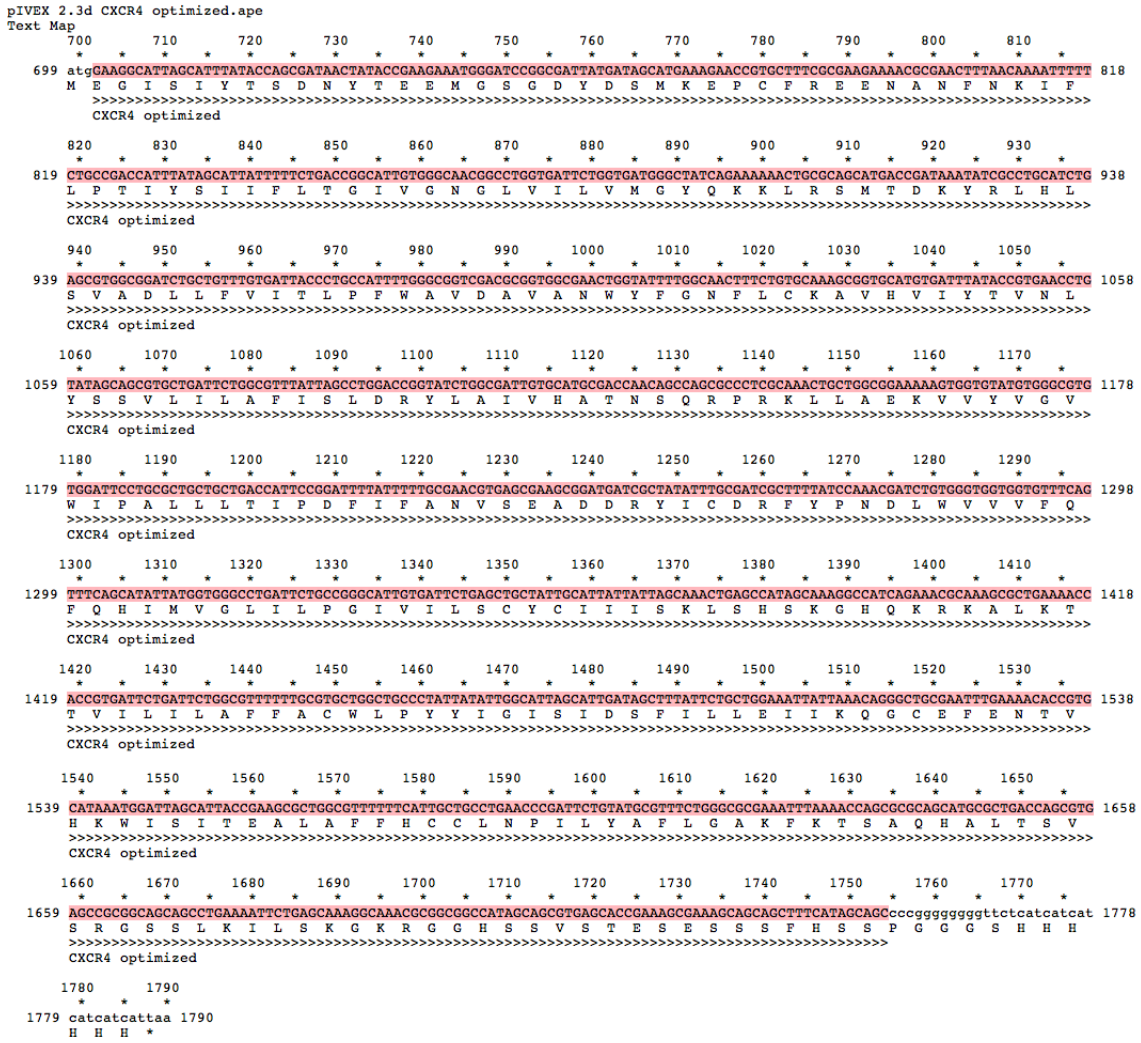

Figure 18.22.: DNA and protein pIVEX 2.3d CXCR4 optimized sequence.

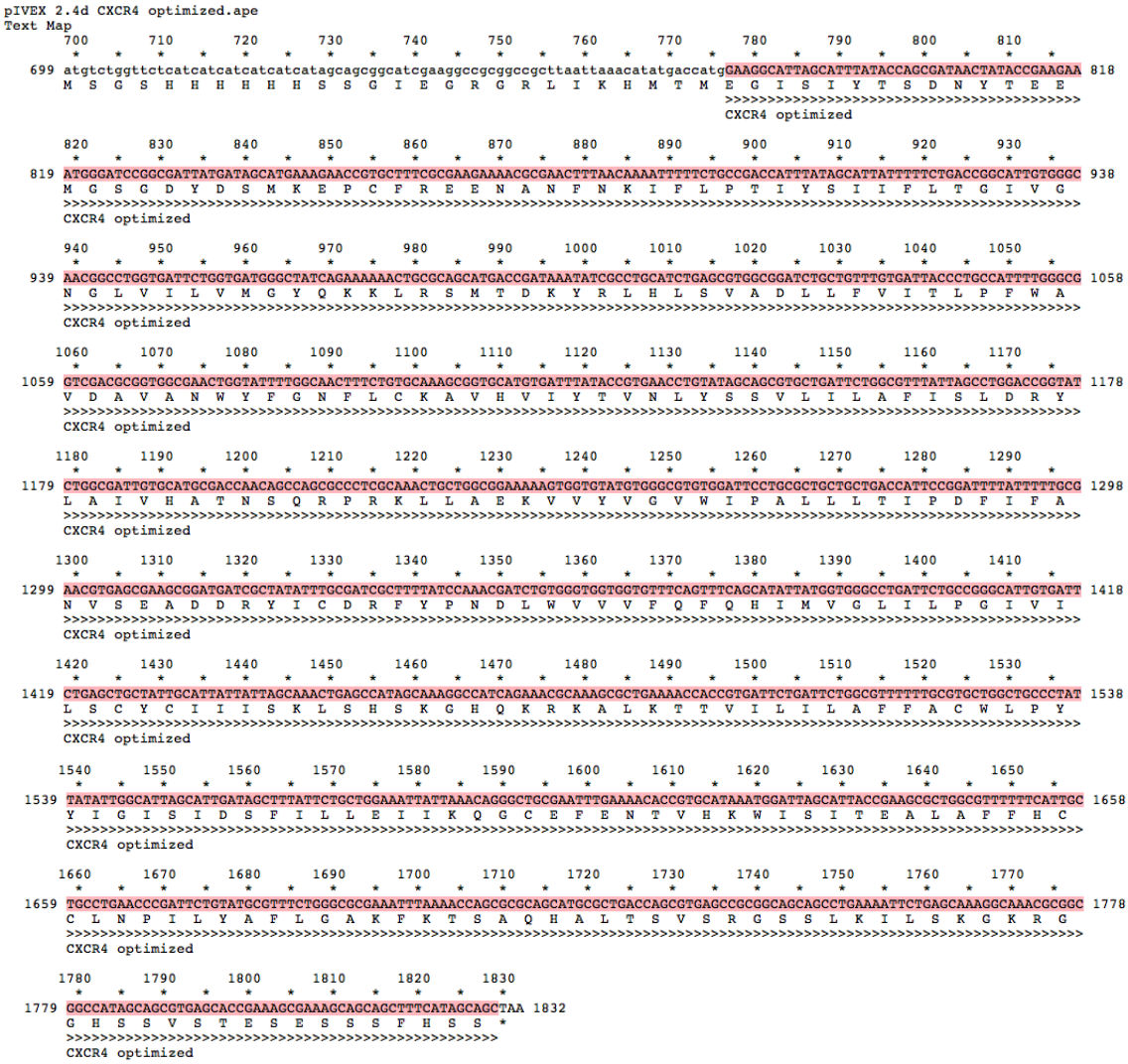

Figure 18.23.: DNA and protein pIVEX 2.4d CXCR4 optimized sequence.

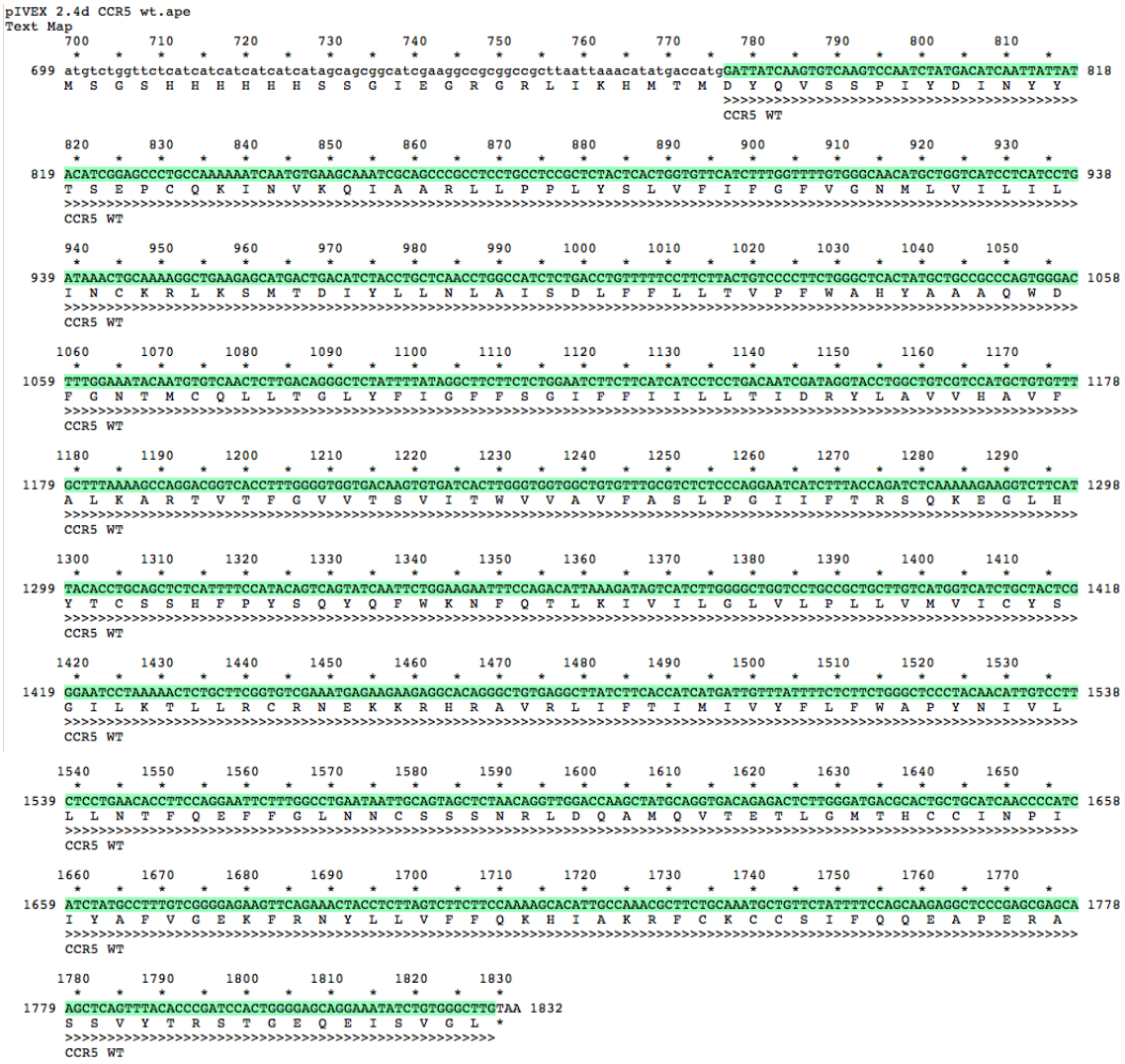

Figure 18.24.: DNA and protein pIVEX 2.4d CCR5 WT sequence.

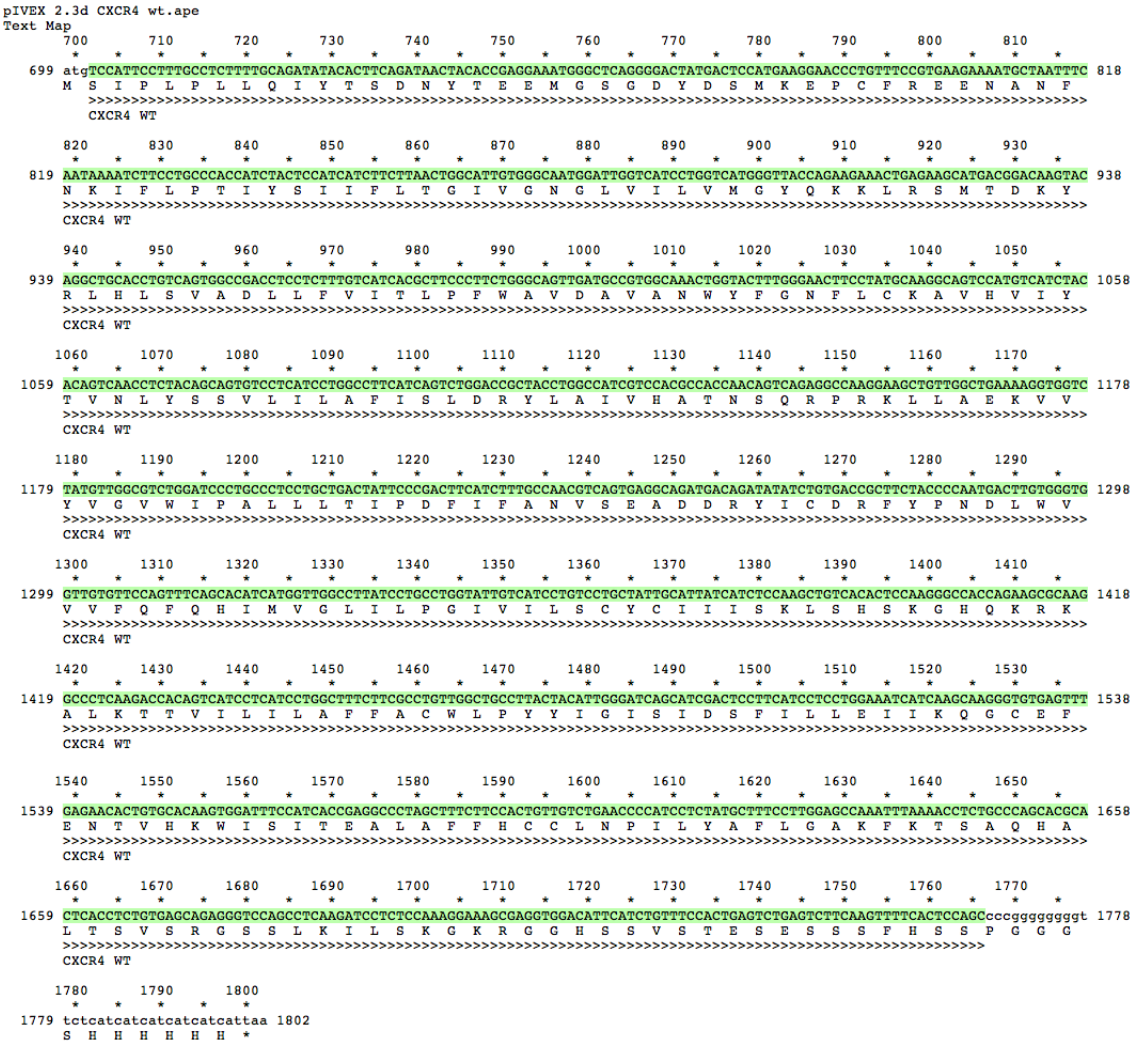

Figure 18.25.: DNA and protein pIVEX 2.3d CXCR4 WT sequence.

Abstract: Chemokine receptors are critical regulators of cell migration in the context of immune surveillance, inflammation and development. The GPCRs (G protein-coupled receptors) CCR5 and CXCR4 are specifically implicated in cancer metastasis and HIV-1 infection. An expression system to over-express these two GPCRs was developed. To overcome the toxicity problem of membrane protein expression in bacterial system, the production approach consists in targeting the proteins towards *E. coli* inclusion bodies thanks to a N-terminal fusion allowing a high yield expression. After purification under denaturing conditions, these GPCRs were then folded using original polymeric surfactants: the amphipols. The validation of this new approach for the chemokine receptor production is one of the goals of this work. In order to assess the functionality of the folded proteins, series of tools have been developed: engineered chemokine ligands (RANTES for CCR5 and SDF1α for CXCR4) were produced. The functionality of chemokines was evaluated at cellular and molecular levels. Interaction between the receptor folded in amphipols and its ligand was evaluated using Surface Plasmon Resonance (SPR) technique. Several types of surfaces, functionalized with the chemokine receptor/amphipol complex have been explored in this work. At the end of this project the productions of chemokines and their receptors has been set up. These established tools open the way to future studies, at the molecular level, in order to, for instance, investigate receptor dimerization and complex stoichiometry.

Keywords: GPCRs, Chemokine receptors, CXCR4, CCR5, chemokines, SDF1α, RANTES, *E. coli* expression system, GPCR folding, amphipols, chemotaxis, Surface Plasmon Resonance, TEVC, Lanthanoid Binding Tag.

Résumé : Les récepteurs de chimiokines sont des régulateurs essentiels de la migration cellulaire dans le cadre de la surveillance immunitaire, et le développement. Les récepteurs CCR5 et CXCR4 sont de plus spécifiquement impliqués dans les métastases cancéreuses et l'infection par le VIH. Nous avons développé un système permettant de sur-exprimer ces deux RCPGs. Afin de s'affranchir des problèmes de toxicité inhérents à l'expression des protéines membranaires en bactérie notre approche de production consiste à adresser les protéines vers les corps d'inclusion d'*E. coli* grâce à une fusion protéique N-terminale permettant de hauts niveaux d'expression. Après purification en conditions dénaturantes, les protéines sont alors repliées en présence de surfactants originaux, les amphipoles. La validation de cette nouvelle approche pour les récepteurs des chimiokines représente un des objectifs principaux de ce travail. Afin de tester la fonctionnalité des protéines repliées, une série d'outils a été développée : des versions modifiées des chimiokines ont été produites (RANTES pour CCR5 et SDF 1α pour CXCR4). La fonctionnalité des chimiokines a été évaluée au niveau moléculaire et cellulaire. L'interaction entre le récepteur replié en amphipole et son ligand a été testé par résonance de plasmons de surface (SPR). Différents types de surfaces fonctionalisées avec le récepteur de chimiokine replié en amphipole ont été explorés au cours de ce travail. A la fin de ce projet, la production des chimiokines et de leur récepteur a été mise au point. L'accès à ces outils ouvre la voie à de futures études moléculaires telles que la compréhension de la dimérisation du récepteur ou la détermination de la stœchiométrie du complexe.

Mots-clés: RCPG, récepteurs de chimiokines, CXCR4, CCR5, chimiokine, SDF1α, RANTES, expression dans *E. coli,* GPCR renaturation, amphipoles, chimiotactisme, Résonance Plasmonique de Surface, TEVC, etiquette de Lanthanid.